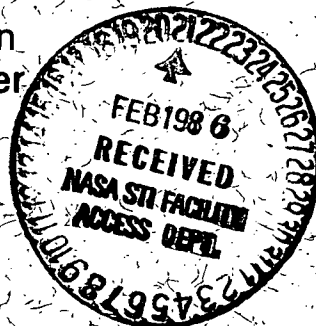# High Dynamic GPS Receiver Validation Demonstration

## Final Report

William J. Hurd
Joseph I. Statman
Victor A. Vilnrotter

FEB1986
RECEIVED
NASA STI FACILITY
ACCESS DEPT

October 31, 1985

| 1. Report No. 85-74 | 2. Government Accession No. | 3. Recipient's Catalog No. |
|---|---|---|
| 4. Title and Subtitle<br><br>High Dynamic GPS Receiver Validation Demonstration<br>- Final Report | | 5. Report Date<br>October 31, 1985 |
| | | 6. Performing Organization Code |
| 7. Author(s) William J. Hurd, Joseph I. Statman, Victor A. Vilnrotter | | 8. Performing Organization Report No. |
| 9. Performing Organization Name and Address<br><br>JET PROPULSION LABORATORY<br>California Institute of Technology<br>4800 Oak Grove Drive<br>Pasadena, California 91109 | | 10. Work Unit No. |
| | | 11. Contract or Grant No.<br>NAS7-918 |
| | | 13. Type of Report and Period Covered<br><br>JPL Publication |
| 12. Sponsoring Agency Name and Address<br><br>NATIONAL AERONAUTICS AND SPACE ADMINISTRATION<br>Washington, D.C. 20546 | | |
| | | 14. Sponsoring Agency Code<br>RE 182 PX-644-11-00-03-20 |

15. Supplementary Notes

16. Abstract

The Validation Demonstration establishes that the high dynamic Global Positioning System (GPS) receiver concept developed at JPL meets the dynamic tracking requirements for range instrumentation of missiles and drones. It was demonstrated that the receiver can track the pseudorange and pseudorange rate of vehicles with acceleration in excess of 100 g and jerk in excess of 100 g/s, dynamics ten times more severe than specified for conventional High Dynamic GPS receivers. These results and analytic extensions to a complete system configuration establish that all range instrumentation requirements can be met. The receiver can be implemented in the 100 in.$^3$ volume required by small missiles and drones, and is ideally suited for transdigitizer or translator applications.

| 17. Key Words (Selected by Author(s)).<br><br>Aircraft Communications and Navigation<br>Electronics and Electrical Engineering<br>Navigation, Detection, and Countermeasures (General)<br>Navigation and Guidance | 18. Distribution Statement<br><br><br>Unclassified - Unlimited |
|---|---|

| 19. Security Classif. (of this report)<br><br>Unclassified | 20. Security Classif. (of this page)<br><br>Unclassified | 21. No. of Pages<br><br>216 | 22. Price |
|---|---|---|---|

JPL 0184 R 9/83

# High Dynamic GPS Receiver Validation Demonstration

## Final Report

William J. Hurd
Joseph I. Statman
Victor A. Vilnrotter

October 31, 1985

# ABSTRACT

The Validation Demonstration establishes that the high dynamic Global Positioning System (GPS) receiver concept developed at JPL meets the dynamic tracking requirements for range instrumentation of missiles and drones. It was demonstrated that the receiver can track the pseudorange and pseudorange rate of vehicles with acceleration in excess of 100 g and jerk in excess of 100 g/s, dynamics ten times more severe than specified for conventional High Dynamic GPS receivers. These results and analytic extensions to a complete system configuration establish that all range instrumentation requirements can be met. The receiver can be implemented in the 100 in.$^3$ volume required by small missiles and drones, and is ideally suited for transdigitizer or translator applications.

# ACKNOWLEDGEMENTS

# CONTENTS

**FIGURES**

ix

TABLES

# CHAPTER 1

## SUMMARY

## 1.1 EXECUTIVE SUMMARY

This Validation Demonstration conclusively establishes that the high dynamic Global Positioning System (GPS) receiver concept developed by JPL meets the dynamic tracking requirements for range instrumentation of high dynamic missiles and drones. Analysis indicates that all range instrumentation requirements can be met, but only the pseudorange tracking capability was demonstrated. It is recommended that a fully functional receiver be developed using the high dynamic tracking concept.

It was demonstrated that the receiver accurately tracks pseudorange and pseudorange rate with acceleration and jerk in excess of 100 g and 100 g/s, respectively, which constitute dynamics ten times more severe than specified for conventional GPS High Dynamic Instrumentation Set (HDIS) receivers [1]. Analysis shows that, at the same time, the receiver position accuracy can meet the HDIS specifications. Accuracy is limited by the GPS Space and Control Segments and by propagation effects, not by the receiver or by vehicle dynamics. This is all accomplished without external aiding by an inertial navigation unit.

The receiver can be implemented in the stated volume goal of 100 in.$^3$ for missiles and small-scale drones. The design is almost entirely digital, and is suitable for miniaturization by use of Very Large Scale Integration (VLSI) Circuits. Still smaller volume appears feasible, but detailed investigation was outside of the scope of study.

The receiver is ideally suited for transdigitizer or translator applications. In these applications, the signal from an instrumented vehicle is relayed to a remotely located processing receiver. The key feature of the new receiver is that high dynamic vehicles can be tracked without inertial aiding, which would be unavailable in typical systems.

## 1.2 OBJECTIVES AND APPROACH

The general objective of this Validation Demonstration is to establish that the new receiver concept meets the high dynamic, low volume requirements for range instrumentation of missiles and drones.

The approach was first to develop and publish a High Dynamic GPS Receiver Validation Demonstration Plan [2]. This Plan, approved by Armament Division, presented objectives, concepts, functional requirements including tests and success criteria, a description of the receiver and the entire Demonstration System, anticipated performance and error budget, and a task schedule. The Plan was implemented by developing the receiver and test instrumentation, conducting the experimental tests and supporting analyses and simulations, and writing this Final Report. To minimize cost, the Demonstration Receiver has only one channel, capable of tracking one simulated satellite in pseudorange and range rate. This is sufficient to validate the high dynamic and low SNR tracking capability. Feasibility to meet the volume goal was established by performing a strawman electronic and packaging design of a complete receiver and estimating the volume and power.

The Plan established the specific objectives of the Demonstration. Armament Division stated a volume requirement of 100 in.$^3$ for final implementation, but did not require specific accuracy, dynamics or SNR threshold. These latter requirements were based on the overall GPS accuracy and SNR, and on envisioned dynamics. The required rms pseudorange accuracy was 17 m with acceleration of 50 g and jerk of 50 g/s, at an input SNR of 34 dB-Hz. Late in the Demonstration, Armament Division issued specifications for HDIS receivers for aircraft dynamics. Although these requirements do not apply to the Demonstration Receiver, and the HDIS operates at much lower dynamics, the Demonstration Receiver has comparable accuracy. An informal goal was established to compare the performance of the new high dynamic receiver to the HDIS specifications.

## 1.3 RESULTS

The receiver performance exceeds all Demonstration requirements and meets the key HDIS requirements. Performance was determined experimentally, by analysis, and by simulation, with close agreement.

Extensive experimental tests and simulations were conducted with dynamics consisting of circular motion with acceleration of 50 g and jerk of 40 g/s. Pseudorange accuracy is 0.4 m rms at the nominal SNR of 38 dB-Hz, 0.6 m rms at 34 dB-Hz, and 1.2 m rms at the HDIS threshold specification SNR of 31 dB-Hz. This is better than the Plan specification of 2 m rms at 34 dB-Hz, and is close to the HDIS low dynamics specification of 1 m at 31 dB-Hz. Loss of lock threshold is 28 dB-Hz at these dynamics, which is 3 dB better than the HDIS low dynamic coherent tracking specification. Accuracy versus SNR is shown in Figure 1-1 for the stated dynamics. Experimental data, simulation results and theoretical performance are shown to agree within approximately 1 dB in SNR at SNRs

below 40 dB-Hz. Instrumentation accuracy of 0.15 m rms dominates at higher SNRs, but meets the HDIS specification of 0.15 m.

The receiver operates accurately at accelerations up to 150 g and jerk up to 150 g/s. At 100 g and 80 g/s, performance versus SNR is within 1 dB of performance at 50 g and 40 g/s. Accuracy is maintained with instantaneous acceleration steps of up to 150 g. Peak transient errors are less than 0.004 m per g of step acceleration, with transient times of approximately 0.14 s.

Total position accuracy was determined for the receiver operating with the GPS Space and Control Segments and accounting for propagation effects. While under dynamics exceeding 50 g and 50 g/s, the receiver accuracy is essentially the same as the HDIS static accuracy specification. This is true whether the receiver is measuring either absolute or relative position.

Elimination of carrier phase tracking is the key concept which enables the receiver to operate at extremely high dynamics. Therefore, receiver velocity accuracy is not as good as the HDIS specifications, because the most accurate velocity estimation depends on tracking carrier phase. Software modifications could be made to enable carrier phase tracking when under lower dynamics, thus meeting the HDIS velocity specifications. Current range rate accuracy is 0.8 m/s at 31 dB-Hz SNR, plus 0.2 m/s for each 1 g/s of jerk.

The receiver can meet all other key performance specifications of the HDIS, with further development. These include acquisition or time to first fix, reacquisition, parameter update rate, data accuracy, data bit synchronization and data detection. Improvements can also be made in SNR threshold. Fast acquisition for transdigitizer applications can be incorporated without changing the basic receiver architecture.

## 1.4 CONCLUSIONS AND RECOMMENDATIONS

The receiver can meet all performance requirements now envisioned for range instrumentation of high dynamic aircraft, missiles and drones. Implementation in a volume of 100 in.$^3$ or less is feasible. The receiver can be implemented to operate either on the vehicles or as a transdigitizer or translator receiver.

It is recommended that a fully functional, rack mounted receiver be developed and tested. Preliminary investigations indicate that the HDIS now being procured could be modified to include the high dynamic tracking concepts. This approach appears to be cost effective and to maximize commonality of range equipment. It is recommended that JPL develop a fully functional high dynamic receiver, using a government furnished HDIS.
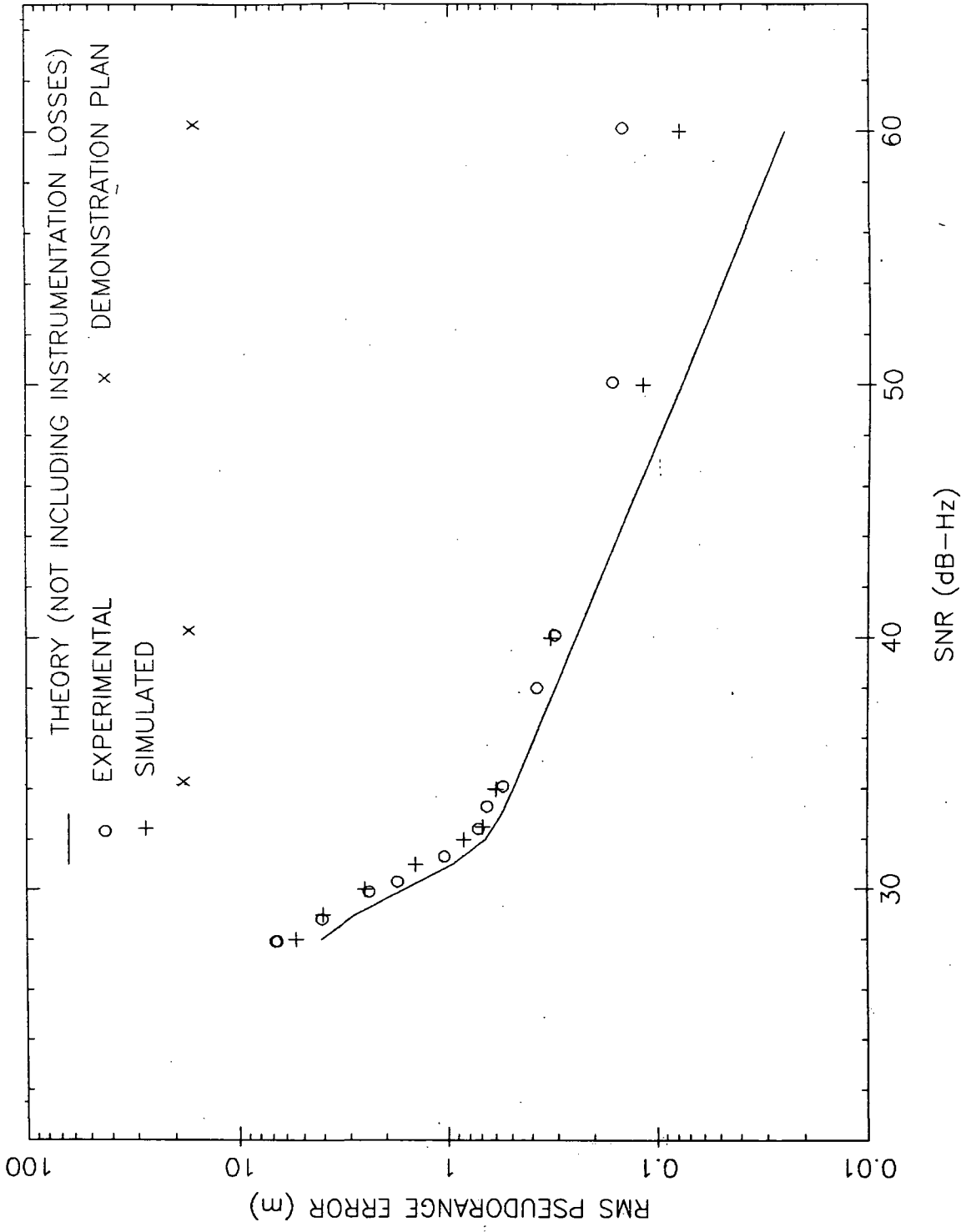
Figure 1-1. Pseudorange Error Versus SNR for 50 g, 40 g/s, Circular Motion

# CHAPTER 2

## PURPOSE AND SCOPE

### 2.1 PURPOSE

The purposes of this final report are to conclusively show that the receiver concept examined in GPS High Dynamic Receiver Validation Demonstration can meet the key requirements for high dynamic range instrumentation receivers, and to document the work for technology transfer. This report fulfills deliverable item g of Task Order RE-182, Amendment 320, "GPS Receiver for High Dynamic and Low Volume Applications" [3], sponsored by the U.S. Air Force Systems Command, Armament Division.

### 2.2 SCOPE

This report fully documents the objectives, concepts, equipment, tests, results and conclusions of the GPS High Dynamic Receiver Validation Demonstration. It describes the receiver, the instrumentation, the demonstration, and the receiver performance, and how the receiver performance was determined analytically, by simulation, and experimentally. A miniaturized design of a complete receiver is presented and its size, volume and power estimated.

Design trades affecting performance, comparisons to other types of receivers, and methods for improving performance are included. The report completely describes the receiver functionally and mathematically, but schematics and software listings are not included.

# CHAPTER 3

## INTRODUCTION

### 3.1 BACKGROUND AND RATIONALE FOR DEMONSTRATION

The U.S. Air Force Armament Division, GPS Range Applications Joint Program Office (RAJPO), is responsible for development of GPS receivers to satisfy Department of Defense range instrumentation requirements.

A new receiver development program has been initiated for range applications, because range requirements are significantly different from those satisfied by the family of receivers under development by the GPS Joint Program Office (JPO). Early in the program, RAJPO concluded that all requirements for manned aircraft and for ground applications, but not for high dynamic missiles were within the current capability of industry. Therefore, the main RAJPO activity has been to specify and procure the aircraft and manpack receivers. In May, 1985, Interstate Electronics Corporation was selected to develop these receivers.

In late 1982, the Jet Propulsion Laboratory presented to RAJPO a concept for a receiver to satisfy the requirements for high dynamic missiles, without requiring inertial aiding. This concept was insufficiently developed and therefore too risky to include in the above procurement. Development and demonstration were required. This Validation Demonstration task began in May 1983 to establish the capability of the JPL-proposed receiver to meet the high dynamic requirements.

### 3.2 DEMONSTRATION DESCRIPTION

The primary physical elements of the Demonstration are the receiver, the Test Instrumentation Subsystem, and the Data Evaluation Subsystem, shown in block diagram form in Figure 3-1. Other key elements of the task are the Demonstration Plan [2], analyses and simulations of the receiver performance, a minimization study, and this Final Report.

### 3.2.1 Hardware Configuration

The hardware elements of the demonstration were built in breadboard form, so as to demonstrate the concept at minimum cost. A photograph of the Receiver and the Test Instrumentation Subsystem is shown in Figure 3-2.

### 3.2.2 Specified Objectives And Accomplishments

Seven specific objectives were set forth in the Demonstration Plan, as key steps validating the receiver concept. These objectives are repeated here, with brief statements as to their accomplishments.

The first objective was to provide a Demonstration System operating at JPL consisting of a receiver breadboard capable of tracking a simulated signal from one satellite, and instrumentation for generation of test signals, for control and display, and for data recording for post-test evaluation. This was accomplished by designing and building a single channel receiver breadboard, a Test Instrumentation Subsystem with a signal simulator, and a Data Evaluation Subsystem with analysis software, all of which comprised a Demonstration System sufficient to validate the receiver concept.

Second was to determine the pseudorange and range rate accuracy of the system with low receiver dynamics, and to demonstrate that this accuracy is consistent with GPS system specifications for receivers. This was accomplished by a series of low velocity tests. At an SNR of 34 dB-Hz, the rms pseudorange and range rate errors were 0.6 m rms and 0.4 m/s rms. The pseudorange error is very small compared to the overall GPS system accuracy of approximately 15 m.

Third was to demonstrate the ability to track at velocities up to 3300 m/s and at accelerations up to 50 g with pseudorange error due to dynamics of less than 15 m, and to determine the accuracy under various dynamics. This was accomplished by high dynamic tests at constant velocity, with step acceleration, and with simulated circular motion trajectories. The rms pseudorange errors due to dynamics were under 0.3 m under all conditions including velocities up to 10,000 m/s, acceleration up to 150 g, and jerk up to 157 g/s.

Fourth was to demonstrate a breadboard design which is capable of miniaturized implementation using technology that is within the state-of-the-art. The receiver is inherently suitable for miniaturization because the design is mostly digital, and thus implementable via VLSI and dense packaging. The RF circuitry in the breadboard consists of a single mixing to baseband with no intermediate frequency (IF). Final implementation would be much simpler than traditional GPS receivers, even if one IF stage is added in final mechanization.

Fifth was to perform a design of an integrated circuit capable of performing the key special purpose high speed signal processing functions within the receiver. Fabrication and testing of this circuit were specifically stated to be outside the scope of the demonstration. The

chip chosen to study was the 11-lag correlator. The breadboard correlator was built using an architecture which enabled the basic operations to be performed at 10.23 MHz, rather than the 20.46 MHz that would have been necessary in a more straightforward design. This speed and the complexity of the circuitry are both well within the state-of-the art for CMOS VLSI. Further design was not deemed to be appropriate at this time.

Sixth was to perform a preliminary hardware design of a complete receiver using the demonstrated concepts, to estimate the size, weight and power consumption of a miniaturized implementation of this design, and to determine the feasibility of meeting the key missile application volume requirement of approximately 100 in.$^3$. This miniaturization study was performed. The volume goal is achievable, as detailed in Chapter 7.

Seventh was to provide a final report covering all work in sufficient detail and in appropriate format for transfer of the demonstrated techniques and technology. This document fulfills this objective.

Additional objectives were informally added as the Demonstration progressed. These included more complete characterization of the receiver performance by analysis, simulation and testing, enhancement of the receiver performance especially in the area of threshold signal-to-noise ratio, and comparison of the receiver to other possible implementations and to the procurement specification for the High Dynamic Instrumentation Set [1]. These goals were accomplished, and the comparisons given in Chapter 5 show that the receiver concept can meet all HDIS specifications, while also having the ability to operate with dynamics 10 times more severe than specified for the HDIS, which uses inertial aiding.
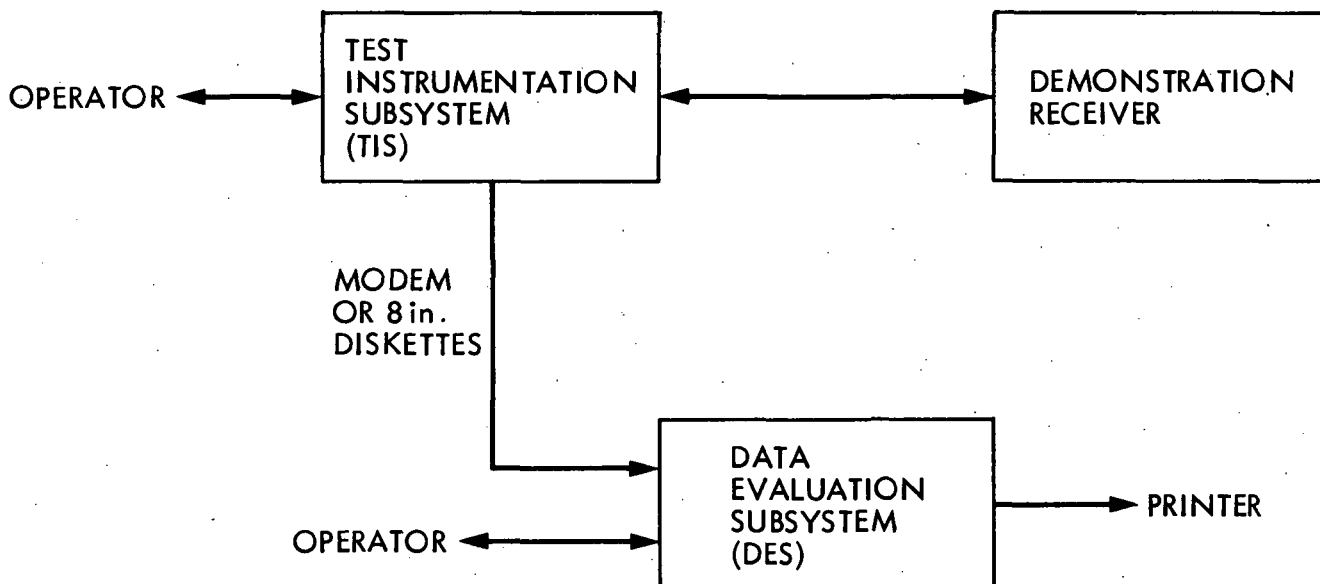
Figure 3-1.    Demonstration System Block Diagram
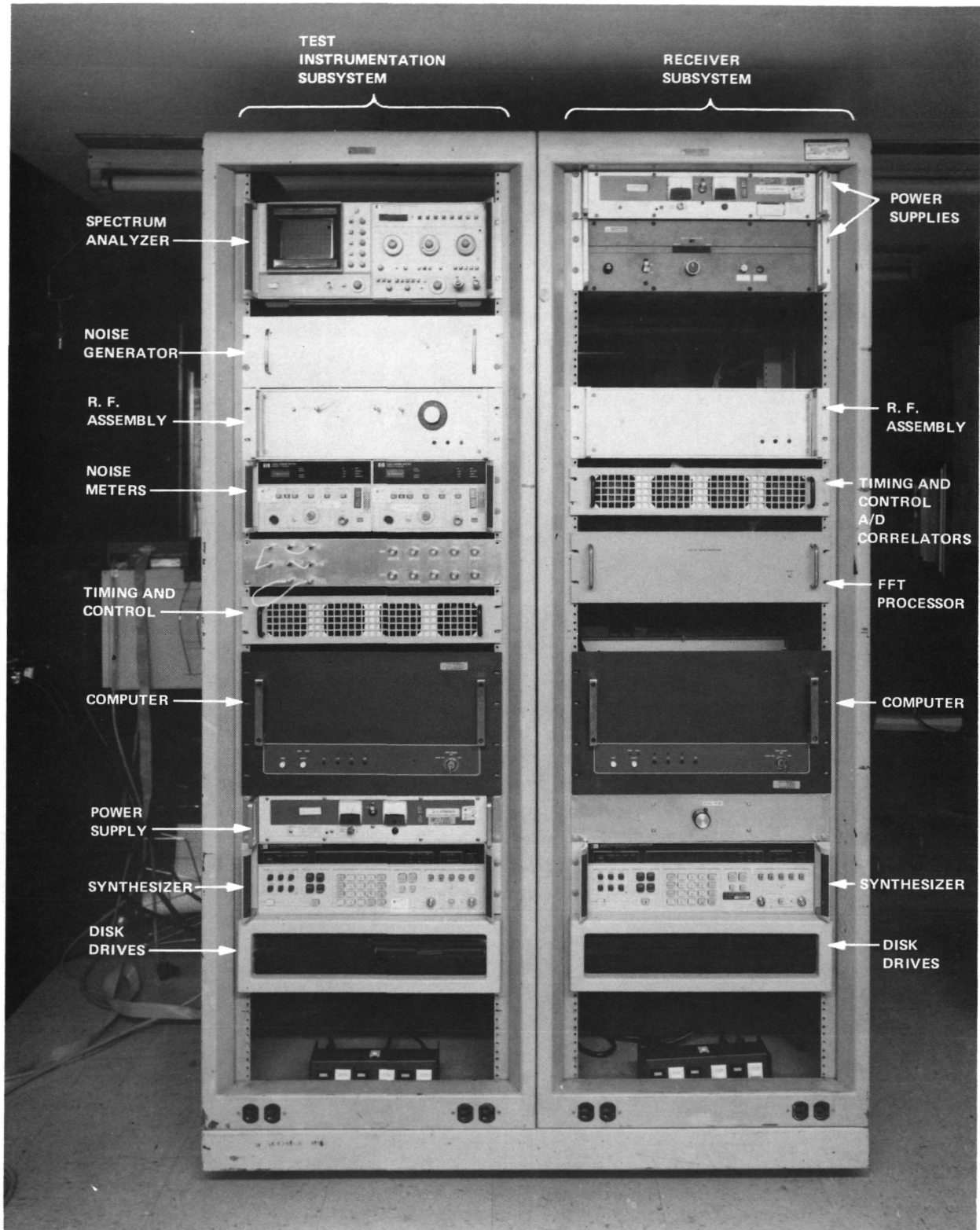
Figure 3-2.    Demonstration System Photograph

CHAPTER 4


SYSTEM DESCRIPTION



     This chapter describes the Demonstration System in detail. Section
4.1 outlines the functional requirements as given by the Demonstration Plan
[2].   Section 4.2 briefly explains the receiver principles.   The elements
of the Demonstration system, the Test Instrumentation Subsystem (TIS), the
Demonstration Receiver,  and the Data Evaluation Subsystem (DES) are
described in Section 4.3. Finally, Section 4.4 highlights system
integration and testing.


4.1 FUNCTIONAL REQUIREMENTS

The functional requirements of the Validation Demonstration are based on
those given in the Demonstration Plan. Appendix A lists the original
requirements, and modifications, in detail. The following is a summary of
key requirements.

     The Demonstration was required to be built, installed and tested at
JPL. It consists of the Demonstration Receiver, a Test Instrumentation
Subsystem (TIS) and a Data Evaluation Subsystem (DES). Real time displays
and post-processing of recorded data are sufficient for the evaluation of
system performance.

     The system demonstrates the capability of the receiver to track a
simulated GPS L1 signal under high receiver dynamics and at low SNR.
Receiver functions not demonstrated include the low noise front end,
acquisition, data bit synchronization, data detection, tracking of actual
satellites, tracking of the C/A code, tracking of the L2 carrier, tracking
of multiple satellites, solution for position and velocity in three

dimensions, and external interfaces. These functions are not necessary to validate the new high dynamic tracking concept.

Performance requirements, all of which were exceeded, are summarized. The pseudorange error requirement was less than 2.0 m rms when under constant velocity of less than 3300 m/s relative to the satellite, with receiver P-code SNR of 34 dB-Hz at the input to the receiver. (This SNR was chosen because it is exceeded with minimum satellite signal levels, an antenna gain of -6 dB and total system noise figure of 3.5 dB.) The required maximum pseudorange lag error due to receiver dynamics is less than 15 m with pseudorange profile corresponding to radial acceleration of 50 g peak, and under step acceleration of 50 g.

The receiver is tested under various conditions of dynamics and signal to noise ratio which might be encountered by a receiver on a high dynamic vehicle. Constant velocity, step acceleration and circular motion are simulated at high, medium and low SNR. High SNR conditions test instrumentation accuracy and dynamic limits. Medium SNR tests normal operating conditions. Low SNR evaluates the performance limitations under adverse conditions.

## 4.2 RECEIVER PRINCIPLES

The main new concept demonstrated here is the method of estimating the pseudorange and range rate of the receiver with respect to the satellites. This is accomplished in a quasi-open loop, approximately maximum likelihood (AMLE) manner, rather than by tracking with phase and delay locked loops, as in other receivers. This approach enhances the ability to maintain tracking under high receiver dynamics, and naturally leads to an all digital implementation suitable for miniaturization. A second feature of the receiver is the use of a high update rate tracking filter, which is necessary for high dynamic tracking. This type of filter is within the capability of current microprocessors.

Appendix B gives a detailed description and analysis of the AMLE concept. Basically, the receiver estimates pseudorange by using a bank of 11 correlators with delay or lag spacing of one-half a P-code chip (approximately 14.7 m). The range rate estimate, which is related to the estimate of Doppler shift, is derived from a bank of 50 Hz wide filters generated by a FFT of the cross correlation between the received baseband signal and a locally generated P-code. Frequency and range feedback are provided by the tracking filter to center the range of the AMLE at the predicted frequency and delay, but the accuracy of this feedback does not affect estimation error as long as the feedback is within the correlator and FFT range. Thus the estimation technique is termed quasi-open loop.

## 4.3 SYSTEM DESIGN

### 4.3.1 System

The Demonstration System consists of three functional blocks. The Test Instrumentation Subsystem (TIS) generates a test signal with the simulated dynamics and SNR. The Demonstration Receiver tracks this signal and reports results back to the TIS for recording and display. The Data Evaluation Subsystem (DES) post-processes the recorded data.

The system configuration is shown in Figure 3-1, while the main interfaces are shown in Figure 4-1. This section presents the assembly level designs of the subsystems, designed to meet the above requirements.

### 4.3.2 Demonstration Receiver

A block diagram of the Demonstration Receiver is shown in Figure 4-2. The principal assemblies are: front end assembly, analog to digital converters, correlation assembly, signal processing assembly, code generator and timing assembly. A functional block diagram of the tracking processor, i.e., the digital portion of the Demonstration Receiver is shown in Figure 4-3.

#### 4.3.2.1 Front End Assembly

The front end assembly accepts the simulated satellite signal and noise from the TIS, and a fixed 20.46 MHz reference frequency from a synthesizer. It multiplies the 20.46 MHz signal by 77 to generate a nominal L1 reference. It amplifies the input signal and demodulates it to baseband in two phase-quadrature channels, using that L1 reference signal. It then low pass filters the baseband signals, amplifies them, and outputs these analog signals to the analog to digital converter assembly. Note that the front end amplifier is not the low noise amplifier that is anticipated for a final receiver, as this is not necessary to demonstrate the high dynamic capability. The front end assembly is presented in Figure 4-4.

#### 4.3.2.2 Analog To Digital Converter Assembly

The analog to digital converters accept baseband analog signals from the front end assembly, and a clock signal from the timing assembly. They perform 3-bit analog-to-digital conversion and output the digital baseband to the correlation assembly. The sampling rate is twice the nominal P code chip rate. The implementation uses two evaluation boards with TRW TDC1029 converters. Although these are 6-bit converters, only 3 bits are used so that the effective resolution is 3 bits.

#### 4.3.2.3 Correlation Assembly

The correlation assembly accepts the digital baseband signal from the analog to digital converters, clock and timing signals from the timing assembly, a code signal from the code generator, and a digital frequency control signal from the signal processing assembly. Each data bit time is

divided into 32 subintervals called correlation intervals. The correlation assembly performs its processing functions over each correlation interval and outputs correlation data for each interval to the signal processing assembly. A complex signal is formed at the frequency specified by the frequency control signal. The baseband input signal, considered a complex number, is multiplied by this frequency reference signal to remove the predicted doppler frequency. The amplitude quantization of the frequency reference is 3-level and of the baseband signal is 3-bit. The product signal is cross-correlated with 11 lags of the code signal input. At the end of each correlation interval, the correlation values are output to the signal processing assembly.

Functionally, the correlators need to operate at the sampling frequency of 20.46 MHz. The implementation accomplishes this with logic clocked at the 10.23 MHz rate of the reference code. The sampled data are demultiplexed into two paths, denoted "even" and "odd", and separate correlations are performed at 10.23 MHz. Finally the results are combined in a particular way to reproduce the 11 complex correlation values. This design is better suited to low power CMOS VLSI implementation.

### 4.3.2.4 Signal Processing Assembly

The signal processing assembly accepts correlation data from the correlation assembly, clock and timing signals from the timing assembly, and initialization data from the TIS. It performs several major functions: acquisition of pseudorange and range rate, synchronization to the bit times of the data modulation, Fast Fourier Transformation (FFT) of the correlation data, formation of raw estimates of pseudorange and range rate from the FFT outputs, smoothing of the raw estimates in a tracking filter, control of the code generator, and output of frequency values to the correlator assembly. The signal processing assembly outputs smoothed values of estimated pseudorange and range rate to the TIS, frequency data based on the smoothed range rate to the correlation assembly, and code phase control data based on the smoothed pseudorange to the code generator.

Synchronization to the data bit times is accomplished by initialization from the TIS. Code Acquisition is accomplished by searching over 1023 chips of the code. In an independent receiver, these functions would be accomplished by detecting the received energy over different candidate time intervals and for different pseudoranges and range rates, using the same basic detection algorithms as for parameter estimation described below. The demonstration receiver does not implement these functions because they are not required to validate the dynamic and noise performance of the receiver concept. It is noted, however, that acquisition and bit synchronization affects only software in the signal processing assembly, and not the hardware.

The correlation data are buffered over the 32 correlation intervals corresponding to one data bit time. Double buffering is done so that one buffer can be loaded while previous data are processed. The correlations are then Fourier transformed, one lag at a time, using a software-implemented FFT. The detected energy is calculated for each FFT frequency

and for each correlation lag, and the maximum value and its lag and frequency are noted. An interpolation algorithm is then used to estimate the raw values of pseudorange and range rate for that bit time from the maximum value of detected energy and from values in adjacent frequencies and lags.

The tracking filter operates on the raw estimates to form smoothed estimates of pseudorange and range rate. The operator can select a second- or third-order filter, with various parameters.

The tracking filter outputs are used to predict the pseudorange and range rate for the next measurement time, which is three data bit times ahead of the last data used. The predicted range rate is used to control the frequency input to the correlator so that the residual frequency (after cross correlation) is within the range of the FFT. The predicted pseudorange is used to control the code phase output from the code generator so that the residual delay is within the range of the correlator.

The signal processing assembly functions are performed by two processors. A Texas Instruments TMS32010 inputs the correlation values, performs the FFTs, and detects the maximum energy. An Intel 8086 with an 8087 floating point coprocessor computes the raw estimates, updates the tracking filter, and controls the hardware. The correlation data is stored in a double buffer over a data bit time, so while the correlator fills the first buffer, one correlation subinterval at a time, the TMS32010 performs FFTs on data from the second buffer, one code lag at a time. The results of the TMS32010 computations are transmitted to the 8086 through a First In First Out (FIFO) buffer.

4.3.2.5 Code Generator Assembly

The code generator assembly accepts clock and timing inputs from the timing assembly and code phase control inputs from the signal processing assembly. It generates a pseudorandom code clocked at the nominal P code chip rate of 10.23 MHz. The code is a short-period, simulated P code, for implementation simplicity. The code phase is controlled by inputs from the signal processing assembly. Although the predicted values of pseudorange are inherently updated only once per data bit time, the code phase is changed during a data bit time in order to compensate for range rate. Updating of the code phase once each correlation time is sufficient. This is accomplished by using the code phase and its rate of change once each data bit time.

4.3.2.6 Timing Assembly

The timing assembly accepts a 20.46 MHz clock from a local oscillator (frequency synthesizer). This is multiplied by 77 to generate the nominal L1 frequency, and the resulting signal is output to the front end. The timing assembly also generates buffered clock outputs at the sampling frequency and at the P code frequency, and outputs them to the other assemblies as required. It generates and outputs all required timing

signals, including correlation interval timing. It generates and outputs reference epoch signals at 1 pps, and resets all timing signals upon command. It also generates a reset signal and a frequency update timing signal for the TIS.

### 4.3.3 Test Instrumentation Subsystem

The TIS generates test signals and inputs them to the receiver, initializes the receiver and supplies it with a frequency reference, and displays and records the test signal parameters and the results of the receiver measurements. A block diagram is shown in Figure 4-5. The principal assemblies are the TIS computer, the test signal frequency synthesis assembly, the code generator assembly, the random noise generator, the signal combiner assembly and the signal to noise ratio instrumentation.

### 4.3.3.1 TIS Computer

The TIS computer is a microprocessor based computer with keyboard, floppy discs, printer, displays and parallel input and output ports. To control the test signal, it accepts control inputs via the keyboard, and timing inputs from the receiver timing assembly. It controls both the frequency synthesis and code generator assemblies. To control the receiver, it accepts initial values of pseudorange and range rate, and initializes the receiver via a parallel port. Tracking results from the receiver are accepted via a parallel port, recorded on floppy discs, and presented on alphanumeric and graphic displays.

### 4.3.3.2 Test Signal Frequency Synthesis Assembly

The test signal frequency synthesis assembly accepts frequency control inputs from the TIS computer, timing information and reset signal from the receiver timing assembly, and a frequency reference input. It switches frequency phase continuously upon command and under timing control, generates phase coherent P code clock and L1 frequency signals, and outputs these signals to the code generator assembly and the signal combiner. Control and accuracy of these signals is such that the pseudorange simulated is known to within 0.2 m at all times when a test is in progress. The frequency update rate is four per data bit time, so as to simulate changing doppler frequency due to acceleration during a bit time.

Figure 4-6 illustrates the TIS frequency synthesis assembly. The input signals are a fixed 19 MHz and a programmed 1.3 MHz. These are mixed and divided by 14 to improve phase stability by a factor of 14. The resulting signal, at approximately 1.046 MHz (programmed), is mixed against the fixed 19 MHz to obtain a phase stable, programmed, 20.46 MHz. This signal is used as the P code times-2 clock, and is multiplied by 77 to obtain the phase coherent, programmed, L1 carrier signal.

### 4.3.3.3 Code Generator Assembly

The code generator assembly accepts the P code clock from the frequency synthesis assembly, and control signals from the computer. It generates a phase controlled, simulated P code and a simulated 50 Hz data pattern, sums these two signals modulo-2, and outputs this data-modulated P code signal to the signal combiner assembly. The assembly is similar to the receiver code generator assembly, except that the receiver code generator does not generate data modulation, but is required to change phase on command.

### 4.3.3.4 Random Noise Generator

The random noise generator generates bandpass random noise in the L1 band and outputs it to the signal combiner assembly. It consists of three stages of high gain L-band amplifiers, separated by bandpass filters. The noise generator is packaged in a separate chassis with its own power supplies, so as to eliminate cross-coupling of the signal into the high gain noise generator amplifiers.

### 4.3.3.5 Signal Combiner Assembly

The signal combiner assembly accepts the L1 carrier signal from the test signal frequency synthesis assembly, the data-modulated P code signal from the code generator, the L1-band random noise from the noise generator, and manual signal level controls. It biphase modulates the carrier with the data and code, sums the signal and noise, filters the summed signal and noise in a filter simulating the satellite transmitter passband, and outputs the filtered signal to the receiver. The filtered noise and the filtered signal are available to the SNR instrumentation.

### 4.3.3.6 SNR Instrumentation

The SNR Instrumentation measures the test generator signal level, noise level and SNR. The SNR for each test is computed using equation (4-1), with measurements made with the set-up shown in Figure 4-7.

$$\text{SNR (dB-Hz)} = P_S - P_N + 10 \log B_N + C - ATT \qquad (4\text{-}1)$$

where

$P_S$ = Signal power (dB)

$P_N$ = Noise power (dB)

$B_N$ = Equivalent noise bandwidth (Hz)

$C$ = Correction factor (dB)

$ATT$ = External attenuation (dB)

$P_S$ and $P_N$ are the signal and noise power as measured by the power meters. The signal is band limited by a 37 MHz filter that simulates the

filter used by the GPS transmitter. The noise is band limited by two 47 MHz filters, with a combined noise bandwidth of $B_N$. $B_N$ was evaluated by integrating the noise transfer function observed on a spectrum analyzer resulting in $B_N = 43$ MHz. The correction factor C includes all the mismatches between devices, cable losses, and unbalanced power dividers. It was evaluated by measuring separately the signal and noise powers at the output of the TIS, with a result of C = 6.0 dB. Note that if we assume perfect line matching, no cable losses, no splitter losses, and perfect attenuators, then C = 10 dB − 4 dB = 6 dB, agreeing with the measurement. The attenuators included in the ATT attenuator were individually calibrated and were within 0.2 dB of their nominal values.

The overall accuracy of SNR calibration is estimated to meet the functional requirement [2] of ± 1.0 dB.

## 4.3.4 Data Evaluation Subsystem

The data evaluation subsystem (DES) consists of operator controlled software on a VAX 11/780. Figure 4-8 shows that the operator controls the selection of a sequence of operations on a corresponding sequence of data types. As the figure depicts, the operator can select from several operations on each data type. The operator is notified if an illegal operation is encountered.

## 4.3.4.1 DES Data Types

In the first step of DES operation, the program reads the TIS outputs, reconstructs the simulated trajectory, and generates four basic data types for further processing. These four data types are described below.

Raw AMLE errors are defined as the differences between measurements at the output of the AMLE and simulated pseudorange, range rate and acceleration. Neither the measurements nor the simulated data are directly affected by the tracking filter. AMLE errors are dominated by random effects: simulated input noise, quantization and roundoff errors, and approximations inherent in the implementation.

Total tracking errors are defined as the differences between the measurements at the output of the tracking filter and the simulated pseudorange, range rate, and acceleration. Tracking errors include all receiver effects. At high SNR, tracking errors are dominated by the transient or steady state error of the tracking filter, and by instrumentation errors. Filtered noise errors are defined as the differences between the measurements at the output of the tracking filter and the simulated pseudorange, range rate, and acceleration, passed through an identical tracking filter. This removes all modelled dynamics effects. At low SNR, the filtered noise errors represent raw AMLE errors, smoothed by the tracking filter. At high SNR, the filtered noise errors are dominated by instrumentation errors.

Monitor data are a set of diagnostic data used mainly in the analysis of test failures. These include the peak power detected by the AMLE, the

4-8

location of the peak power, the feedback to the NCO and code generators, and any adjustments to the data bit syncronization pointer.

## 4.3.4.2 DES Processing

The DES performs summaries on the above defined data types. Often utilized summaries are:

1. Time summary. Time summary data consists of plots of the simulated pseudorange, range rate and acceleration, and of appropriate errors (raw noise, filtered noise, or total tracking errors) as a function of time. These plots are the primary tools in the diagnosis of test success or failure. Under operator control, the DES can overlay data corresponding to repeats of the same simulated inputs to emphasize transient errors.

2. Bin distribution. Bin distribution summaries describe the location of the AMLE maximum detected energy in range and frequency, as a function of time. These summaries provide a measure of how many range and frequency bins are used, as a function of dynamics. They also indicate when the maximum detected energy occurs in an incorrect or outlying bin, due to low SNR.

3. AMLE bias. These summaries measure the effect of the approximation formulas used for range and frequency interpolation. The summaries consist of plots of average pseudorange and range rate errors vs. simulated pseudorange and range rate where the simulated variables are modulo the corresponding bin size. The measurement biases are the differences between the average measurements and the simulated values, as a function of pseudorange and range rate (modulo bin size).

4. Statistical summary. Statistical summaries consist of the sample means and sample variances for specified errors. Statistics are computed for pseudorange, range rate, and acceleration.

5. FFT and Fourier analysis. Some of the error signals (e.g. the AMLE bias) are analyzed to determine the dominant Fourier coefficients. This is a way to characterize AMLE bias.

## 4.3.5  A Typical Test Sequence

A typical test consisted of four steps: first the operator commanded the TIS with the desired test parameters, then the test was executed and data stored, then the data was transferred to the VAX, and finally the performance evaluation was conducted by the DES.

The TIS set up was via an interactive menu.  The operator set the following parameters:

1.  Test identification: test name, operator, location.

2.  Trajectory type: constant velocity, circular motion, or
    acceleration. The operator also selected the velocity,
    acceleration and period that specified the trajectory.

3.  SNR parameters: measured signal and noise power, and the
    value of the fixed attenuator.

4.  Type of tracking filter and tracking filter parameters.

5.  Displays: control of graphic and alphanumeric real time
    displays.

6.  Miscellaneous parameters: type of AMLE interpolation
    formulas, ON/OFF control for AMLE feedback, method of code
    acquisition, etc.

Once the TIS was set up, relevant parameters were sent to the Demonstration
Receiver, the test was conducted and results were stored in the TIS memory.
Then the data were sent to the VAX either via modem or through 8 in.
diskettes that served as intermediate storage. Finally, the DES generated
the required performance evaluation summaries. All the data were saved on
9 track magnetic tapes for later processing.


## 4.4 SYSTEM INTEGRATION AND TESTING

### 4.4.1 Implementation

The demonstration system was built in two 19 in. instrumentation
racks, seen in Figure 3-2, clearly separating the TIS from the Receiver.
The TIS rack includes a computer assembly, a digital assembly, an RF
assembly, a noise generator, and SNR instrumentation. The computer, housed
in a MULTIBUS chassis, was based on an Intel 86/14 CPU board and included
memory, disk controller, real-time clock, and serial and parallel
interfaces. It also included a PROTEON PRO-80 synthesizer that under
computer control generated the frequencies simulating Doppler effects. The
digital assembly (mainly code generator and timing signals) was built on a
single prototyping board in a separate chassis. The RF assembly performed
the frequency synthesis and the signal combing functions. The noise
generator was built from a series of high gain amplifiers and bandpass
filters. The SNR instrumentation consisted of two power meters that
measured the signal and noise powers separately. The noise power was
nominally fixed, but varied with ambient temperature. The signal power was
controlled by fixed and variable attenuators on the front of the RF
assembly.

The main components in the Demonstration Receiver rack are the
MULTIBUS chassis, correlator assembly, FFT assembly, and RF assembly. The
computer was identical to that used in the TIS. The correlator assembly
consisted of four prototyping cards: two correlator cards, a code generator

and timing card, and two A/D modules. The correlator resided on two cards, separating the correlation of the even samples from that of the odd samples, allowing 10.23 MHz hardware to operate on a 20.46 signal. The FFT assembly used a TMS320 Evaluation Module to perform the needed FFTs, and included all the buffering to the correlators and to the FFT. The RF assembly included the L1 frequency generator, the I-Q mixers and the baseband analog circuitry.

During the testing two displays were utilized. The alphanumeric display shown in Figure 4-9 displayed the simulated data and the tracking error with and without filter smoothing. The graphic display shown in Figure 4-10 displayed simulated data and tracking data, under operator control. In the figure, the display shows the simulated velocity and the position tracking error for a circular motion test. This particular real time graphic display presents the simulated velocity and the position error. The simulated velocity scale is $\pm 1400$ m/s while the pseudorange error scale is $\pm 24$ m.

## 4.4.2  Test Plans And Procedures

A Test Plan and Procedures document was issued approximately three months prior to testing, as a JPL Interoffice Memorandum (IOM) [4]. It defines the required tests during the integration phase, i.e. tests that validate the subsystems, the subsystem interfaces and the complete system. It also identifies the Validation Demonstration tests in detail, including types of dynamics, SNR conditions, test logs, and supplemental tests.

## 4.4.3 Test Schedule

The originally planned Validation Demonstation tests started at the end of November 1984 and were concluded by the end of December 1984.

Additional tests were conducted through June 1985 to verify new interpolation formulas, to evaluate the outlier detection performance and the resulting SNR threshold, and to identify the performance improvement achieved by narrowing the AMLE window.

## 4.4.4  Equipment Performance

During the Validation Demonstration there were no equipment failures. The operation was automated so that a sequence of tests, each test with different dynamics but with the same SNR, could be conducted without operator intervention between tests. The size of the sequence was limited only by the disk storage on the VAX disk, typically permitting 100 minutes of testing.

## 4.4.5  Measured Spectra

During system integration, the frequency spectra of the generated signal and noise were recorded. Figure 4-11a shows the noise spectrum. The

passband is defined by two 3-pole, 47 MHz, Chebychev filters. Figure 4-11b shows the spectrum of the L1 signal, a $(sin(x)/x)^2$ type spectrum with nulls separated by 20.46 MHz. Figures 4-11c and 4-11d show the combined signal and noise at $C/N_0$ of 70 dB-Hz and 80 dB-Hz. (The nominal SNR for a 0 dB antenna is approximately 40 dB-Hz, at which level the spectrum appears to contain only noise.)
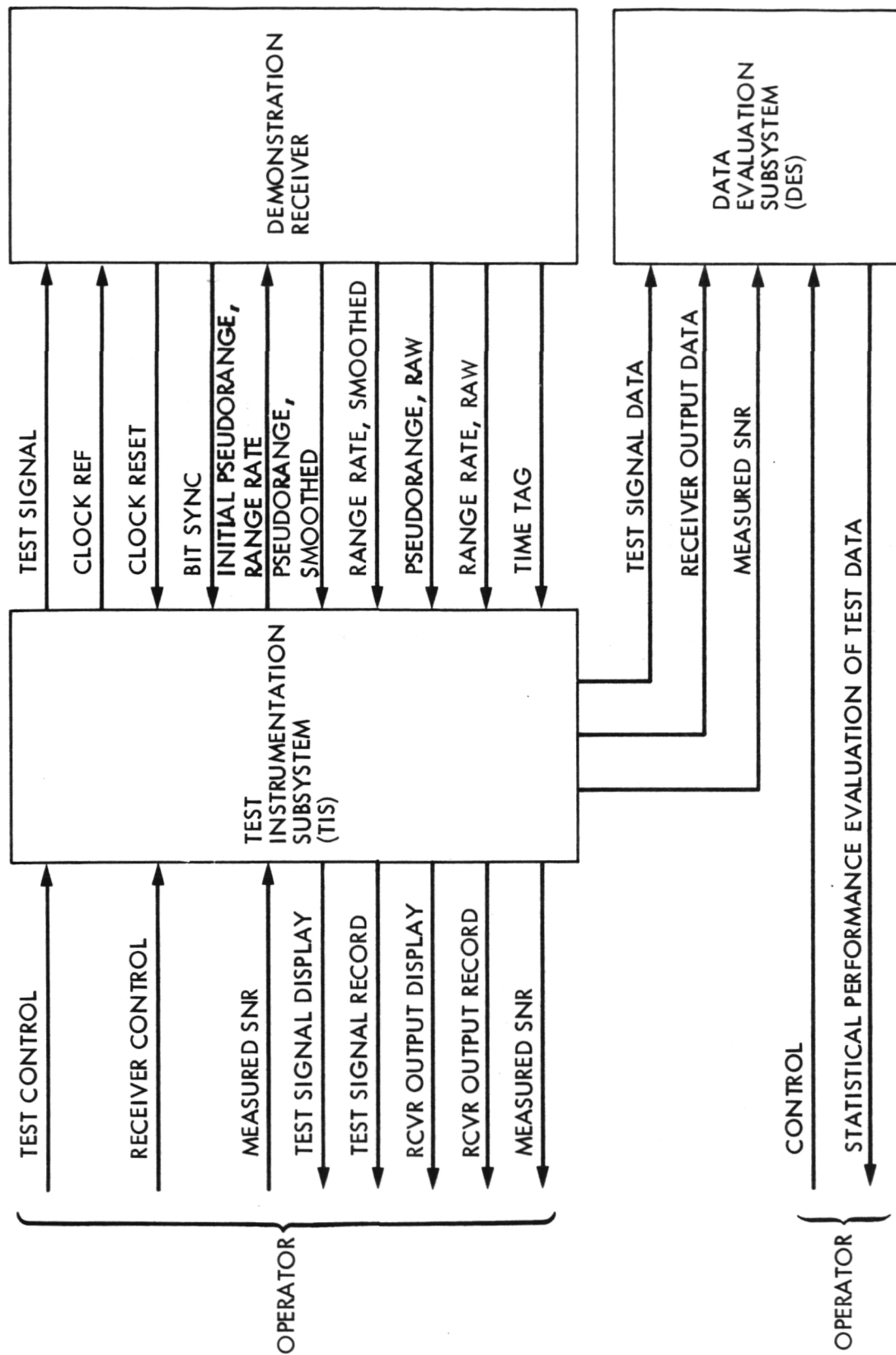
Figure 4-1.   Demonstration System Interface Diagram
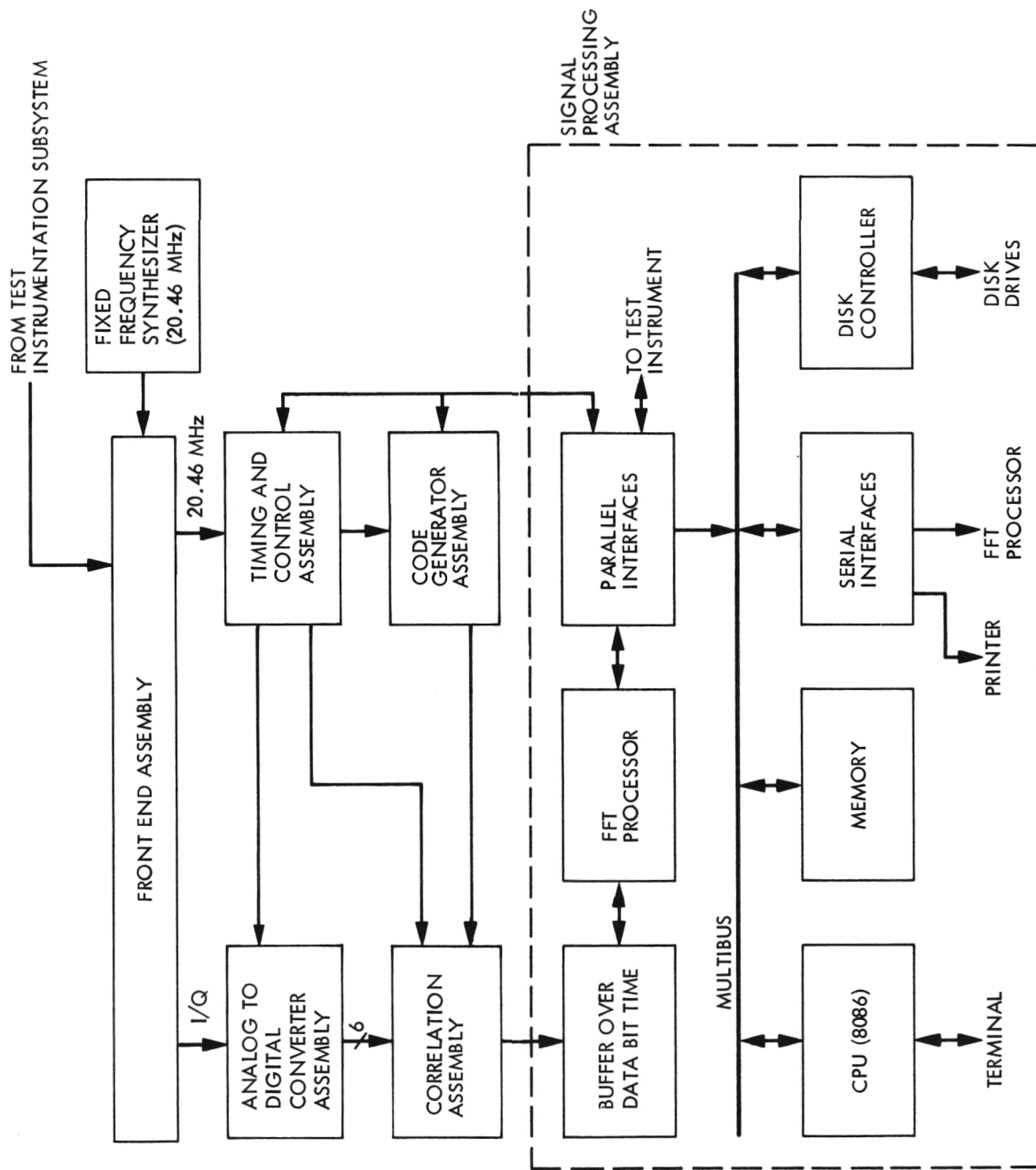
Figure 4-2. Demonstration Receiver Block Diagram
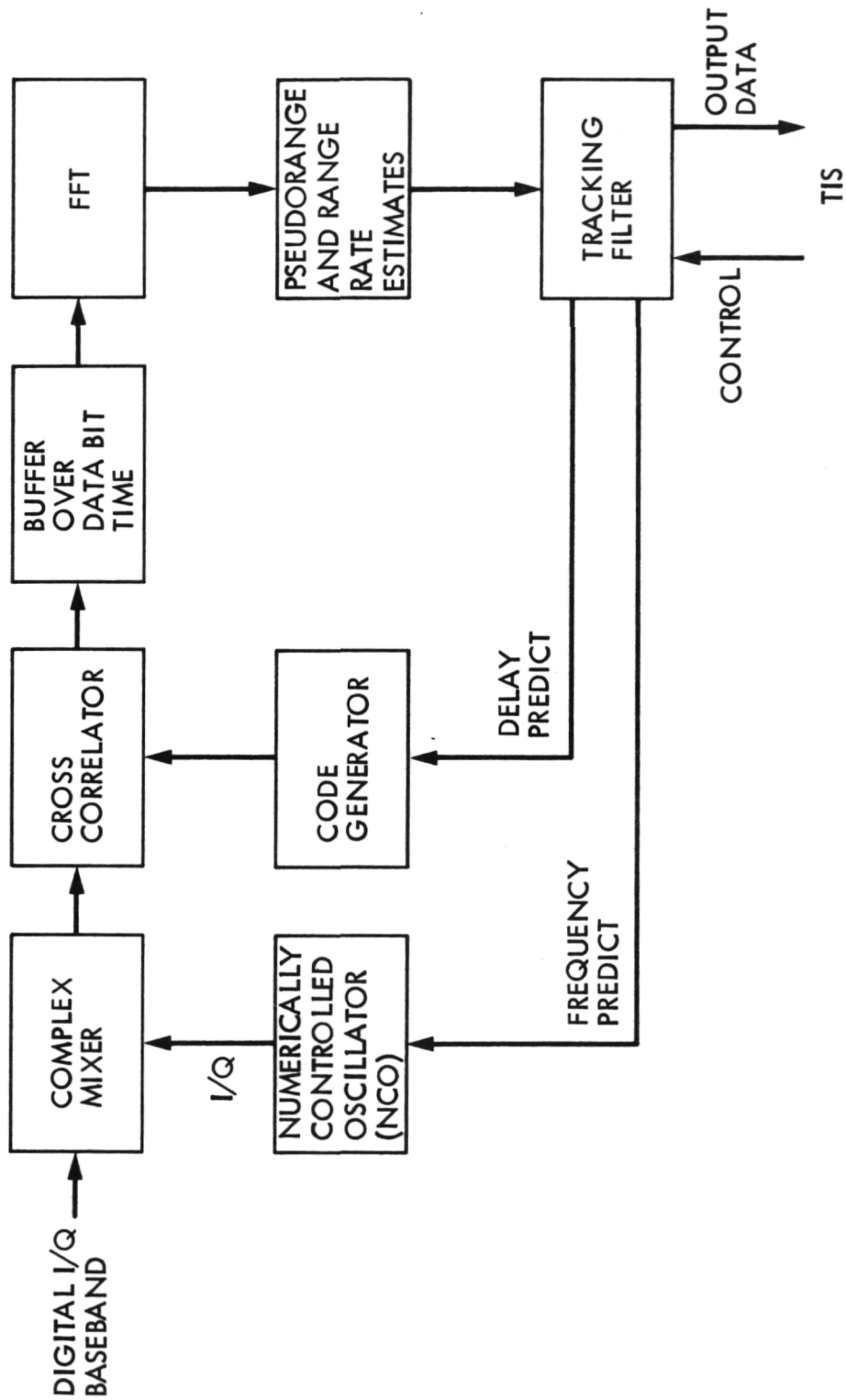
Figure 4-3. Tracking Processor Functional Block Diagram
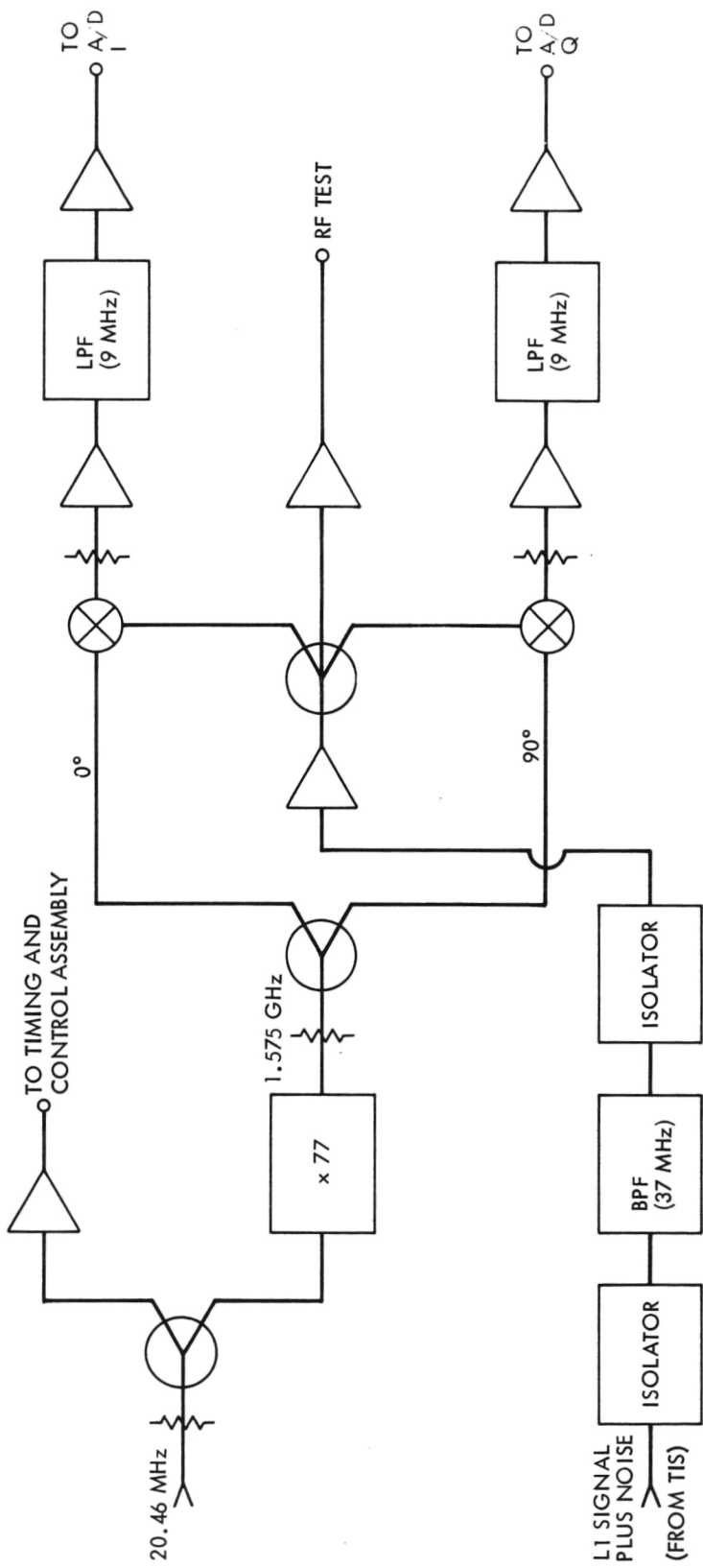
**Figure 4-4.** Demonstration Receiver RF Assembly
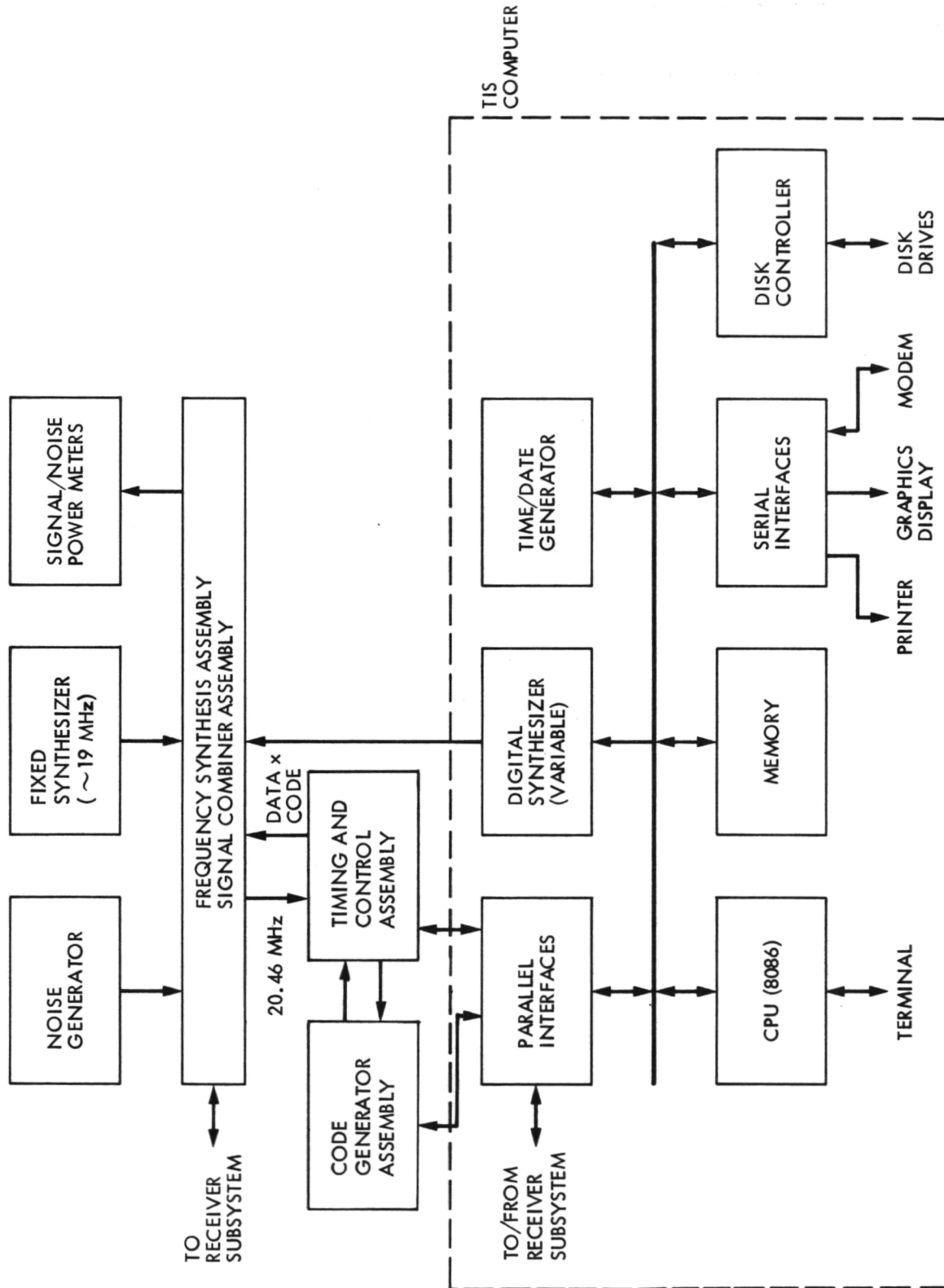
Figure 4-5. Test Instrumentation Subsystem Block Diagram

4-17
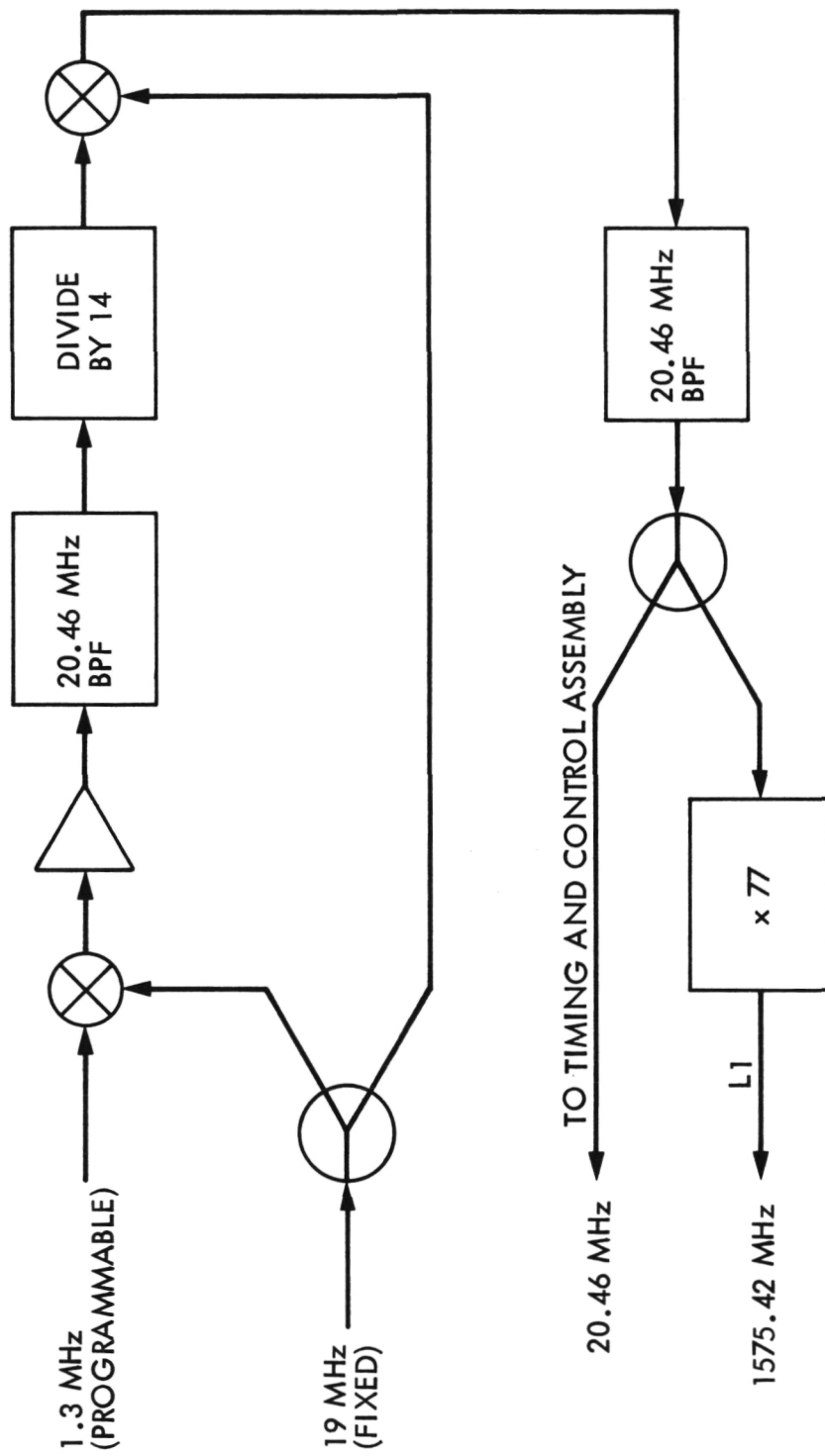
Figure 4-6. Test Instrumentation Subsystem – Frequency Synthesis Assembly
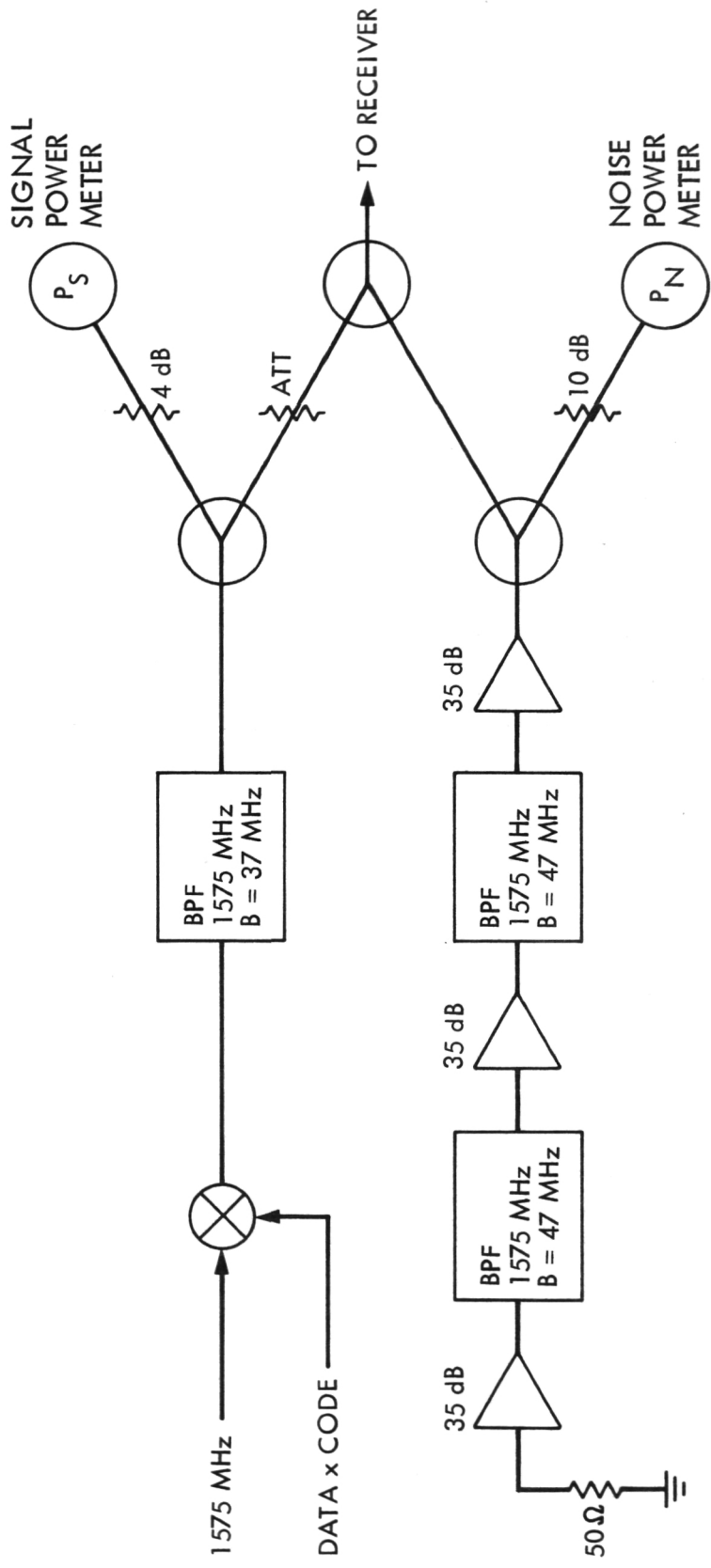
Figure 4-7.   TIS Signal Combiner and SNR Instrumentation

Figure 4-8.    DES Flow Chart

Simulated Position (meters) : 35114.64
Simulated Velocity (m/s) : .00
Simulated Acceleration (g) : .00

Smoothed Position Error (meters) :
Smoothed Velocity Error (m/s) :
Smoothed Acceleration Error (g) :

Raw Position Error (meters) :
Raw Velocity Error (m/s) :

Run-Time Operator Menu

^A  Issue code lock message
^B  End the test
^C  Increase DT (1 ms)
^D  Decrease DT (1 ms)

Date: 1/7/85
Time: 13:38:35
Kb= 39.08

Elapsed: 197/150

DUPE EDTL          FDX 9600
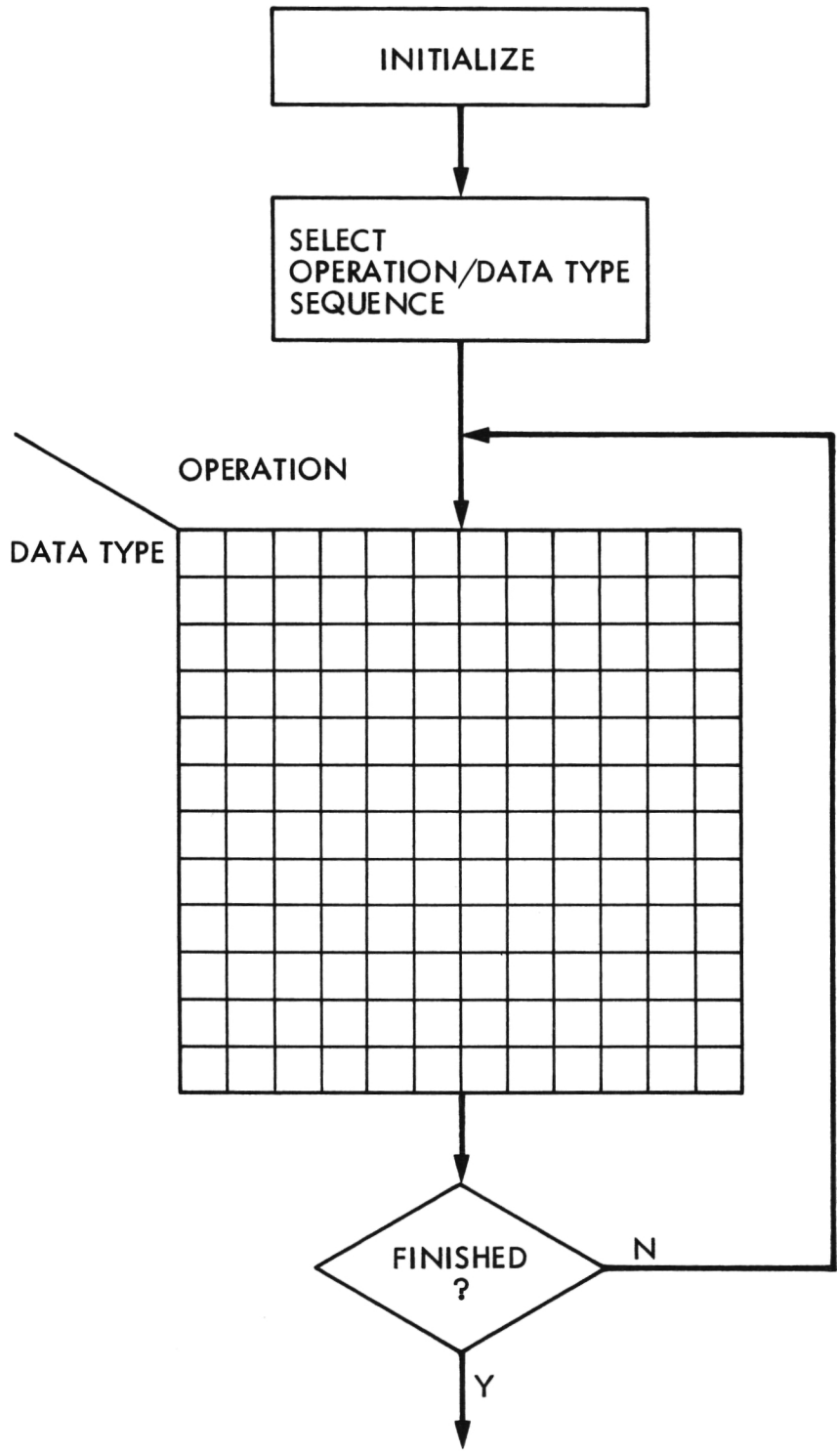
Figure 4-9.  The Alphanumeric Display.
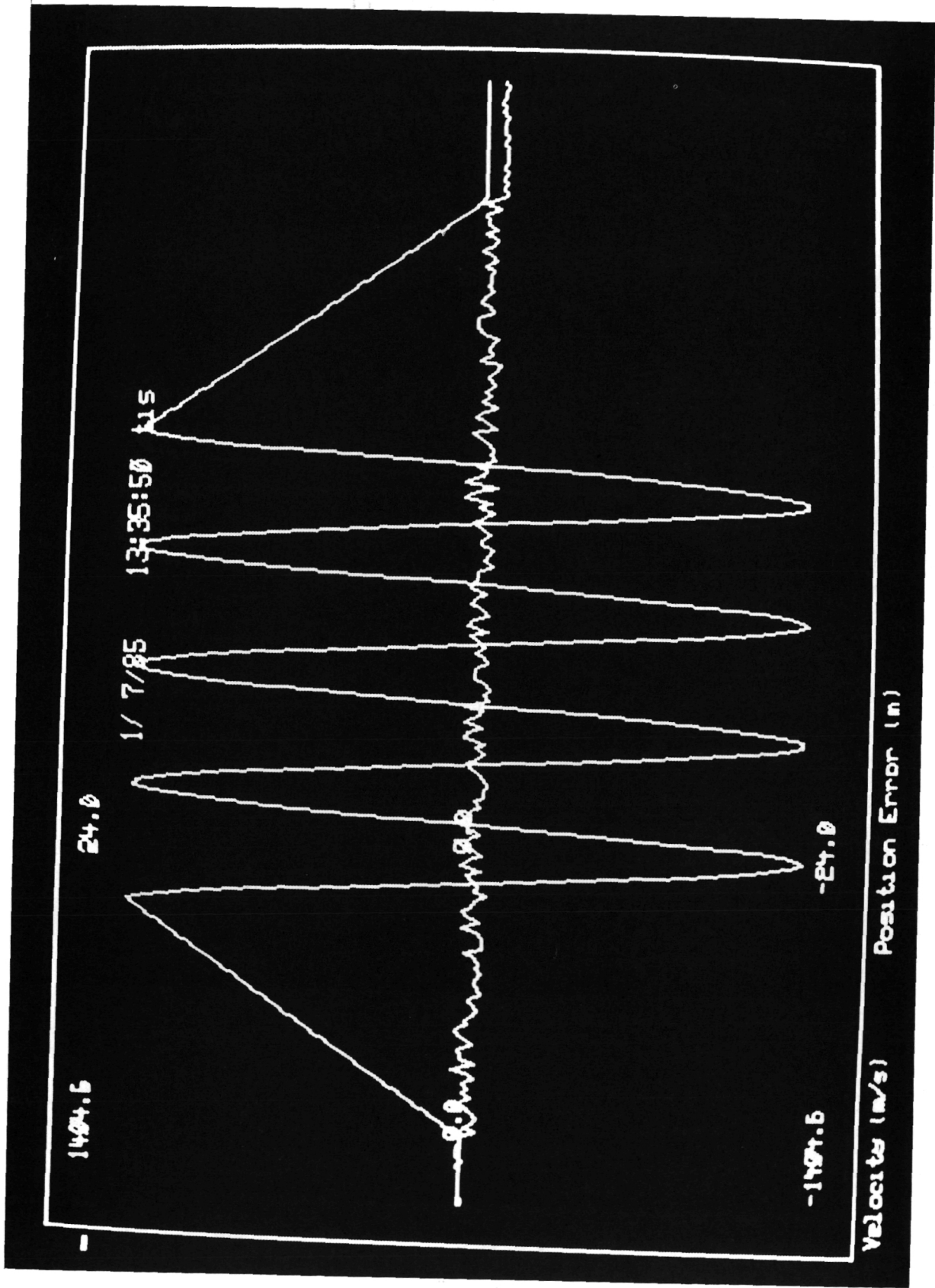
Figure 4-10. Real Time Graphic Display
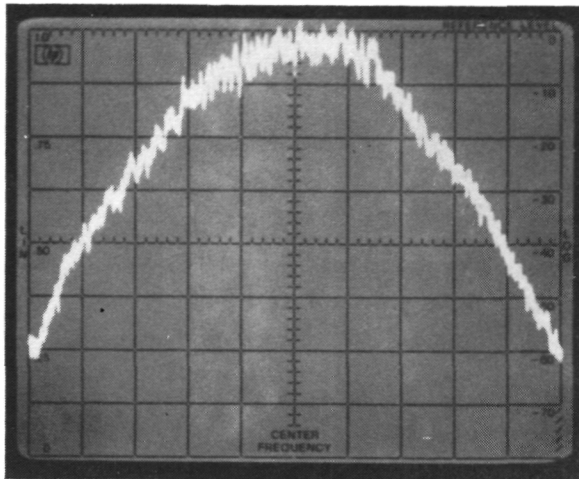
(a) SIMULATED NOISE
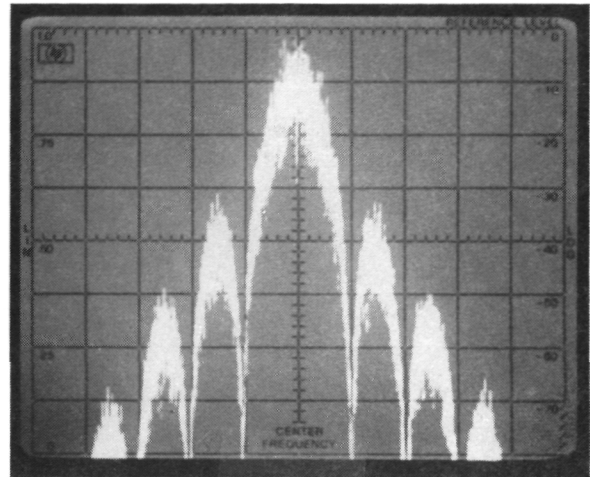
(b) SIMULATED SIGNAL
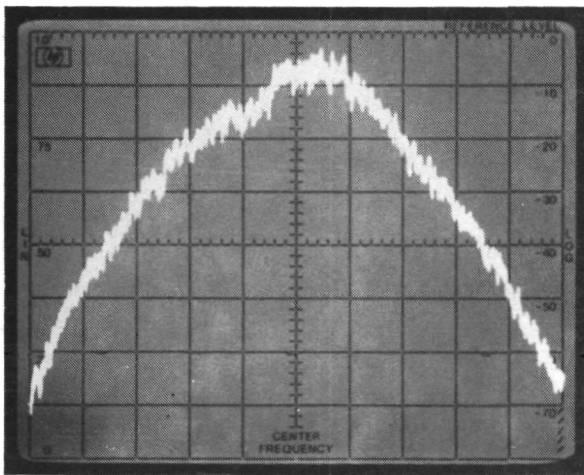
(c) SIGNAL + NOISE, $C/N_0$ = 70 dB-Hz
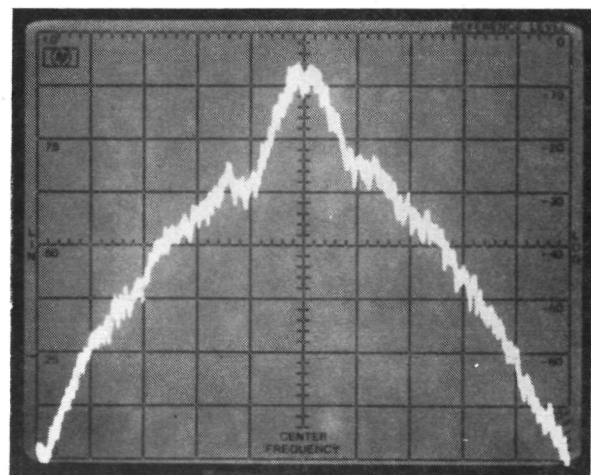
(d) SIGNAL + NOISE, $C/N_0$ = 80 dB-Hz

Figure 4-11. Measured Spectra 10 MHz/div, 5 dB/div

# CHAPTER 5

## PERFORMANCE AND ERROR BUDGET

This chapter presents performance predictions and error budgets for both the Demonstration Receiver and for a completely functional receiver which could be developed using the principles and concepts demonstrated. The critical and unique performance characteristics have been established by analysis, simulation, and demonstration. These include all pseudorange and range rate errors due to receiver noise, dynamics, and all effects characteristic of the receiver.

Errors which depend on GPS system effects outside of the receiver are included for the sake of completeness. Data for these effects are taken from the recent Armament Division procurement specification for high dynamic (HDIS) receivers [1]. Performance of the Demonstration Receiver is compared to the HDIS specification, and it is shown that all important and applicable specifications are met even at the much higher dynamics where the Demonstration Receiver operates. This is true even though the receiver was not designed to these requirements.

Performance characteristics important to a receiver implementation but outside of the scope of the Demonstration are discussed in 5.3. These characteristics were determined by analysis. The characteristics include acquisition, reacquisition, data bit synchronization, data bit detection, parameter update rates, and data accuracy.

Performance estimates are included for some modified receiver configurations which were not tested. These configurations include C/A code tracking, combined P and C/A code tracking, and phase locked tracking under conditions of SNR and dynamics which permit phase locking.

Performance predictions for these cases, made by analysis and simulation, are presented in 5.4.

## 5.1 SINGLE CHANNEL PERFORMANCE

This section presents the pseudorange and range rate measurement performance for a single channel receiver alone, excluding errors due to the GPS Space and Control Segments. Performance is characterized in terms of the input signal to noise ratio and dynamics, the receiver processing losses, the approximate maximum likelihood estimator (AMLE) performance, and the tracking filter performance. The performance was determined by measurement, analysis, and simulation.

Error budgets are presented for the processing losses in the receiver, and for pseudorange and range rate errors, under both static and dynamic conditions. The analyses and simulation results which justify the error budgets are presented in Appendix B. The experimental results are presented in Chapter 6 and Appendix C.

### 5.1.1 Receiver SNR Losses in Processing

Table 5-1 presents a summary of the SNR losses in the receiver, as detailed in Appendix B. These losses represent all losses from ideal theoretical performance due to receiver effects and transmitter bandwidth. The total SNR loss is 1.5 dB ± 1.0 dB.

Table 5-1. Receiver SNR Loss Summary

| Effect | Loss (dB) |
|---|---|
| Transmitter filter (gain due to definition of carrier power) | -0.3 ± 0.1 |
| Correlation loss due to bandwidth in receiver | 0.5 ± 0.1 |
| Analog to digital conversion, 3 bit | 0.3 ± 0.1 |
| Reference sine wave 3-level quantization | 0.4 ± 0.1 |
| FFT filter loss, offset from center frequency | 0.3 ± 0.1 |
| Dynamics losses, 50 g maximum acceleration and 50 g/s maximum jerk | 0.3 ± 0.2 |
| Miscellaneous | 0.0 ± 0.3 |
| Total SNR losses | 1.5 ± 1.0 |

### 5.1.2 Loss-of-Lock Threshold SNR

Loss-of-lock occurs when the error in either pseudorange or range rate, at the feedback inputs to the AMLE, is so large that the actual input values are outside of the range of the AMLE. This occurs either at very low SNRs, or with very high dynamics, or at a combination thereof. When under the required dynamics, loss-of-lock occurs at SNRs that are well below the linear region of the AMLE, because occasional large errors at the AMLE output are averaged out by the tracking filter, just as a phase locked loop averages out large errors at the phase detector output. The loss-of-lock thresholds realized by the receiver are significantly better than the 34 dB-Hz specified in the Demonstration Plan [2], because the Plan neglected this smoothing effect.

Loss-of-lock thresholds for various dynamics have been determined experimentally, analytically, and by simulation. The threshold SNR for dynamics up to 50 g acceleration and 50 g/s jerk is 28 dB-Hz. Methods of improving threshold are discussed in 5.4.

To compare the loss-of-lock threshold to the HDIS specification, one needs to know the total system noise figure of the receiver. This total noise figure includes all noise sources through the output of the receiver front end, including antenna input noise, cable losses, pre-selection filter losses, and amplifier noise. A total noise figure of 3.5 dB is practical, as suggested in the specification. This corresponds to a noise spectral density of -174 dBm/Hz. For the signal level of -142 dBm specified for the lowest signal strength satellite, the SNR is 31 dB-Hz. Thus the receiver threshold of 28 dB-Hz is 3 dB better than that requirement, even when under accelerations of up to 50 g.

## 5.1.3 Static Errors Due To Receiver Noise

The static errors due to receiver noise are determined by the input SNR less the processing losses, the AMLE performance, and the tracking filter noise reduction.

The AMLE is analyzed in B.3. The performance is approximately linear in SNR in the normal range of $C/N_0$ from approximately 32.5 dB-Hz to 40 dB-Hz. Below 32.5 dB-Hz, performance degrades due to thresholding; above 40 dB-Hz, instrumentation errors become significant. In the linear region, the AMLE rms pseudorange error is

$$\sigma_\tau(AMLE) = 87.1(C/N_0)^{-0.5} \qquad (m) \qquad\qquad (5-1)$$

and the rms range rate error is

$$\sigma_{\dot{\tau}}(AMLE) = 31.1(C/N_0)^{-0.5} \qquad (m/s) \qquad\qquad (5-2)$$

The tracking filter reduces the rms pseudorange and range rate errors, as analyzed in B.4. In the AMLE linear region, the pseudorange error is reduced by a factor of 3.5, and the range rate error is reduced by a factor of 1.2. The resulting rms error at the filter output is

$$\sigma_\tau = 24.9 (C/N_0)^{-0.5} \qquad (m) \qquad\qquad (5-3)$$

and the rms range rate error is

$$\sigma_{\dot{\tau}} = 25.9(C/N_0)^{-0.5} \qquad (m/s) \qquad\qquad (5-4)$$

At low SNRs, noise sometimes causes pseudorange and range rate estimation errors larger than would be expected from the above linear theory. These large errors are called outliers, and a theory including

outlier effects is developed in B.3. Outlier effects become significant at SNRs below approximately 32.5 dB-Hz. Loss-of-lock threshold, discussed in 5.1.2, occurs when there are so many outliers that the large tracking filter output error causes the signal to be outside the range of the AMLE. This occurs at approximately 28 dB-Hz.

## 5.1.4 Instrumentation Errors and Channel Bias

The implementation of the receiver generates instrumentation errors which are not accounted for by SNR effects or by dynamics. These effects are most apparent at high SNRs. The high SNR tests were specified in the Plan specifically to measure these effects. The rms pseudorange bias ranges from 0.09 m at low dynamics to 0.15 m at high dynamics, and the higher 0.15 m figure is assumed for the overall error budget. The rms range rate instrumentation effect is 0.13 m/s, and is essentially independent of dynamics. Note that the 0.15 m rms error meets the HDIS procurement specification of 0.5 ft (0.15 m).

## 5.1.5 Total Static Pseudorange Error

Static pseudorange error is all receiver-induced pseudorange error except that due to dynamic lag in the tracking filter. It includes errors due to receiver noise, processing losses and channel bias. The static error indirectly depends on dynamics because the processing losses depend on dynamics. Figure 1-1 presents the total rms of all random pseudorange errors in the receiver, for dynamics up to 50 g acceleration and 50 g/s jerk.

The total error is close to the HDIS P code specification of 3.2 ft (1.0 m) at the required threshold SNR of 31 dB-Hz even though the Demonstration Receiver operates at much higher dynamics, and therefore uses an averaging time of only approximately 0.14 s, compared to the 1 s assumed in the HDIS specification.

## 5.1.6 Total Static Pseudorange Rate Error

Figure 5-1 presents the total static pseudorange rate error for all receiver effects, for dynamics up to 50 g acceleration and 50 g/s jerk.

The range rate errors for this receiver do not compare to the delta pseudorange specifications for the HDIS because the HDIS specification requires phase coherent carrier tracking. Section 5.4.3 discusses how this receiver can accomplish phase coherent tracking and meet this specification at appropriate dynamics, if desired.

## 5.1.7 Dynamic Tracking Errors

The tracking filter selected for the Demonstration is a third order filter, so the dynamic tracking errors in both pseudorange and range rate are determined primarily by jerk. For steady state jerk, i.e., for jerk which is constant for a time long compared to the filter time constant of approximately 0.14 s, the lag errors are

$$\text{Pseudorange error} = 0.00136 \ j \ (\text{m}) \qquad (5\text{-}5)$$

$$\text{Range rate error} = 0.197 \ j \ (\text{m/s}) \qquad (5\text{-}6)$$

where j is jerk in g/s.

For a receiver in circular motion, or turning with a constant radial jerk, the lag errors in pseudorange and range rate are approximately proportional to jerk. The maximum errors are again given by equations (5-5) and (5-6).

Transient errors due to step acceleration are proportional to the size of the step, and have peak errors of approximately 0.0039 m/g in pseudorange and 0.48 (m/s)/g in range rate. Transient errors due to very high jerk for a short length of time are approximately the same as errors due to step acceleration of an amount equal to the jerk magnitude multiplied by the duration of the jerk. This approximation holds when the duration of the jerk is comparable to or less than the filter time constant of 0.14 s, with lower transient errors resulting for longer jerk at lesser magnitude.

Tracking errors for 50 g and 50 g/s maneuvers are summarized in Table 5-2. These errors are much lower than those specified for the HDIS at much lower dynamics, even for the inertially aided HDIS.

Table 5-2. Dynamic Errors at 50 g and 50 g/s Maneuvers

| Condition | Pseudorange Error (m) | Range Rate Error (m/s) |
|---|---|---|
| Steady state error due to 50 g/s jerk | 0.068 | 9.83 |
| Peak error in 50 g, 50 g/s circular motion | 0.068 | 9.74 |
| Peak transient error due to 50 g step accel | 0.196 | 24.0 |

Since the dynamic pseudorange error is very small even at 50 g/s jerk, it may appear that the filter time constant could be lengthened to reduce random errors and threshold SNR while retaining an acceptable dynamic performance error. In fact this cannot be done because the filter time constant is limited by the frequency range of the FFT and by the range rate

prediction error fed back to the AMLE. This prediction error exceeds the range rate tracking error by approximately a factor of 2 for step acceleration. With a 100 g step acceleration, the peak range rate prediction error is 90 m/s (with peak tracking error of 48 m/s), compared to a maximum FFT range of 160 m/s.

## 5.2 COMPLETE RECEIVER PERFORMANCE

This section presents the overall accuracies achievable with a complete high dynamic receiver. The overall accuracies include effects of the Space and Control Segments, with the same assumptions as to the error components as presented in the HDIS specification. The results in this section are presented in ft and ft/s to allow easy comparison to the HDIS specification.

### 5.2.1 Static Accuracies

The static accuracy is evaluated at 38 dB-Hz and at 31 dB-Hz. As shown in B.3, the loss-of-lock condition defined for the HDIS P code L1 signal, -142 dBm, corresponds to 31 dB-Hz with a total system noise figure of 3.5 dB. The following results present the HDIS specifications parenthetically next to the performance of the Demonstration Receiver.

### 5.2.1.1 Position Static Accuracy

Static position accuracy is not dominated by receiver noise or channel bias in either the Demonstration Receiver or the HDIS. Rather, in the absolute mode, accuracy is dominated by the Space and Control segment errors. In the differential mode, accuracy is dominated by multipath.

Table 5-3 presents the static component of the position accuracy, in the absolute and differential tracking modes. The errors for the Demonstration Receiver are identical to those of the HDIS specification.

Table 5-3 - Static Position Accuracy
(HDOP=1.5, VDOP=2.5)

| Parameter | rms Position Error (ft) | | | |
| | Absolute | | Differential | |
| | 38 dB-Hz | 31 dB-Hz | 38 dB-Hz | 31 dB-Hz |
|---|---|---|---|---|
| Horizontal | 21   (21) | 23   (23) | 6   (6) | 6   (6) |
| Vertical | 35   (35) | 38   (38) | 11  (11) | 13   (13) |

( ) - HDIS specification


Table 5-4 presents the error budget for static pseudorange accuracy, or User Equivalent Range Error (UERE), for tracking in the absolute mode. The UERE is identical to the rms pseudorange error used in the previous text. The Demonstration Receiver, as designed for extreme dynamics, is within 0.2 ft of the HDIS specification. The specification is met if the receiver tracking filter is modified for the HDIS maximum dynamics.

Table 5-4 - Static Absolute Pseudorange Accuracy

| Parameter | Error Budget   (ft) | | | |
| | 38 dB-Hz | | 31 dB-Hz | |
|---|---|---|---|---|
| Space Segment | 10 | (10) | 10 | (10) |
| Control Segment | 8.6 | (8.6) | 8.6 | (8.6) |
| User Segment | | | | |
|   Ionospheric delay | 1.3 | (1.3) | 5.3 | (5.3) |
|   Tropospheric delay | 1.3 | (1.3) | 1.3 | (1.3) |
|   Receiver noise, | | | | |
|     quantization, and biases | 1.2 | (0.8) | 4.0 | (3.2) |
|   Multipath | 4.0 | (4.0) | 4.0 | (4.0) |
| UERE (rms) | 14.0 | (13.9) | 15.4 | (15.2) |

( ) - HDIS specification

Table 5-5 presents the static pseudorange accuracy or UERE budget for tracking in the differential mode. In the differential mode, the processing cancels the effects of the Space and Control Segments as well as some of the ionospheric and tropospheric delays. As in the case of absolute mode accuracy, the Demonstration Receiver, as designed for extreme dynamics, is within 0.4 ft of the HDIS specification. The specification is met if the receiver tracking filter is modified for the HDIS maximum dynamics.

Table 5-5 - Static Differential Pseudorange Accuracy

| Parameter | Error Budget (ft) | | | |
|---|---|---|---|---|
| | 38 dB-Hz | | 31 dB-Hz | |
| Ionospheric/Troposphere delay | 0.5 | (0.5) | 0.5 | (0.5) |
| Channel bias | 0.5 | (0.5) | 0.5 | (0.5) |
| Receiver noise | 1.2 | (0.8) | 4.0 | (3.2) |
| Multipath | 4.0 | (4.0) | 4.0 | (4.0) |
| UERE (rms) | 4.2 | (4.2) | 5.7 | (5.3) |

( ) - HDIS specification

In summary, the static position accuracy of the Demonstration Receiver is essentially identical to that specified for the HDIS.

5.2.1.2 Velocity Static Accuracy

The Demonstration Receiver, as designed for extreme dynamics, does not perform the phase coherent tracking required of the HDIS. Therefore, the velocity static accuracy is not directly comparable to that of the HDIS. Table 5-6 presents the horizontal and vertical velocity errors.

Table 5-6 - Static Velocity Accuracy

| Parameter | rms position error (ft/s) | | | |
|---|---|---|---|---|
| | 38 dB-Hz | | 31 dB-Hz | |
| Horizontal | 1.7 | (0.6) | 3.7 | (0.7) |
| Vertical | 2.9 | (1.0) | 6.1 | (1.1) |

( ) - HDIS specification

## 5.2.2 Dynamic Accuracies

The dynamic environment of the HDIS, defined in Table XI of attachment 5 of [1], is repeated in Table 5-7. The conditions for the aided HDIS correspond to acceleration of 10.4 g and jerk of 10.4 g/s for 0.1 s. In contrast, the Demonstration Receiver operates with acceleration in excess of 100 g and jerk in excess of 100 g/s, for any duration consistent with maximum velocity and acceleration.

Table 5-7  -  HDIS and Demonstration Receiver Worst Case Dynamics

| Parameter | HDIS (aided) | HDIS (unaided) | Demonstration Receiver |
|---|---|---|---|
| Velocity (ft/s) | 5000 | 580 | > 32,000 |
| Acceleration (ft/s$^2$) | 330 for 10 s | 130 | > 3,200 |
| Jerk (f/s$^3$) | 330 for 0.1 s | 130 for 0.1 s | > 3,200 |

As shown in B.4, if all the receiver channels use the same tracking filter, the worst case tracking error of the receiver is identical to that exhibited by a single channel when the jerk is in the direction between the receiver and the tracked satellite. Since we assume that in the implemented Demonstration Receiver all channels use identical steady state gain tracking filters, the effect of GDOP can be ignored.

The third order tracking filter used in the Demonstration Receiver has zero pseudorange and range rate tracking errors for any constant velocity or constant acceleration. The errors in a 10.4 g, 10.4 g/s circular motion are 0.045 ft and 6.6 ft/s for position and velocity, respectively. This position accuracy is significantly better than the HDIS specification, even for the aided HDIS receiver. The velocity accuracy is better than that of the unaided HDIS but not as good as that of the aided HDIS. This is due to the noncoherent nature of the tracking.

Table 5-8 presents the dynamic error specifications for the HDIS, and the dynamic errors generated by the Demonstration Receiver at much higher dynamics.

Table 5-8 - Dynamic Component of Accuracy

| Parameter | Position Error (ft) | Velocity Error (ft/s) |
|---|---|---|
| HDIS - average under dynamics of Table 5-7 | | |
|     - aided | 1.0 | 1.0 |
|     - unaided | 7.6 | 13.5 |
| | | |
| Demonstration Receiver | | |
|    constant velocity | 0. | 0. |
|    constant accel. | 0. | 0. |
|    100 g/s jerk | 0.42 | 63. |
|    50g,50 g/s circular | 0.21 | 32. |

## 5.3 OTHER PERFORMANCE CHARACTERISTICS

This section discusses some performance characteristics of interest that could be achieved with the Demonstration Receiver concept, but were not demonstrated. Rationale for the performance predictions is included.

### 5.3.1 Acquisition

The Demonstration Receiver can be especially powerful in fast acquisition applications because of the wide search capability of the AMLE window. All HDIS requirements can be easily met. Also, the techniques could be extended to meet the extremely fast acquisition time which might be required for a transdigitizer receiver.

During initial acquisition, data bit synchronization is unknown. To overcome the problem of having data transitions occur during the FFT detection time, the detection interval is reduced to one half bit time, and each possible time delay is examined over two consecutive intervals. At least one of these detection intervals will always be transition free. The number of input data points in the FFT could be maintained at 32 by reducing the correlation interval to one half of the normal length. The resulting frequency range of the FFT is ± 1600 Hz, which corresponds to ± 980 ft/s at L1.

In the pseudorange domain, the AMLE window, using 11 correlators separated by one-half P-code chip, can detect pseudorange uncertainties of ± 250 ft. All this detection is accomplished in a single data bit time, i.e., 20 ms.

The HDIS specifications for Time-To-First-Fix (TTFF) are given in Table I, Attachment 5 of the HDIS specification. The specified SNR, 38 dB-Hz, is high enough so that the false detection rate is very low, and detection over one pair of 10 ms intervals, or a single bit time, is sufficient. The worst case specified velocity uncertainty is within the uncertainty of the AMLE window, so no search in frequency is required.

Because of the 10 minute uncertainty in user clock, the acquisition must start with a full search over the 1023 chips of the C/A code, including recovery of the data bit boundary (bit synch, see 5.3.3). Then, the 50 Hz data stream is detected, and finally, P code acquisition is obtained.

The budget for the Demonstration Receiver TTFF is given in Table 5-9. The total acquisition time is 62 s, or approximately half of the HDIS specification of 120 s.

<div align="center">Table 5-9   -   Time-To-First-Fix Budget</div>

| Step | Duration | |
|---|---|---|
| | bits | sec |
| Search set up | 2 | 0.04 |
| Search C/A code (1023 chips) | 1023 | 20.46 |
| Identification of bit synch, positioning of the code | 500 | 10.00 |
| Preparation for data recovery | 2 | 0.04 |
| Recovery of a data frame (1500 bits) | 1500 | 30.00 |
| Verification of data | 2 | 0.04 |
| Transfer to P-code lock, confirmation | 50 | 1.00 |
| Tracking filter transient time (0.14 s time constant) | 14 | 0.28 |
| Total | 3093 | 61.86 |

The search time, 20.46 s, is based on moving the window in steps of one chip, and using one bit time in each step to compute the FFTs for the two 10 ms intervals. This results in each point appearing at least four times within the AMLE window. The repeat appearances can be used to accommodate lower SNRs than the specified 38 dB-Hz by adding the FFT outputs noncoherently, e.g., an approximate 6 dB improvement is obtained by the four repeats. An additional 3 dB improvement could be achieved by detecting over 2 bit times, increasing the TTFF by 20.26 s.

## 5.3.2 Reacquisition

The unaided HDIS specification requires that under the conditions given by Table 5-10, reacquisition shall be established within 2 s. This section shows that the reacquisition time for the proposed receiver is 0.5 s.

Table 5-10 - Reacquisition Conditions

| Parameter | units | unaided | aided |
|-----------|-------|---------|-------|
| $C/N_0$ at input to preamplifier | dB-Hz | 38 | 38 |
| Duration of signal loss | s | 10 | 60 |
| Position uncertainty | ft | 1000 | 200 |
| Velocity uncertainty | ft/s | 200 | 3.5 |
| Acceleration uncertainty | $ft/s^2$ | 20 | 0.003 |

Because the velocity window for 20 ms integration is $\pm$ 490 ft/s, no velocity search is required. The pseudorange uncertainty is the position uncertainty added to the effect of an unknown receiver oscillator frequency offset. As an example, a frequency offset of 1 part in $10^9$ causes 1 ft of pseudorange drift per second of signal loss, or 10 ft and 60 ft for signal outages of 10 s and 60 s specified for the unaided and aided HDIS, respectively. With an AMLE window of $\pm$ 250 ft, the pseudorange search over the total maximum uncertainty of 1060 ft can be completed in five data bit times.

We assume that the receiver is tracking the P-code, and the reacquisition is performed without returning to C/A code. As presented in Table 5-11, the total reacquisition time is 0.5 s, well under the HDIS specification of 2 s.

Table 5-11 - Reacquisition Time Budget

| Step | Duration | |
|---|---|---|
| | bits | sec |
| Search set up | 2 | 0.04 |
| Search P code (1060 ft uncertainty) | 5 | 0.10 |
| Re-position P-code | 2 | 0.04 |
| Confirm reacquisition | 2 | 0.04 |
| Tracking filter transient time (0.14 s time constant) | 14 | 0.28 |
| Total | 25 | 0.50 |

## 5.3.3 Data Bit Synchronization

Data bit synchronization can easily be obtained in software once acquisition is accomplished. Bit synchronization is quantized to the nearest correlation time, so there are only 32 possible synch phases. Synch is obtained by finding the phase which maximizes the value of the AMLE detection function. This can be done analogously to data bit synchronization such as in a transition tracking bit synchronizer [5,6].

At $C/N_0 = 38$ dB-Hz, a data bit sync loop bandwidth of 0.5 Hz will achieve an rms timing error of one-quarter of a correlation interval, which is sufficient to obtain sync to the nearest correlation interval. Conservatively, loop lock will occur within five inverse loop bandwidths, or 10 s.

## 5.3.4 Data Bit Detection

The receiver can also perform data bit detection in software. This capability is inherent since the FFT measures carrier phase. Data bits are detected differentially by observing when the measured phase in one bit time differs from the phase in the previous bit by more than 90 degrees. The phase in the early bit time must be extrapolated ahead one bit time to compensate for range rate and for the feedback frequency at the AMLE input. Data detection will not be possible at very high dynamics, when the phase extrapolation process breaks down. This dynamic limit has not been established, but is comparable to the dynamic limit for a receiver using phase coherent tracking.

## 5.3.5 Parameter Update Rates

The inherent update rate of the Demonstration Receiver is 50 times per second, or once every data bit time. This rate is higher than the 10 times per second update rate specified for the HDIS (Table XIII, Attachment 5, [1]). In fact, the receiver implementation can be simplified if the signal channels continue to be updated at 50 times per second, while a flash solution for time and position is computed at a lower rate, reducing the computational requirements.

## 5.3.6 Data Accuracy

The Demonstration Receiver computes or has otherwise available all of the output data items specified for the HDIS (Table XIII, Attachment 5, [1]), except for the Inertial Reference Unit (IRU) status. The Demonstration Receiver does not require an IRU even for tracking under very high dynamics; nevertheless, an IRU can be integrated with the receiver if so desired.

The accuracies specified for the UERE and position are met, as discussed in 5.2. The accuracy of GPS system time, 100 ns, is equivalent to a position error of 100 ft and is met under all the specified conditions.

The velocity accuracy of the Demonstration Receiver is better than that specified for the unaided HDIS but not as good as that of the aided HDIS. This is because the receiver uses noncoherent tracking rather than the HDIS phase locked loop tracking.

Data resolution specified for the HDIS can easily be met.

## 5.4 RECEIVER MODIFICATIONS AND ENHANCEMENTS

This section discusses some modifications and enhancements which can be incorporated into the receiver. These include C/A code tracking, phase coherent (PLL) tracking, and threshold enhancement by combined P and C/A code tracking.

## 5.4.1 C/A Code Tracking

Implementation of the receiver would require the addition of C/A code tracking capability for acquisition. In some applications, notably with translators or transdigitizers, only C/A tracking might be used.

Capability for both P and C/A code can be implemented with only minor changes in digital logic and the addition of a C/A code generator. It is not necessary to add a second IF-baseband channel with restricted bandwidth, new A/D converters, or a new sampling clock. The existing correlators can be run at the existing clock rate, but with increased lag spacing via digital delays.

There is a performance advantage to processing the C/A code with the existing sampling rate. For acquisition, the lag spacing can be one-half chip. After acquisition, the lag spacing can be reduced to one-quarter chip or less. This reduces the rms pseudorange error, as shown in Appendix B.3.

One quarter chip spacing gains root 2 in rms error over the normal half chip spacing. Assuming this one-quarter chip lag spacing, the rms pseudorange error above threshold would be

$$\sigma_{\tau(C/A)} \simeq 177 \ (C_{C/A}/N_0)^{-0.5} \qquad (m)$$

where $C_{C/A}$ is the received C/A code power. At a C/A code SNR of 34 dB-Hz, the rms pseudorange error would be 3.5 m.

For a C/A code only receiver, such as for a transdigitizer, the sampling rate and processing rate would be reduced to 2.046 MHz, and one-half chip lag spacing would be used. The rms error would be root 2 greater than above.

## 5.4.2 Threshold SNR Versus Dynamics

Threshold SNR depends on the design point maximum dynamics and on the parameters of the tracking system. The frequency tracking in the Demonstration Receiver is equivalent to a second order frequency locked loop (FLL). Achievable threshold varies in approximate inverse proportion to the square root of maximum jerk. Thus threshold can be reduced to approximately 18 dB-Hz if the system is designed for 1 g/s maximum jerk. This threshold is better than the non-coherent tracking threshold required for the HDIS at low dynamics.

Threshold extension is achieved by increasing the AMLE estimation time and the tracking filter time constant. Since the coherent-integration (FFT) time in the AMLE cannot be longer than one data bit time, the estimation time is increased by accumulating energy over several bit times, for each correlation lag and frequency.

Tracking at dynamics in excess of those demonstrated can be accomplished at the cost of SNR threshold, by decreasing the detection time and the filter time constant, and increasing the filter update rate. Tracking with jerk in excess of 500 g/s is possible with a threshold of approximately 31 dB-Hz.

Figure 5-2 shows the maximum jerk versus threshold SNR for the demonstrated FLL tracking technique, with modified detection times and tracking filter time constants. Also shown are maximum jerk versus threshold for phase locked loop tracking, discussed in 5.4.3, and for threshold extension by combined P and C/A code tracking, Section 5.4.4.

In Figure 5-2, the curve for the Demonstration Receiver FLL is based upon the demonstrated tracking capability at 100 g/s jerk and a SNR of 28 dB-Hz. Actual performance is not a smooth curve, because integration

time can be varied only in multiples or factors of the data bit time.

## 5.4.3 Phase Coherent Tracking and Threshold

Because the FFTs in the AMLE inherently measure carrier phase, phase coherent carrier tracking can be implemented by changing the tracking loop filter software. Coherent tracking is optimized by the FFT signal processing, because the integration times are matched to the data bit times. Effectively, the loop is an optimum Costas loop with arctangent-type phase detection.

Phase coherent tracking is limited by the phase lag error due to dynamics and by the rms phase error due to noise in the loop bandwidth. At 10 g/s jerk, a third order loop with a loop bandwidth, $B_L$, of 15 to 20 Hz can achieve satisfactory dynamic phase error. Larger loop bandwidths are not feasible without decreasing the phase detector measurement time to less than one bit time, thus increasing threshold. Tracking threshold occurs with a loop SNR of approximately 15 dB. Allowing 1.5 dB processing losses, as for the non-coherent tracking, the threshold $C/N_0$ is approximately 28 dB-Hz. Maximum jerk versus threshold is shown in Figure 5-2. Capability to track jerk varies as $B_L$, or as the cube root of threshold $C/N_0$, since the PLL is assumed to be third order. The estimated accuracy of the curve is $\pm$ 2dB at $C/N_0$ = 28 dB-Hz. Performance is worse than shown at low SNRs due to squaring loss, which has not been accounted for.

An adaptive receiver would be desirable. Such a receiver could monitor both dynamics and SNR and select appropriate tracking. Coherent tracking could be used at low and moderate dynamics and with SNRs above 28 dB-Hz. Non-coherent tracking with the demonstrated filter time constants would be used for high dynamics. Non-coherent tracking with a longer time constant would be used at low dynamics and low SNR, to extend SNR threshold.

## 5.4.4 Threshold Extension by Combined P and C/A Code Tracking

Since the P and C/A code signals are carrier-phase coherent with a known 90 degree phase difference, tracking threshold can be improved by phase coherently combining the P code and C/A code signals. Since the L1, C/A code signal is 3 dB stronger than the P code signal, the potential threshold improvement is 4.77 dB in terms of P code power [7].

Threshold improvement can be achieved both with frequency tracking, as in the high dynamic demonstration, and tracking carrier phase with a PLL. Phase detection of both signals must be relative to the same local oscillator. The AMLE implementation with the FFT is ideal.

Tracking capability (maximum jerk) is shown in Figure 5-2 for combined P and C/A code tracking both with PLLs and with FLLs. At a P code SNR of 23 dB-Hz, maximum jerk of 10 g/s can be tracked non-coherently. At very low dynamics, non-coherent FLL tracking is possible with a P code SNR of approximately 13 dB-Hz.
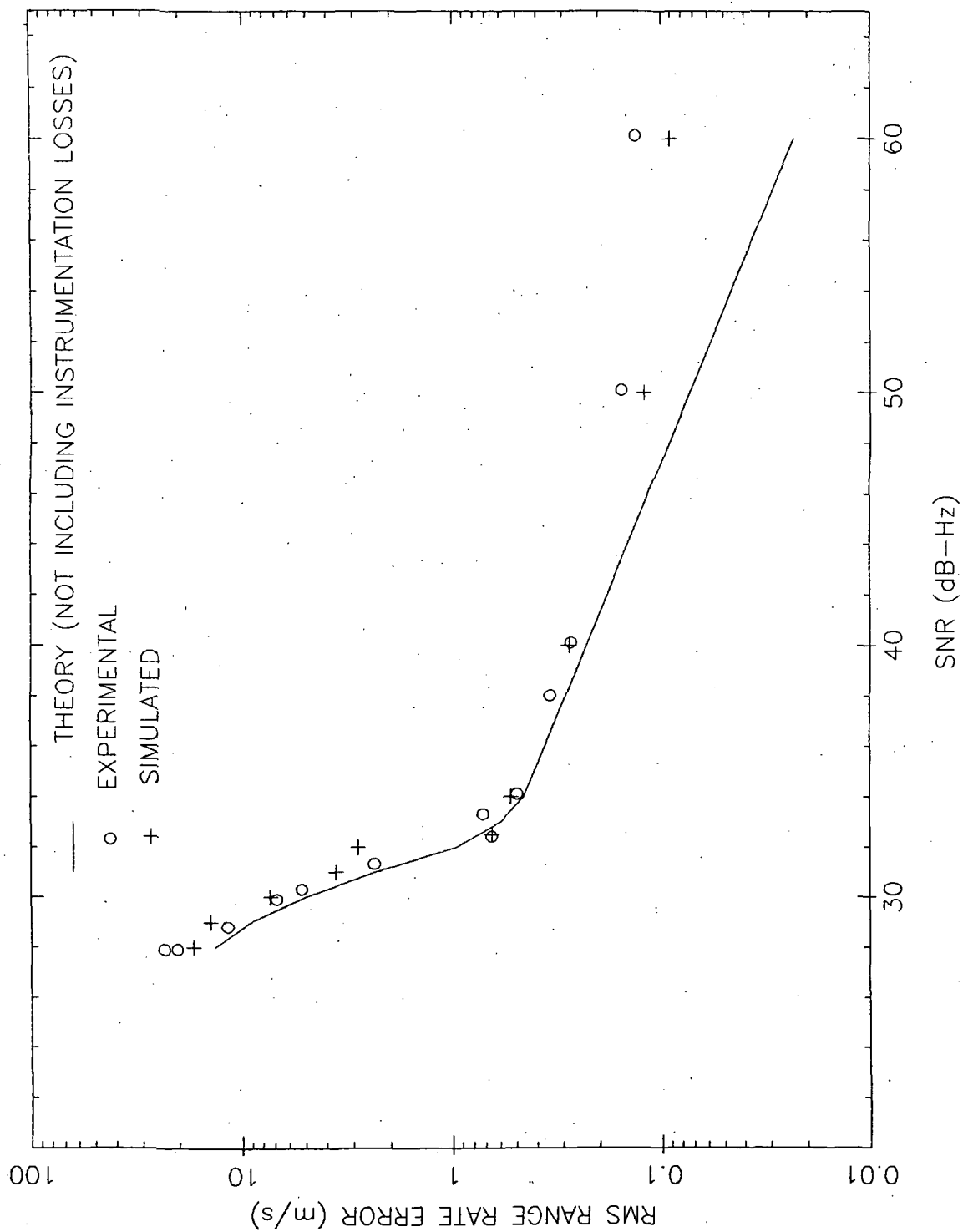
Figure 5-1. Range Rate Errors, with Dynamic Component Removed, Versus SNR for 50 g, 40 g/s, Circular Motion
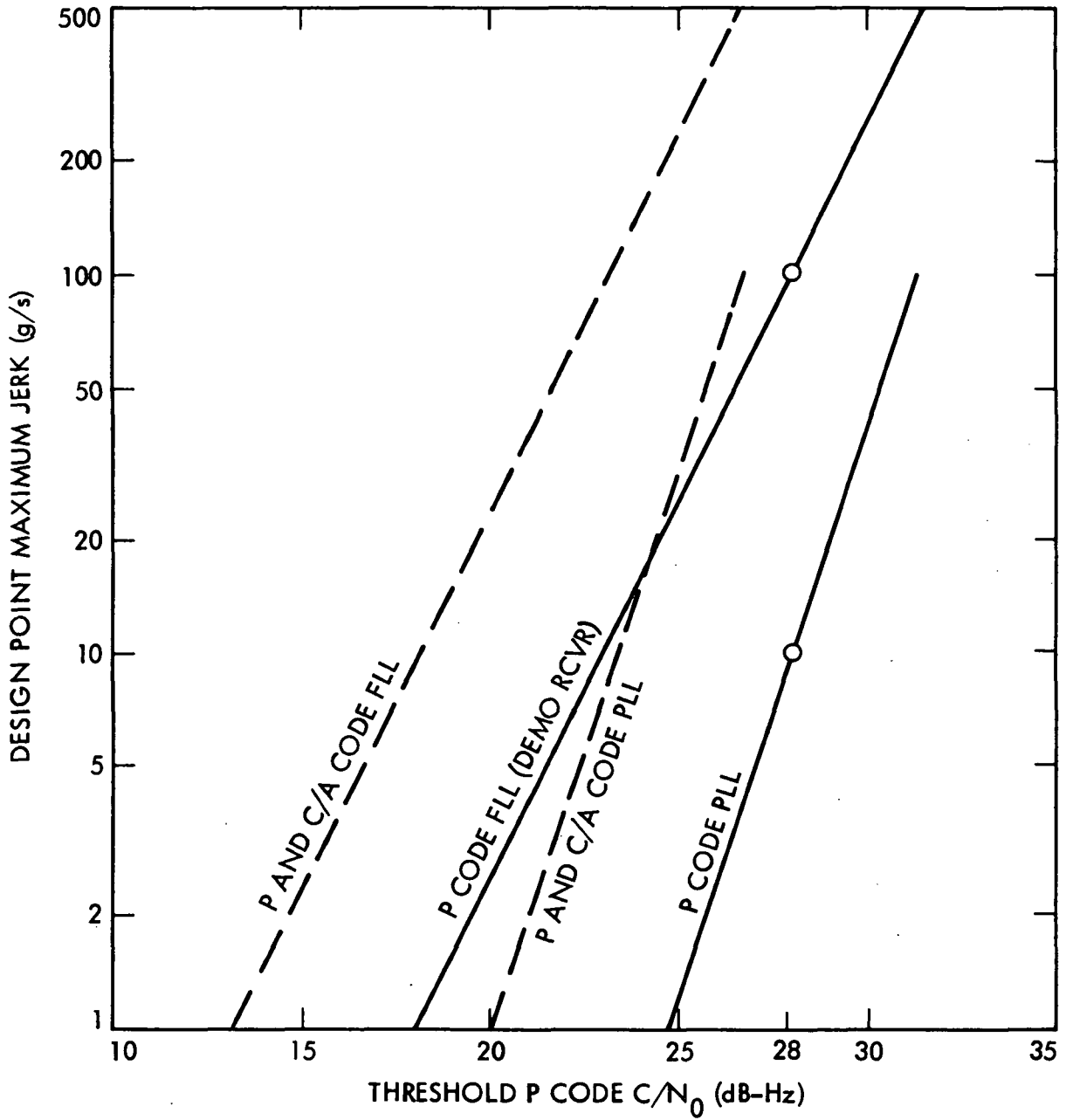
Figure 5-2. Maximum Jerk Versus SNR Threshold for Various Tracking Methods

# CHAPTER 6

## DEMONSTRATION TESTS AND RESULTS

The Demonstration tests are divided into four categories: AMLE evaluation, tracking filter evaluation, tracking under high dynamic conditions, and performance at low SNR. This chapter presents the experimental performance and compares it to the performance predicted by analysis and simulation.

The results of the Validation Demonstration tests meet or exceed all the performance requirements of the Plan (Appendix A) and are in close agreement with system analysis and simulations (Appendix B). Details of the test results are presented in Appendix C.

## 6.1 SUMMARY OF TEST CONDITIONS

In the Demonstration tests, the Test Instrumentation Subsystem (TIS) generated three types of simulated trajectories: constant velocity, step acceleration, and circular motion. For simplicity, the simulated variables (pseudorange, range rate and acceleration) are with respect to a GPS satellite rather than relative to Earth. In the worst case, the satellite-Earth motion may add 750 m/s and 0.1 g to the range rate and acceleration, respectively.

In step acceleration tests, constant positive and negative accelerations are applied for 6 s intervals, separated by intervals of high range rate and no acceleration. For example, in a 50 g test the peak range rate and acceleration are $\pm 1470$ m/s and $\pm 490$ m/s$^2$, respectively. In circular motion tests, the pseudorange is sinusoidal, simulating the component of circular motion in the receiver-satellite direction. The amplitude of the waveform is selected to correspond to the specified acceleration and period. In constant velocity tests, the range rate is

constant for the duration of the test. Note that short intervals of constant velocity are part of the step acceleration tests.

Tests were conducted at three SNR levels - high (60 dB-Hz), medium (40 dB-Hz) and low (34 dB-Hz), for each type of trajectory and with different magnitudes of dynamics. The high SNR level tested instrumentation effects and the signal level dynamic range of the receiver. Medium SNR tests simulated the nominal conditions with minimum specified satellite signal level, 3.5 dB receiver noise figure, and a 0 dBi antenna. The low SNR is the SNR that occurs with a -6 dBi antenna gain, which is common with missile antennas. Still lower SNRs were used to determine the minimum or threshold SNR for satisfactory tracking.

## 6.2 AMLE EVALUATION TESTS

The AMLE evaluation tests measured the errors in pseudorange and range rate estimation caused by the Demonstration Receiver implementation. The tests confirmed the detailed structure of the AMLE function over the discrete set of points where it is evaluated, and bounded the bias error in fine estimation caused by the interpolation formulas. Averaged over pseudorange and range rate, the pseudorange and range rate estimation bias errors were 0.5 m and 0.1 m/s rms, respectively. After the end of the planned tests, new interpolation formulas were introduced which reduced the bias errors to less than 0.1 m and 0.1 m/s, respectively. Details of the AMLE evaluation tests are presented in Appendix C.

## 6.3 TRACKING FILTER EVALUATION TESTS

The pseudorange and range rate estimates generated by the AMLE are passed through a tracking filter achieving three objectives: smoothing of measurement noise, estimation of receiver state (pseudorange, range rate and acceleration), and prediction of pseudorange and range rate to position the AMLE window. Various filters were compared by analysis, simulation, and experiment to select a filter for the Demonstration Receiver. Filter selection and mechanization for a complete receiver are outside the scope of the testing.

Filter selection is driven by three criteria. First, the filter must be computationally efficient to allow a 50 times per second update rate. Second, the filter must estimate the state and provide predictions to the AMLE under the required high dynamics. Third, the filter must reduce the pseudorange noise by as much as possible consistent with the above.

Three classes of filters were evaluated: second- and third-order fading memory filters, and a second-order Kalman filter. All filters had fixed gains to minimize the computational complexity; in particular, the Kalman filter used steady state gains obtained by various assumptions on process noise and measurement noise. In each class, 12 to 15 filters were tested, with different filter parameters, i.e. filter time constant and weighting for the fading memory filters, and standard deviation of process

and measurement noise for the Kalman filter. The tests were 50 g, 1470 m/s step acceleration trajectories, with high, medium, and low SNR.

Details of the filter analysis and simulations are given in B.4. Experimental results, presented in Appendix C, agreed with the analysis and simulations in all cases. The filter selected for the rest of the Demonstration was a third-order fading memory filter, with a time constant of 0.14 s.

## 6.3.1 Transient Response

Figures 6-1 and 6-2 show the transient responses to 50 g step acceleration and 50 g circular motion. The figures were generated by overlaying repetitions of the indicated trajectories: 8 repetitions for step acceleration and 30 repetitions for circular motion. In the step acceleration tests, during the constant acceleration intervals, the dynamic components of the pseudorange and range rate errors are zero after the transient decays, as expected for a third order filter. The step acceleration causes a range rate transient with a peak of 24 m/s, which decays to a negligible value within twice the filter time constant, or 0.28 s. There is no significant pseudorange transient. In the circular motion test, the pseudorange and range rate errors have sinusoidal components with magnitudes that are proportional to the maximum jerk. For the test of Figure 6-2, the maximum jerk is approximately 40 g/s and the peak errors due to dynamics are 0.06 m and 8 m/s, respectively.

## 6.3.2 Noise Response

The noise response of the filter is best evaluated by tests at low SNR, since instrumentation effects dominate at high SNR. As shown in 6.4, the dynamics of the test have a negligible effect on noise performance as long as the dynamic component of the error is removed from the tracking results. At 34 dB-Hz, the pseudorange and range rate estimates generated by the AMLE have standard deviations of 1.7 m and 0.6 m/s respectively. The tracking filter reduces these by a factor of 3.5 for pseudorange and a factor of 1.2 for range rate, resulting in standard deviations of 0.6 m and 0.4 m/s for filtered pseudorange and range rate, respectively.

## 6.4 PERFORMANCE UNDER HIGH DYNAMICS

Performance as a function of dynamics and SNR is evaluated by using simulated constant velocity, step acceleration, and circular motion trajectories, under various SNR conditions. The tracking errors have dynamic components that are introduced by the tracking filter lags, and random components that are caused by thermal noise and instrumentation effects. The random errors are approximately independent of receiver dynamics. This is only an approximation because the nonlinearity of the AMLE operation and the nature of some instrumentation effects introduce some dependence on receiver dynamics. Nevertheless, as the tests demonstrated, performance under high dynamics can be approximated by

evaluating these two error components separately.

To separate the dynamic error from the random error, the DES uses two error measures, as defined in Chapter 4. The "total tracking error" is the tracking result minus the simulated trajectory. These errors include both the random and dynamic components. The "filtered output noise" is the tracking result minus a filtered version of the simulated trajectory (i.e., passed through a tracking filter identical to that used in the Demonstration Receiver). Thus "output noise" error, at SNRs below 50 dB-Hz, is dominated by thermal noise. Instrumentation errors dominate at SNRs above 50 dB-Hz.

### 6.4.1 Constant Velocity Tests

Tests were conducted at constant velocities up to 10,000 m/s. The results showed that there is only minimal degradation at the high velocities. Figure 6-3 shows the rms pseudorange and range rate errors under high, medium, and low SNR, as a function of velocity. The figure presents both the unfiltered and filtered output noise where the unfiltered noise is at the AMLE output and the filtered noise is at the output of the tracking filter. Note that for the constant velocity test, the dynamic components of pseudorange and range rate are zero, hence the total tracking error is identical to the filtered output noise. At low SNR, 34 dB-Hz, the rms pseudorange and range rate errors are under 0.8 m and 0.6 m/s, respectively. The dynamic components of the errors are zero, thus the errors are due only to thermal noise and instrumentation effects.

As Figure 6-3 shows, there is a slight increase in the various error components as the velocity increases above 300 m/s. This is caused by coupling between instrumentation and dynamics effects. The main cause of degradation is the method by which the local code generator is corrected to account for dynamics. A detailed explanation is presented in Appendix B.

At very low velocities, there is also a slight increase in rms error. This is caused by the original AMLE interpolation formulas. As discussed in Appendix C, this bias was later removed using better interpolation formulas, but only after the completion of the illustrated tests.

Tests at velocities that were approximate multiples of 1800 m/s showed a high rate of false detections and loss-of-lock regardless of the SNR. There were no similar problems at other velocities (e.g. 3000 m/s and 10000 m/s) and there is no analysis or simulation that explains the problem. The problem is believed to be in the instrumentation and not fundamental to the design. This area is targeted for further investigation.

## 6.4.2 Step Acceleration Tests

The step acceleration tests were conducted with step accelerations of up to 100 g. The transient response for a 50 g step acceleration test is shown in Figure 6-1. Figure 6-4 presents the rms pseudorange and range rate errors with the transient removed, at various SNRs and accelerations. At low SNR, the random errors are independent of the acceleration and are under 0.7 m and 0.6 m/s for pseudorange and range rate, respectively.

The theoretical peak transient errors for a 100 g step acceleration are 0.39 m and 48 m/s for pseudorange and range rate, respectively. Figure 6-5 presents the measured peak transient errors as functions of dynamics and SNR. The pseudorange transient error is comparable to the ambient noise and cannot be accurately measured. The peak transient range rate error for a 100 g step in acceleration is 48 m/s and is proportional to the acceleration, as expected for a linear filter. These results agree with the analysis and simulations.

The maximum magnitude of the step acceleration, for reliable tracking, is determined by the size of the AMLE prediction error compared to the width of the FFT filter bank. For the Demonstration Receiver, the prediction peak error under 100 g step acceleration is approximately 100 m/s, or 500 Hz. This error is close to the limits of the AMLE window, $\pm$ 800 Hz, allowing perhaps a maximum step acceleration of 150 g. Note that as the prediction error increases, there is a reduction in SNR due to the 1600 Hz lowpass filtering caused by integration over the correlation time. Higher dynamics can be accomodated if a different tracking filter is used, or if the range of the FFT is increased by using shorter correlation intervals and more points in the transform.

## 6.4.3 Circular Motion Tests

Circular motion tests were conducted for various accelerations and jerks and for low, medium, and high SNR. Circular motion corresponds to sinusoidal motion in pseudorange. The period of the sinusoids were 8 s, resulting in peak jerks of $\pi/4$ times the peak accelerations, in consistent units.

Figure 6-6 presents random pseudorange and range rate errors as functions of dynamics and SNR. The output noise is independent of the dynamics and depends mainly on the SNR. At low SNR, the rms pseudorange and range rate errors at the output of the tracking filter are under 0.6 m and 0.5 m/s, respectively.

The theoretical rms dynamic errors for the 100 g, 80 g/s, circular motion trajectory are 0.08 m and 11.3 m/s for pseudorange and range rate, respectively. Figure 6-7 shows the total measured total tracking error as a function of dynamics and SNR. The dynamic component of the pseudorange error is negligible compared to the random effects. For range rate, the dynamic component dominates the rms error, and is proportional to acceleration.

The prediction errors for circular motion tests are proportional to jerk. Successful tests were conducted up to 150 g, 157 g/s circular motion, and operation may be acceptable for jerk of up to 250 g/s. If even higher dynamics are needed, receiver processing (tracking filter and length of correlation interval) can be changed to accommodate the dynamics at a cost in SNR threshold, as discussed in 5.4.2.

## 6.5 PERFORMANCE AT LOW SNR

Low SNR tests were conducted to determine the performance of the receiver as a function of the SNR, and to determine the minimum acceptable SNR, or tracking threshold, as a function of dynamics. The tests demonstrated that the receiver can track reliably down to 28 dB-Hz, almost independent of the test dynamics.

Circular motion tests were used to determine low SNR performance. Figure 1-1 shows the agreement between the analysis, simulation, and experimental results for a 50 g, 40 g/s, circular motion trajectory. For SNRs between 32 dB-Hz and 50 dB-Hz, the mean square pseudorange error is inversely proportional to SNR. At lower SNRs, many false detections (or outliers) occur, causing large increases in error as the SNR decreases. For SNRs over 50 dB-Hz, instrumentation errors dominate. These errors are not included in the theoretical model or in the simulation, causing the observed discrepancy between simulations and experimental results.

Figure 6-8 shows the tracking errors for different dynamics: accelerations of 3 g, 50 g, 100 g and 150 g. The dynamics have little or no effect on the loss of lock threshold, and only minor effect on the rms pseudorange error due to random noise. The minor increase in pseudorange error at high dynamics is due to changes in the carrier frequency over the measurement time and to instrumentation effects, both in the TIS and in the Demonstration Receiver, as explained in Appendix B.

Figure 6-9 demonstrates that the removal of the dynamic component of the tracking error has only a minimal effect on the pseudorange error, even at dynamics as high as 50 g, 40 g/s, circular motion. This is because the rms dynamic component at such dynamics is less than 0.05 m, which is negligible compared to random noise and instrumentation errors.
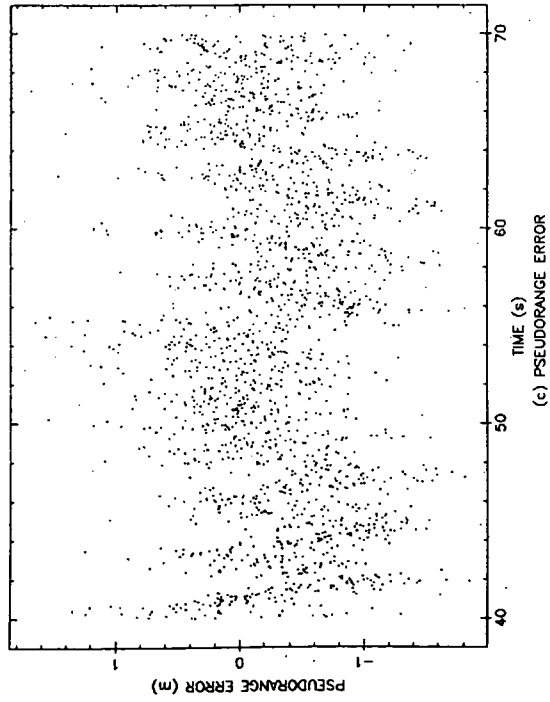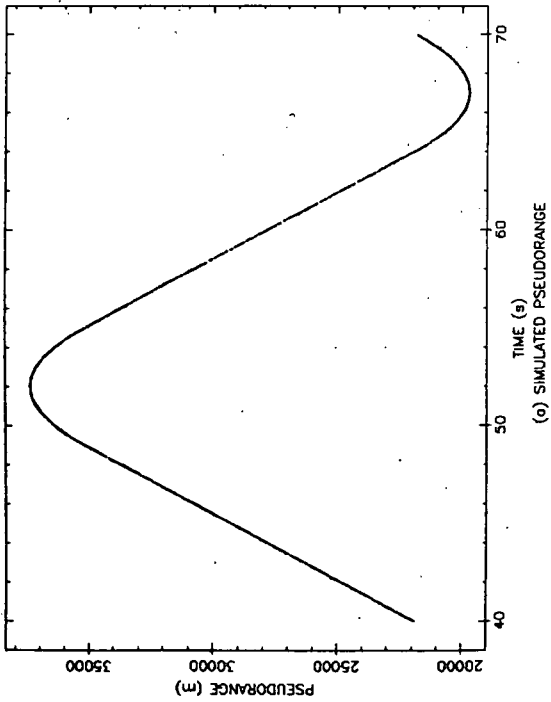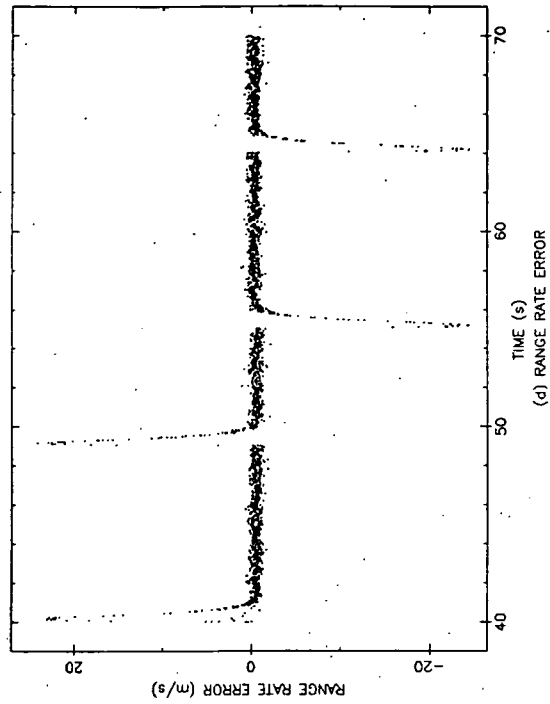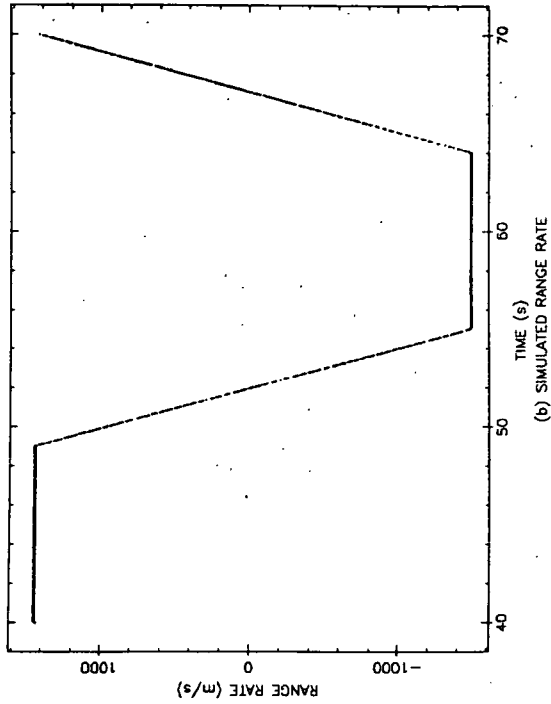
Figure 6-1. Transient Responses to 50 g Step Acceleration, SNR = 34 dB-Hz
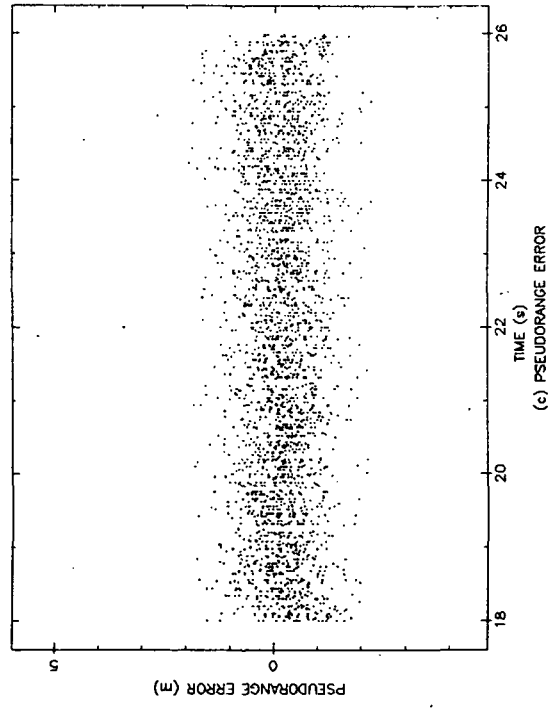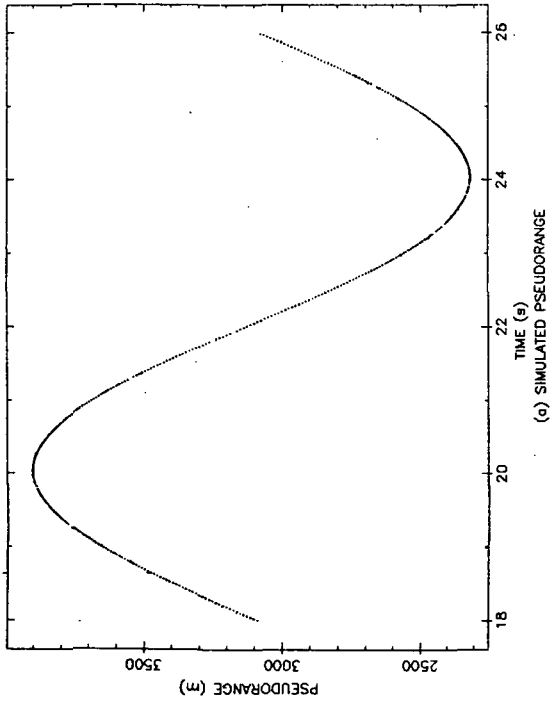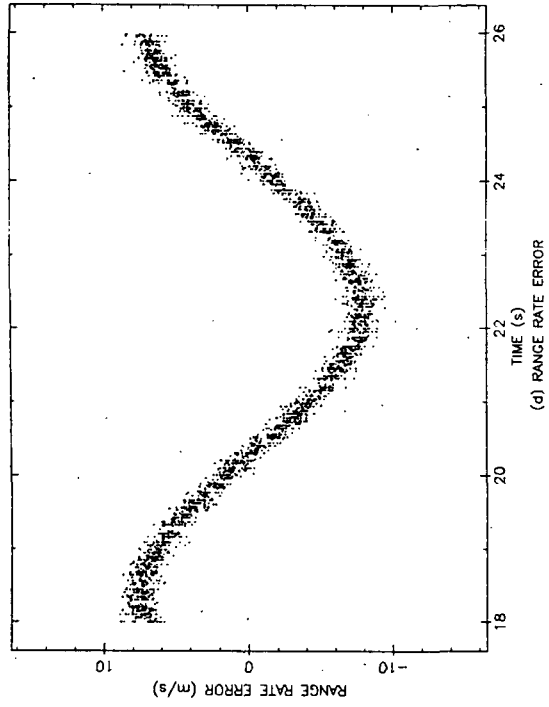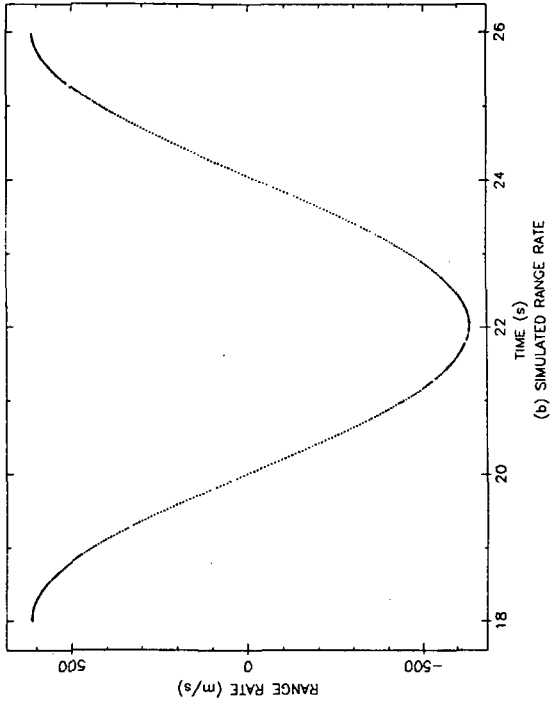
Figure 6-2.  Transient Responses to 50 g, 40 g/s, Circular Motion, SNR = 33 dB-Hz
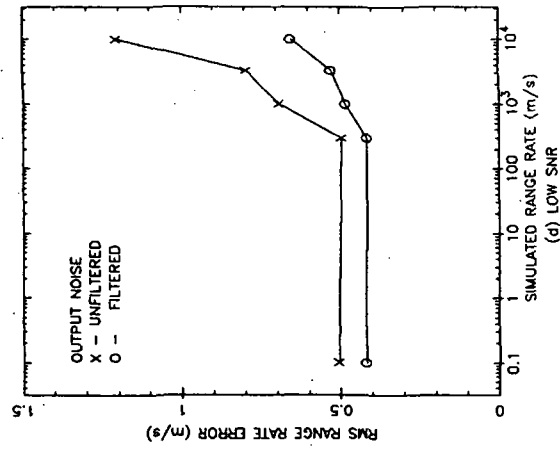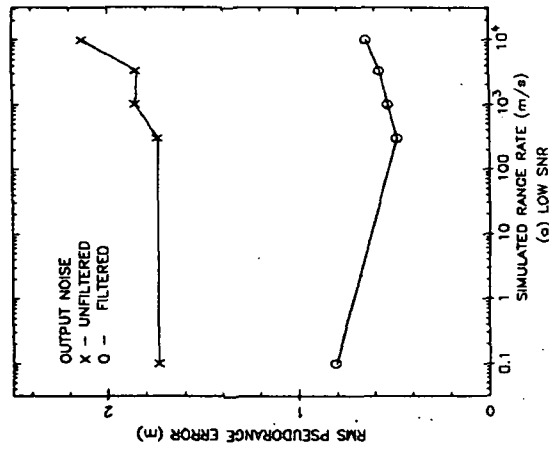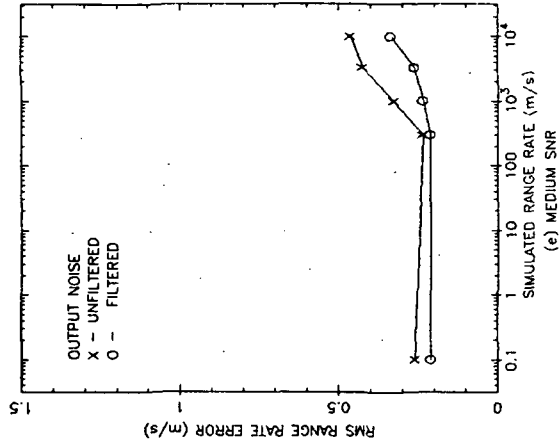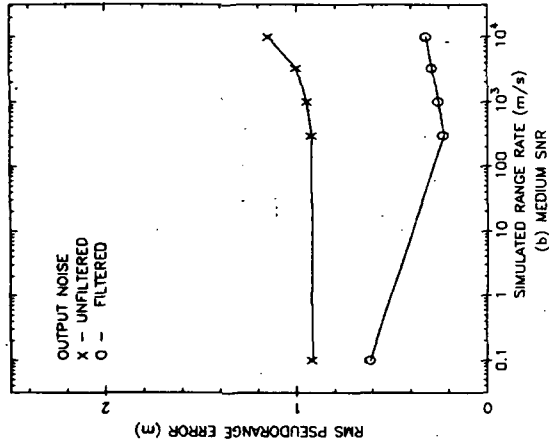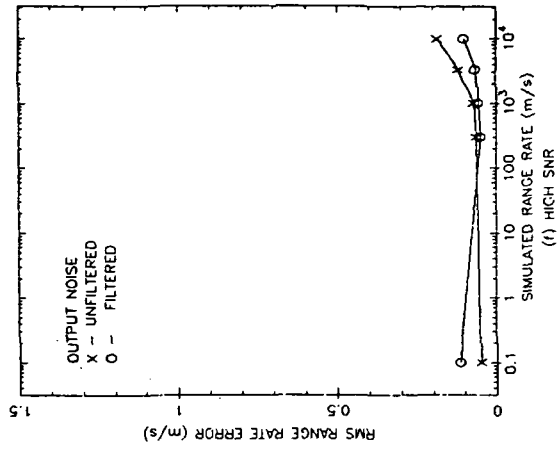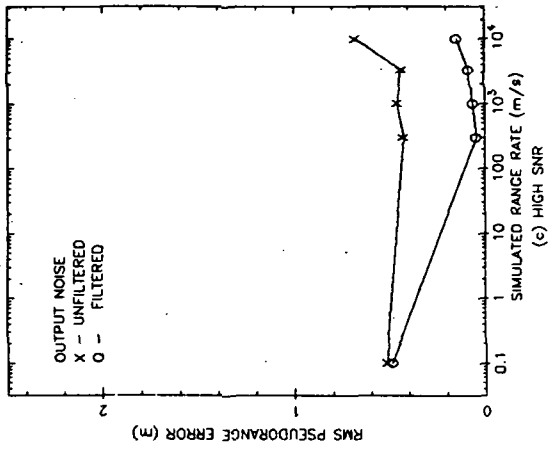
Figure 6-3. Random Errors Versus Velocity for Constant Velocity Tests
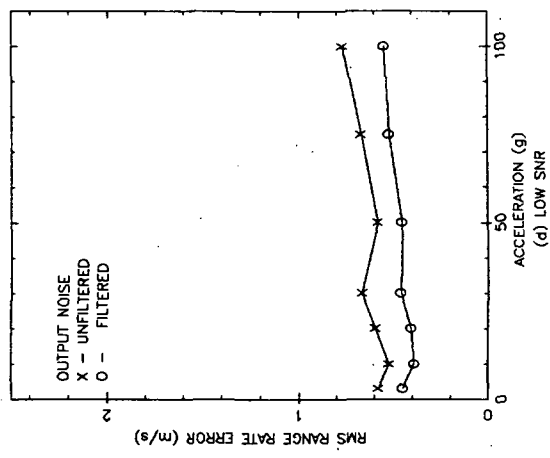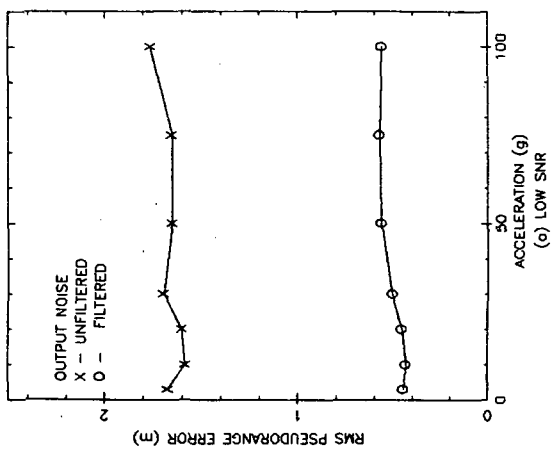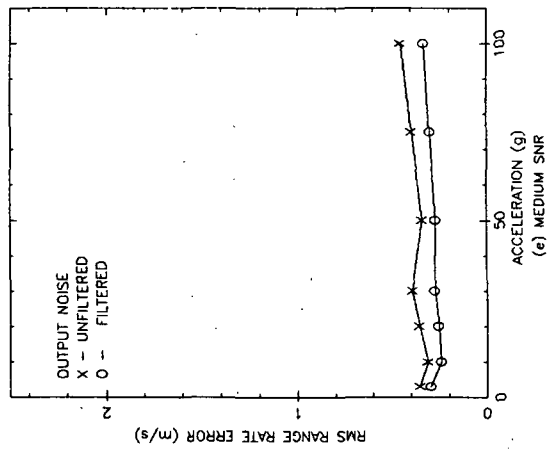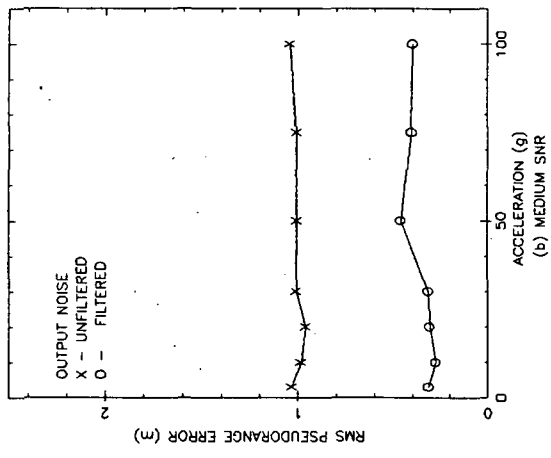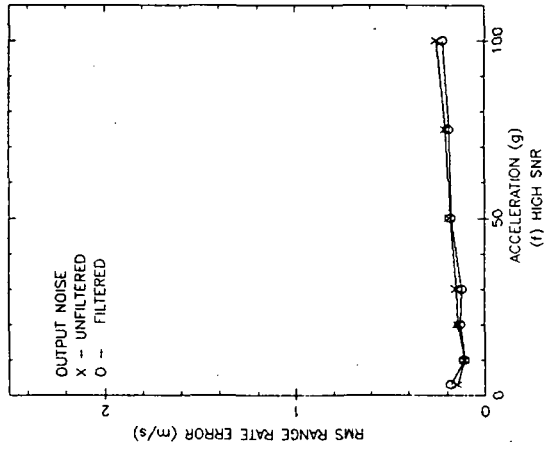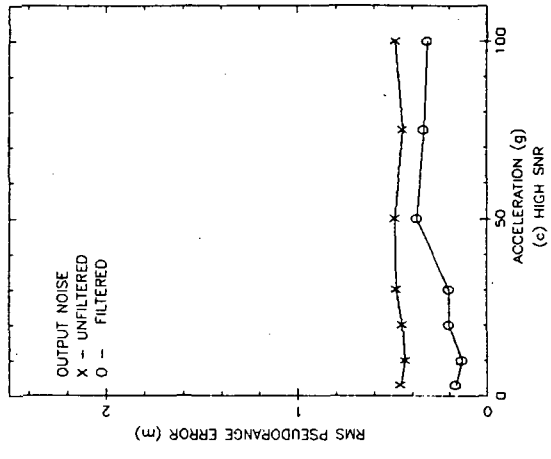
Figure 6-4. Random Errors Versus Acceleration for Step Acceleration Tests
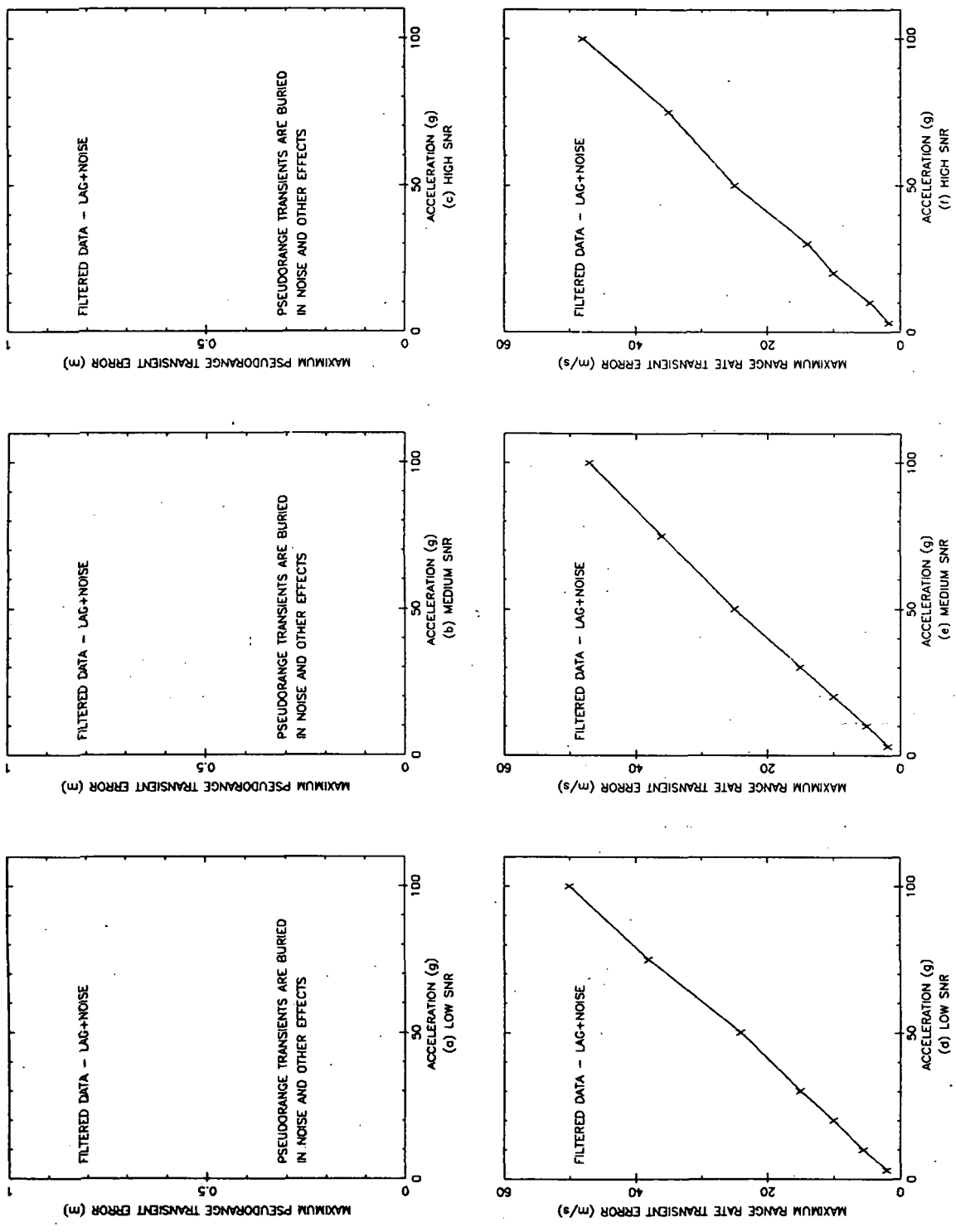
**Figure 6-5.** Peak Transient Errors Versus Acceleration for Step Acceleration Tests
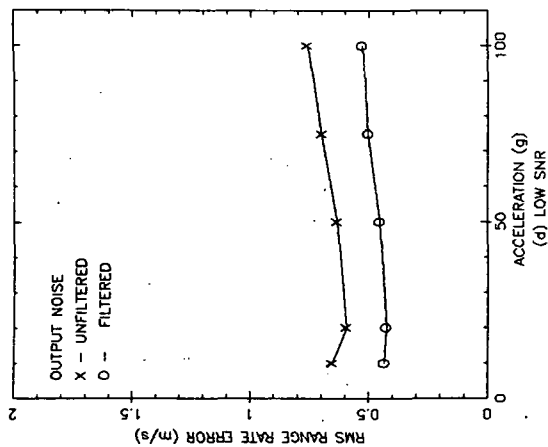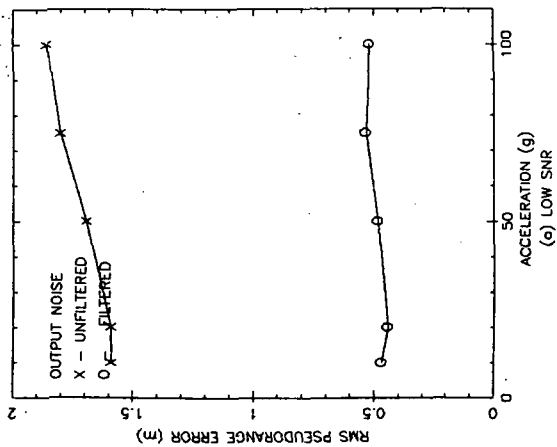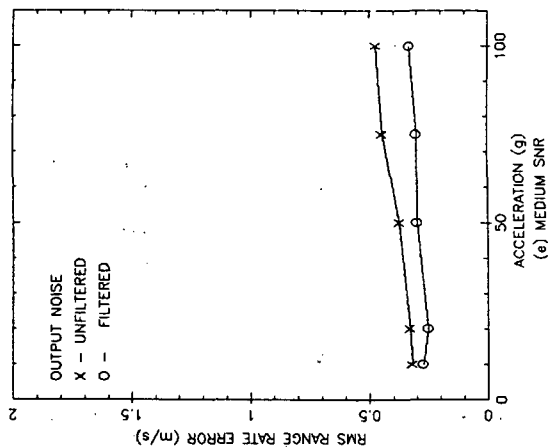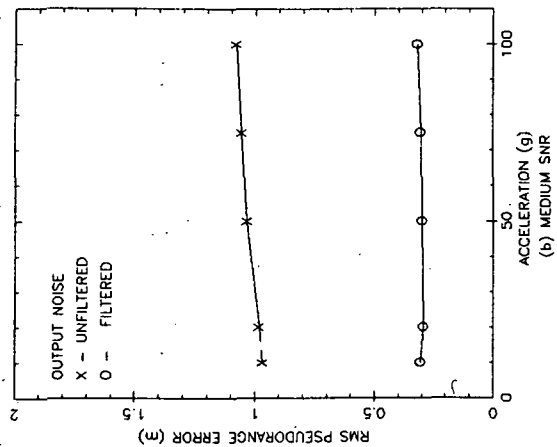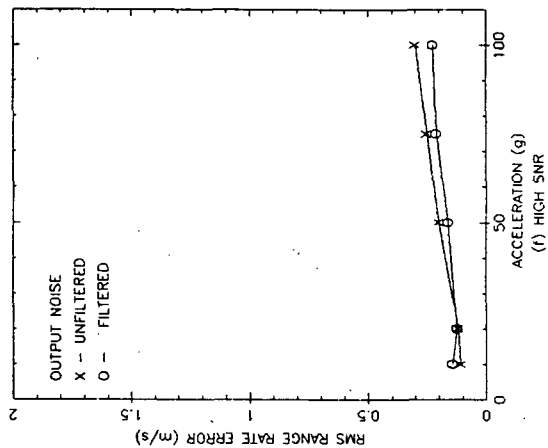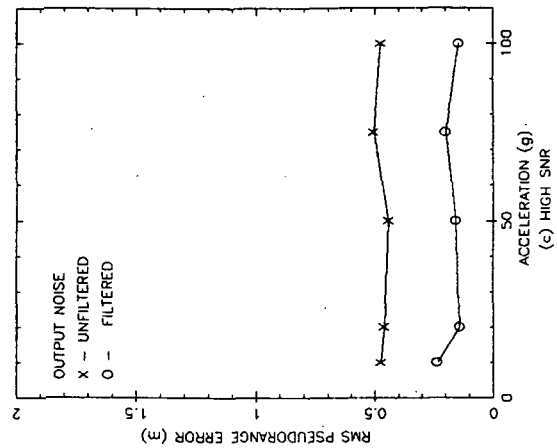
Figure 6-6. Random Errors Versus Acceleration for Circular Motion Tests
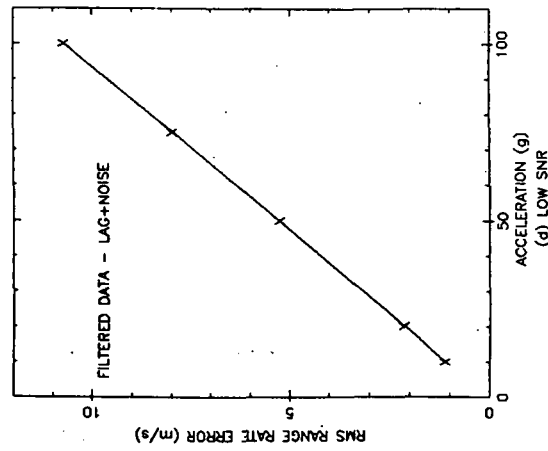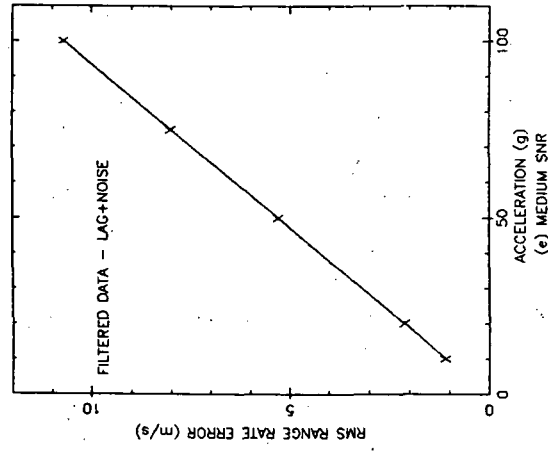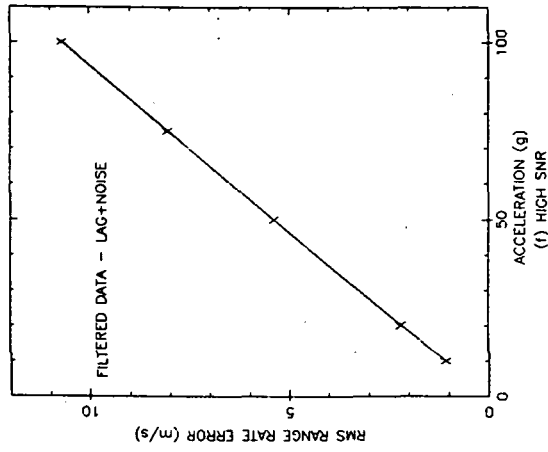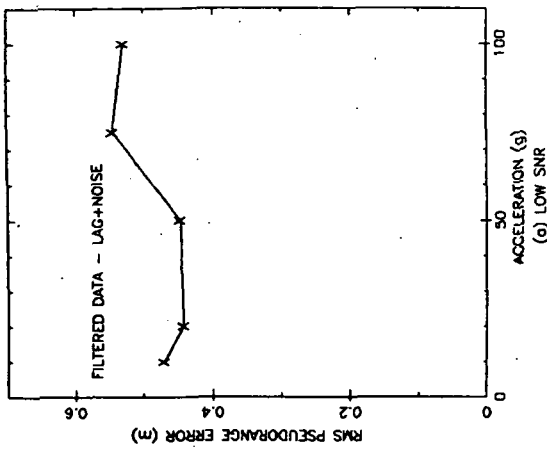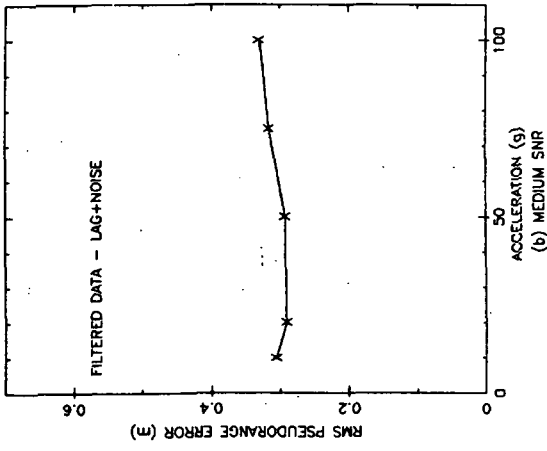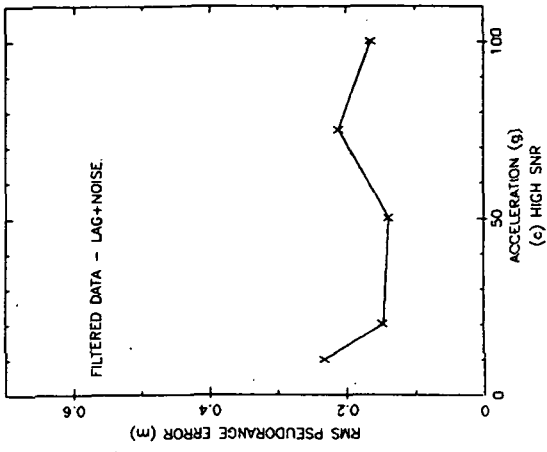
Figure 6-7. RMS Tracking Errors Versus Acceleration for Circular Motion Tests
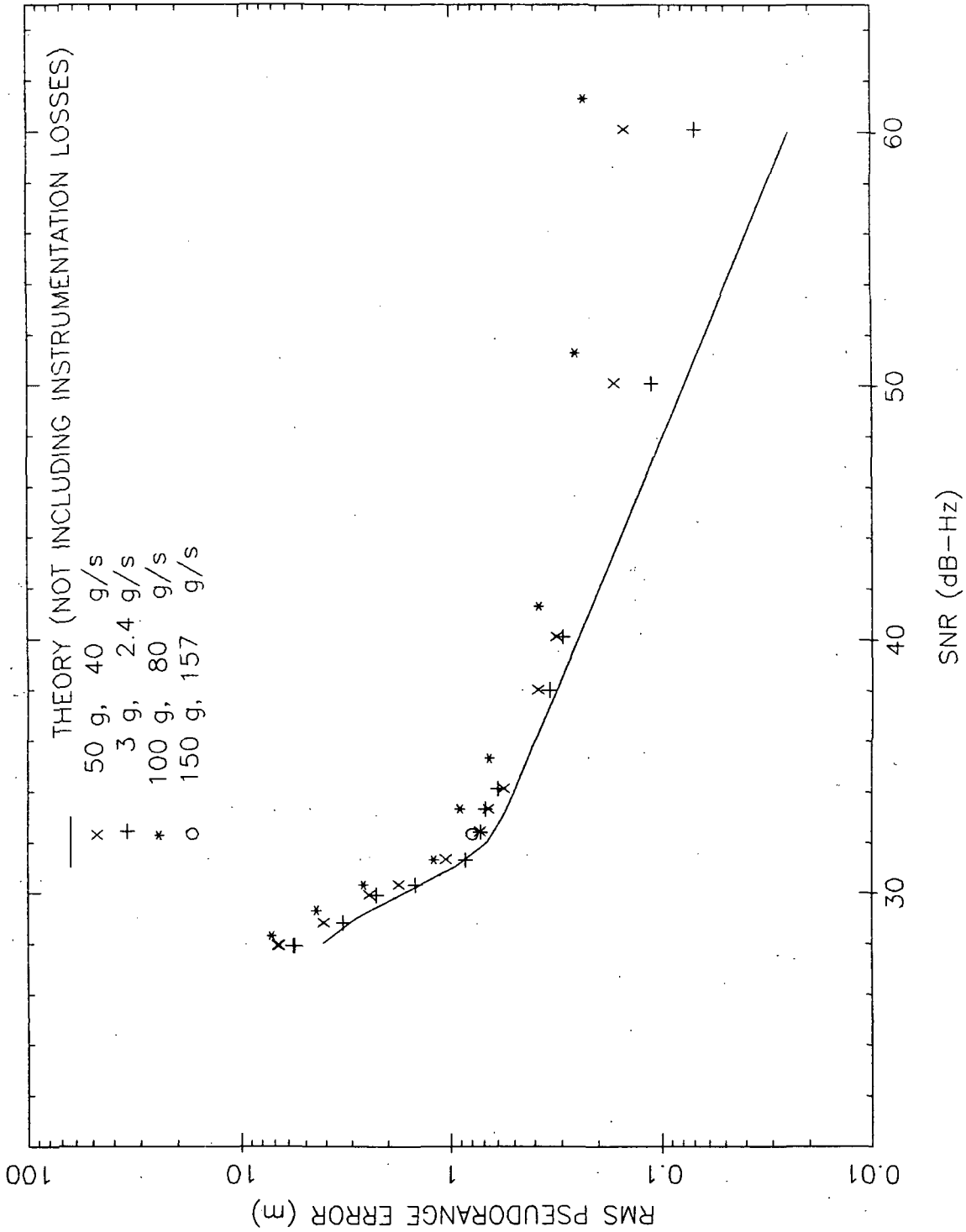
**Figure 6-8.** Pseudorange RMS Error Versus SNR for Circular Motion
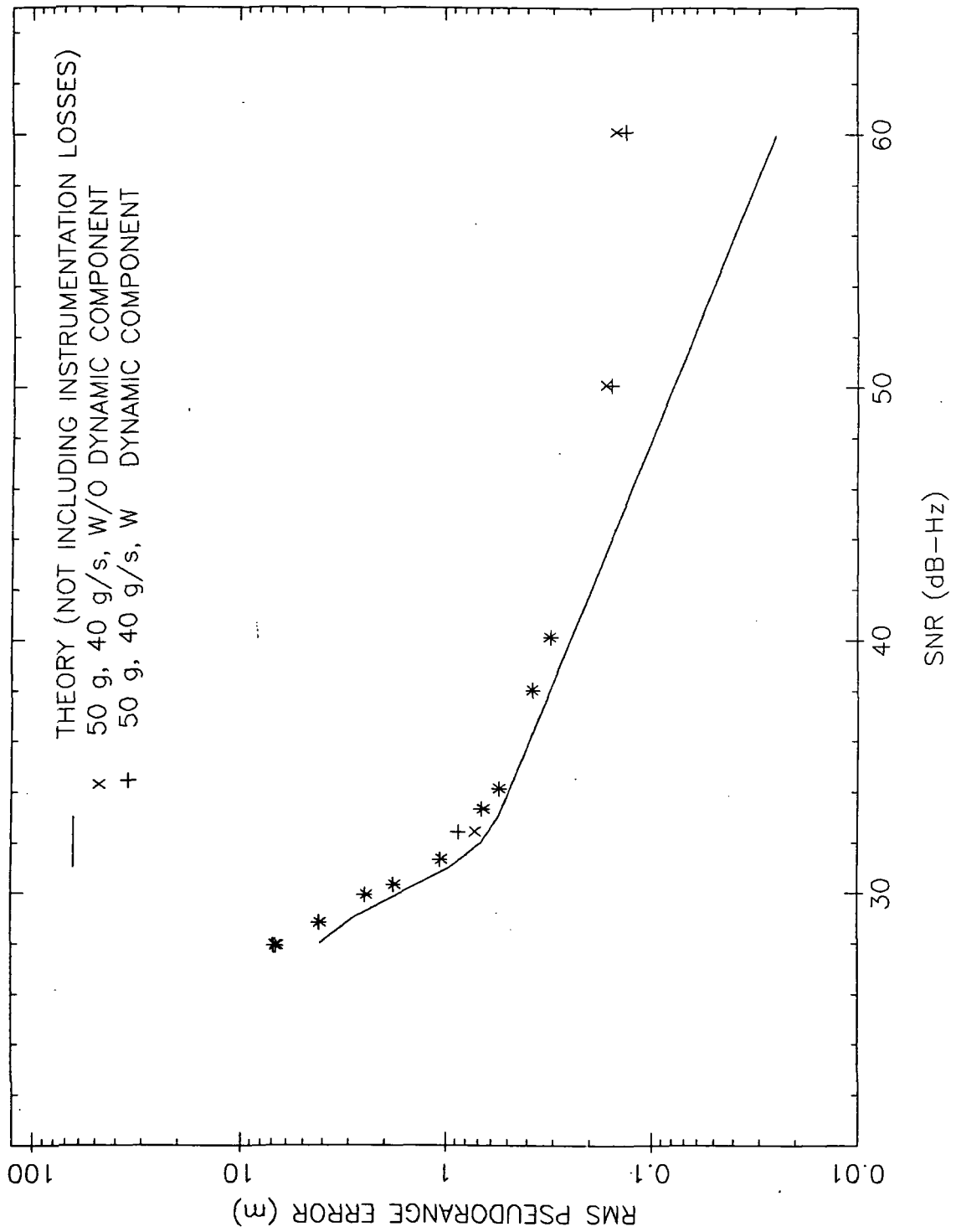
**Figure 6-9.** Pseudorange RMS Error With and Without Dynamic Component

# CHAPTER 7

## A CANDIDATE COMPLETE RECEIVER DESIGN AND MINIATURIZATION

This chapter presents a preliminary design of a candidate complete low volume, high dynamic, GPS receiver, with estimates of size and power. This work was completed and reported orally and in viewgraph form in early 1984, and represents the knowledge at that time. This report specifically does not take into account the recent Armament Division solicitation and specifications for GPS receivers [1], or the resulting selected receiver designs.

Section 7.1 lists major trade-offs in the design of a complete miniaturized receiver. Section 7.2 describes the block diagram design of a GPS receiver consisting of single or dual L-band antennas, RF and digitizer circuits, five signal processors, a navigation and control unit (NCU), and host interface via a 1553 bus. The design emphasizes digital technology and minimizes the analog sections, thus lending itself to miniaturization. Section 7.3 shows that by using advanced technologies such as CMOS processors, gate array and custom VLSI, leadless chip carriers, and two-sided substrate boards, the receiver can be packaged in a small volume. To illustrate this an example is shown of the receiver packaged in a section of an air-to-air missile, using approximately 100 cubic inches of space.

The power estimate for the receiver is approximately 80 W. This estimate is believed to be conservative. More study is needed to refine the power estimate and its accuracy, and to determine whether the heat generated in the receiver can be dissipated in the thermodynamic environment of specific missiles. This work is outside of the current scope.

## 7.1 DESIGN TRADE-OFFS

There are several design trade-offs that have significant effects on the volume, power and cost of the GPS receiver. A full analysis of the cost effectiveness of each trade-off is beyond the scope of this report. The following is a qualitative summary of the relevant trade-offs.

The receiver can operate with a single antenna or with multiple antennas. Additional antennas enhance the operation of the receiver during partial masking of GPS satellites. On an aircraft, antennas may be placed on the top and bottom surfaces, or on the wing tips, so that GPS signals can be received even during banking or rolling. The additional masking immunity has to be weighted against the added hardware and software costs. There are risks associated with adaptive selection of the "right" antenna by the receiver, and in the synchronization of switching between antennas. In our design we elected to use one antenna.

The GPS receiver uses the L2 band signal to calibrate ionospheric delay, thus improving real time accuracy. In range applications, the receiver might perform ionospheric calibration by receiving data from a host vehicle or a control center, or by operating in a differential GPS mode. Furthermore, it may be acceptable to operate with degraded accuracy during real time operation (satisfying the range safety requirements), but achieve full accuracy during post-test analysis when the ionospheric calibration data is added. In our design, we elected to use L2 so that self-contained real time accuracy is maintained.

A factor contributing to the size of the receiver is the presence of L1 and L2 bandpass filters in the front of the RF section. These filters reject out-of-band interference and reduce the risk of pre-amplifier saturation. To achieve low receiver noise temperature, the filters are typically built as tuned cavities with significant volume. In a range missile application it may be acceptable to ignore interference signals, and build the receiver without the bandpass filters. In our design we conservatively elected to include the bandpass filters.

The number of signal processing channels depends on the receiver application. A high dynamic receiver needs four channels to continuously track the four satellites used in the Time-Space-Position Information (TSPI) solution. A fifth channel can be used to search and acquire more satellites, to solve for the ionospheric calibration based on L1-L2 measurements, and to serve as backup during masking. If size and power are not a limitation (such as for a transdigitizer receiver), enough channels can be provided to track all the visible satellites. However, if size and power are at premium, the receiver can be built with only one or two channels with reduced dynamic performance and SNR threshold. We conservatively selected a full five channel receiver.

There are variations in the structure of the signal processor channel. The demonstration system uses an 11-lag correlator, a FFT processor, and an 8086 CPU as key components. The span of the correlator is important during acquisition, but can be reduced during tracking, so a different span can be

used in the final receiver. Doppler frequency detection is performed in a TMS32010 processor using 64-point complex FFTs. If the number of lags and the number of frequencies is reduced, the size and complexity of the interface between the correlators and the FFT processor is reduced, and the processing may be performed by a Discrete Fourier Transform (DFT). In other alternatives, the functions performed by the 8086 might be performed in an 8-bit processor, or the 8086 and TMS32010 functions might be combined in the TMS32010 or an upgraded chip, reducing both size and complexity. We conservatively elected to use the signal processor configuration of the Demonstration Receiver.

There are two schemes to compensate for pseudorange variations during integration time. In the Demonstration, the local code is delayed or advanced when the accumulated pseudorange is an integer number of correlator lags. An alternate approach is to re-clock the received signal at a rate that depends on pseudorange variation. This approach requires more circuitry but improves the threshold. We selected the "code control" method of the Demonstration Receiver in our design.

The TSPI solution can be performed in two ways. One method is to combine all raw pseudorange and range rate data and all orbit data in a single tracking filter residing in the Navigation and Control Unit (NCU). Another method is to smooth the raw pseudorange and range rate in the signal processing channel, and then combine the smoothed results and the orbit data in a NCU TSPI solution, distributing the processing load. We selected the second approach in our design.

## 7.2 CANDIDATE BLOCK DIAGRAM FOR COMPLETE RECEIVER

A candidate top level functional design of a high dynamic receiver is shown in Figure 7-1. The design shown is for a single antenna, five channel, L1 and L2 band, P and C/A code receiver.

The signal from the antenna is amplified, demodulated to in-phase and quadrature baseband components, and digitized in four analog to digital converters. There is only one signal channel for each of L1 and L2 up to this point, not one channel for each satellite. The local oscillators and the sampling clocks are derived in open-loop fashion from a single fixed frequency oscillator, the local oscillators being at the nominal L1 and L2 center frequencies and the sampling clock at twice the P code chip rate. This is a significant simplification over receivers which demodulate the signals from each satellite separately in phase-locked loop channels requiring seperate frequency-controlled oscillators. The receiver has only one oscillator and one frequency generator.

Both P and C/A code signals are recovered through the same baseband circuitry and A/D converters. The outputs of the analog to digital converters are input to five identical tracking processors (TPs), one for each channel. These units implement the approximate ML estimation of the pseudorange and range rate to the satellites. In the implementation shown, the tracking processors also perform the tracking filter function, that is,

they filter the raw estimates to reduce random noise effects. The smoothed estimates of pseudorange and range rate are output to the NCU, which converts them to position, velocity, and clock offset.

The NCU interfaces to a system input-output interface unit, which in turn interfaces to the outside world. The NCU accepts initialization and control from the I/O interface unit, and tracking filter outputs from the tracking processors . It performs all necessary ephemeris, clock and propagation calculations, based either on data received from the I/O interface unit or on data extracted from the satellite data signals. Using this data and the tracking filter output data, it calculates receiver position and velocity, and outputs them to the I/O interface unit along with status information. It also controls the tracking processors, and provides them with pseudorange and range rate estimates during acquisition and reacquisition.

If the implementation is such that all smoothing is done in the NCU, this unit outputs pseudorange and range rate estimates to the tracking processors at all times.

## 7.2.1 RF Modules

Figure 7-2 describes the structure of a RF module. The signal from the L-band antenna is split into L1 and L2 paths, and then band-limited by a narrow bandpass filter (approximately 30 MHz) to reject interference. The filtered signal is split into in-phase and quadrature (I and Q) components, then mixed down to baseband. After the mixers, the signals are filtered by 10 MHz lowpass filters. Each RF module produces four analog baseband signals: L1-I, L1-Q, L2-I, and L2-Q.

## 7.2.2 Analog-to-Digital Converter Module

The Analog-to-Digital Converter (ADC) module described by Figure 7-3 consists of four ADC circuits, one for each incoming signal. The ADCs sample at twice the frequency of the P-code ( 20.46 MHz) and output three bits for each sample of the analog signal.

## 7.2.3 Signal Selector

The signal selector (Figure 7-4) allows the connection of the ADC outputs to the tracking processors. Logically, the signal selector is a switch box with two inputs from L1 and L2, and five outputs to the tracking processors. Each switched output signal is 6-bits wide: 3 bits I, 3 bits Q. The signal selector is controlled from the tracking processors with L1-L2 selection independent for each channel. When expanding the design to two antennas, the signal selector becomes a larger switch with four inputs and five outputs, with independent antenna selection for each channel to optimize SNR performance.

## 7.2.4 Tracking Processor Unit

There are five identical tracking processors, one for each channel.

Each unit accepts the signal from one pair of ADCs via the signal selector, implements the approximate ML estimation of raw pseudorange and range rate, smooths the raw estimates in a tracking filter, and outputs the smoothed estimates to the NCU.

A functional block diagram of the tracking processor is shown in Figure 4-3. The main elements of this unit are the numerically controlled oscillator (NCO), the complex multiplier, the code generator, the correlator, the FFT buffer, the FFT processor and a microprocessor to extract pseudorange and range rate estimates from the FFT outputs and implement the tracking filter.

The first step in the processing is to translate the frequency of the received signal by the previous best estimate of carrier frequency, so that the residual frequency (to be estimated by the FFT) is near zero. This is accomplished by the sine cosine generator and the complex multiplier. The sine-cosine generator generates sine and cosine functions at the current best estimate of carrier frequency, using the tracking filter frequency estimate, or, during acquisition, an input from the NCU. The complex multiplier digitally multiplies the signal input by the cosine and sine functions, considered as a complex numbers, thus accomplishing the frequency translation. The sine and cosine functions are quantized to 3 levels for implementation simplicity, with an SNR loss of only 0.4 dB.

The output of the complex mixer is cross-correlated with eleven lags of the code. The FFT integration interval, equal to the data bit time T, is divided into K subintervals of length T/K, with K chosen to be 32. These subintervals are called correlation intervals. The correlations for each lag are sums over the correlation intervals of the products of the code lags multiplied by the complex mixer output. One effect of the summing is to low pass filter the product signals with a low pass filter of bandwidth $K/(2T)$, which is negligible when the frequency error is small.

The correlator results for each lag are input to the FFT buffer at the end of the correlation interval. These correlation values are then output to the FFT processor one lag at a time. In other words, the buffer can be viewed as a matrix which is filled by the row and emptied by the column.

The FFT buffer outputs are input to the FFT processor. This circuit computes a FFT for each correlation lag, using data from the K correlation intervals. A straightforward FFT over T seconds with K input points results in computing the energy in K filters, each of bandwidth 1/T Hz, spaced 1/T Hz apart. Since the gain responses of these filters cross over at the -4 dB points, causing significant degradation when the actual received frequency is at or near one of these crossover points, additional computations are made to compute the response of additional filters, centered at the crossover points of the original filters. This is done by appending K zeros to the K data points and doing a 2K-point FFT.

There is also a complication because the time delay is not constant over the integration time. At high velocity, the delay can change by several lags in one integration time. To account for this, the code

generator lag is updated each correlation time, rather than each integration time. The average rate of change of code phase is analogous to the code oscillator offset frequency in a code locked loop.

The remaining functions are implemented in the TP microprocessor. The energy outputs of the FFTs are maximized over time lag and frequency to find the correlator time lag and the FFT frequency closest to the actual delay and frequency. The approximate ML estimates are then calculated by interpolation using two adjacent lags and two adjacent frequencies, and output to the tracking filter. The tracking filter is a fixed gain filter operating at an update rate of 50 per second.

## 7.2.5 Navigation and Control Unit

The NCU computes receiver position and velocity from the tracking filter outputs and from the satellite ephemerides, clock offsets, and propagation corrections. In some applications, such as short time-of-flight missiles, the satellite data could be input to the receiver from a host vehicle. These data could also be extracted from the received satellite signals by the tracking processors, but this extraction might not be reliable under extreme conditions of high acceleration and low SNR. The needed data could also be obtained using the receiver itself in an initialization mode prior to launch.

The NCU also interfaces to the receiver input-output interface unit, which communicates with the outside world. It determines which satellites are to be tracked, initializes and controls the tracking processors, performs acquisition in conjunction with the tracking processors, and maintains data bit synchronization. All of these are software implemented functions.

## 7.2.6 Input-Output Interface

The Input-Output Interface unit interfaces between the NCU and the host system. The 1553 bus was selected for this design because it is a standard bus for aircraft. It is a bi-directional high-speed serial bus and is used to interface between the receiver and the host vehicle.

## 7.2.7 Voltage Regulating Module

The voltage regulating module converts the host vehicle's supply voltage to those required by the receiver, at the correct power. It also includes a backup battery for data storage.

## 7.2.8 Clock Module

The clock module, Figure 7-5, uses a crystal as a frequency reference to create the needed clocks. As an example, using a crystal at the P-code frequency, two multipliers create the L1 and L2 frequencies from which one can derive all the other required frequencies.

## 7.3 PACKAGING, COMPONENT COUNT, SIZE AND POWER

This section discusses several advanced technologies that contribute to the packaging of the proposed receiver, proposes implementations of various receiver modules, defines the new integrated circuits that need to be developed, and estimates total volume and power.

### 7.3.1 Technology Review

The recent advances in electronic technology allow for building smaller and denser components both in the digital and analog sections of the receiver.

One of the most power consuming parts in the circuit is the microprocessor (CPU). Recently, Harris introduced a CMOS version of the 8086 processor. CMOS technology reduces power consumption, while the 8086 provides a 16-bit processing capability. Other companies are (and will be) offering similar products.

Many of the 16-bit processors currently available have coprocessors that perform high speed floating point arithmetic. These allow the high update rate for tracking filters, orbit determination, and TSPI solutions. Examples are the Intel 8087 and National's floating point unit.

Only a few years ago, the high cost of development restricted VLSI to products that were manufactured in large volume (e.g. 100,000 or more chips). Today, Gate Array and Semi-Custom technologies reduce the prices substantially. The development of a gate array, with 2500-4000 gates, may cost under $100K and be more cost effective than Medium Scale Integration/Small Scall Integration (MSI/SSI) circuits for production of as few as 100 to 1000 units.

Many new ICs are offered in Ceramic Leadless Carrier Chip (CLCC) packages in addition to the standard dual-in-line package (DIP). The new package offers reduced area and volume. Typical volume improvement is 8:1 over DIPs and 2:1 over Ceramic Flatpacks. In addition, the CLCC package allows for better thermal management. In surface mounting, the CLCC uses more area than silicon dice, but is easier to mount and replace.

Hybrid technology combines several components on a single substrate, where the interconnection patterns are photo-etched. The components can be complex (e.g. VLSI dice) or simple (e.g., resistors, transistors). This technology allows for mixing of digital and analog components, in a manner similar to a printed circuit board.

The dense packaging of RF circuits is facilitated using micro-strip circuits. These are hybrid circuits using microwave components, such as power-splitters, filters, amplifiers, and mixers.

Monolithic Microwave Integrated Circuits (MMIC) are the analog equivalent of MSI/SSI. A typical MMIC replaces a whole microstrip on a

single die of silicon or GaAs. The technology is new but not beyond the current state-of-the-art.

### 7.3.2 Module-by-Module Design And Estimates

The following are implementation schemes for each of the functional blocks described in Section 7.2. The implementation uses components that are either available now or in the near future. The component selection is tentative and depends heavily on the selected microprocessors and VLSI components. Table 7-1 summarizes the new VLSI circuits that need development.

Table 7-1
Summary of New IC Development

| Function | Module | Number |
|---|---|---|
| Routing of a signal from ADCs to TPs | Signal Selector | 1 |
| Code generator, mixer, computer interface | Tracking Processor | 1 |
| Controls for the FFT buffer | Tracking Processor | 1 |
| Correlator | Tracking Processor | 1 |
| Tracking processor interface to the NCU | Tracking Processor | 1 |
| Interface inside the Tracking Processor | Tracking Processor | 1 |
| NCU interface to 1553 | I/O interface | 1 |
| Interfaces inside NCU, NCU to signal selector and tracking processors | NCU | 1 |
| Digital divider chains | Clock | 1 |
| Total | | 9 |

In each module the design includes major components and also some discrete components for biasing, surge protection, etc. The microprocessors selected are in the Intel 8086 family. Similar designs can be made with National Semiconductor (NSC) 32016 or Motorola's MC68020. Gate arrays have 2500 to 8000 equivalent gates per device and are available from companies such as Hughes, Harris, Motorola, LSI systems, and NSC. The memory components used in the rest of the discussion are NSC's 8Kx8 static CMOS RAM NMC6164 and Advanced Micro Devices' 64Kx8 EPROM AM67512. We assume each new VLSI chip to be CMOS and to consume 0.25W.

## 7.3.2.1 RF Module

The RF module is estimated to consume 10 W. The input stages are tuned cavity bandpass filters to minimize the noise temperature. The rest of the circuit can be mounted on a microstrip: the intermediate bandpass filters are side-coupled L-band photo-etched filters and take approximately 2 in.$^2$ for each, the lowpass filters are discrete component LC filters, requiring approximately 1 in.$^2$ each.

## 7.3.2.2 ADC Module

Each ADC module uses four 6-bit ADC chips (Analog Devices AD9000), a voltage reference, two operational amplifiers, and the associated resistors and capacitors. The total power for each module is estimated to be 5 W. For the two-antenna receiver, the reference circuitry need not be duplicated in the second ADC module.

## 7.3.2.3 Signal Selector

The signal selector has two 6-bit inputs, five 6-bit outputs, a 5-bit control word (1 bit per tracking processor), and power connections. It can be implemented using a single gate array, consuming 0.25W.

## 7.3.2.4 Signal Processor

The signal processor is implemented as follows:

1. The correlator uses one semi-custom VLSI chip or 1 to 2 gate arrays. Cell count indicates that, even using an 8000-gate device, two gate arrays may be needed. They would be identical.

2. The FFT buffer uses three chips. The memory portion uses two RAM devices to implement 16-bit access, while the control portion uses a single gate array chip. The total memory size is 4 to 8 Kbytes.

3. The FFT uses one processor and two ROM chips. The processor is the Texas Instruments TMS32010, used in the Validation Demonstration.

4.  The NCO is a single chip, Stanford Telecommunication Inc. ST-1172. This is a CMOS device that is used in the Validation Demonstration.

5.  The code generator uses a single gate array device. It creates the P-code and C/A codes and, under computer control, advances or retards them to compensate for Doppler shift. The code generator also controls the location of the bit synchronization pulse. The mixer is part of the code generator gate array.

6.  The computer consists of a CMOS CPU (Harris 80C86), two chips of program memory, (128 KBytes), four chips of data memory (32 KBytes) and two gate array chips. One gate array is dedicated to the interface to the NCU, while the other performs all the interfaces inside the signal processor. It may be possible to combine the two gate arrays into a single chip.

The tracking processor uses a total of 18 to 20 chips, mostly CMOS. The total estimated power is 5 W.

### 7.3.2.5 NCU

The NCU consists of a CPU (Intel 80286), a floating point coprocessor, two chips of program memory (128 Kbytes), eight chips of data memory (64 KBytes), and one gate array chip, for a total of 13 chips. The gate array chip performs all the interfaces within the NCU and between the NCU and the tracking processors and signal selector. The estimated NCU power consumption is 5 W.

### 7.3.2.6  I/O Interface

The 1553 I/O interface can be implemented with commercial hybrid components and a single gate array chip. For example, ILC Data Device Corporation manufactures a DDC65122 that, with the addition of two line transformers (DDC25679), provides a complete 1553 interface. The volume for the three components is 1.22 in.$^3$ and the required power, for 25% duty cycle, is 7 W. The gate array chip performs all the interface functions between the NCU and the DDC65122.

### 7.3.2.7  Power Distribution Module

To obtain high efficiency, a switching power supply must be used. It is projected that 80% efficiency can be achieved.

### 7.3.2.8  Clock Module

The clock module consists of analog and digital sections. The analog sections are on a microstrip and consist of five frequency multiplying circuits. Each circuit has an amplifier, a frequency multiplier, and a

band pass filter, and takes approximately 2 to 3 in.$^2$. The digital section consists of a single gate array circuit chip.

### 7.3.3  Packaging, Volume and Power

This section illustrates the packaging of the receiver in a section of an air-to-air missile. As shown in Figures 7-6 and 7-7, the components are mounted on circular plates (substrates). The plates can be single- or dual-sided, depending on the thermal environment. At the edge of each plate, space is provided for an interconnection harness. Each plate has 17 to 19 in.$^2$ of usable area and can contain, for example, 20 44-pin VLSI packages.

The RF module can be packaged on two single-sided plates. The ADC modules and the signal selector occupy one single-sided plate. Three double-sided plates are used for the five tracking processors, the NCU, and the I/O interface. The clock module occupies a single-sided plate.

We assume that each plate occupies 10 in.$^3$ (i.e., a cylinder of 5 in. in diameter and 0.5 in. height). Then all the electronics discussed above requires 70 in.$^3$. Adding 30 in.$^3$ for the power distribution module, the total volume is approximately 100 in.$^3$. The heights of the individual plates may be adjusted to provide better heat distribution or easier access.

The power dissipation is estimated as follows. Each of the tracking processors consumes approximately 5 W. The NCU also consumes approximately 5 W. Adding the power used by the other modules and considering the efficiency of the power distribution module, the total power is approximately 80 W. Table 7-2 summarizes the volume and power estimates.

There is concern about dissipation of the estimated power in the limited volume, and in the missile environment. To refine the estimates would require:

    1.  Definition of the thermal environment, e.g., missile skin temperature, duration of operation etc.

    2.  Definition of the specific components to be used, rather than using assumptions such as 250 mW per gate array chip. This will affect the number of components as well as power.

    3.  Refined power estimates for the microstrip circuits in the RF and clock modules.

This work is outside of the scope of the present task.

Table 7-2
Volume and Power Estimates

| Module | Volume (in.$^3$) | Power (W) |
|---|---|---|
| RF | 20 | 10 |
| ADC and signal selector | 10 | 10 |
| Tracking processors (5) | 25 | 25 |
| NCU and I/O interface | 5 | 12 |
| Clock | 10 | 7 |
| Power Distribution | 30 | 16 |
| Total | 100 | 80 |
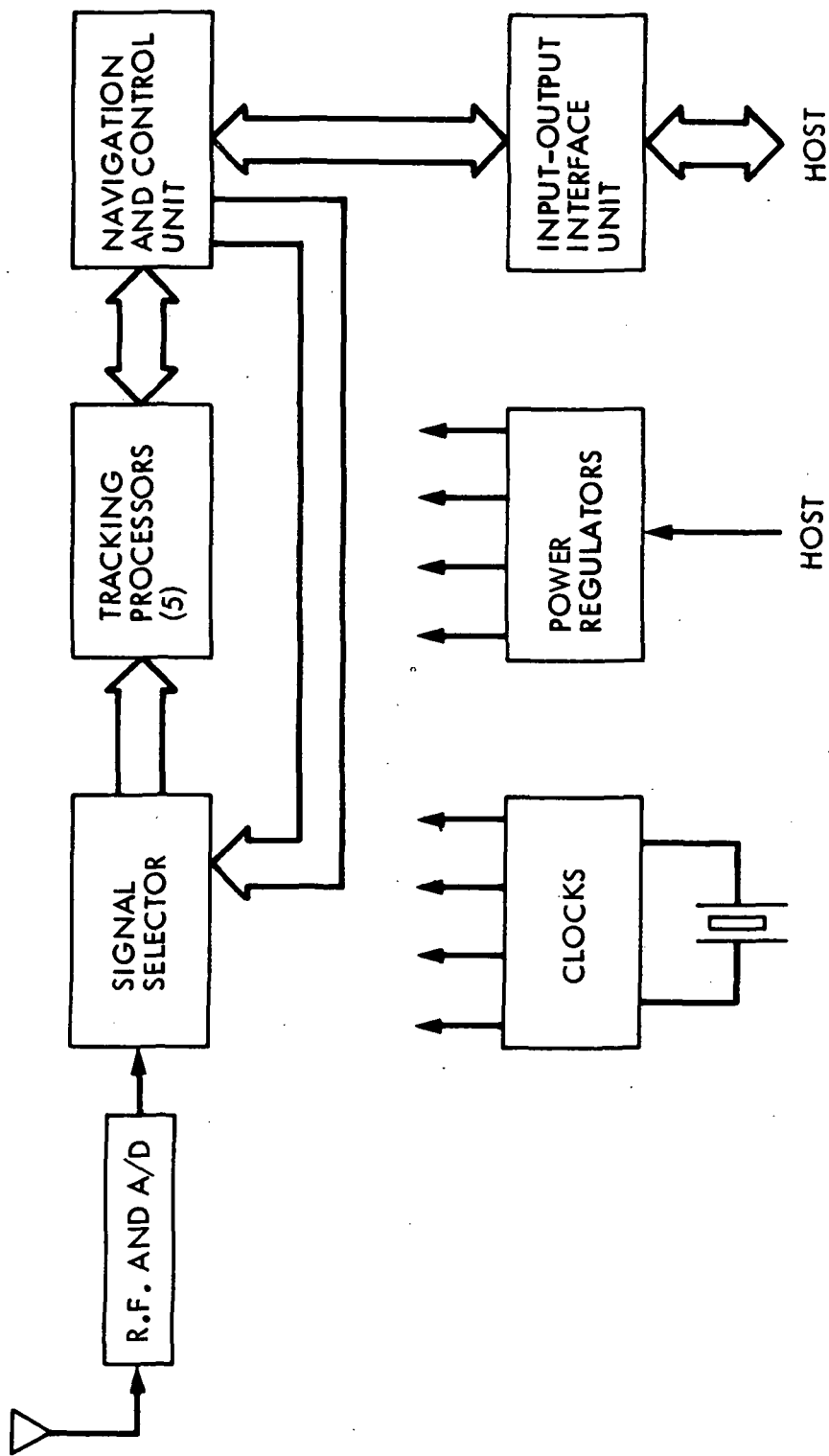
Figure 7-1. GPS Receiver Functional Block Diagram

Figure 7-2.    RF Module

SAMPLING CLOCK
(f = 20.46 MHz)

REFERENCE VOLTAGES

L1-I SIGNAL

A/D

3-BIT SAMPLES

L1

L1-Q SIGNAL

A/D

L2-I SIGNAL

A/D

L2

L2-Q SIGNAL

A/D

Figure 7-3.   Analog to Digital Converter Module

Figure 7-4.    Signal Selector

Figure 7-5. Clock Module

POWER CONVERTER

CLOCK MODULE

PROCESSOR (2)

PROCESSOR (2)

PROCESSOR (2)

RF AMP & A/D CONVERTER

RF AMP & A/D CONVERTER

5.75 in.

5.00 in.
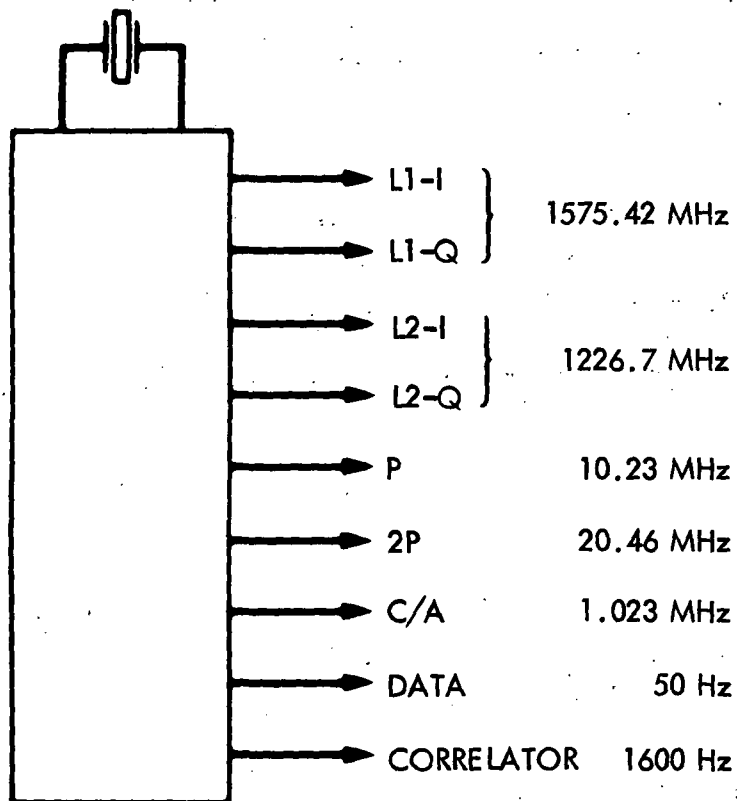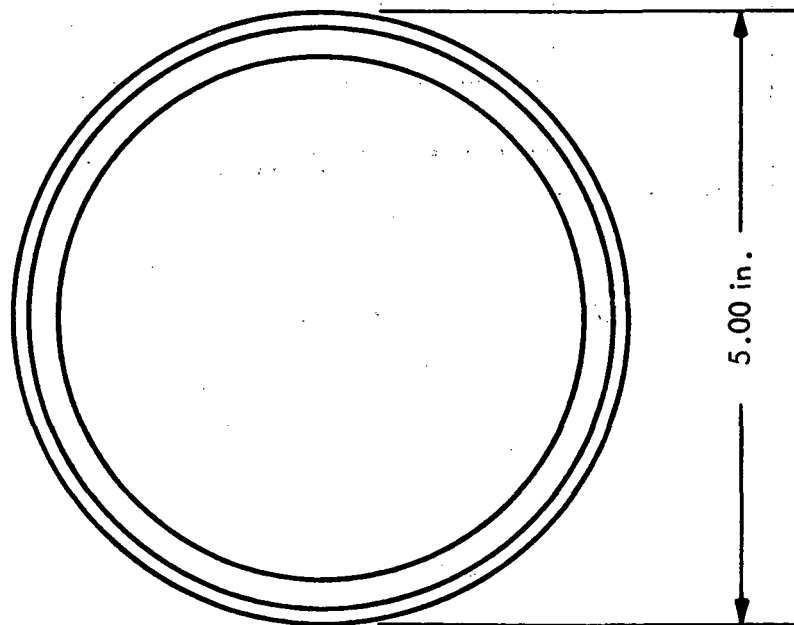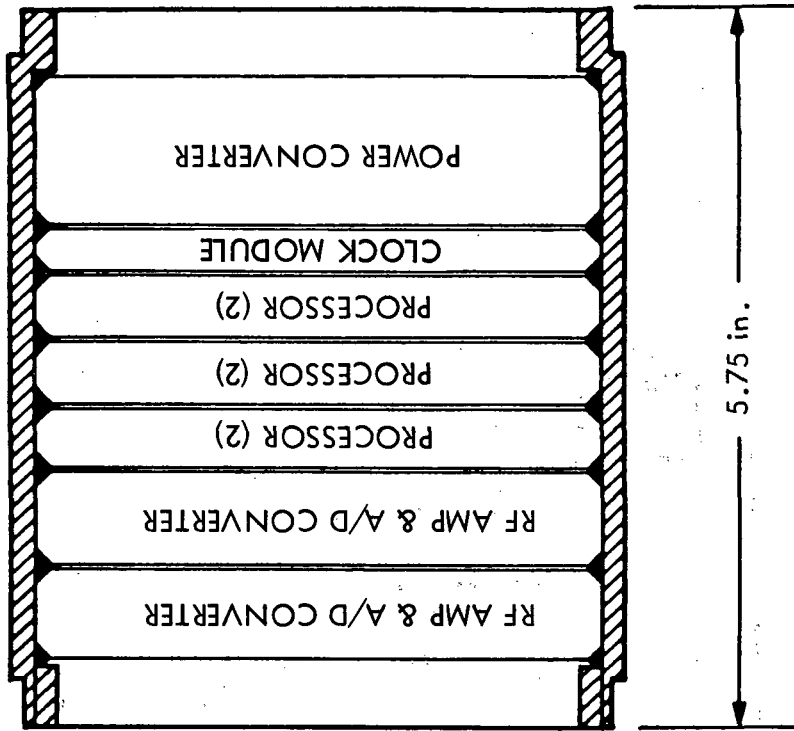
Figure 7-6.   Receiver Packaging Concept

C-2
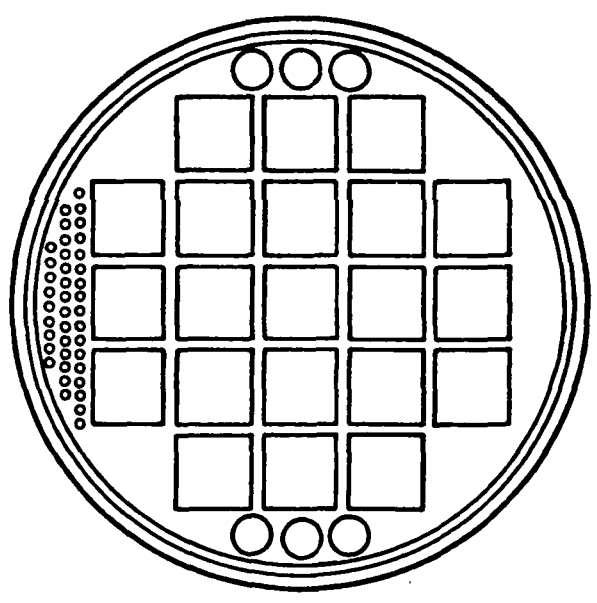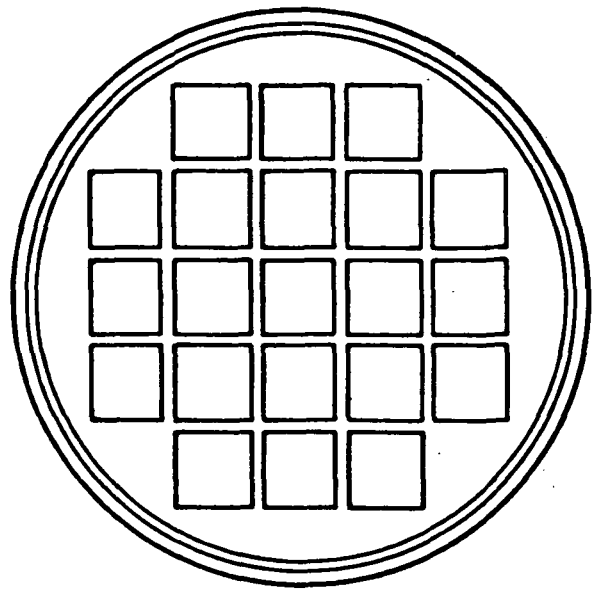
Figure 7-7. Packaging Concept for Tracking Processors

# CHAPTER 8

## OPEN QUESTIONS AND FUTURE WORK

The Demonstation has not answered all questions about GPS receivers, and, indeed, has generated new ideas for potential improvements. This chapter briefly discusses some open questions and suggestions for answering them. The issues are categorized as applicable to a high dynamic P code receiver, to an optimized P and C/A code receiver, to a transdigitizer receiver, and to a miniaturized receiver.

## 8.1 HIGH DYNAMIC P CODE RECEIVERS

The Demonstration Receiver tracks only on the P code, although the C/A code would be used for acquisition in an implemented receiver. This section discusses potential improvements which can be realized while tracking P code only.

### 8.1.1 Critical Velocity Problem in Demonstration Receiver

The Demonstration Receiver has higher errors and higher SNR threshold when the pseudorange rate is approximately 1800 m/s, and at multiples of this rate. There is no problem at other rates tested, up to the maximum test rate of 10,000 m/s. Analysis and simulations did not reveal the same behavior. Therefore, the behavior is believed to be caused by an instrumentation effect peculiar to the hardware. The problem could be either in the Receiver or in the TIS. The problem is not believed to be fundamental to the receiver design, but it should be resolved.

### 8.1.2 AMLE Parameter Optimization

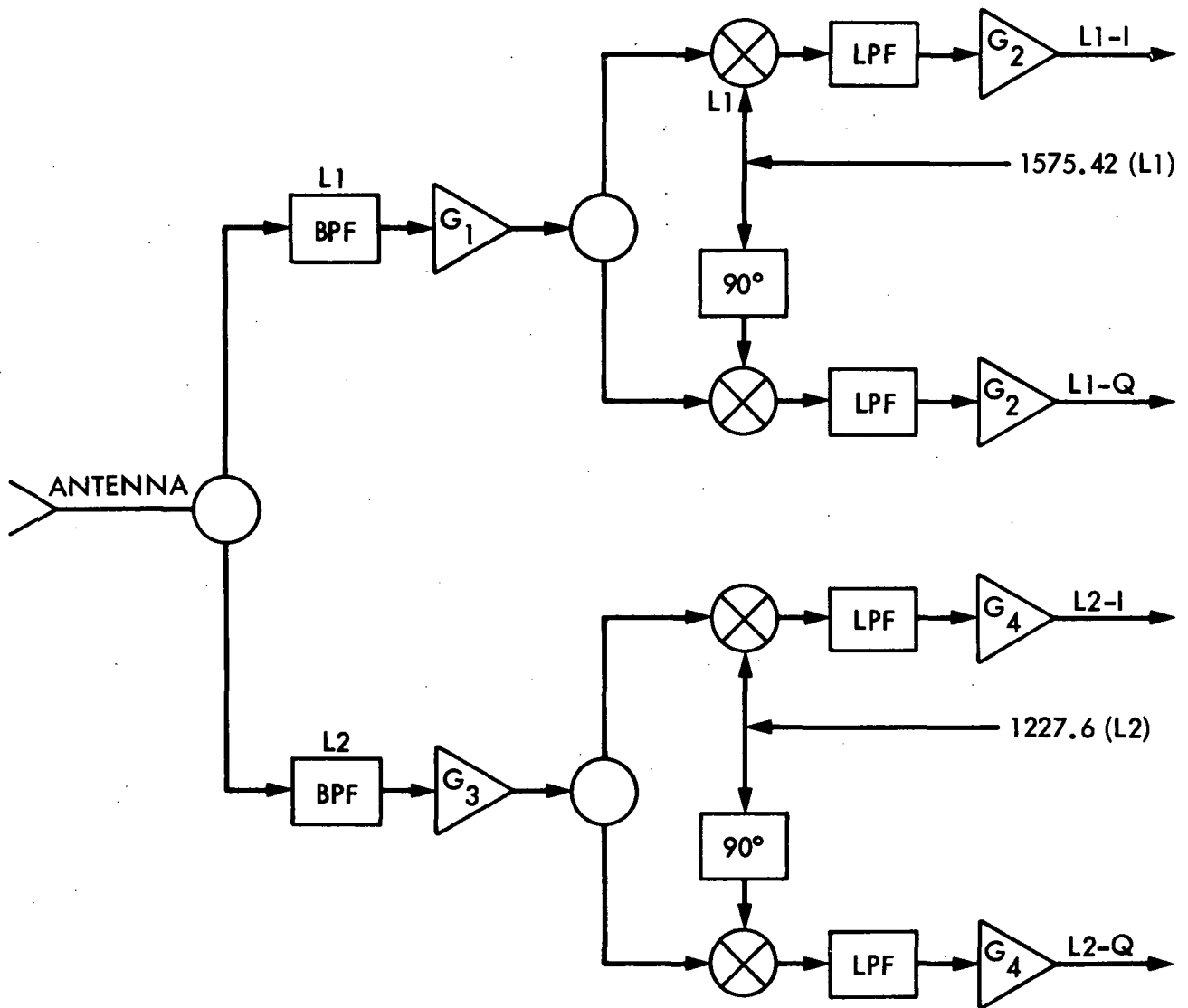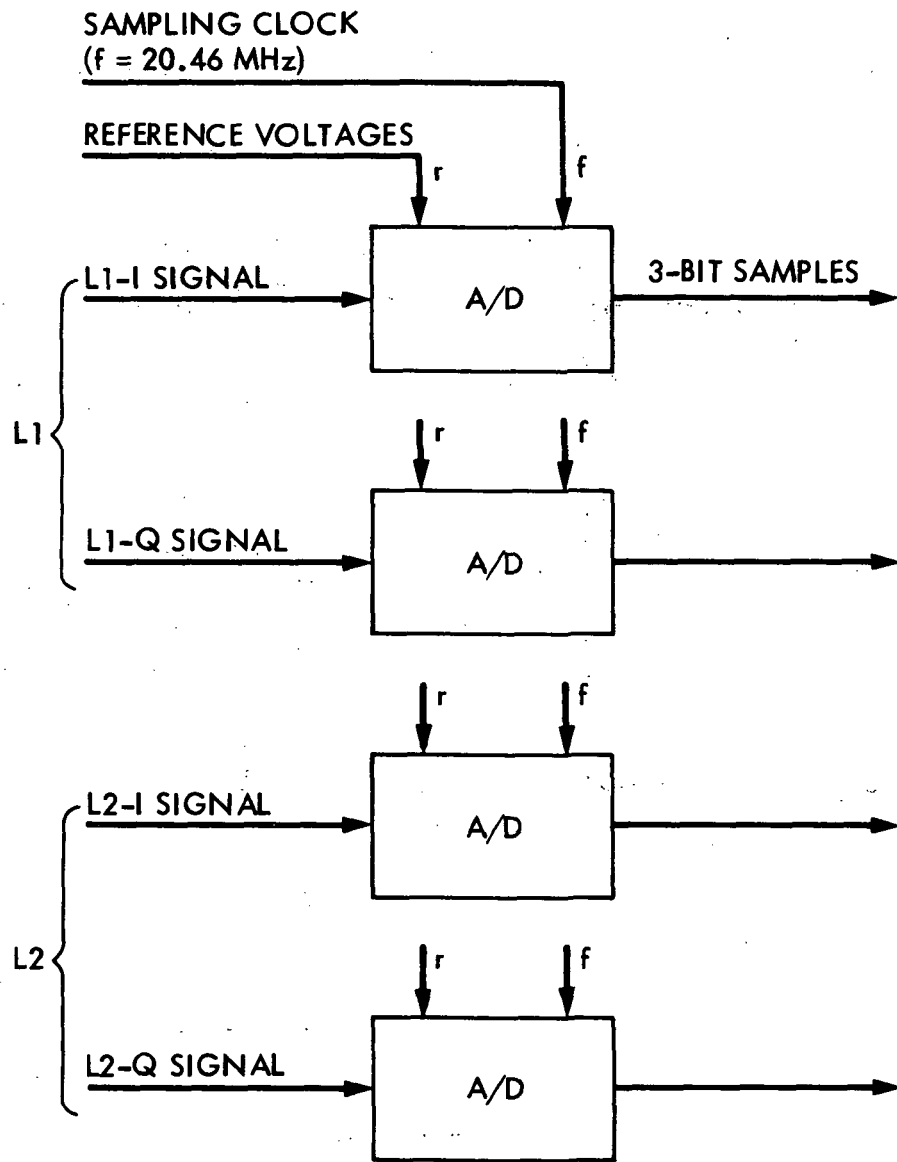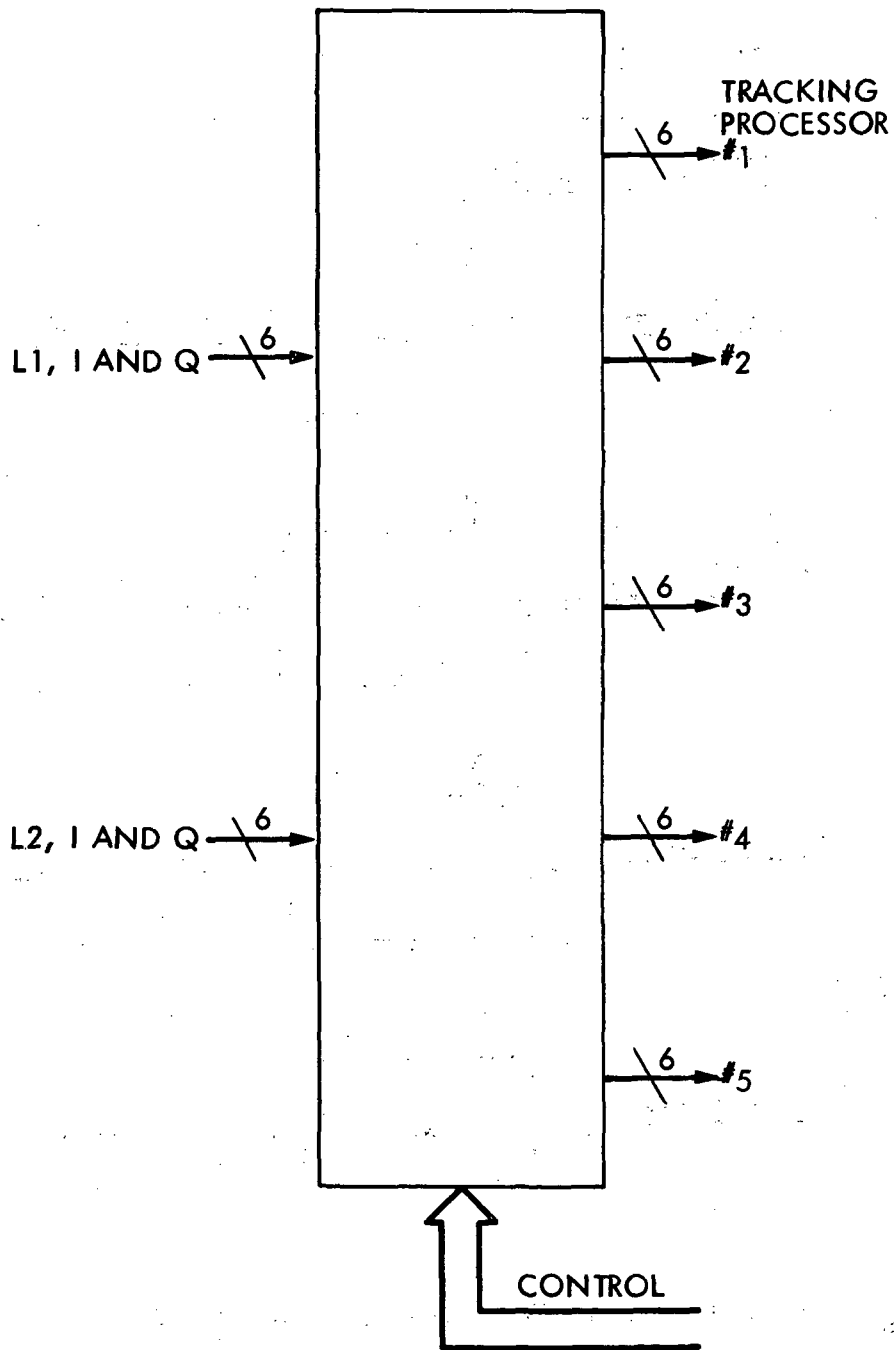The AMLE in the Receiver maximizes over nine correlator lags and 64 frequencies. Higher jerk or step acceleration can be tracked if the frequency range is widened. The penalty in performance is that threshold SNR would increase slightly, because there would be more places for outliers to occur. On the other hand, some reduction in threshold SNR can be achieved by reducing the number of correlator lags, with three lags probably being sufficient after acquisition. The number of frequencies can also be reduced when the maximum dynamics are less. These trades should be investigated by simulations. Experimental verification with reduced number of correlator lags would be easy to do with the Demonstration Receiver, but changes in the frequency domain would be more complex. Increasing the range in the frequency domain would require more points in the FFT.

### 8.1.3   Tracking Capability and Oscillator Effects

Further refinement of the tracking filter is desirable.  Also, the performance should be determined for trajectories with different dynamics, and for the situation in which oscillator frequency offsets occur due to acceleration.  These oscillator frequency offsets appear to the receiver as changes in velocity.  Thus a step acceleration would cause the signal processing to see what appears to be simultaneous steps in frequency and acceleration.  For an oscillator sensitivity of $2 \times 10^{-9}$/g, a 100 g step acceleration would cause a maximum frequency shift of 315 Hz, which is well within the range of the FFT in the AMLE, so no problem is anticipated. Performance should be verified both by simulations and by receiver tests.

### 8.1.4   Phase Coherent and Adaptive Tracking

As discussed in 5.4.3, the Receiver is inherently capable of phase coherent tracking when dynamics permit.  Various phase locked loops should be compared analytically and by simulation, and dynamics capabilities determined.  Stability is a concern, because of the transport delay in the AMLE, loop filter calculations and NCO, and because the desired loop bandwidth for high dynamic tracking is not very small compared to the loop filter update rate of 50/s.  One way to add coherent tracking without sacrificing maximum dynamics would be to adaptively switch between frequency and phase tracking, depending on dynamics and SNR.

### 8.1.5   Parallel FLL and PLL Tracking, and Smoothing

High dynamic FLL tracking and phase coherent tracking could be conducted in parallel.  The receiver would operate as demonstrated to achieve high dynamics and low SNR threshold capability.  In parallel with this, the receiver would track carrier phase in software, without feedback. The velocity measurement capability of a PLL would be achieved without the loss of lock problems.  Loss of phase lock would occur under some conditions, but would cause only a temporary loss of accuracy in measuring velocity and acceleration.  Tracking would continue with the FLL.

A further refinement could be accomplished by using a Kalman or other type of smoothing filter.  A smoothing filter uses data acquired up to the present time to estimate parameters for an earlier time.  Smoothing filters are better than standard tracking filters both in their errors due to random noise and in dynamic response.  Improvements of 6 dB or more are possible [8].  This benefit could probably be realized with a delay of approximately 0.5 s.  There is some cost in complexity.  Considerable analysis and simulation is required to determine feasibility, cost and benefits.

### 8.2   COMBINED P AND C/A CODE TRACKING

Combined P and C/A code tracking, discussed in 5.4.4, has the potential to reduce tracking SNR threshold by 4.8 dB relative to the received P code power, or relative to the total received L1 power.  This can be accomplished either for the demonstrated FLL tracking, or using PLL

tracking. What is necessary is to correlate the received signal against the P and C/A codes simultaneously, and to combine these correlations in the proper phase. Separate correlators are required for the two codes, or else a more complicated correlator is required that can process both codes simultaneously with proper carrier phase. Performance should be established by simulation. Verification with actual satellite signals is desirable.

## 8.3 ENHANCEMENTS FOR TRANSDIGITIZER RECEIVERS

The following potential enhancements are particularly applicable to transdigitizer or translator receivers.

### 8.3.1 Optimum C/A Code Pseudorange Estimation

The performance of the AMLE or of a delay locked loop can be improved by reducing the correlator lag spacing. This is mentioned in 5.4.1, and the expression for rms pseudorange error in Appendix B includes this effect. The rms pseudorange error is proportional to the square root of the lag spacing, when the lag spacing is not too small, when the SNR is sufficiently high, and when the received signal is not bandlimited.

The key requirement appears to be received signal. Suppose the C/A signal were received with a 10 MHz bandwidth and sampled at 20.46 MHz, as in the Demonstration Receiver. Using a lag spacing of one sampling time results in 20 correlator lags per chip. There is a potential gain of root 10 over a typical two lag per chip implementation. Since the theoretical rms pseudorange error at an input SNR of 32.5 dB-Hz is less than one lag spacing, it appears likely that most of this theoretical improvement could be realized. This gain is most likely realizable in a receiver which uses only the C/A code but is not bandwidth limited. In a translator or transdigitizer receiver, the bandwidth is limited. Analysis and simulations are in order to see how much improvement can be realized.

### 8.3.2 Code Locking and Restricted Sampling Rates

The main concern addressed here is that the sampling rate of a transdigitizer might not be compatible with the Demonstration Receiver, and that the Receiver sampling rate might not be compatible with the HDIS sampling rate. This would complicate possible modifications to the HDIS to include the high dynamic tracking capability. These concerns are unwarranted.

The Demonstration Receiver does not code delay lock in the usual sense. Instead, code delay for each data bit time is quantized to the lag spacing. In delay locked loop implementations, code phase is maintained as close as possible to the received code phase.

As implemented, operation of the Demonstration Receiver depends on having the sampling rate be twice the nominal chip rate. Other digital receivers typically offset the sampling rate from twice the chip rate. What is important here is that there is no fundamental reason why the high

dynamic tracking concepts cannot be used with other sampling rates and with the usual type of code locking. The cost would be in required correlator speed, since the half speed correlation technique used in the Receiver would not be applicable. It is likely that there would be a reduction in instrumental pseudorange bias. Thus the high dynamic concepts could be incorporated using the sampling rate of the HDIS and a matched transdigitizer.

### 8.3.3 Smoothing

Kalman, or other least squared estimator, smoothing would be ideal for use in a transdigitizer receiver. The delay of under 1 s would be acceptable. The added computational complexity could be tolerated, because size and production cost are not critical. Both real time and delayed solutions could be provided. Smoothing could be used either with phase locked or frequency locked tracking, or with both. It would also be possible to use a different time constant for the delayed solution than for the real time tracking, or to use an adaptive smoother. It may be possible for the near real time smoother solution for a C/A code transdigitizer receiver to be comparable in accuracy to a P code receiver. This deserves serious investigation.

### 8.3.4 Data Aiding

A PLL transdigitizer should have the capability of using data aiding from a local reference receiver. However, it is desirable that the receiver also be capable of achieving good performance without this aiding. This would probably improve reliability and operability. One of the inherent disadvantages of data aiding is the delay or transport lag introduced, which reduces the dynamic tracking capability of a PLL. Use of the frequency locked high dynamic tracking concepts for real time tracking, and phase locked tracking with data aiding and smoothing, may be ideal.

### 8.3.5 Fast Acquisition and Reacquisition

Fast acquisition and reacquisition are required in a high dynamic transdigitizer receiver. One of the key advantages of using a transdigitizer receiver rather than a receiver on a vehicle is that it is much more feasible to achieve fast acquisition in a ground based receiver.

The Demonstration Receiver concept is ideal for fast acquisition. The multiple lag correlator and the FFT are inherent to the architecture. More correlator lags and more FFT frequencies need to be implemented. Fastest acquisition is obtained by correlating against all lags of the C/A code simultaneously, and performing all FFTs in real time. Since acquisition ideally should be possible at all SNRs at which tracking is possible, an integration time of 0.1s to 0.2 s is desirable. Complete acquisition could be accomplished in under 0.5 s.

The above completely parallel acquisition is probably unnecessary. Searching of approximately one-tenth of the delay-frequency bins in

parallel would result in acquisition time of 1 s to 2 s. Since the same FFT computations are required regardless of the order of bin searching, it is hardware-efficient to build a limited number of correlator lags and to do the FFTs for all of these lags in parallel. Computation of all required FFTs is feasible with current technology. Possible approaches are special purpose logic, parallel signal processing microprocessors, or array processors. The challenges are in determining realistic requirements, and then in meeting them at low cost.

## 8.4 MINIATURIZATION

The packaging study of Chapter 7 accomplished its goal of establishing the feasiblity of a 100 in.$^3$ high dynamic receiver. Determining the minimum possible size was outside of scope. Also, significant technology advances have occurred since the packaging study was conducted. Finally, there is a program to develop 6 in.$^3$ receivers, sponsored by the Defense Advanced Research Projects Agency (DARPA). The DARPA receivers have either single or multiple channels, include front ends, control, display and batteries, and have power consumption consistent with the volume. A very rough estimate is that a high dynamic receiver would be 1.2 to four times more complicated than the DARPA receivers, depending on the number of channels in both receivers, and could be implemented in a corresponding volume of 7 in.$^3$ to 25 in.$^3$. Acquisition would be faster than required for the HDIS, but not extremely fast as for a transdigitizer receiver. Reacquisition would be very fast.

# CHAPTER 9

## REFERENCES

1.  System Specification for Global Positioning System (GPS) High Dynamics Instrumentation Set (Medium Volume), type A, YISP-83-14, USAF Armament Division, Deputy for Range Systems, Eglin AFB, FL, 20 July 1984.

2.  Hurd, William J., "High Dynamic GPS Receiver Validation Demonstration Plan," JPL D-1181, Jet Propulsion Laboratory, Pasadena, California, Nov. 30, 1983. (JPL internal document.)

3.  Contract NAS7-918, Task Order RE-182, Amendment No. 320, "GPS Receiver for High Dynamic and Low Volume Applications."

4.  Hurd, William J., "GPS Receiver Test Plans and Procedures, Final version," JPL Interoffice Memorandum 331-84-277A, August 3, 1984. (JPL internal document.)

5.  Hurd, William J. and Anderson, T. O., "Digital Transition Tracking Symbol Synchronizer for Low SNR Coded Systems," IEEE Trans. on Comm. Vol. COM-18, April 1970.

6.  Holmes, J.K., "Coherent Spread Spectrum Systems," John Wiley & Sons, 1982.

7.  Hurd, William J., "High Dynamic, Low Volume GPS Receiver," NTC 83, San Francisco, November 1983.

8.  Pomalaza-Raez, C.A., and Hurd, W.J., "Improved Carrier Tracking by Smoothing Estimators," IEEE Trans. on Aerospace and Electronic Systems, September 1985.

9.  Spilker, J.J., "GPS Signal Structure and Performance Characteristics," J. Inst. Navigation, Vol. 25., No. 2, Summer 1978.

10. Wozencraft, J.M. and Jacobs, I.M., "Principles of Communication Engineering," John Wiley & Sons, New York.

11. Hurd, W.J., and Statman, J.J., "High Dynamic GPS Unaided Pseudorange Tracking Demonstration," IEEE International Telesystems Conference, Las Vegas, 1984.

12. Ekstrand, B., "Analytic Steady-State Solution for a Tracking Kalman Filter," IEEE Transactions on Aerospace and Electronic Systems, November 1983, pp. 815-819.

13. Statman, J. I., "Fading Memory Filter as a Special Case of Kalman Filter," JPL Interoffice Memorandum 331-85.5-40, July 17, 1985. (JPL internal document.)

14. Statman, J. I., "Position Error Caused by Unmodeled Dynamics," JPL Interoffice Memorandum 331-85.5-41, July 17, 1985. (JPL internal document.)

# CHAPTER 10

## ABBREVIATIONS

ADC(A/D)  - Analog to Digital Converter

AMLE      - Approximate Maximum Likelihood Estimator

BPF       - Bandpass Filter

C/A-code  - Coarse/Acquisition Code (also known as SPS)

CLCC      - Ceramic Leadless Chip Carrier

CM        - Circular Motion (simulated trajectory)

CMOS      - Complementary Metal Oxide Semiconductor

CPU       - Central Processing Unit

CV        - Constant Velocity (simulated trajectory)

DARPA     - Defense Advanced Research Projects Agency

DES       - Data Evaluation Subsystem

DFT       - Discrete Fourier Transform

DIP       - Dual In-line Package

EPROM     - Erasable Programmable Read Only Memory

FIFO      - First In First Out (Buffer)

| | | |
|---|---|---|
| FFT | – | Fast Fourier Transform |
| FLL | – | Frequency-Locked Loop |
| g | – | Gravity-induced acceleration (approximately 9.8 m/s$^2$) |
| GDOP | – | Geometric Dilution Of Precision |
| GPS | – | Global Positioning System |
| HDIS | – | High Dynamics Instrumentation Set |
| HDOP | – | Horizontal Dilution Of Precision |
| I | – | In-phase signal |
| IC | – | Integrated Circuit |
| IF | – | Intermediate Frequency |
| I/O | – | Input/Output |
| I-Q | – | In phase – Quadrature signals |
| IRU | – | Inertial Reference Unit |
| JPL | – | Jet Propulsion Laboratory |
| JPO | – | (GPS) Joint Program Office |
| L1 | – | L-band frequency (1575.42 MHz) |
| L2 | – | L-band frequency (1226.7 MHz) |
| LDIS | – | Low Dynamics Instrumentation Set |
| LPF | – | Lowpass Filter |
| MLE | – | Maximum Likelihood Estimator |
| MMIC | – | Monolithic Microwave Integrated Circuit |
| MSI | – | Medium Scale Integration |
| NCO | – | Numerically Controlled Oscillator |
| NCU | – | Navigation and Control Unit |
| NSC | – | National Semiconductors Corp. |
| P-code | – | Precision Code (also known as PPS) |

PLL       – Phase-Locked Loop

PPS       – Precision Positioning Service (P-code)

Q       – Quadrature signal

RAJPO       – (GPS) Range Applications Joint Program Office

RAM       – Random Access Memory

RMS       – Root Mean Square

ROM       – Read Only Memory

RF       – Radio Frequency

s       – seconds

SA       – Step Acceleration (simulated trajectory)

SNR       – Signal to Noise Ratio

SPS       – Standard Positioning Service (C/A-code)

SSI       – Small Scale Integration

TIS       – Test Instrumentation Subsystem

TP       – Tracking Processor

TSPI       – Time, Space, Position Information

TTFF       – Time To First Fix

UERE       – User Equivalent Range Error

VDOP       – Vertical Dilution Of Precision

VLSI       – Very Large Scale Integration

# APPENDIX A

## DEMONSTRATION FUNCTIONAL REQUIREMENTS

The functional requirements on the Validation Demonstration were given in the Demonstration Plan [2]. This appendix presents the requirements from the Plan, with subsequent changes indicated by an asterisk in parentheses, (*). The deviation from the original requirements are summarized in Section A.4. The functional requirements are presented in terms of requirements on the Demonstration itself, on the Demonstration System, and on the Demonstration Tests. Requirements are presented on a functional level rather than at the design level.

### A.1 GENERAL DEMONSTRATION REQUIREMENTS

#### A.1.1 Location

The Demonstration System will be installed and the Validation Demonstration conducted at JPL.

#### A.1.2 System Configuration

The system shall be configured so as to clearly distinguish between the receiver being tested and the test and control instrumentation.

The functions of each unit shall be identified, and the interfaces shall be clearly defined. The hardware configuration of the receiver shall be such as to allow identification of the relationship between areas of the breadboard receiver and areas of a miniaturized implementation.

A.1.3 Real Time Displays

Real time displays will be provided during all performance tests showing, as a minimum, the pseudorange of the simulated input signal and the pseudorange estimated by the receiver. There is a design goal to provide a real time comparison of these data if this can be done within schedule and budget.

A.1.4 Data Recording

Sufficient data shall be recorded during all tests to enable statistical post-test analysis to determine performance.

A.1.5 Data Analysis

Post-test data analysis shall be conducted of all test data sufficient to determine the receiver performance.

A.1.6 Facilities

No facilities shall be required other than those available in a typical electronics laboratory at JPL.

A.1.7 Special Test Equipment

No test equipment shall be required that is not normally available at JPL or is not identified as part of the Demonstration System.

A.1.8 Data Processing Facilities

All data processing shall be done on computers which are part of the Demonstration System, or on computers available at JPL. No special data processing facilities shall be required.

A.1.9 Pre-Demonstration System Testing

The Demonstration System, including both the receiver and the test instrumentation, shall undergo system tests according to documented test procedures prior to start of the Validation Demonstration tests.

A.1.10 Test Conduct

All Validation Demonstration tests shall be conducted according to documented test procedures.

A.1.11 Documentation

The following documentation of the Demonstration is required:

1. As built engineering drawings,

2. Software requirements, design, acceptance test and operations documents in JPL Interoffice Memorandum (IOM) form,

3. System Test Procedures, in JPL IOM form,

4. Validation Demonstration Test Procedures, in JPL IOM form, and

5. Final Report, as a deliverable document.

## A.2 DEMONSTRATION SYSTEM REQUIREMENTS

### A.2.1 General Description

The Demonstration System shall consist of the Demonstration Receiver to be tested, a Test Instrumentation Subsystem (TIS) and a Data Evaluation Subsystem (DES). The Demonstration Receiver is to be evaluated as to its capability to measure pseudorange and range rate under conditions simulating receiver velocities to 3300 m/s (Mach 10) and accelerations to 50 g, and under various noise conditions.

The relative velocity between receiver and satellite is up to 4100 m/s, including the maximum satellite velocity relative to the surface of the Earth of approximately 800 m/s, so both the receiver and the TIS must accommodate this velocity. Satellite acceleration is negligible.

The TIS will not generate a signal with an actual P code, but instead will use a short period pseudorandom sequence clocked at the P code chip rate. The receiver will process signals with this simplified code and thus will not be able to track actual GPS satellites. The actual L1 carrier frequency will be generated, or else a carrier at another frequency but with phase and frequency variations which would occur at the actual L1 frequency.

Only functions specified in this Plan are required to be demonstrated. Receiver functions which are not required to be demonstrated include the low noise front end, acquisition, data bit synchronization, data detection, tracking of actual satellites, tracking of the C/A code, tracking of the L2 carrier, tracking of multiple satellites and solution for position and velocity in three dimensions, and external interfaces. These functions are not necessary to validate the new concept for high dynamic tracking performance.

### A.2.2 Interfaces

Interfaces are separated as to external interfaces, i.e., between the system and the operator or external instruments, and internal interfaces, i.e., between subsystems.

### A.2.2.1 External Interfaces -

External interfaces to the Demonstration System are defined by

subsystem.

A.2.2.1.1 Receiver External Interfaces -

There are no interfaces from the Demonstration Receiver external to the system.

A.2.2.1.2 TIS External Interfaces -

The Test Instrumentation Subsystem has the following interfaces external to the system:

Inputs:

1. Test signal generation control

2. Test signal generation parameters (range versus time, SNR)

3. Receiver initialization and control

4. Frequency reference

5. Clock synchronization and reset

6. Measured SNR (if not automated)

7. Measured clock epoch offset (if not automated, *)

Outputs:

1. Test signal real time display

2. Test signal hard copy (*)

3. Test signal machine readable

4. Receiver output real time display

5. Receiver output hard copy (*)

6. Receiver output machine readable

7. Clock epoch comparison, real time, hard copy and machine readable (*)

8. Measured SNR, real time, hard copy and machine readable (*)

A.2.2.1.3 DES External Interfaces -

The Data Evaluation Subsystem has the following interfaces external to the system:

Inputs:

1. Control

Outputs:

1. Statistical performance evaluation of test data

A.2.2.2 Internal Interfaces -

Internal interfaces are defined by subsystem pairs.

A.2.2.2.1 Receiver - TIS Interfaces -

TIS to Receiver:

1. Test signal including random noise

2. Carrier frequency reference

3. Clock frequency reference

4. Clock reset signal (*)

5. Initial data bit synchronization (*)

6. Initial estimates of pseudorange and range rate

Receiver to TIS:

1. Estimated pseudorange, smoothed

2. Estimated range rate, smoothed

3. Estimated raw pseudorange

4. Estimated raw range rate

5. Measurement time tag

6. Receiver clock epoch (*)

A.2.2.2.2 Receiver - DES Interfaces -

There are no interfaces between the Receiver and the Data Evaluation Subsystem.

A.2.2.2.3 TIS - DES Interfaces -

TIS to DES:

1. Test signal machine readable

2. Receiver output machine readable

3. Measured SNR, machine readable

4. Measured clock epoch offset, machine readable (*)

DES to TIS: None

A.2.3 Processing

Processing is defined by subsystem.

A.2.3.1 Receiver Processing -

The receiver accepts clock frequency, clock reset, and initial data bit synchronization signals from the TIS, generates all required timing signals, time tags its output data, and provides an output clock epoch signal. It accepts initial estimates of pseudorange and range rate, a signal plus noise input and a carrier reference input from the TIS. It demodulates the signal against the carrier reference, measures the pseudorange and range rate each data bit time, smoothes the measured data, and outputs the smoothed estimates of pseudorange and range rate. Pseudorange is measured relative to the receiver internal clock, and the output estimates are time tagged by that clock.

A.2.3.2 Test Instrumentation Subsystem Processing -

The Test Instrumentation Subsystem accepts the listed external inputs and generates a test signal with the specified simulated pseudorange versus time history and the specified signal to noise ratio. The test signal consists of a simulated P code signal, biphase modulated by a pseudorandom data bit pattern at 50 bps, with this signal modulated onto an actual or simulated L1 frequency carrier. All components of the generated signal must have phase variations corresponding to the simulated receiver dynamics. The SNR of the output signal is measured and this value is output in real time, in hard copy and in machine readable form, perhaps with operator assistance. The test signal is output to the Receiver and the parameters of the signal are output in machine readable form to the DES and externally, and selected simulated pseudorange and range rate data are output on a real time display and in hard copy form.

The TIS generates phase coherent carrier and clock reference signals and outputs them to the receiver. These signals are at fixed frequencies, unaffected by the simulated signal. The frequencies of these signals are controlled by external inputs. The purpose of generating these signals in the TIS rather than using a reference internal to the Receiver is so that

the frequency can be generated relative to the same primary standard as the test signal, and so that the effects of frequency offsets can be evaluated. The TIS also generates a clock reset signal and an initial data bit synchronization signal and outputs these to the Receiver.

The TIS accepts all output data from the Receiver and outputs these in machine readable form to the DES and externally, and outputs selected data on a real time display and in hard copy form. It also accepts the clock epoch signal from the Receiver, compares this to its own clock epoch, and outputs the difference, in real time, in hard copy and in machine readable form, perhaps with operator assistance.

### A.2.3.3 Data Analysis Subsystem Processing -

The Data Analysis Subsystem accepts time tagged simulated pseudorange and range rate, time tagged smoothed and raw receiver estimates of pseudorange and range rate, signal-to-noise ratio and clock epoch comparison data from the TIS, performs statistical analyses on these data, and outputs the results.

### A.2.4 Performance Requirements

Performance requirements are defined by subsystem.

### A.2.4.1 Receiver Performance -

The pseudorange error shall be less than 2.0 m rms when under constant velocity of less than 3300 m/s relative to the satellite and with receiver P code power to noise spectral density ratio of 34 dB-Hz at the input to the Receiver. (This SNR will be exceeded with an antenna gain of -2 dB and a receiver noise temperature of 300 K or with and antenna gain of -7 dB and a receiver noise temperature of 100 K.)

The pseudorange lag error due to receiver dynamics shall be less than 15 m with pseudorange profile corresponding to radial acceleration of 50 g peak and jerk of 50 g/s peak, and under linear acceleration of 50 g. (*)

### A.2.4.2 Test Instrumentation Subsystem Performance -

The simulated pseudorange versus time shall be controlled to within 10 m (goal 0.1 m) and known to within 1.0 m (goal 0.1 m). All components of the simulated signal shall meet this requirement.

The signal-to-noise ratio shall be controlled to within 2 dB (goal 0.5 dB) and measured to within 1 dB (goal 0.5 dB).

The TIS shall not introduce errors in recording of receiver pseudorange of more than 0.05 m and in range rate of more than 0.01 m/s.

### A.2.4.3 Data Analysis Subsystem Performance -

The DES shall not introduce errors in evaluation of pseudorange

performance of more than 0.05 m or in evaluation of range rate performance of more than 0.01 m/s.

## A.3 VALIDATION DEMONSTRATION TESTS

The specified validation demonstration tests are intended to test the receiver under various conditions of dynamics and signal-to-noise ratio which might be encountered by a receiver on a high dynamic vehicle. Constant velocity, step acceleration and circular motion are simulated each at high, medium and low signal-to-noise ratios. High SNR conditions test instrumentation accuracy and dynamic limits. Medium SNR tests simulate normal operating conditions. Low SNR tests evaluate the performance limitations under adverse conditions. The velocities, accelerations and SNRs specified here are subject to change due to the results of analysis or earlier tests, or to simulate cases deemed to be of specific interest.

For each test iteration, the initial conditions of the case may be achieved by any method convenient to the actual mechanization of the Receiver and the TIS. The test iteration begins after the Receiver has acquired tracking of the signal input at the specified velocity and SNR.

Signal to noise ratios are specified as the ratio of received P code power to noise spectral density at the receiver input, in dB-Hz. The selected SNRs are 60 dB-Hz, 40 dB-Hz and 34 dB-Hz for high, medium, and low SNR, respectively. The high SNR corresponds to maximum GPS signal strength and antenna gain, the medium SNR corresponds to the minimum specified GPS signal, a 0 dB to -1 dB antenna gain, and a 100 K system temperature, and the low SNR corresponds to minimum signal strength with a -6 dB to -7 dB antenna gain, which might occur in bad circumstances.

### A.3.1 Constant Velocity Tests

### A.3.1.1 Objectives -

The objectives of these tests are to determine the performance of the receiver as a function of signal-to-noise ratio when operating at constant velocity, and to validate that the receiver achieves a pseudorange accuracy of better than 2.0 m rms at a SNR of 34 dB-Hz and at velocities of up to 3300 m/s.

### A.3.1.2 Test Description -

The receiver will be tested simulating constant velocity motion at 300 m/s, 1000 m/s and 3300 m/s at high, medium and low SNR. At 1000 m/s, data will be taken at several additional SNRs sufficient to fully characterize performance. Each test condition shall be simulated for approximately 10 minutes.

### A.3.1.3 Anticipated Results -

The anticipated results for the constant velocity tests are shown in

Figure A-1. The dashed line indicates the calculation error for SNRs above threshold, and the dots indicate anticipated data. At 34 dB-Hz and 40 dB-Hz, the results should be close to theoretical. At high SNR, the errors will be greater than theoretical due to instrument accuracy. At very low SNR, the errors will be lower than the dashed line due to thresholding.

A.3.1.4 Success Criteria -

The constant velocity tests are successful if the rms pseudorange error is less than 2.0 m at a SNR of 34 dB-Hz at all velocities up to 3300 m/s.

A.3.2 Step Acceleration Tests

A.3.2.1 Objectives -

The objectives of the linear acceleration tests are to evaluate performance under constant acceleration and at various SNRs, and to validate that the receiver will operate under constant acceleration of 50 g with a pseudorange error due to acceleration of less than 15 m.

A.3.2.2 Test Description -

The receiver will undergo the following test at accelerations of approximately 3 g, 10 g, 20 g, 30 g and 50 g and at low, medium and high SNRs. The receiver will be operated simulating constant velocity in one direction, then step to constant acceleration until reaching the same speed but the opposite direction, then constant velocity, then constant acceleration of the same magnitude but opposite sign as the previous acceleration until the initial velocity is reached. For each chosen acceleration, the duration of acceleration will be approximately 12 s and the duration of constant velocity will be approximately 8 s so that each cycle takes approximately 40 s. Figure A-1 shows the profiles of position, velocity and acceleration for the 50 g step acceleration case. The velocity will change from approximately -3000 m/s to +3000 m/s. The cycle will be repeated approximately 15 times for each test. Additional cases may be added to determine performance limitations. (*)

A.3.2.3 Anticipated Results

After being at zero acceleration 1 s or more, the range error due to acceleration will be approximately zero. After a step of acceleration, the range error will rise to its steady state value of approximately -0.2 m/g, reaching 90 percent of the steady state value in approximately 0.6 s. When the acceleration is stepped back to zero, the error will decay towards zero, again with a 90 percent rise (fall) time of approximately 0.6 s. There will be no overshoot.

A.3.2.4 Success Criteria -

The step acceleration tests are successful if at a constant acceleration of 50 g, the rms pseudorange error near the end of the

intervals of constant acceleration, is less than 15 m, 16 m and 17 m for high, medium and low SNRs, respectively. If loss of lock occurs at low SNR, the tests are successful if it is determined statistically that the rate of loss of lock is less than once per 15 cycles of the test trajectory (once per 360s of 50 g acceleration). (*)

## A.3.3 Circular Motion Tests

### A.3.3.1 Objectives -

The objectives of these tests are to evaluate the performance of a receiver in turns at various speeds, radial accelerations and SNRs, and to validate that the pseudorange error due to acceleration and jerk is less than 15 m at high SNR and under acceleration of 50 g or jerk of 50 g/s.

### A.3.3.2 Test Description -

The receiver will be operated with inputs simulating sinusoidal range variations at peak accelerations of 10 g, 20 g and 50 g and at high, medium and low SNRs. The period of the sinusoidal motion shall be such that the angular velocity is unity and thus the maximum jerk is equal to the maximum acceleration, in consistent units. Approximately 100 cycles will be made for each test. Additional cases may be added to determine performance limitations. (*)

### A.3.3.3 Anticipated Results -

The range error due to sinusoidal range changes at unity radian frequency is also sinusoidal at unity radian frequency. The peak range error is approximately 0.2 m for each g of peak acceleration, and the range error lags the range input by approximately 15 degrees.

### A.3.3.4 Success Criteria -

The tests are successful if for the 50 g acceleration test at high, medium, and low SNRs, the rms pseudorange error is less than 15 m, 16 m, and 17 m, respectively, at the phases of maximum error, averaged over 100 or more points. If loss of lock occurs at low SNR, the tests are successful if it is determined statistically that the rate of loss of lock is less than once per 100 full sinusoidal cycles at 50 g peak acceleration. (*)

## A.4 CHANGES DURING IMPLEMENTATION

When comparing the original functional requirements to the resulting Demonstration System implementation, it is observed that only minor deviations occurred. None of these deviations interferred with the demonstration objectives as stated in the plan. The deviations are in these areas:

1. Hard copy outputs at the testing site

The test data was stored on magnetic media - first on 8"

A-10

floppy diskettes and then on 9-track magnetic tapes for processing on a VAX computer. Separate printer outputs were not created at the TIS.

2. Clock reset

At the beginning of each test, the receiver generated a reset pulse for the timing circuits in the receiver and the TIS. This performed clock reset and initial data bit synchronization functions. This is a change from having an external common reset signal.

3. Clock epoch comparison

Clock epoch signal, in the form of 50 pps pulses, were available for observation. The receiver and TIS clocks were compared on a logic analyzer and the continuous data bit synchronization was verified. However, clock epoch data was not recorded on the diskettes.

4. Requirements on pseudorange lag errors

The requirements for the lag errors in pseudorange assume a second order fading memory dynamic filter. During the demonstration, a third order filter with better response was used. Hence performance was much better than the original requirements.

5. Test trajectories

Test trajectories were slightly modified. For example, circular motion tests used radian frequency of 0.785 rather than unity; this resulted in each cycle being an integer number of seconds.

RESULTS INDEPENDENT OF
VELOCITY, 300 TO 3300 m/s

$$\sigma = \frac{44\,m}{SNR^{\frac{1}{2}}}$$
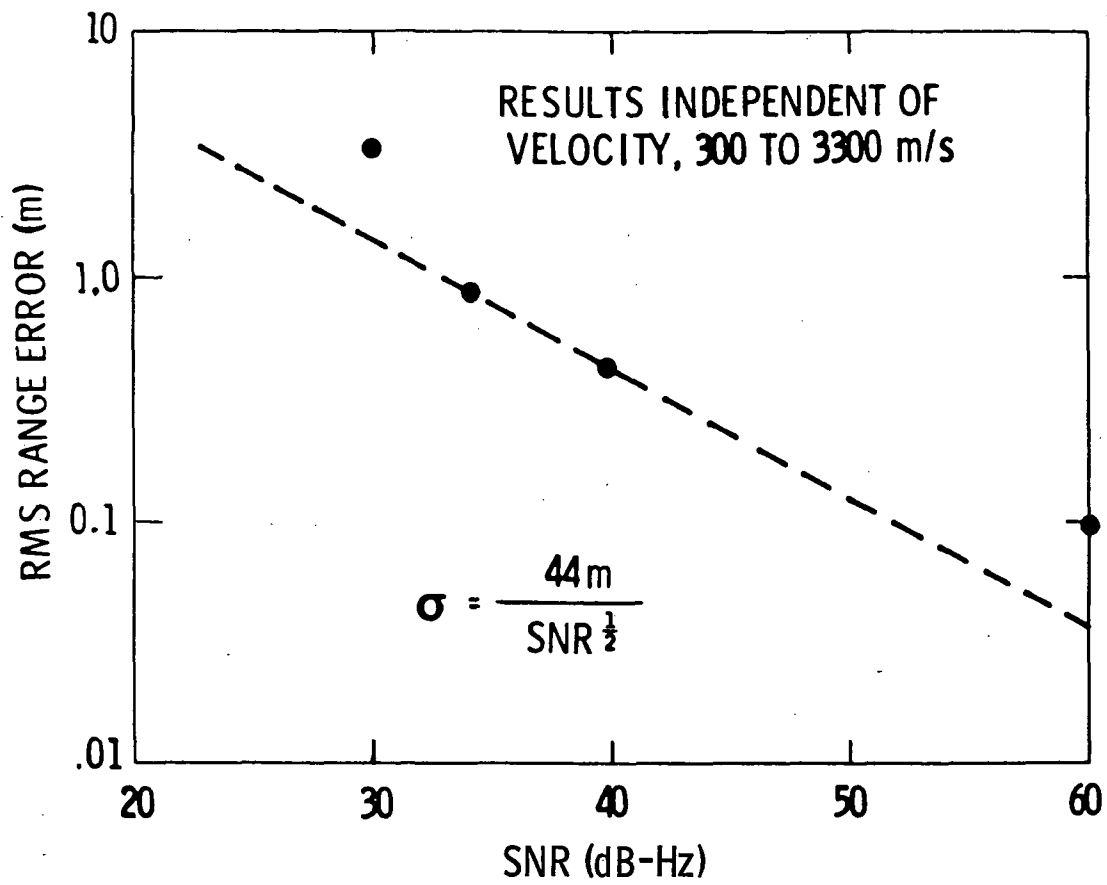
Figure A-1. Anticipated Performance

APPENDIX B


ANALYSIS AND SIMULATIONS



This appendix presents a summary of the analysis and simulation performed for the GPS High Dynamic Receiver Validation Demonstration program.


## B.1 RECEIVER CONCEPT

The main new concept described here is in the method of estimating the pseudorange and range rate of the receiver with respect to the satellites. This is accomplished in a quasi-open loop, approximately maximum likelihood (ML) manner rather than by tracking with phase and delay locked loops, as in other receivers. This enhances the ability to maintain tracking under high receiver dynamics, and naturally leads to an all digital implementation suitable for miniaturization. A second feature of the receiver is the use of a high update rate navigation or tracking filter, which is necessary for high dynamic tracking and which is within the capability of current microprocessor technology.

## B.1.1 GPS Signal Characteristics

The GPS satellites transmit pseudonoise signals at two L-band frequencies, denoted L1 and L2. Two different pseudonoise signals are used on each satellite, a P code signal and a C/A code signal. The P code is a long period pseudonoise sequence with a chip (clock) rate of 10.23 MHz, and the C/A code is a period 1023 pseudonoise code clocked at 1.023 MHz. Both codes are biphase modulated by binary data at 50 bps. The L1 carrier is phase modulated by both pseudonoise signals, with the C/A code lagging the P code by 90 degrees. The L2 carrier is modulated by either the P or the C/A signal, but not both at the same time. The L1 carrier frequency is 154 times the P code chip rate, and the L2 carrier frequency is 120 times the P code chip rate. All frequencies are phase coherent. On L1, the C/A signal has twice the power of the P code signal. The carriers are completely suppressed.

The L1 signal can be expressed as

$$AD(t)p(t) \cos (\omega_1 t + \phi_1) + BD(t)c(t) \sin (\omega_1 t + \phi_1) \qquad (B.1.1)$$

where

$$
\begin{aligned}
A &= \text{P signal amplitude} \\
B &= \text{C/A signal amplitude} \\
D(t) &= \text{data signal at 50 bps} \\
p(t) &= \text{P code signal} \\
c(t) &= \text{C/A code signal} \\
\omega_1 &= \text{L1 radian carrier frequency} \\
\phi_1 &= \text{constant but random carrier phase.}
\end{aligned}
$$

This signal is filtered before transmission to restrict its bandwidth to approximately 37 MHz. This effect is neglected in the estimation process, but is considered as "correlation loss" in B.3.3.2.

## B.1.2  Maximum Likelihood Estimation for One Code

A receiver observes a noise-corrupted, attenuated, doppler-shifted version of the transmitted signal delayed by the propagation delay between satellite and receiver. The receiver has a different clock than the satellite, hence by observing the signal from one satellite only it cannot tell the difference between the clock offset and the signal delay due to range.

When only the P code signal is present, the received signal r(t) is

$$r(t) = AD(t-\tau)p(t-\tau) \cos (\omega (t-\tau) + \phi) + n(t) \qquad (B.1.2)$$

where

> A = amplitude of received L1,P signal
> τ = time delay plus clock offset, proportional to pseudorange
> φ = phase of received L1 signal suppressed carrier
> n(t) = white Gaussian noise
>
> ω = received radian carrier frequency

The transmitter filtering effects are ignored.

Now assume that the signal is observed over a period of time T, such as one data bit time, during which all parameters A, D,τ,ω and φ, are constant. The parameters of interest for tracking are ω and τ, and the maximum likelihood estimates are the values of $\tau_m$ and $\omega_n$ which maximize

$$\left| \int_T r(t) \; p \; (t - \tau_m) \; e^{-j\omega_n t} \; dt \right|^2 \qquad (B.1.3)$$

The value of D does not affect the magnitude of the complex integral. The phase of the complex integral can be used to recover the modulation or to perform phase tracking. The ML method for the P code signal is to multiply the received signal by all possible delays of the P code, and then for each of these products to measure the energy at all frequencies. The values of time delay and frequency for which the energy is a maximum are the maximum likelihood estimates of these parameters.

B.1.3 Approximate ML Method for One Code

In practice, one can not actually measure the energy at an infinite number of lags and at an infinite number of frequencies. But suppose that the delay and frequency are known to be within some small intervals. It is then practical with current technology to calculate the products for a set of discretely spaced lags within the interval of possible time delays, and for each lag to calculate the energy at a set of discretely spaced frequencies using a Fast Fourier Transform (FFT). A receiver using this estimation method is called an approximate maximum likelihood estimator (AMLE) receiver.

B.1.4 Approximate ML Method Versus PLL Tracking

Typical GPS receivers estimate time delay by tracking the P code in a delay locked loop, using two lags of the code to generate an error signal. This type of loop may lose lock when the time delay error exceeds approximately one-half of the lag spacing. If N lags are used in the (AMLE) method, good delay estimates can be obtained even as the tracking filter

pseudorange error approaches approximately N/2 lags. This improves the ability to track when there are large errors due to vehicle dynamics.

In an analogous manner, the AMLE receiver can tolerate errors in estimating carrier frequency of approximately one half of the frequency span of the FFT. A phase locked loop implementation is similar to having only one filter, and thus is much less tolerant to tracking errors due to vehicle dynamics.

## B.1.5  Combined ML Estimation for Both Codes

The L1 carrier is modulated by both the P code and the C/A code, and the delays of both signals can be independently estimated by the method presented above. This is not optimum, however, because the time delay, frequency and phases of the two signals have known relationships. In particular, the P and C/A signals have the same carrier frequency and the same delay, and the C/A carrier phase lags the P carrier phase by 90 degrees. The overall maximum likelihood method is to choose the $\tau_m$ and $\omega_n$ which maximize

$$\left| \int_T r(t) \left[ p(t-\tau_m) + \sqrt{2}\ c(t-\tau_m)\ e^{j\pi/2} \right] e^{-j\omega_n t}\ dt \right|^2 \qquad (B.1.4)$$

The factor of the square root of two arises because the C/A signal amplitude is that much higher than the P code signal amplitude.

Use of the overall maximum likelihood method would yield significant protection against tracking failure under very weak signal conditions, and would yield some improvement in random noise performance under normal SNR conditions. Good performance depends on having a high enough SNR so that the lag and the FFT filter which have maximum detected energy are the lag and frequency closest or next-closest to the correct answers. Very low SNRs can cause other lags and filters to have maximum energy. Simultaneous detection of the P and C/A code signals increases the effective SNR by about 4.8 dB over the P code only SNR, because the C/A code is twice as strong as the P code. This would improve the threshold performance of the receiver by almost 4.8 dB. Under normal SNR conditions, there would be only a small improvement in random noise performance, because due to its wider bandwidth the time delay estimation performance of the P code would dominate.

Implementation cost and performance tradeoffs should be made for a combined maximum likelihood receiver versus a receiver detecting the P code and the C/A code signals independently.

## B.2 RECEIVER IMPLEMENTATION MODEL

This section presents the mathematical model of the Demonstration Receiver, based on the actual hardware and software implementation. The theoretical background for this implementation is given in Appendix B.1, a description of the software simulation in Appendix B.5, and more detail of the hardware implementation is presented in Chapter 4.

The receiver model is illustrated in Figure B-1. The main functional blocks are the predict removal block, AMLE window, predict addition block, tracking filter, predictor, and bit synchronization tracker. All variables in the figure are column vectors composed of pseudorange, range rate, and acceleration. The variables are defined as

$$\overline{X} = (\tau, \dot{\tau}, \ddot{\tau})^T = \text{simulated inputs}$$

$$\overline{\Delta X} = (\Delta\tau, \Delta\dot{\tau}, \Delta\ddot{\tau})^T = \text{differential AMLE inputs}$$

$$\overline{\Delta X}_a = (\Delta\tau_a, \Delta\dot{\tau}_a, \Delta\ddot{\tau}_a)^T = \text{differential AMLE outputs}$$

$$\overline{X}_a = (\tau_a, \dot{\tau}_a, \ddot{\tau}_a)^T = \text{unfiltered state estimate}$$

$$\overline{X}_f = (\tau_f, \dot{\tau}_f, \ddot{\tau}_f)^T = \text{filtered state estimate}$$

$$X_f = (\tau_p, \dot{\tau}_p, \ddot{\tau}_p)^T = \text{AMLE predicts}$$

The formulas in the following sections are specific to the Demonstration Receiver and may change in other implementations of the AMLE concept. Examples of implementation dependent features are the spacing of pseudorange lags and range rate bins, the method of code dithering, and the loop delay caused by the pipelined implementation.

### B.2.1 Prediction Removal

The prediction removal block, implemented in hardware and software, centers the AMLE window at the predicted pseudorange and range rate. It performs three functions: range rate predict removal, pseudorange predict removal at the center of the bit-time, and stepping of pseudorange each correlation time to compensate for range rate.

Code stepping is used to adjust the phase of the local code during a bit time. In the Demonstration Receiver, the local code generator is clocked at a fixed 20.46 MPPS rate. Since the change in received code delay may be more than one correlator in one bit time, it is necessary to adjust the phase of the local code each correlation interval. The Demonstration Receiver measures the accumulated phase of the local code (or the accumulated pseudorange) in two parts: the integer number of lags is maintained in software, while the fractional part is stored in hardware,

represented by a 7-bit counter. The counter scaling is such that a full count corresponds to one code lag, or 14.7 m. At the beginning of every correlation interval the counter is incremented by a step that is proportional to the unquantized range rate predict. The counter value is constant over a data bit time and is given by

$$D_1^{n+1} = \text{round}\left(k_1 \cdot \tilde{\tau}_p^{n+1}\right) \qquad \text{(B.2.1)}$$

$$k_1 = (128 \cdot T)(31 \cdot L) \simeq 0.0056 \text{ counts/(m/s)} \qquad \text{(B.2.2)}$$

where

$$D_1^{n+1} = \text{code step for } (n+1)^{th} \text{ bit}$$

$$T = \text{data bit time (0.02 s)}$$

$$L = \text{distance corresponding to a lag (14.7 m)}$$

Since pseudorange and range rate values are referenced to the data bit center, the code stepping occurs in locations that are approximately symmetrical with respect to this center. To accomplish this, the counter setting at the center of the data bit, i.e., after the sixteenth correlation interval, is forced to be 63, approximately half the full scale of the counter. Note that code stepping does not occur until the change in pseudorange over a bit time becomes approximately one lag. Thus, code stepping begins to occur at a range rate of roughly 750 m/s, or mach 2.5.

The pseudorange predict at the center of each bit time is quantized to an integer number of lags. This means that the hardware counter must have the value 63 at these times. Thus the change in accumulated pseudorange from the center of one bit time to the center of the next bit time must be an integer number of lags. This is implemented in three parts: code stepping over the first bit, code stepping over the second bit, and a phase shift at the bit transition. The phase shift at the bit transition is implemented as a one time increment of the code phase counter, given by:

$$D_2^{n+1} = k_2 \left(\tau_p^{n+1} - \tau_p^n\right) - \left(15 D_1^n + 16 D_1^{n+1}\right) \qquad \text{(B.2.3)}$$

where

$$D_2^{n+1} = \text{code phase increment between the } n^{th} \text{ and } (n+1)^{th} \text{ bits}$$

$$k_2 = 128/L \simeq 8.7 \text{ counts/m}$$

To remove the range rate predict, the range rate predict is converted to frequency and quantized to the nearest 50 Hz, with zero frequency omitted. The incoming signal is mixed with a complex signal at this quantized frequency.

B.2.2 AMLE Window

The AMLE window processing consists of three steps. First, every 1/1600 s, correlation values are computed for eleven code lags. Then, every bit time, an FFT is computed for each lag and the peak FFT power over the AMLE window is identified. Finally, interpolation formulas are applied to estimate the location of the AMLE peak relative to the discrete points where the AMLE is evaluated.

Correlation is performed by multiplying the noisy complex samples by an unfiltered, shifted version of the code sequence, and summing. For each lag, 32 complex zeroes are appended to the 32 complex correlation values over the data bit time, and a 64-point complex FFT is performed. This results in a 64 by 11 matrix of FFT power values. The matrix spans 1575 Hz (63 multiplied by 25 Hz) in frequency, and 147 m (14.7 m multiplied by 10) in pseudorange. The maximum of the discrete AMLE function is defined as the largest number in the matrix, excluding the first and last lags. Once the maximum is identified, fine pseudorange and range rate estimates are obtained using one of the following interpolation formulas.

The interpolation formulas are divided into three categories based on the assumed shape of the fitted function. The first category assumes that the three input points, peak AMLE power or amplitude and two adjacent points, are on an isosceles triangle. The formulas use two of the points to determine the slope of the triangle's equal sides and the third to locate the peak. The second group assumes that the points are on a parabola, solve for the parabola coefficients, and estimate the location of the peak. The third group uses the measured correlation function and the ratio of the two points with the highest power (or amplitude) to compute the peak of the function. Computation is by a second or third order polynomial. The TIS operator controls the selection of the interpolation formulas. For most Demonstration tests, the first group was used for delay and the second group for frequency. After completion of the originally planned tests, it was found that the third group is superior in bias, as shown in Appendix C.

B.2.3 Predict Addition Block

The predict addition block, implemented in software, adds the delta pseudorange and range rate computed by the AMLE to the predicts:

$$\tau_a = \tau_p + \Delta\tau_a$$

$$\dot{\tau}_a = \dot{\tau}_p + \Delta\dot{\tau}_a$$

$$\ddot{\tau}_a = \ddot{\tau}_p + \Delta\ddot{\tau}_a$$

## B.2.4 Tracking Filter

The tracking filter, implemented in software, is described in B.4. It accepts pseudorange and range rate data, after predict addition, and estimates filtered pseudorange, range rate, and for a third order filter, acceleration. The tracking filter has the generic form

$$
\begin{pmatrix} \tau_f \\ \dot{\tau}_f \\ \ddot{\tau}_f \end{pmatrix}_{n+1} = A \begin{pmatrix} \tau_f \\ \dot{\tau}_f \\ \ddot{\tau}_f \end{pmatrix}_n + B \begin{pmatrix} \tau_a \\ \dot{\tau}_a \\ \ddot{\tau}_a \end{pmatrix}_{n+1}
\tag{B.2.4}
$$

where the matrices A and B depend on the filter parameters.

## B.2.5 Predictor

The predictor, implemented in software, generates pseudorange and range rate predicts which are used to close the feedback loop. The prediction consists of two steps: compensation for the loop delay, and quantization of the predicts to discrete values.

As implemented, the forward data path has a delay of three data bit times, i.e., 60 ms. The delay is caused by the pipelining of the processing phases. Unquantized predicts, corrected for this delay, are given by

$$
\tilde{\tau}_p^{n+3} = \tau_f^n + 3T\dot{\tau}_f^n + (9T^2/2)\,\ddot{\tau}_f^n
\tag{B.2.5}
$$

$$
\tilde{\dot{\tau}}_p^{n+3} = \dot{\tau}_f^n + 3T\ddot{\tau}_f^n
\tag{B.2.6}
$$

$$
\tilde{\ddot{\tau}}_p^{n+3} = \ddot{\tau}_f^n
\tag{B.2.7}
$$

The quantized predicts are generated as follows. The pseudorange predict is quantized to the nearest pseudorange lag, i.e., to the nearest multiple of 14.7 m. The range rate predict is quantized to the nearest multiple of 9.5 m/s (50 Hz). If the range rate predict is zero, a 50 Hz offset is inserted. The following formulas summarize the prediction quantization.

$$
\tau_p = L \cdot \text{round } (\tilde{\tau}_p/L)
\tag{B.2.8}
$$

$$
\dot{\tau}_p = k \cdot \text{round* } (\tilde{\dot{\tau}}_p/k)
\tag{B.2.9}
$$

where

$$L \simeq 14.7 \text{ m}$$
$$k \simeq 9.5 \text{ m/s}$$
$$\text{round* = "round to nearest non-zero value."}$$

## B.2.6 Bit Synchronization Tracker

The bit synchronization tracker updates the bit synchronization pointer as needed. In the Demonstration Receiver, initial bit synch is accomplished by initialization from the TIS. During tracking, bit synch is adjusted, in units of 1/32 of a data bit time, by redefining the first correlation interval in the data bit. Changes in bit synchronization occur when the accumulated pseudorange is close to a multiple of 187 km, with an initial offset of 93.5 km. Hysteresis was provided to avoid rapid switching when the receiver stays close to a transition point. The change in pseudorange that is equivalent to a unit change in bit synch can be computed from

$$\Delta s = c/f_{1600} \simeq 187 \text{ km} \qquad (B.2.10)$$

where

$$f_{1600} = \text{frequency of correlation intervals (1600 Hz)}$$
$$c = \text{speed of light}$$
$$\Delta s = \text{change in pseudorange}$$

When bit synch changes, additional operations must be performed to align the correlation buffers over the data bit, and to adjust the accumulated pseudorange. For example, residual accumulated pseudorange in the center of the data bit time, as represented by the corresponding 7-bit counter, must be set to 63.

## B.3 SNR ANALYSIS

Performance analyses are presented in support of the performance and error budget of Chapter 5.

### B.3.1 Input Signal to Noise Ratio

The signal to noise ratio of interest for performance analysis is the ratio of code power to noise spectral density at the output of the receiver front end, i.e., at the input to the signal processing equipment. This SNR is determined by the satellite signal strength at the input to the antenna, the antenna gain at the proper polarization, and the system noise figure. The GPS signal strength is specified such that the power at the output of a

0 dBi antenna with right circular polarization (RCP) is at least -133 dBm for L1, P code; -130 dBm for L1, C/A code; and -136 dBm for L2, either code. This is met whenever the satellite elevation is over 5 degrees and the atmospheric loss is less than 2 dB.

Receiving system noise is specified in terms of either system noise figure, $F_S$(dB), or system noise temperature, $T_S$ (Kelvins, K). Noise temperature is the thermal noise generated in a resistor at temperature $T_S$. System noise figure is the noise that the system would add to a resistor at room temperature, 290 K. Thus

$$F_S = 10 \log_{10} (1 + T_S/290)$$ (B.3.1)

A total system noise figure of 3.5 dB is practical, and is the noise figure specified for the HDIS procurement [1]. System noise figure includes amplifier noise and noise added and losses caused by all other components, such as cables and filters.

The 3.5 dB noise figure corresponds to a system temperature of 359K. The resulting system noise spectral level is

$$N_0 = 4k \, T_S$$ (B.3.2)

where k is Boltzmann's constant. This results in

$$N_0 = -173 \text{ dBm/Hz}$$ (B.3.3)

For antenna gain of G dB, the input SNR is

$$C/N_0 \text{ (dB-Hz)} = C \text{ (dBm)}$$
$$+ G \text{ (dB)}$$
$$- N_0 \text{ (dBm/Hz)}$$ (B.3.4)

For a 3.5 dB noise figure and minimum specified L1, P-code signal strength, this is G + 40 dB-Hz.

The HDIS procurement specification requires a loss of lock threshold of -142 dBm on the weakest satellite, with a 3.5 dB system noise figure. The -142 dBm signal corresponds to minimum satellite signal strength and a -9 dBi antenna gain. Thus threshold SNR is specified indirectly: the receiver must track for all SNRs exceeding 31 dB-Hz, measured at the point in the system where system noise figure is specified to be 3.5 dB or less.

B.3.2  Theoretical Performance of Approximate ML Estimator

First, the performance of the approximate ML estimator is presented assuming that the SNR is high enough that the errors in time delay and frequency estimation are almost always small, i.e., the rms errors are small compared to the time lag and FFT filter frequency spacings. Low SNR performance is then presented, using outlier theory. Loss of lock threshold depends on the tracking filter as well as the AMLE, and is discussed in section B.3.5.

## B.3.2.1 Pseudorange Estimation at High SNR

Suppose that the range rate or received frequency is constant and known. Then the ML method for pseudorange is to measure the received energy at all possible code delays, at the appropriate frequency. In the approximate implementation, only a finite number of code delays can be used. The pseudorange estimation error can then be calculated as a function of the spacing between the code lags. There is also an effect due to sampling and due to bandwidth limiting filtering before sampling. Here, we ignore the bandwidth limitaion. We assume that there are N samples per code chip, and that the pre-sampler filter integrates its input over the time between samples. With these assumptions, it can be shown that the rms error in pseudorange estimation is

$$\sigma_\tau = cT_c (4NT)^{-0.5} (C/N_0)^{-0.5} \qquad (B.3.5)$$

where

| | | |
|---|---|---|
| c | = | speed of light |
| $N_0$ | = | noise spectral density |
| C | = | effective code power |
| T | = | integration time |
| $T_c$ | = | chip time |
| N | = | number of lags per chip time |

For N = 2, T = 20 ms and for the P code, this evaluates to

$$\sigma_\tau = 73.3 \ (C/N_0)^{-0.5} \qquad (B.3.6)$$

This result does not depend on the phasing between the code lags processed, or on having the actual delay be constant over the integration interval. Note that in this approximate calculation, the rms error goes to zero as the lag spacing goes to zero. This is explained by the assumptions made in the calculations not being valid as this occurs. For any fixed SNR, the assumption that the rms delay error is small compared to the lag spacing breaks down as the lag spacing is decreased.

The result can be compared to a coherent delay locked loop. For example, it agrees with the result of Spilker [9], with N=1 corresponding to a 1-Delta delay locked loop and T corresponding to $1/(2B_L)$ where $B_L$ is the bandwidth of the delay locked loop.

## B.3.2.2 Pseudorange Rate at High SNR

Pseudorange rate estimates are made by estimating received carrier frequency. Assuming perfect delay estimation, frequency estimation in the AMLE is analogous to maximum likelihood reception of Frequency Position Modulation. This is treated by Wozencraft and Jacobs [10, Chapter 8].

Transforming the notation of [10] to our notation, equation (8.116a) of the reference becomes

$$\sigma_{\dot{\tau}} = (c/2\Pi f_{L1}) \ 6^{0.5} \ T^{-1.5} \ (C/N_0)^{-0.5} \tag{B.3.7}$$

where c is the speed of light and $f_{L1}$ is the carrier frequency. Since this equation is independent of $T_c$, it holds for both P and C/A codes. One factor of T arises because frequency estimation inherently improves as coherent measurement time increases. The remaining factor of $T^{0.5}$ arises because the signal energy in the measurement time is proportional to T.

For T = 20 ms,

$$\sigma_{\dot{\tau}} = 26.2 \ (C/N_0)^{-0.5} \ (m/s) \tag{B.3.8}$$

### B.3.2.3  Low SNR Effects

At low SNR, nonlinear estimation is often accompanied by threshold effects that may cause catastrophic deterioration in system performance. The SNR at which rapid degradation begins to occur is generally referred to as the threshold. In the AMLE, loss-of-lock typically occurs several dB below threshold. Thresholding is caused by the appearance of large noise spikes, which can result in pseudorange and range rate estimates that are essentially independent of the actual parameters embedded in the received signal.

The operation of the AMLE below threshold can be explained in terms of the decision array generated by the FFT. Each element of the array represents the energy of both signal and noise at a particular frequency and delay. (In this domain, delay and frequency are proportional to pseudorange and range rate, respectively.) The total number of coherence-areas, or "degrees of freedom" in the decision array is estimated to be 32 x 5 = 160 (32 independent time-samples derived from each waveform, over a range of 9 delay-lags corresponding to 5 independent correlation intervals). A coherence region that contains only noise can be modelled by a Rayleigh random variable, while the coherence region containing the signal is Rician. Since the AMLE selects the coordinates of the largest element, the probability of correct decision, $P_c$, is the probability that the Rician random variable exceeds each of the 159 Rayleigh random variables. Detection of a maximal coherence area corresponding to a Rayleigh random variable is often called an " outlier ". The probability of choosing an outlier is $q = 1 - P_c$. The variation of q with SNR is shown in Figure B-2.

Conditioned on an outlier occurring, the variance of range and range rate estimates can be obtained by treating them as continuous uniformly

distributed random variables over their domains. The conditional variance in pseudorange estimation becomes $(R^2)/12$, while in range rate it evaluates to $(V^2)/12$. (Here $R = 29.4 \times 4$ is the total extent of range, and $V = 9.5 \times 32$ is the extent of range rate in an AMLE window.) The estimation variance at any SNR can be represented as a linear combination of outlier and non-outlier results. Using the high SNR results from B.3.2.1 and B.3.2.2, the following general expressions are obtained :

$$\sigma_\tau^2 = q(R^2/12) + (1 - q)(cT_c)^2(4NT)^{-1}(C/N_0)^{-1} \qquad (B.3.9)$$

$$\sigma_{\dot\tau}^2 = q(V^2/12) + (1 - q)\left(\frac{c}{2\Pi f_{L1}}\right)^2 6T^{-3}(C/N_0)^{-1} \qquad (B.3.10)$$

These expressions do not take into account the various processing losses encountered in the receiver. The effect of these losses is the same as a reduction in $C/N_0$ of 1.5 dB, as per B.3.3 and B.3.4.

## B.3.3  Processing Losses and SNR Corrections

The AMLE performance can be characterized in terms of the effective $C/N_0$ at its input. This effective SNR is the SNR at the output of the receiver front end, including all system noise effects, minus losses in signal processing. These losses include effects both ahead of and in the AMLE. The effects are summarized in B.3.3.8 and are discussed individually in the following paragraphs.

### B.3.3.1  Transmitter Filter

The theoretical analyses assumed that the P code signal is not band limited. The actual transmitted P code signal is bandlimited to 37 MHz, or ± 18.5 MHz about the carrier frequency. The transmitter filter reduces the signal power by 0.3 dB. Since the specified power, C, is the power in the 37 MHz band, the signal power density within the band is 0.3 dB higher than if the total power were not band limited. Since the power near the carrier frequency dominates the solution, there is an effective gain of 0.3 dB ± 0.1 dB.

### B.3.3.2  Correlation Loss

After being mixed to baseband, the signal is low pass filtered prior to A/D conversion. This reduces the peak of the cross-correlation function between the input signal and the local P code by 0.8 dB. The noise is also affected, since the correlator noise is the product of the local P code and the filtered receiver noise. The spectral density of this product

noise, at zero frequency, is 0.3 dB less than $N_0$, the receiver noise density at zero frequency. The net effect is a reduction in effective SNR by 0.5 dB ± 0.1 dB.

### B.3.3.3 A/D Conversion

The next loss is due to signal quantization. A three-bit analog to digital converter is used. With optimum signal level, a 3-bit A/D converter would have a loss of 0.2 dB. We conservatively estimate the actual loss to be 0.3 dB ± 0.1 dB, averaged over the likely range of input signal levels.

### B.3.3.4 Sine Wave Reference Quantization

The next loss is due to 3-level quantization of the reference sine wave at the input to the digital complex multiplier. This loss is 0.4 dB, since the total power in the three level signal exceeds the power in the fundamental frequency component by this amount. The tolerance is ± 0.1 dB.

### B.3.3.5 FFT Filter Passband

There is a loss in SNR when the frequency of the signal at the input to the FFT is not at the center frequency of one of the FFT filters. The mechanization uses filters spaced by one-half of the filter bandwidth, with responses crossing over at the -1 dB points. The maximum loss is 1 dB, and the average loss is 0.3 dB ± 0.1 dB.

### B.3.3.6 Dynamics Effects

There are also losses in SNR due to receiver dynamics. Acceleration causes the signal bandwidth to expand, because the carrier after code removal is effectively a chirped sinusoid. Jerk causes the reference frequency fed back to the AMLE complex multiplier to be in error, which means that the frequency at the correlator outputs is offset from zero. This causes signal attenuation because the 1/1600 s correlation time corresponds to a low pass filter. Each of these effects is approximately 0.3 dB maximum and 0.1 dB average with circular motion of 50 g maximum acceleration and 50 g/s maximum jerk. Since jerk is the derivative of acceleration, maximum acceleration occurs when the jerk is zero, and the two losses are not both high at the same time. We conservatively assume an average total loss of 0.3 dB ± 0.1 dB. (The loss is approximately 1 dB at maximum acceleration and jerk of 100 g and 100 g/s.)

### B.3.3.7 Miscellaneous Losses

There may be miscellaneous losses which have not been accounted for, and there may be errors in estimating the above losses. In the Demonstration Plan [2], we assumed miscellaneous losses of 1.5 dB ± 1.5 dB, and we also carried a correlation loss for transmitted waveform of 1 dB. As a result of the simulations and demonstration tests, we now believe that the Plan was overly conservative, and that all significant effects have now been accounted for. We add an additional tolerance of ± 0.3 dB.

### B.3.3.8  Processing Loss Summary

The total processing losses are summarized in Table B.3-1.  The total loss in effective SNR is 1.5 dB ± 1.0 dB.

#### Table B.3-1  Processing Losses Affecting AMLE

| | |
|---|---|
| Transmitter filter (gain due to definition of C) | -0.3 dB ± 0.1 dB |
| Correlation loss due to bandwidth in receiver | 0.5 dB ± 0.1 dB |
| Analog to digital conversion, 3-bit | 0.3 dB ± 0.1 dB |
| Reference sine wave 3-level quantization | 0.4 dB ± 0.1 dB |
| FFT filter loss, offset from center frequency | 0.3 dB ± 0.1 dB |
| Dynamics losses (50 g accel., 50 g/s jerk) | 0.3 dB ± 0.2 dB |
| Miscellaneous | 0.0 dB ± 0.3 dB |
| | |
| Total processing losses | 1.5 dB ± 1.0 dB |

### B.3.4  AMLE PERFORMANCE INCLUDING LOSSES

The effect of processing losses on the rms pseudorange error is to decrease the effective signal to noise ratio in the expression for rms error.  Let $F_p$ be a processing loss factor which multiplies the SNR; this factor is $F_p = 0.708$ for the nominal 1.5 dB processing loss.  Then the rms pseudorange estimate error in the high SNR region, including losses, is

$$\sigma_\tau \text{(AMLE)} = cT_c \ (4NT)^{-0.5} \ (F_p C/N_0)^{-0.5}$$

$$= 87.1 \ (C/N_0)^{-0.5} \ \text{(m)}$$

(B.3.11)

The rms pseudorange rate estimate in the high SNR region, including losses, is

$$\sigma_{\dot\tau} \text{(AMLE)} = (c/2\Pi f_{L1}) \ 6^{0.5} \ T^{-1.5} \ (F_p C/N_0)^{-0.5}$$

$$= 31.1 \ (C/N_0)^{-0.5} \ \text{(m/s)}$$

(B.3.12)

The same loss factor applies in the low SNR region, with appropriate modifications of equations (B.3.9) and B.3.10).

## B.4 TRACKING FILTER

The signal processing channels of the GPS receiver provide raw estimates of pseudorange and range rate once every data bit time, or 20 ms. A tracking filter is used to achieve three objectives: first, to derive the system state from the observables (e.g. estimate platform acceleration), second, to smooth the random noise effects, and third, to predict pseudorange and range rate for the purpose of positioning the AMLE window. In the following discussion, the noise response and the dynamic response of various filters are presented, an optimal filter is selected for the single tracking channel demonstration, and different forms of filter implementation for the final receiver are discussed.

### B.4.1 State Model and Filter Formulations

In the demonstration, two types of filters were considered: the fading memory filter [11], and the Kalman filter [12]. The fading memory filter weights each measurement by an exponentially decaying weight, based on the filter time constant. The Kalman filter includes each measurement in the state estimate, based on the modeled measurement noise and state (process) noise. The fading memory filter can be expressed as a special case of a general Kalman filter, by making particular assumptions on measurement and process noise [13].

As in many tracking applications, it is assumed that filter gains reach steady state values. The use of steady state gains reduces the computational load associated with filter updates and removes potential sources of numerical instability. Fading memory filter steady state gains depend on the weighting matrix and on the filter time constant. Gains for the second order filter are presented in [11]; similar expressions for a third order filter were derived during the Demonstration. The Kalman filter steady state gains depend on the measurement noise and process noise covariance matrices. Formulas for the steady state gains of a second order Kalman filter, derived by Ekstrand [12], were used in the Demonstration.

### B.4.2 Response to Random Noise

The pseudorange and range rate measurement noise in the following discussion are modeled as independent white Gaussian random variables with zero mean and covariance matrix R, with

$$R = \sigma_x^2 \begin{pmatrix} 1 & 0 \\ 0 & 0 \end{pmatrix} + \sigma_{\dot{x}}^2 \begin{pmatrix} 0 & 0 \\ 0 & 1 \end{pmatrix} = \begin{pmatrix} \sigma_x^2 & 0 \\ 0 & \sigma_{\dot{x}}^2 \end{pmatrix} \qquad (B.4.1)$$

where

$\sigma_x$ = standard deviation of pseudorange measurement

$\sigma_{\dot{x}}$ = standard deviation of range rate measurement

A convenient way to compute the covariance of state estimate due to measurement noise is to separately compute the covariance due to pseudorange noise with standard deviation of 1 m, denoted E1, and due to range rate noise with standard deviation of 1 m/s, denoted E2. These matrices can be easily obtained because the tracking filters are implemented with steady state gains. Then, because the filters are linear, the covariance of the state estimate, E, is expressed as:

$$E = \sigma_x^2 E_1 + \sigma_{\dot{x}}^2 E_2 \qquad (B.4.2)$$

Figure B-3 presents the variation of the state estimate covariance matrix as a function of the parameters of the second order fading memory filter. The two top plots are the variances of pseudorange and range rate estimates caused by pseudorange measurement noise with standard deviation of 1 m, i.e. the (1,1) and the (2,2) elements of $E_1$. The two bottom plots are the comparable results for range rate measurement noise, i.e., the (1,1) and (2,2) elements of $E_2$. Using equation (B.4.2), the response to a given measurement noise can be computed. Figures B-4 and B-5 present similar results for the third order fading memory filter and for the second order Kalman filter. The variables R and S in the figures are defined in [12]. These variables are related to the statistics of the process and measurement noise assumed in the derivation of the Kalman filter, and serve to define the relevant filter parameters.

In the Demonstration system the standard deviations of pseudorange and range rate measurements were 1.8 m and 0.6 m/s, respectively, at an SNR of 34 dB-Hz. For a third order filter with time constant of 0.14 s and range rate weight 0.1, the resulting pseudorange estimate has a standard deviation of 0.6 m, mostly due to pseudorange measurement noise. In a similar way, the range rate estimate standard deviation, 0.4 m/s, is mostly due to range rate measurement noise.

The results presented in the figures are related to filter bandwidth. For a single-input single-output filter, the one-sided bandwidth is

$$B_L = \left(\frac{1}{2T}\right) \frac{\sigma_{OUT}^2}{\sigma_{IN}^2} \quad (Hz) \qquad (B.4.3)$$

where

$$\sigma_{IN}^2 = \text{variance of input noise}$$
$$\sigma_{OUT}^2 = \text{variance of output noise}$$
$$T = \text{time between samples}$$

The filters discussed so far have two inputs and two or three outputs, thus the definition of bandwidth is not straightforward. Nevertheless, the (1,1) element of $E_1$ can be used to obtain the pseudorange bandwidth, and the (2,2) element of $E_2$ can be used to obtain the range rate bandwidth. For a third order fading memory filter with a time constant of 0.14 s and range rate weight of 0.1, these bandwidths are 2 Hz and 16 Hz for pseudorange and range rate, respectively.

## B.4.3 Response to Dynamics

The selection of a tracking filter is driven by two conflicting requirements: the filter should smooth the noise on the measurement, while tracking high platform dynamics, without losing lock. In this section we evaluate the responses of the filters to various dynamic conditions.

The modeled dynamics are divided into three groups. The first includes trajectories where the pseudorange is a polynomial in time. Examples are constant velocity and constant acceleration, where the pseudorange is a second order or third order polynomial in time. The measure of filter performance is the steady state lag error. The second order tracking filters have no steady state tracking errors under constant velocity and operate with errors proportional to the acceleration when under constant acceleration. The third order tracking filter has no steady state pseudorange error when under either constant velocity or constant accceleration.

A second group of trajectories includes those represented by piecewise polynomials, with the segments separated by discontinuities in one of the derivatives. Examples are trajectories with step changes in velocity or acceleration. The filter response is composed of a transient error that converges to the steady state error discussed above. The peak of the transient error and the settling time are both of interest. Figures B-6 and B-7 show responses of second and third order filters to step acceleration. The errors due to step dynamics can be treated as a limiting case for continuously changing dynamics. For example, the peak transient error due to 100 g/s jerk for 1 s is comparable to that due to a 100 g acceleration step.

The third group of trajectories are those represented by a sinusoid, i.e. pseudorange, range rate and acceleration, which are all sinusoids of the same frequency with appropriately scaled amplitudes and phases. These trajectories model platform turns. As shown in Figure B-8, because the filters are linear, tracking errors also have the form of sinusoids.

In the following subsections, variation of filter response as a function of the filter parameters are evaluated for four trajectories: a velocity step of 100 m/s, an acceleration step of 100 g, constant acceleration of 100 g, and circular motion at 50 g with a period of 8 s. Due to the linearity of the system, results can be extended to other velocities and accelerations.

## B.4.3.1 Second Order Fading Memory Filter

Results for the second order fading memory filter are presented in Figures B-9 and B-10. Peak pseudorange transient error caused by a velocity step increases with filter time constant and with range rate weight. On the other hand, peak range rate transient error is almost as high as the velocity step, and does not depend heavily on the filter variables. Peak pseudorange transient error caused by an acceleration step increases with filter time constant and with range rate weight. Peak range rate transient errors increase with the increase in filter time constant, but decreases with increasing range rate weight.

When under constant acceleration, and $T \ll \tau$, steady state pseudorange lag error for $w=0$ is

$$e = \left(\frac{\alpha T}{1 - \alpha}\right)^2 a \simeq \tau^2 a \qquad (B.4.4)$$

where

$$
\begin{aligned}
a &= \text{acceleration} \\
e &= \text{pseudorange error} \\
\tau &= \text{filter time constant} \\
T &= \text{sample time} \\
w &= \text{range rate weight} \\
\alpha &= \exp(-T/\tau)
\end{aligned}
$$

Peak pseudorange errors for circular motion increase with increasing filter time constant and with increasing range rate weight. Peak range rate errors for circular motion increase with increase in filter time constant and decrease with increase in range rate weight.

## B.4.3.2 Third Order Fading Memory Filter -

Results for the third order fading memory filter are presented in Figures B-11 and B-12.

The peak pseudorange transient error caused by a 100 m/s velocity step increases with filter time constant and decreases with range rate weight. For weights of 0.1 and higher, pseudorange error is under 1 m. The peak range rate transient error is almost as high as the velocity step, and does not depend heavily on filter variables. Peak pseudorange transient error caused by an acceleration step increases with filter time constant and decreases with range rate weight. Again, for weights of 0.1 and higher, pseudorange error is under 1 m for a 100 g/s step. Peak range rate transient error increases with increase in the filter time constant, but decreases with increasing range rate weight.

Peak pseudorange and range rate errors for sinusoidal motion increase with increasing filter time constant and decrease with increasing range

rate weight as shown in Figure B-12. Steady state error due to acceleration is zero for the third order filter.

B.4.3.3 Second Order Kalman Filter

Results for the second order Kalman filter are presented in Figures B-13 and B-14. These results are similar to those of the second order fading memory filter.

B.4.4 The Demonstration Tracking Filter

The tracking filter for the Demonstration has to meet several requirements. Some, such as loss-of-lock conditions and computational efficiency, are absolute and must be met. Others, such as noise bandwidth and dynamic response, can be selected using a-priori optimization criteria.

The in-lock condition is that under all specified dynamics, AMLE detection must occur within the AMLE window. Using conservative safety margins, we define the maximum tracking errors in pseudorange and range rate to be 50 m and 80 m/s, respectively, since the AMLE ranges are ± 73 m and ± 160 m/s. We consider only fixed gain filters, hence the filter update computation time is a function of only the order of the filter. The dynamic response criteria is that when under 50 g circular motion or under 50 g step acceleration, the pseudorange error shall not exceed 15 m. The required noise response is not as significant as the dynamic response as long as the standard deviation of the pseudorange estimate is at most half of the standard deviation of the pseudorange measurement.

The third order fading memory filter appears superior to the second order filters. It has better dynamic response, especially in the range rate estimation, at a cost of minor degradation in noise performance. The longer computation time of a third order filter can be accommodated. The filter selected is the third order fading memory filter, with a time constant of 0.14 s and a range rate weight of 0.1.

Peak transient pseudorange and range rate errors due to a 100 g step acceleration are 0.4 m and 48 m/s, respectively. Peak pseudorange and range rate errors in a 50 g, 8 s, circular motion trajectory are 0.05 m and 7 m/s respectively. All of these errors are less than the maximum allowable dynamic errors.

The noise reduction of this filter depends on the ratio of the standard deviations of the input pseudorange and range rate measurements. Figure B-15 shows the noise reduction factors as functions of this ratio. For the Demonstration system, the pseudorange and range rate noise are reduced by 3.5 and 1.2, respectively, at SNRs above 32 dB-Hz. These are different at 32 dB-Hz, because "outliers" cause the ratio of the standard deviations to change.

## B.4.5 Tracking Filter for a Complete Receiver

There are two methods of tracking filter implementation. The more powerful method inputs the pseudorange and range rate observed by all the signal channels into a single tracking filter, and simultaneously solves for all of the navigation parameters. The second method tracks the dynamics of the signal from each satellite separately, forming smoothed estimates of pseudorange, range rate and perhaps acceleration, and then forms a memoryless flash solution for the navigation parameters, without further smoothing. This method is not as powerful as the first, but it often has distinct implementation advantages without significant loss in performance. Many navigation receivers use a combined method, in which the individual signals are tracked and smoothed in phase locked loops, and then the loop outputs are further smoothed in the navigation filter. A special case is when all channels use the same tracking filter, with fixed steady state gains, followed by a flash solution for position, velocity, and time. For this case, the position errors due to random noise are determined by the measurement standard deviation multiplied by the Geometric Dilution of Precision (GDOP) factor, while the magnitude of position error due to unmodeled dynamics is identical to the error of a single channel under the same dynamics, i.e., with no GDOP factor applied [14].

## B.5 SIMULATED DEMONSTRATION SYSTEM

The software simulation program is summarized in the following subsections.

The main reasons for simulating the GPS High Dynamic Receiver are to establish independent confirmation of system performance. In the simulation, the relevant operations performed by the actual Demonstration System are modeled, taking into account the various degradations and losses suffered by the signal as it propagates through the system. Once a reliable correspondance has been established between simulation predictions and hardware results, additional simulations can be used to verify potential improvements offered by possible extensions and modifications to the current system, before incorporating the proposed changes into the existing hardware.

## B.5.2 Simulation Description

The software simulation is based on the following model. During each T-second bit interval, the received P-code signal can be modeled as a sinusoidal carrier of frequency $f_{L1}$ = 1.575 GHz and doppler-shift $f_d$, modulated by a time-delayed PN sequence of length N = 1023 and chip duration $T_c$ = 0.1 microsecond. The unknown doppler-shift and time delay (both, in general, slowly varying functions of time) are due to relative motion between the two ends of the link. The received signal is observed in the presence of additive thermal noise generated in the receiver's front end. The receiver structure is based on the "maximum likelihood" principle, according to which those values of delay and doppler frequency are selected that maximize the likelihood function defined in B.1.2. The

implementation is approximate in the sense that decisions are based on a discrete set of observables over a restricted delay-frequency window, rather than on a continuum of values over the entire relevant section of the delay-frequency plane.

In the receiver, in-phase and quadrature components are created by mixing the received signal with properly phase-shifted local signals of nominal frequency $f_1$. The I and Q waveforms are filtered and subsequently multiplied by nine replicas of the unfiltered PN sequence, each shifted in time by the quantized delay estimate, and further delayed with respect to one another by integer multiples of a lag. Over the T-second bit time, each of the resulting waveforms is converted to 32 time-samples by means of short-time integration over successive T/32 second intervals. The in-phase and quadrature samples are combined to form complex numbers, and 32 (complex) zeros are appended to each sequence in order to improve frequency resolution before the FFT is performed.

It is convenient to represent the received waveform as

$$r(t) = AD(t-\tau)p(t-\tau) \cos \phi_r(t) + n_c(t) \cos \phi_r(t) + n_s(t) \sin \phi_r(t)$$

$$(B.5.1)$$

where

$$\phi_r(t) = 2\pi (f_{L1} + f_d) t + \phi$$

and $n_c(t)$ and $n_s(t)$ are independent Gaussian noise processes with identical spectral densities $S_n(f)$, and identical correlation functions $R_n(\tau)=(N_0/2)\delta(\tau)$. When the noise processes are integrated for T/32 s, the mean and variance of the noise samples become $E(n) = 0$, and Var $(n) = N_0 T/64$. In the simulation, the magnitude of the complex signal is set to one. Using this condition, the equivalent noise sample variance is

$$\sigma_n^2 = \left(\frac{N_0}{2}\right) \left(\frac{32}{CT}\right) \gamma \qquad (B.5.2)$$

$$= \frac{800 \gamma}{(C/N_0)}$$

$$\gamma \simeq 0.93$$

Therefore, the variance of the noise samples can be determined once the code power and the noise spectral level are specified. The attenuation factor $\gamma$ is required to account for the reduction in the effective noise spectral level due to the filtering and multiplication operations (the reduction in signal level is accounted for in a signal correlation table).

While the noise samples for a given lag are essentially uncorrelated random variables, noise samples between adjacent lags are not. This is because the lag spacing is equivalent to one-half chip. This effect has been taken into account in the generation of the noise sequences employed in the software simulation program.

The rest of the simulation follows closely the processing operations carried out by the Demonstration Receiver. The sample sequence from each lag serves as input to a 64-point FFT, whose output is ultimately arranged in the form of an 9x64 element array. The coordinates of the element with the greatest magnitude are declared to be the "rough" estimates of delay and frequency. Refined estimates are subsequently obtained by means of three-point triangle interpolation for delay, and three-point parabolic interpolation for frequency. These refined estimates are then used to compute the final pseudorange and range rate estimates, and also serve as input to the tracking filter described in Section B.4. The filter output (which includes an acceleration estimate along with the smoothed pseudorange and range rate estimates) provides the parameters needed to project pseudorange and range rate estimates ahead by three bit-times. The projected estimates are quantized, and subtracted from the observed input trajectory in an attempt to maintain the delay-frequency plane centered at all times. The projected (quantized) estimates are subsequently added back into the AMLE output. Therefore, under normal operating conditions, the projected estimates do not affect the accuracy of the final pseudorange and range rate estimates generated either at the output of the AMLE or at the output of the tracking filter.

During high-dynamic maneuvers, the received trajectory may change significantly over 20 ms (the duration of a bit), possibly causing a reduction in the detection SNR. Both the Receiver and the simulation compensate for this effect by using pseudorange and range rate estimates to determine if the observed delay changes by an entire lag within the bit-interval, and effectively increment the local PN code by a full lag when this occurs. Significant degradations in detection SNR due to dynamics are minimized by the use of this incremental compensation technique.

## B.5.3  Simulation Operation and Results

The simulation program emulates the GPS high dynamic receiver demonstration hardware. Upon activation, the program reads a data file containing tabulated values of the Butterworth filter correlation function (this correlation function was computed using the transfer-function of an ideal third order Butterworth filter). Next, the program reads pseudorange, range rate and acceleration data from an external data file containing the trajectory parameters. The program then executes the necessary steps to arrive at pseudorange and range rate estimates based on the available trajectory information. The length of the simulation and the type of trajectory are user-controlled items. A typical run may correspond to simulated circular motion (sinusoidal acceleration, velocity and range trajectories) of 32-second duration. The simulation output generally consists of trajectory graphs as a function of time, along with a time history of pseudorange, range rate and acceleration errors. Such an output

is shown in Fig. B-16, corresponding to circular motion with 50-g acceleration and 8-second period, at an input SNR of 31 dB-Hz. The trajectory error is measured at the output of the tracking filter. Note the occasional appearence of large error spikes caused by "outliers" (defined in Section B.3.2.3 ). Under benign dynamic conditions, outliers begin to occur at approximately 31 dB-Hz, which defines the threshold of the simulated GPS receiver. Operation a few dB below threshold is generally feasible, until the SNR becomes so low that outliers begin to dominate the detection statistics, at which point the receiver tends to lose lock.

## B.6 FREQUENCY LOCKED LOOP

This section presents an alternate form of range rate tracking for the Demonstration Receiver. While Section B.4 discusses a two-input, two- or three-output filter that estimates pseudorange, range rate and acceleration simultaneously, the following discussion focuses on tracking only the range rate. Performance of the resulting frequency locked loop is compared to that of the phase locked loop.

The AMLE measures the pseudorange (or time delay between the received signal and a locally generated replica of the signal) and the Doppler frequency offset between the two signals (which is proportional to range rate). As seen in Figure B-17, the raw estimates of pseudorange and range rate are passed through a two-input, two-output estimator-predictor that provides feedback to the AMLE. The estimator-predictor uses the fact that range rate is the derivative of pseudorange to improve the overall performance of the tracking loop.

Another interesting case is illustrated in Figure B-18, where a separate tracking loop is used to track only the range rate. This form of range rate (or frequency) tracking has the same structure as the standard phase locked loop, except that the observable is frequency rather than phase. For the rest of the discussion, it will be called Frequency Locked Loop (FLL).

The standard PLL uses a multiply and accumulate (or multiply and integrate) device as a phase detector, resulting in nonlinear periodic discriminator characteristics. In some implementations, such as with an AMLE, both the sine and cosine components are available and the nonlinearity of the phase detector is avoided. This is called an "arctangent phase detector." In either case to prevent ambiguities, the absolute value of the phase error must remain under 0.25 cycles. In contrast, the FLL discriminator for the Demonstration Receiver is linear for frequency errors between -800 Hz and 800 Hz and has a period of 1600 Hz. The discriminators are presented in Figure B-19.

To compare the PLL and FLL, we assume that both loops use a single input fading memory filter (B.4) as an estimator. The computational delay inherent in implementation is neglected, thus a predictor is not needed. To make a fair comparison, the PLL uses a third order filter while the FLL a second order filter. With these assumptions, both filters have finite non-

zero steady state errors, at the discriminator output, when the input dynamics correspond to phase jerk. The steady state errors are

$$E(PLL) = jX^3 \text{ (cycles)} \qquad (B.6.1)$$

$$E(FLL) = jX^2 \text{ (Hz)} \qquad (B.6.2)$$

where

$$
\begin{aligned}
j &= \text{jerk, in cycles/s}^3 \\
X &= \alpha T/(1-\alpha) \\
\alpha &= \exp(-T/\tau) \\
T &= \text{time between samples} \\
\tau &= \text{filter time constant}
\end{aligned}
$$

The input jerk, in m/s$^3$, is obtained by multiplying j by the carrier wavelength, in m. Note that as the filter time constant increases, the value of x approaches the filter time constant, thus

$$E(PLL) \simeq j\tau^3 \text{ (cycles)} \qquad (B.6.3)$$

$$E(FLL) \simeq j\tau^2 \text{ (Hz)} \qquad (B.6.4)$$

The one-sided bandwidths of both filters are:

$$B(PLL) = \left(\frac{1}{2T}\right) \frac{(1 - \alpha)(1 + 6\alpha + 16\alpha^2 + 24\alpha^3 + 19\alpha^4)}{(1 + \alpha)^5} \underset{\tau \gg T}{\to} \frac{1.03}{\tau} \qquad (B.6.5)$$

$$B(FLL) = \left(\frac{1}{2T}\right) \frac{(1 - \alpha)(1 + 4\alpha + 5\alpha^2)}{(1 + \alpha)^3} \underset{\tau \gg T}{\to} \frac{0.625}{\tau} \qquad (B.6.6)$$

A convenient benchmark for the comparison of PLL to FLL is their loss-of-lock conditions due to noise and due to dynamics. The loops have two distinct modes of losing lock. At one extreme, even at high SNR high dynamics cause the tracking error to fall outside the range of the discriminator. At the other extreme, even in the absence of dynamics, the SNR is so low that loss-of-lock occurs due to the noise. Both modes are related to loop bandwidth since as the filter bandwidth increases, the lag errors caused by dynamics decrease and the noise at the loop output

increases. Let the dynamic performance measure be the maximum phase jerk before the loop loses lock. The value of the maximum jerk is:

$$J_{max}(PLL) = \frac{0.25}{E(PLL)} = 0.25 \left(\frac{1 - \alpha}{\alpha T}\right)^3 \qquad (B.6.7)$$

$$J_{max}(FLL) = \frac{800}{E(FLL)} = 800 \left(\frac{1 - \alpha}{\alpha T}\right)^2 \qquad (B.6.8)$$

Figure B-20 presents the maximum jerk in g/s as a function of filter bandwidth. The maximum allowed tracking errors for the PLL and FLL are selected to be 0.25 cycles and 800 Hz, respectively. We observe that for the same filter bandwidth, the PLL loses lock at significantly lower dynamics than the FLL. Also, the maximum phase jerk is a cubic function of the bandwidth for the PLL while it is only a quadratic function for the FLL, when $T \ll \tau$.

The noise performance measure is the input signal to noise spectral density at which the loop loses lock. If we assume that both loops lose lock at the same SNR (say $SNR_0$ dB) then the loss-of-lock signal to noise spectral density can be expressed as

$$\left(\frac{C}{N_0}\right)_{LL} = SNR_0 + B \qquad (dB-Hz) \qquad (B.6.9)$$

Alternately, the loss-of-lock $C/N_0$ is proportional to loop bandwidth. This means that in Figure B-20 the label on the horizontal axis can be replaced by $(C/N_0)_{LL}$, with the appropriate change in units. These results can be only partially extended to compare PLL and FLL tracking in the GPS receiver. The PLL model does not account for the Costas loop, or for the actual filters used in such loops. The FLL model does not evaluate the effects of estimating pseudorange and range rate in separate filters. They also do not account for the outlier (B.3) effects that occur both in PLLs and FLLs, and for processing delays. Nevertheless, the basic tradeoff between maximum phase jerk and minimum signal to noise spectral density is believed to hold. As an example, Figure 5-2 presents PLL and FLL curves having 3:1 and 2:1 slopes, respectively. The curves are anchored at known operating points for GPS receivers: PLL curve uses 10 g/s jerk at 28 dB-Hz specified for the HDIS receiver, while the FLL curve is defined by the 100 g/s jerk at 28 dB-Hz measured in the Demonstration.

TRACKING FILTER

PREDICTOR

BIT SYNCHRO-NIZATION TRACKER

PREDICT ADDITION

AMLE WINDOW

PREDICT REMOVAL

$\overline{X_f}$

$\overline{X_a}$

$\overline{\Delta X_a}$

$\overline{\Delta X}$

$\overline{X}$

$\overline{X_p}$
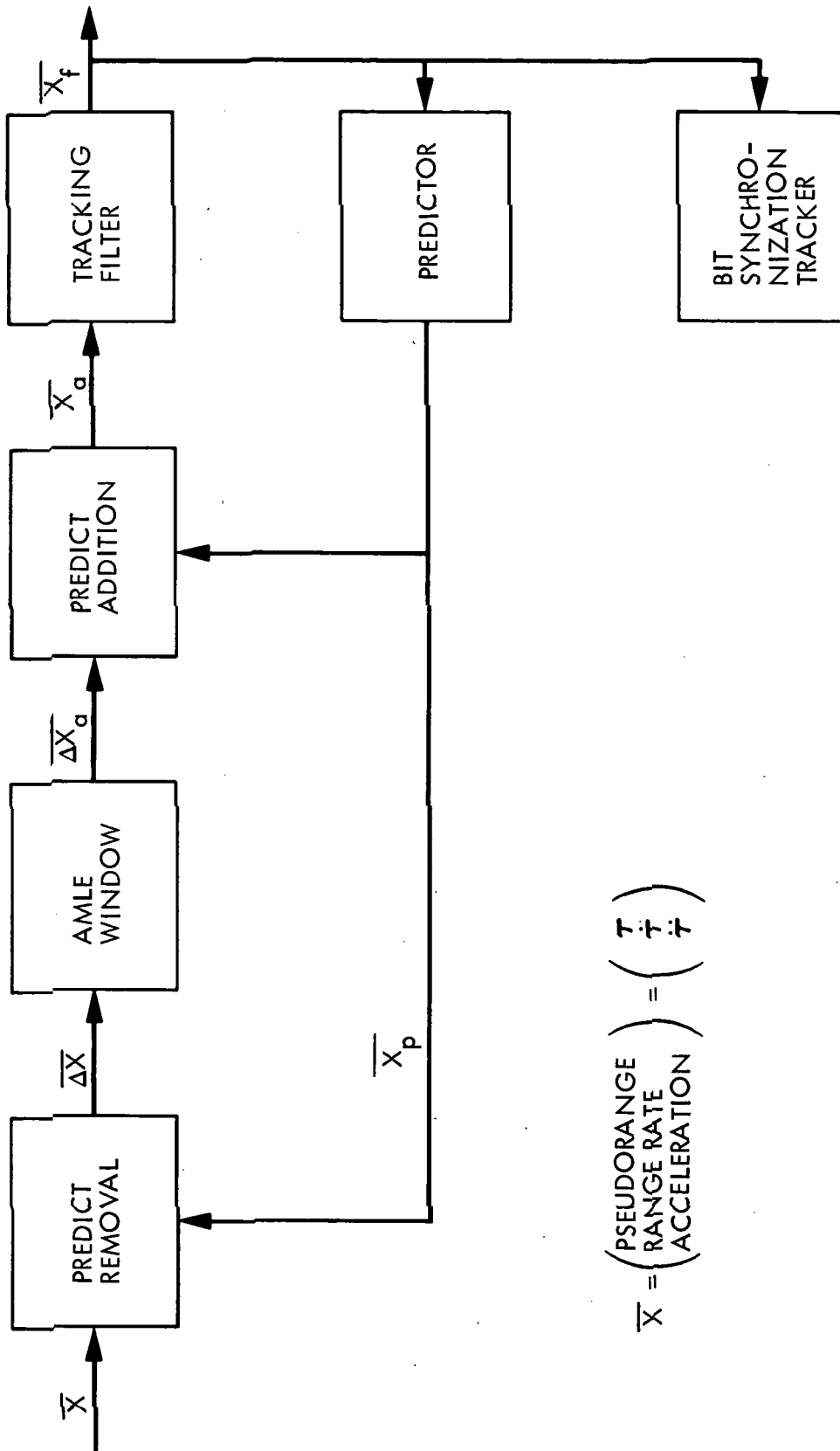
$$\overline{X} = \begin{pmatrix} \text{PSEUDORANGE} \\ \text{RANGE RATE} \\ \text{ACCELERATION} \end{pmatrix} = \begin{pmatrix} \tau \\ \dot{\tau} \\ \ddot{\tau} \end{pmatrix}$$

Figure B-1. Receiver Model
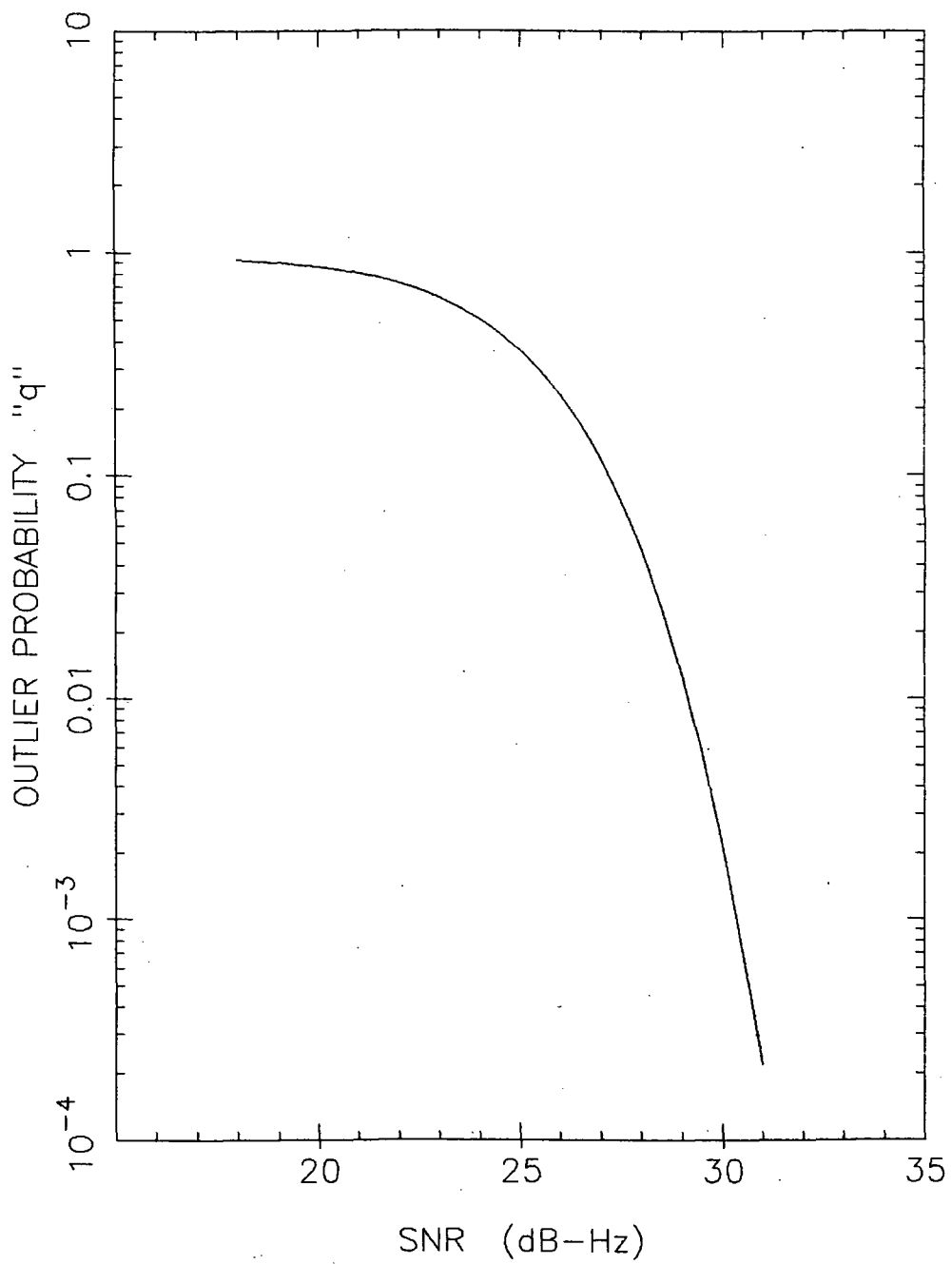
Figure B-2.    Outlier Probability as a Function of SNR
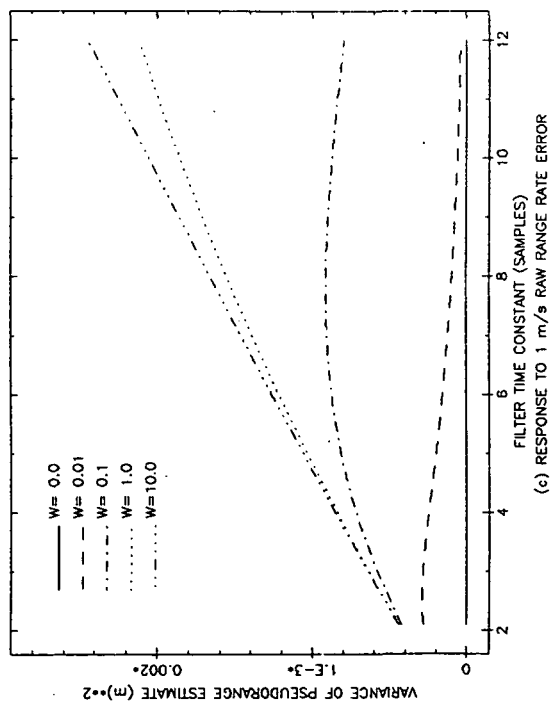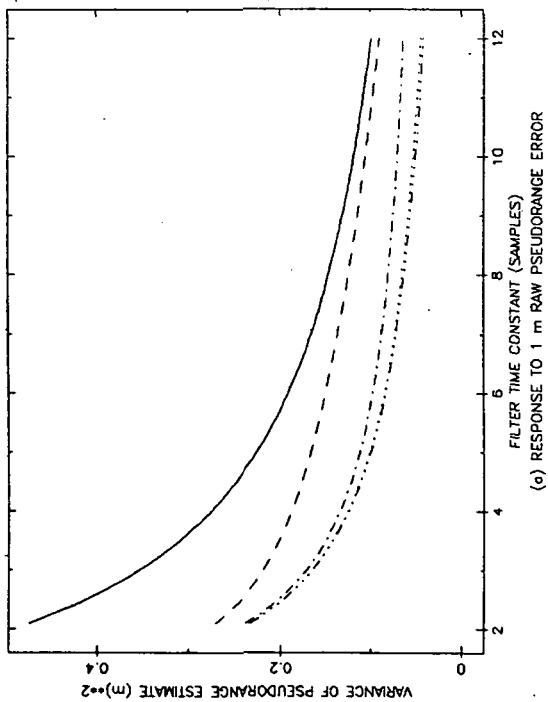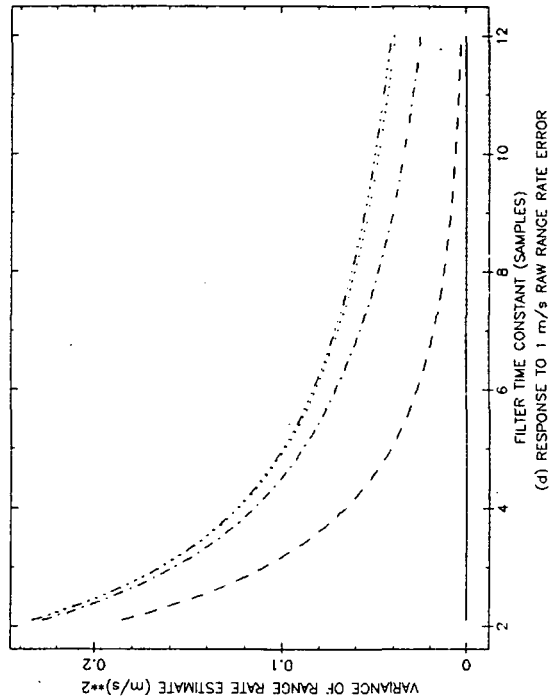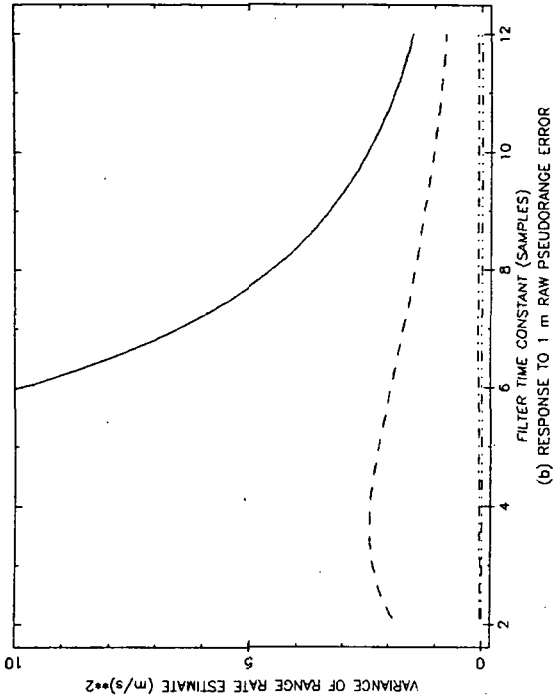
Figure B-3.   Second Order Fading Memory Filter – Noise Response
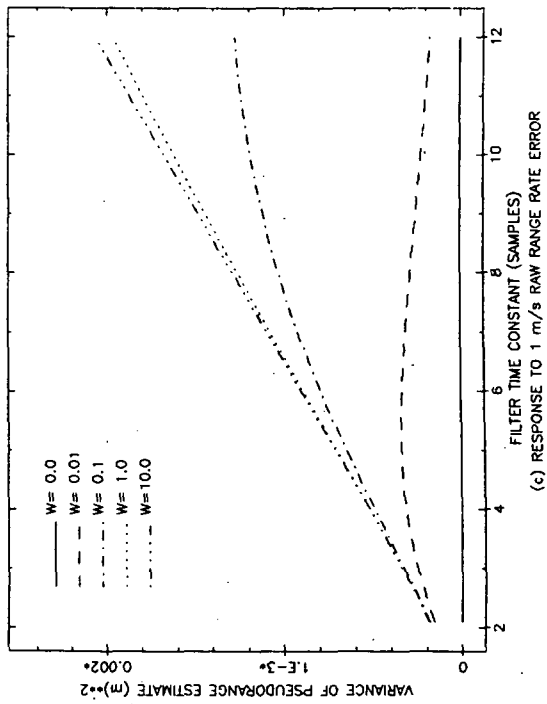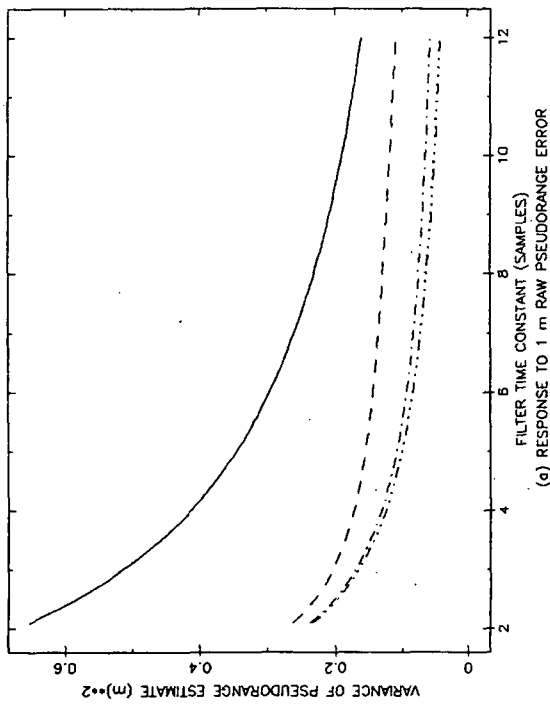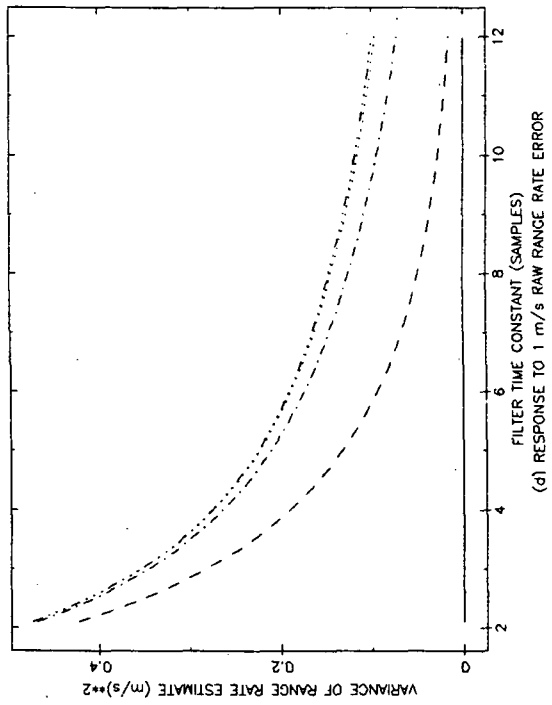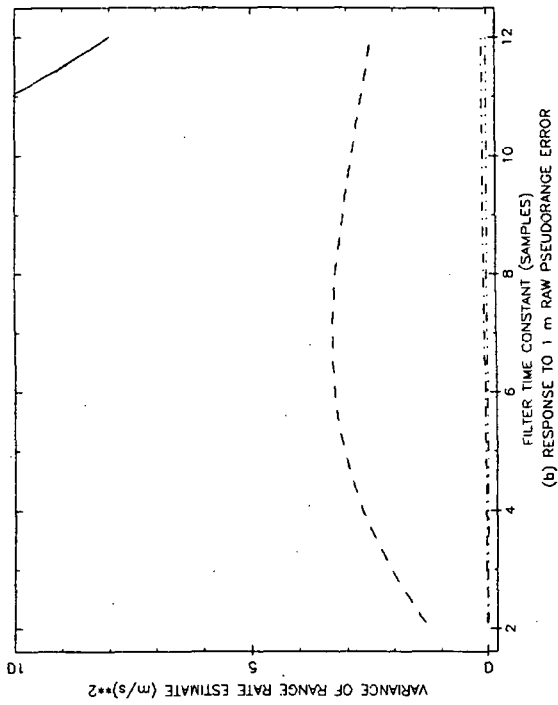
Figure B-4. Third Order Fading Memory Filter – Noise Response
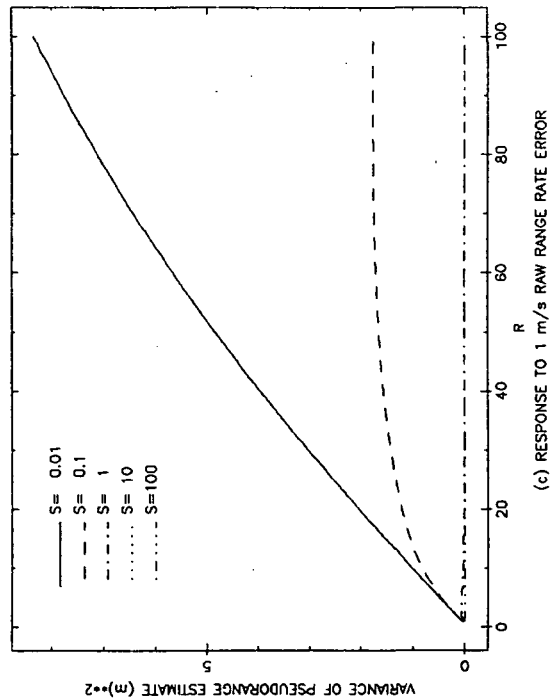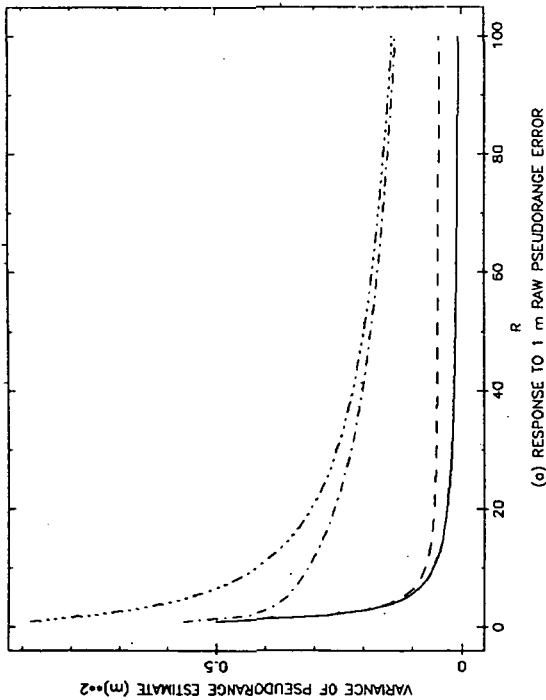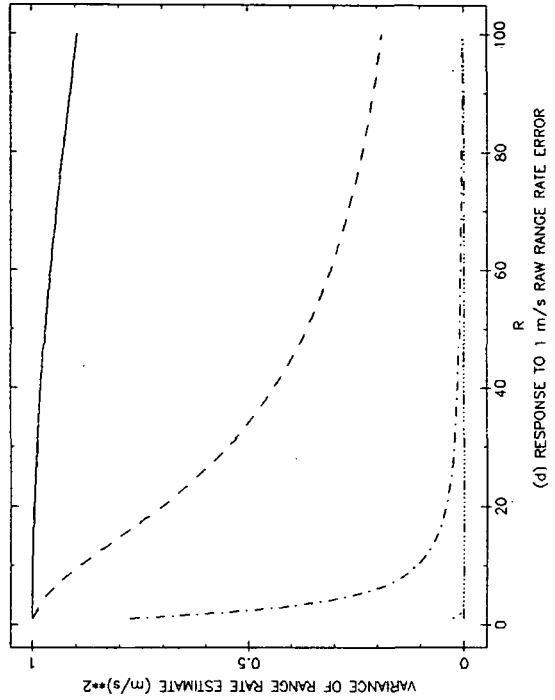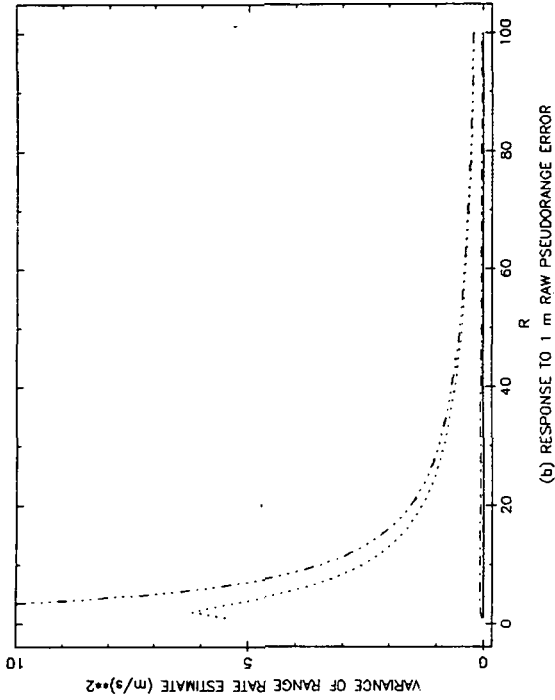
Figure B-5. Second Order Kalman Filter - Noise Response
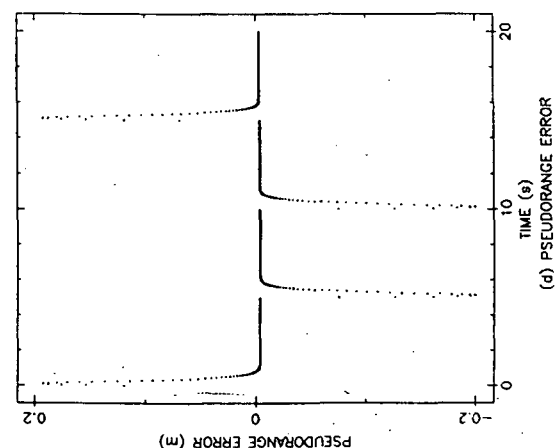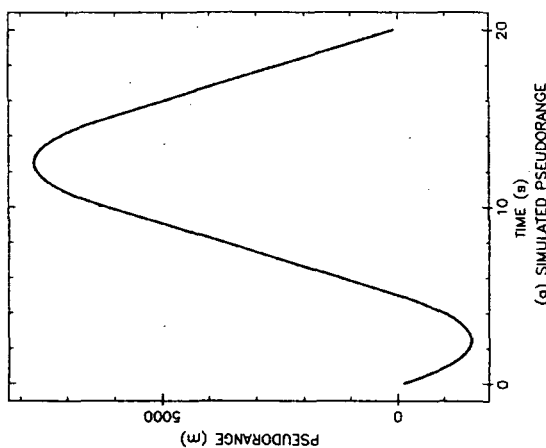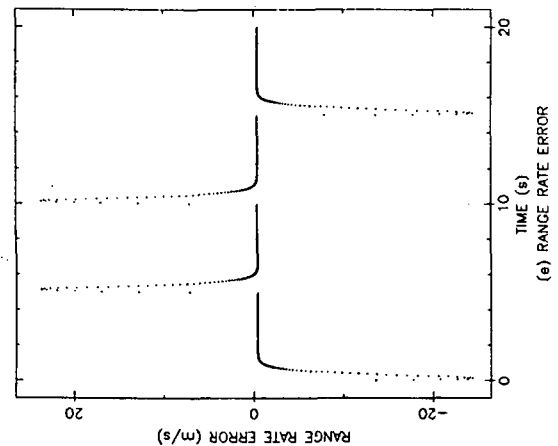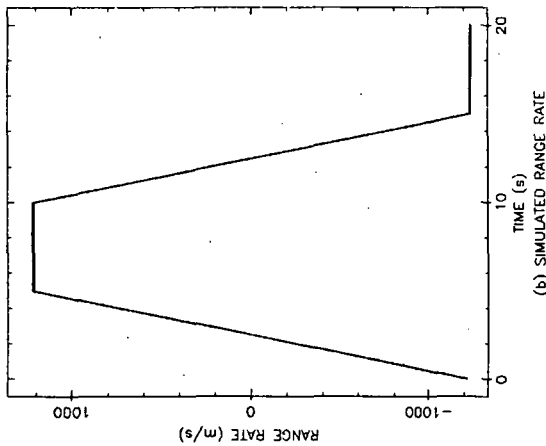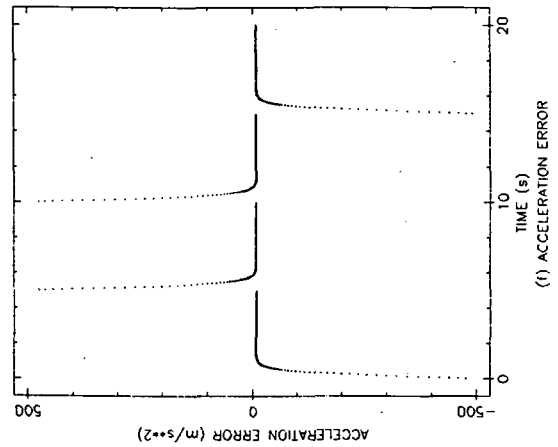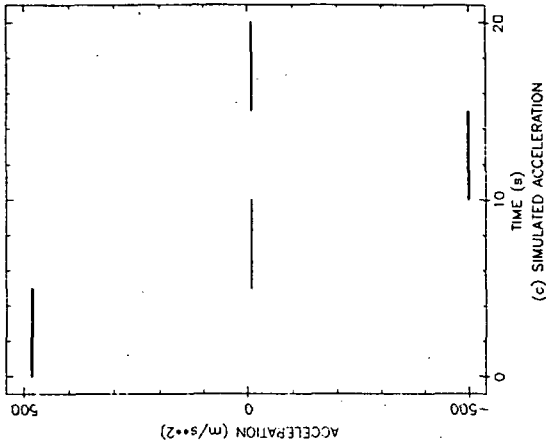
**Figure B-6.** Third Order Fading Memory Filter - Transient Response to Step Acceleration
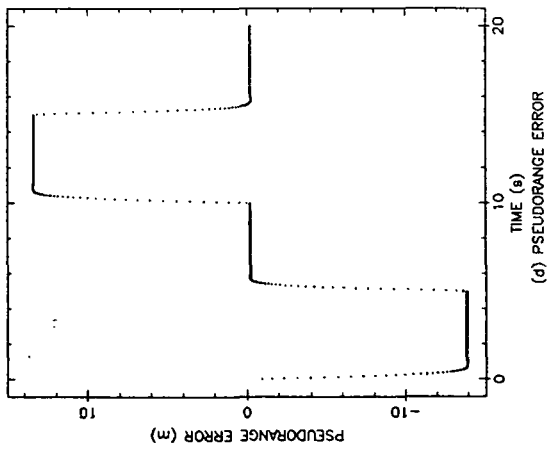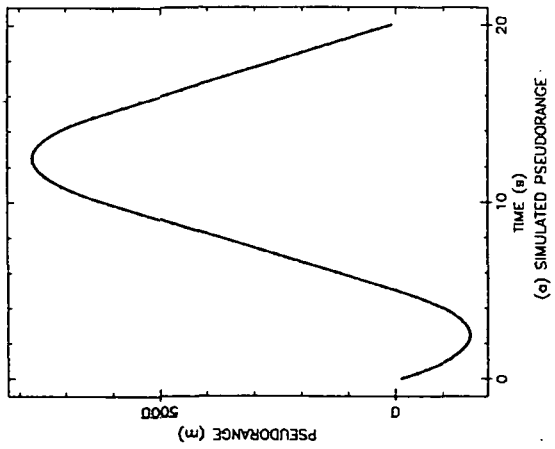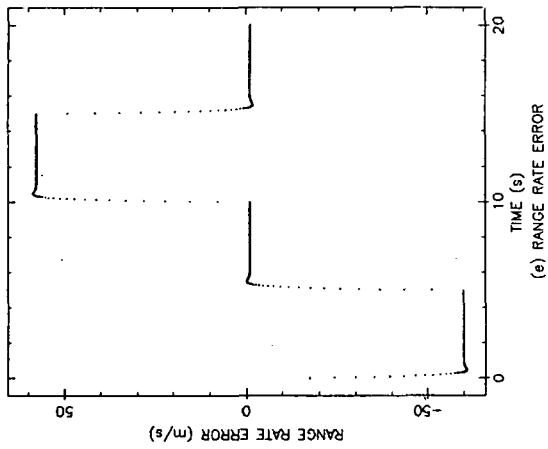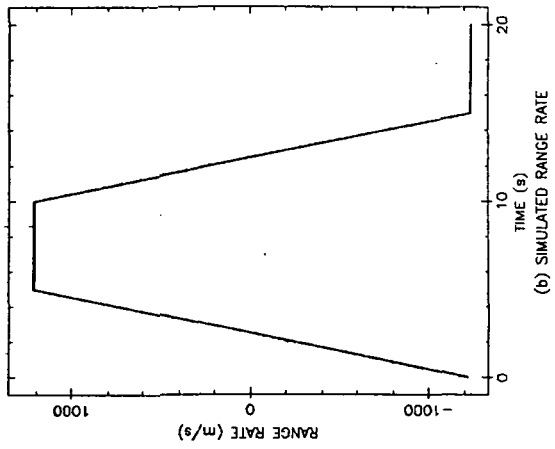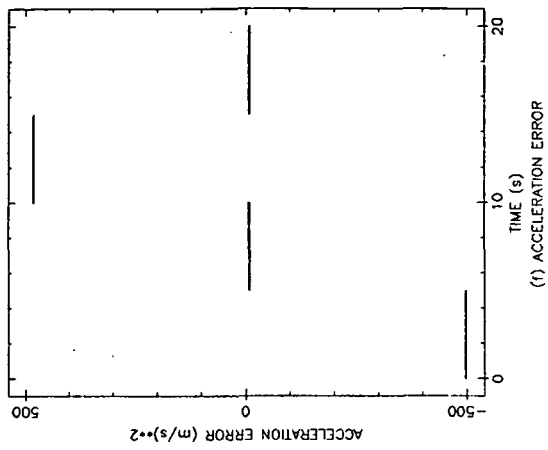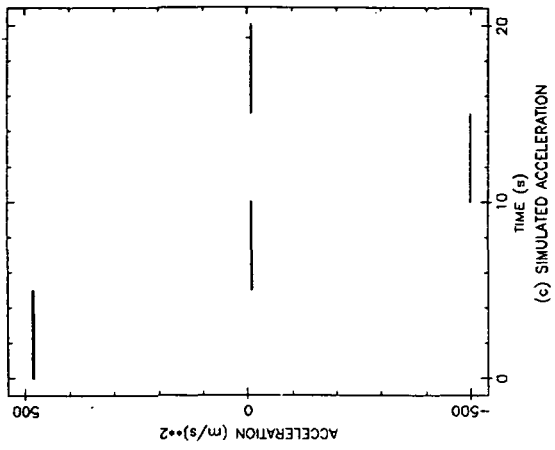
**Figure B-7.** Second Order Fading Memory Filter – Transient Response to Step Acceleration
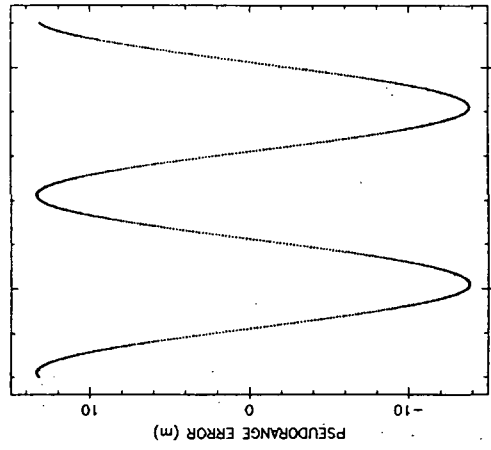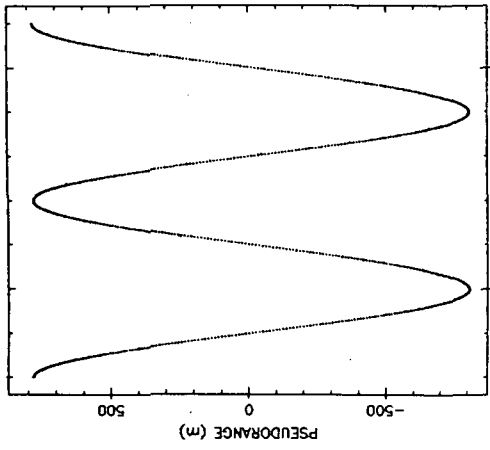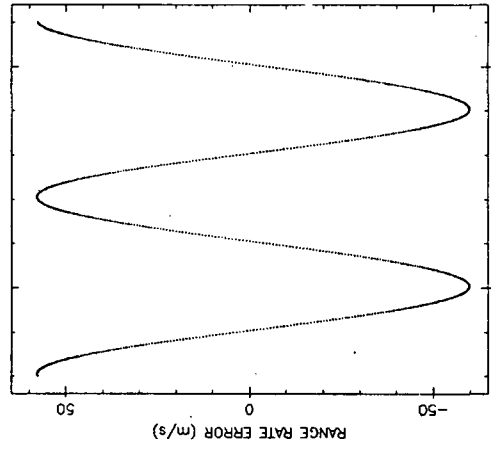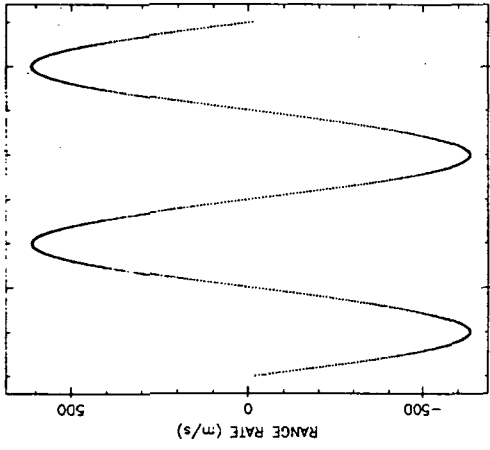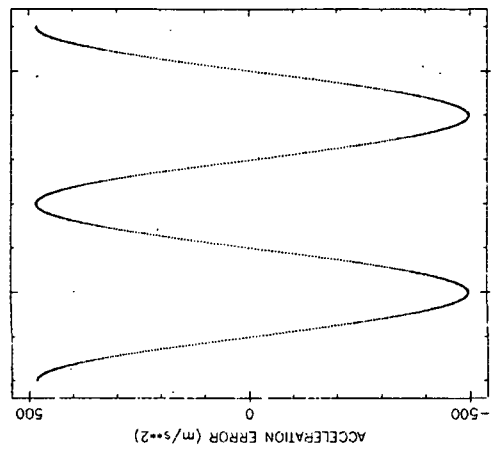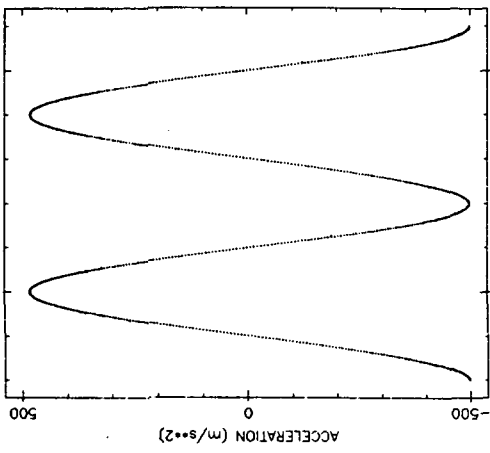
Figure B–8. Second Order Fading Memory Filter – Response to Sinusoidal Motion
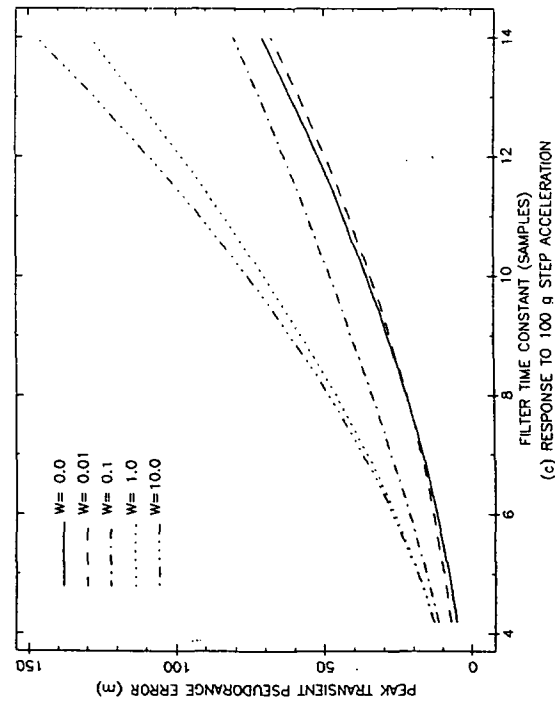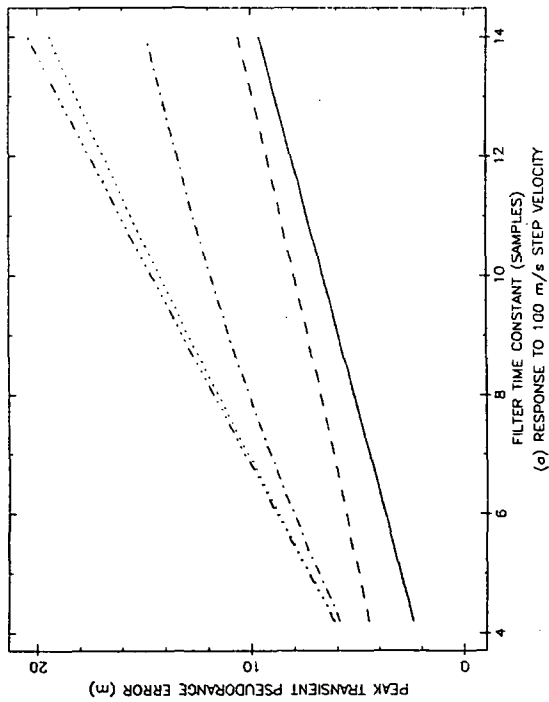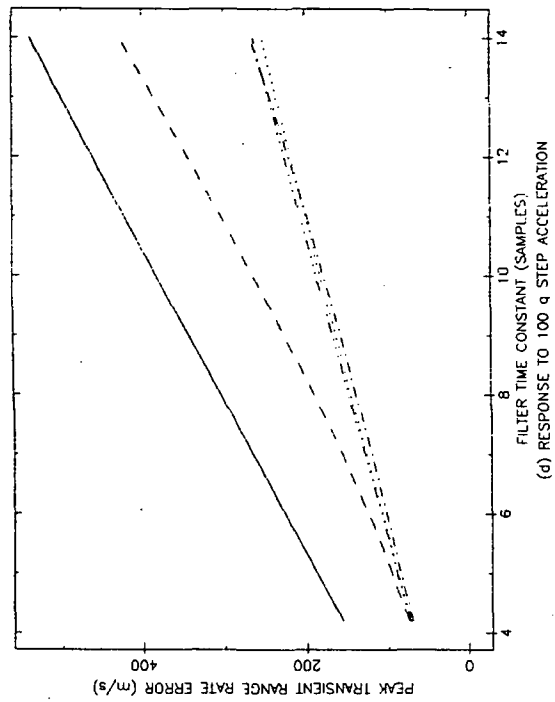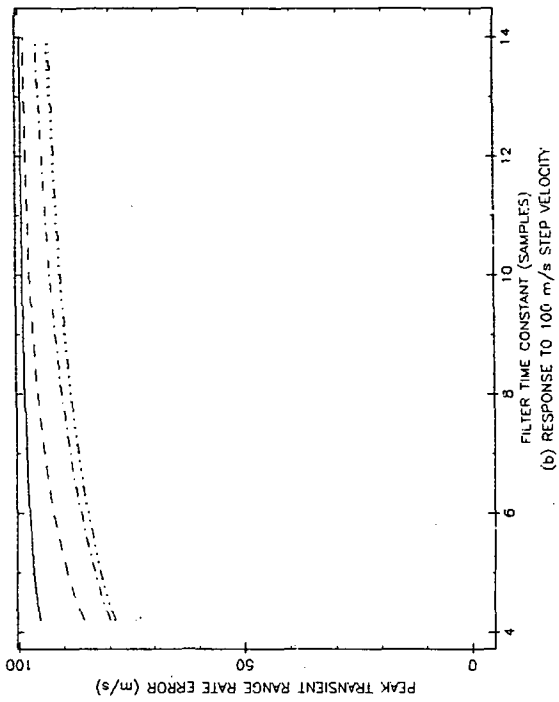
Figure B-9. Second Order Fading Memory Filter - Transient Response
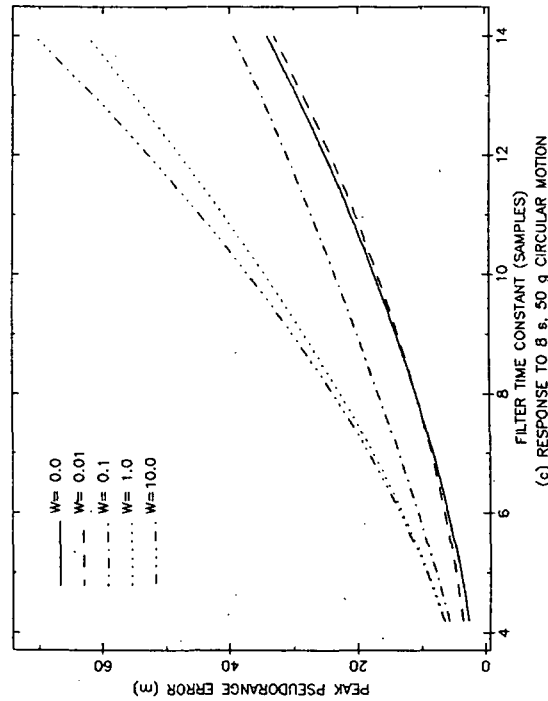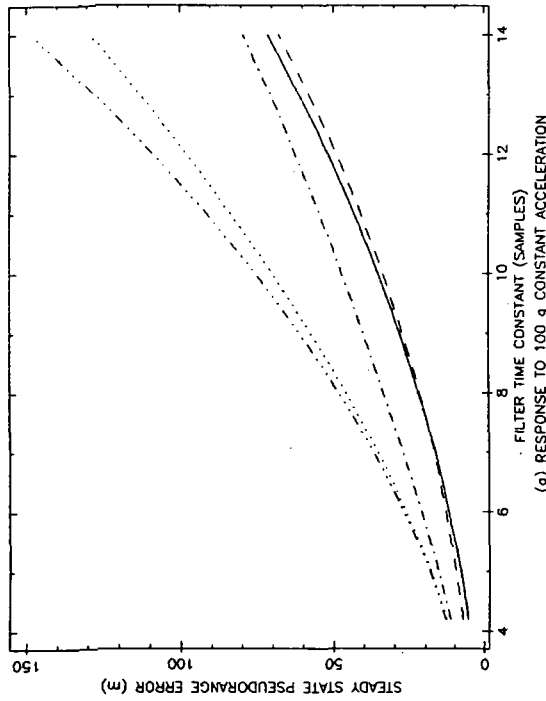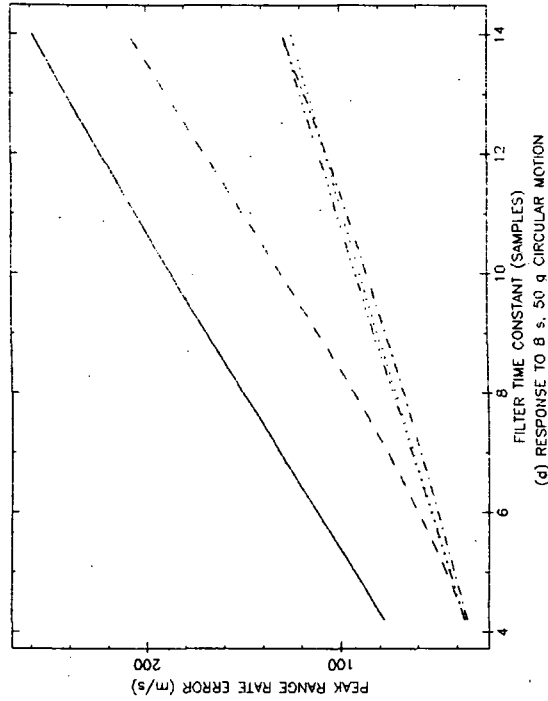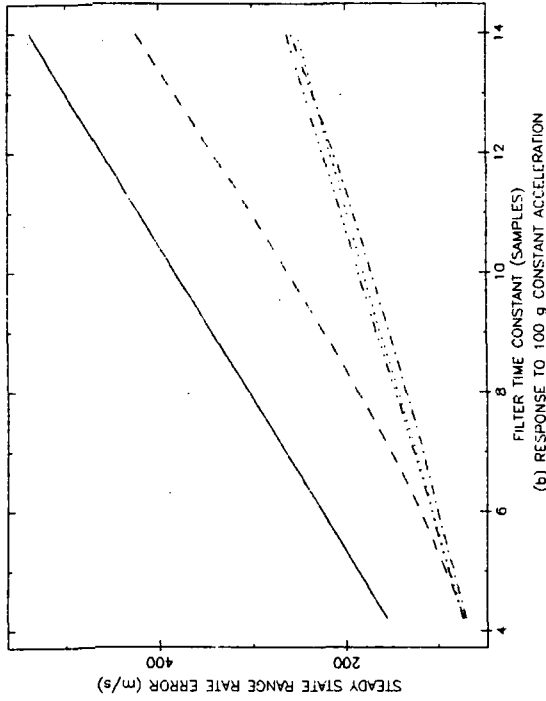
Figure B-10. Second Order Fading Memory Filter - Response to Constant
Acceleration and Sinusoids
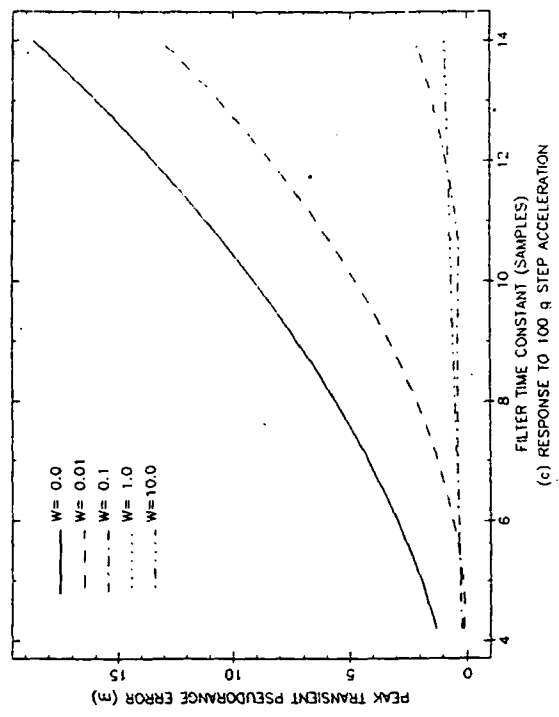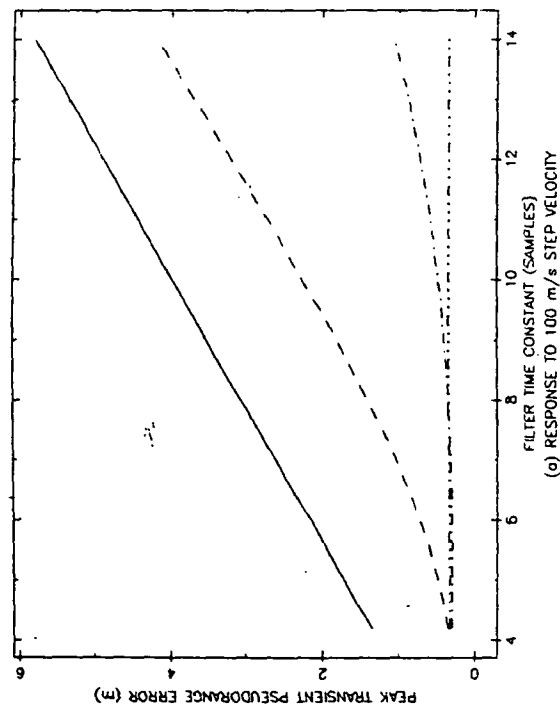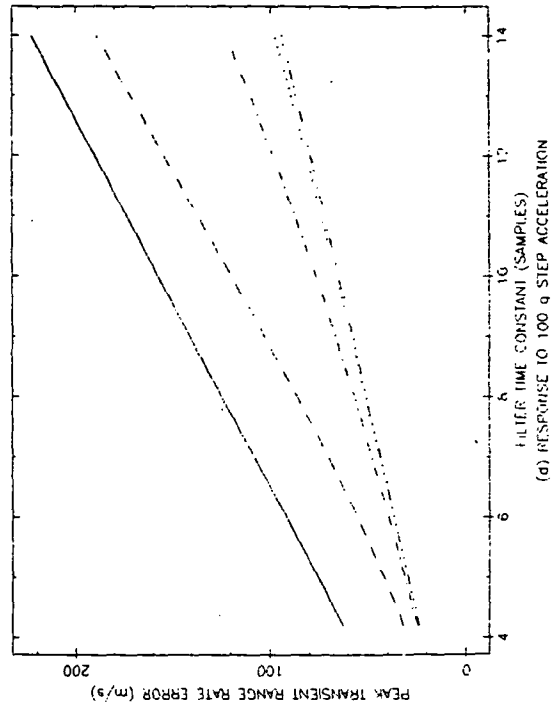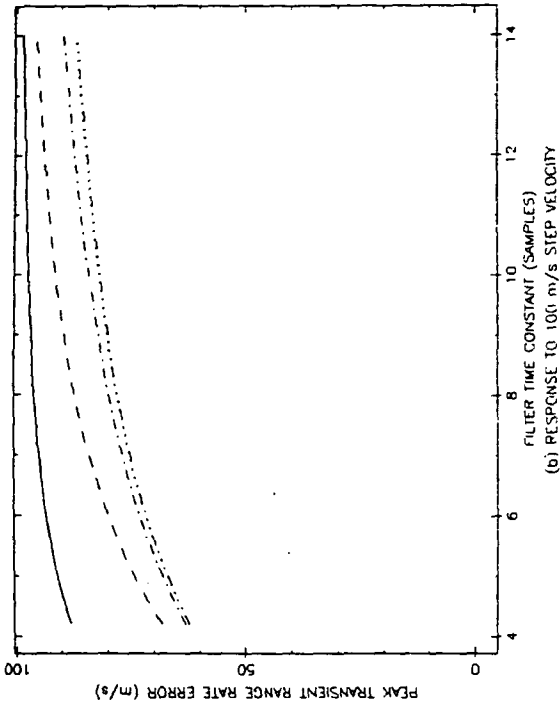
Figure B-11. Third Order Fading Memory Filter - Transient Response

**Figure B-12. Third Order Fading Memory Filter -- Response to Sinusoids**
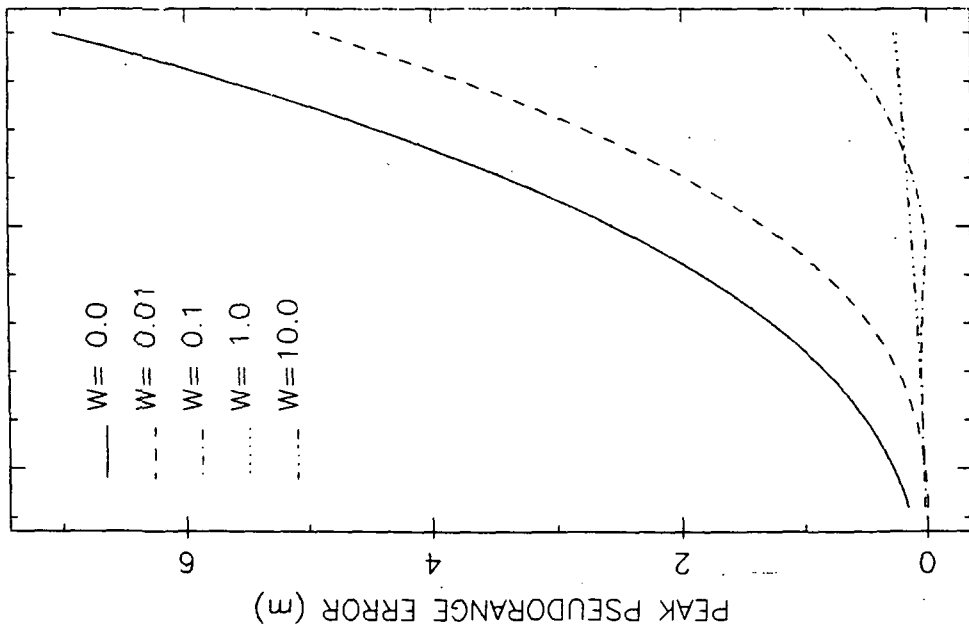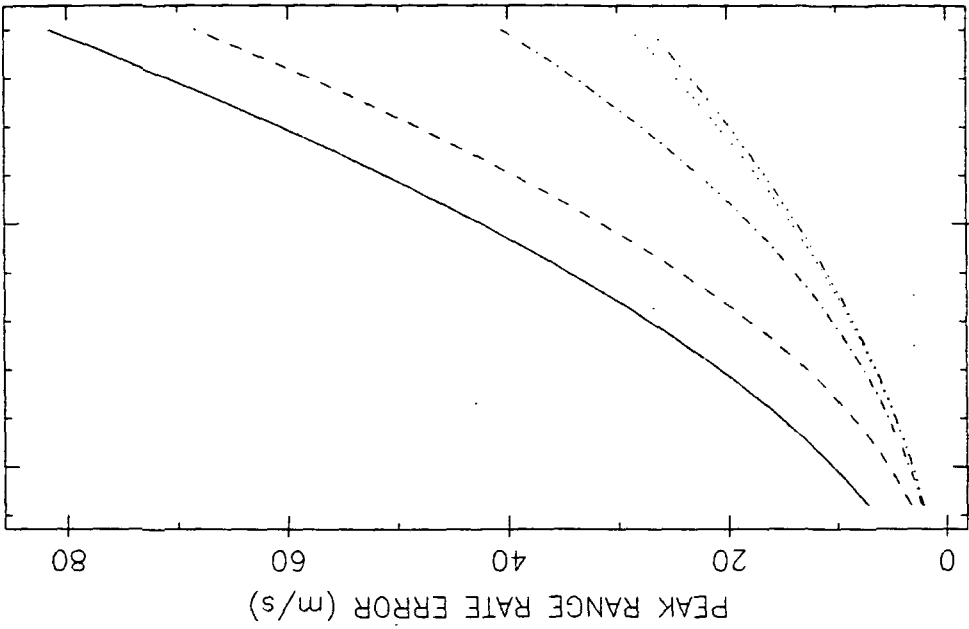
(a) RESPONSE TO 8 s, 50 g CIRCULAR MOTION

(b) RESPONSE TO 8 s, 50 g CIRCULAR MOTION
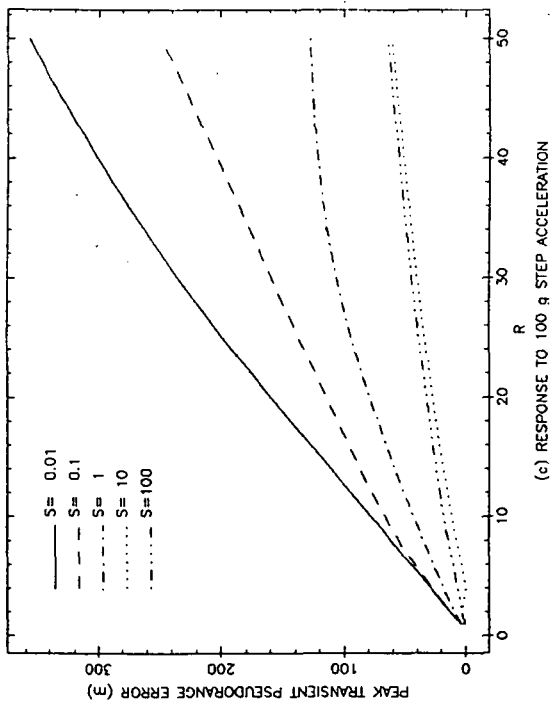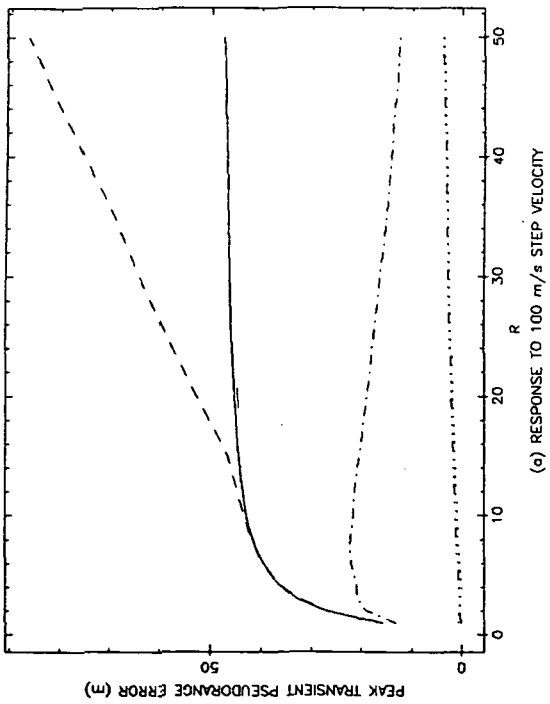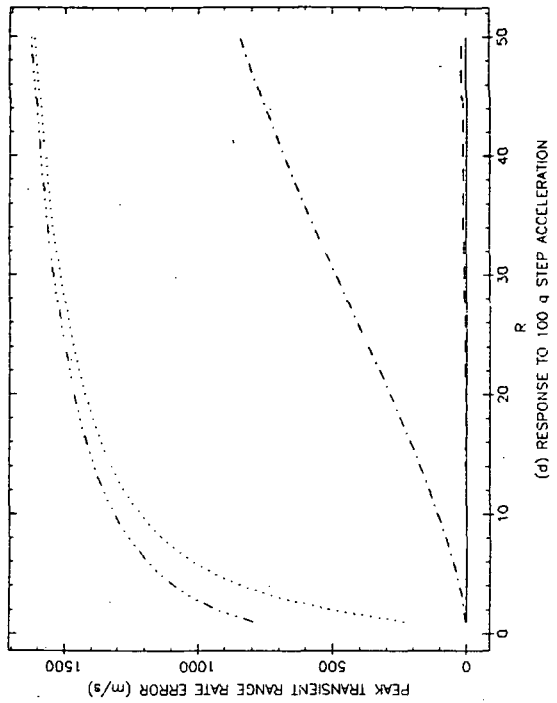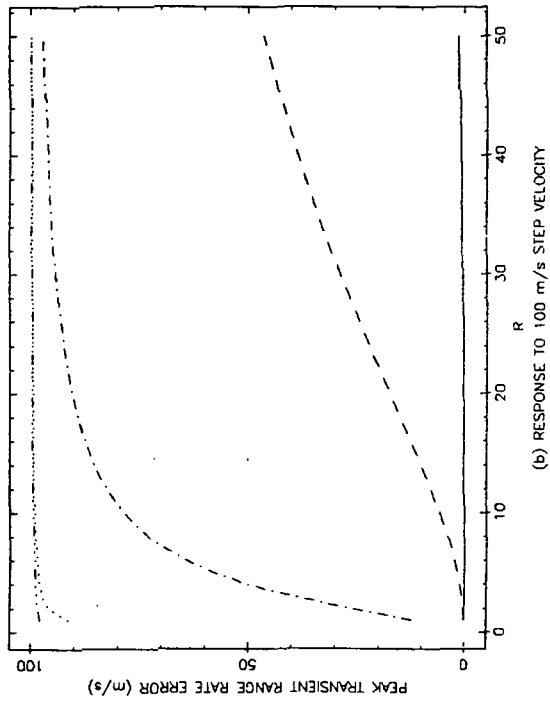
Figure B-13. Second Order Kalman Filter - Transient Response
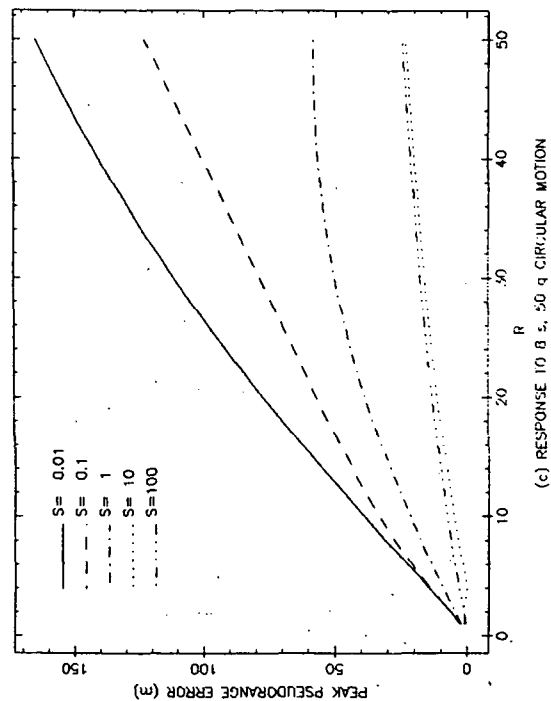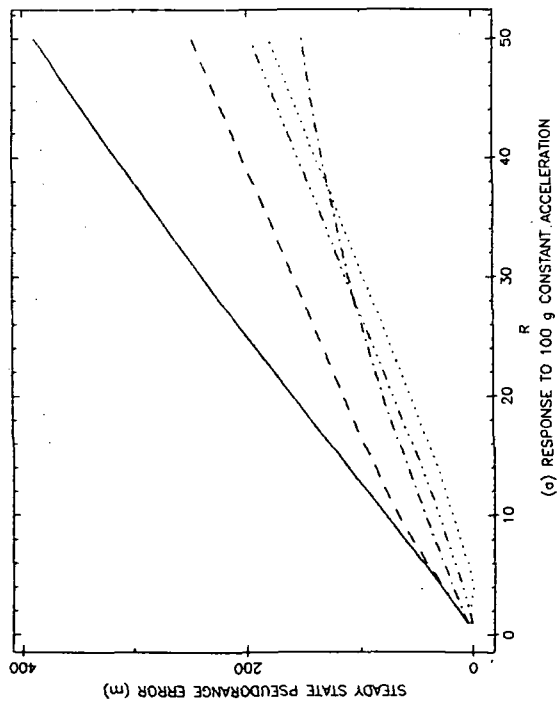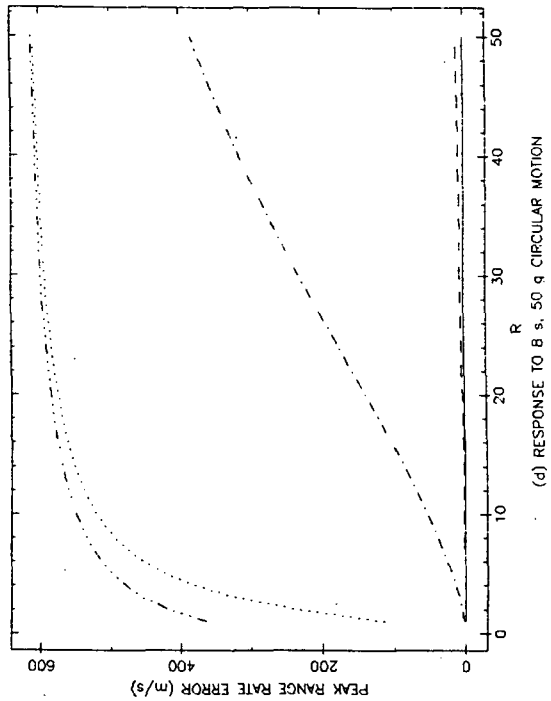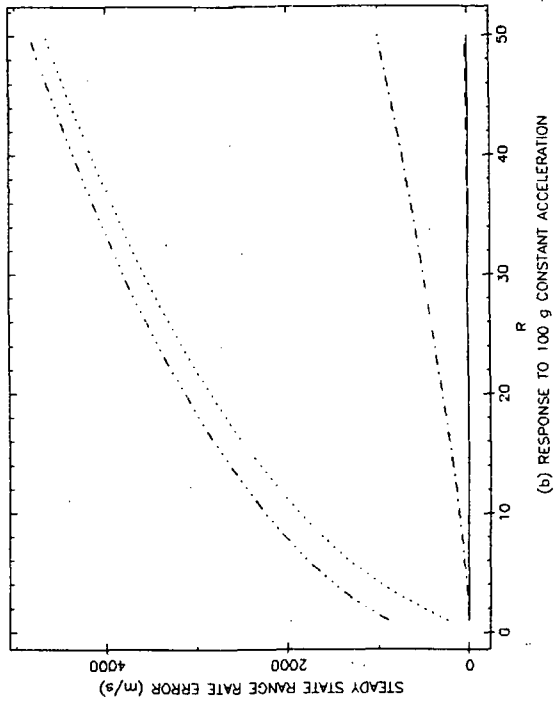
**Figure B-14.** Second Order Kalman Filter - Response to Constant Acceleration and Sinusoids
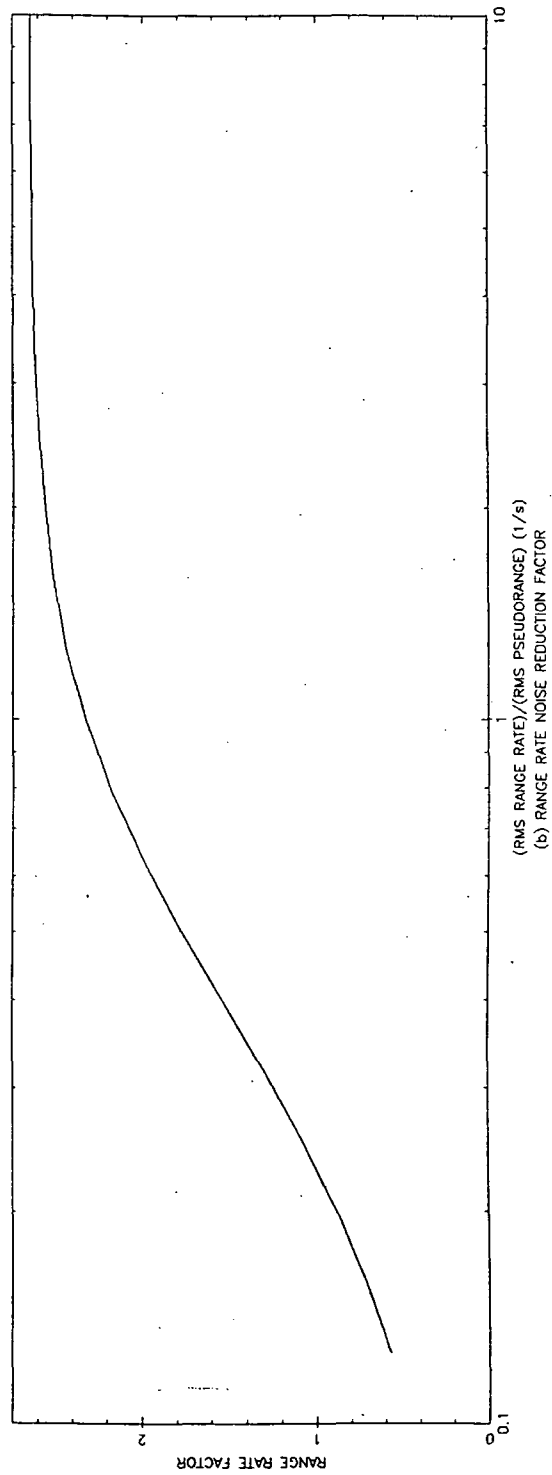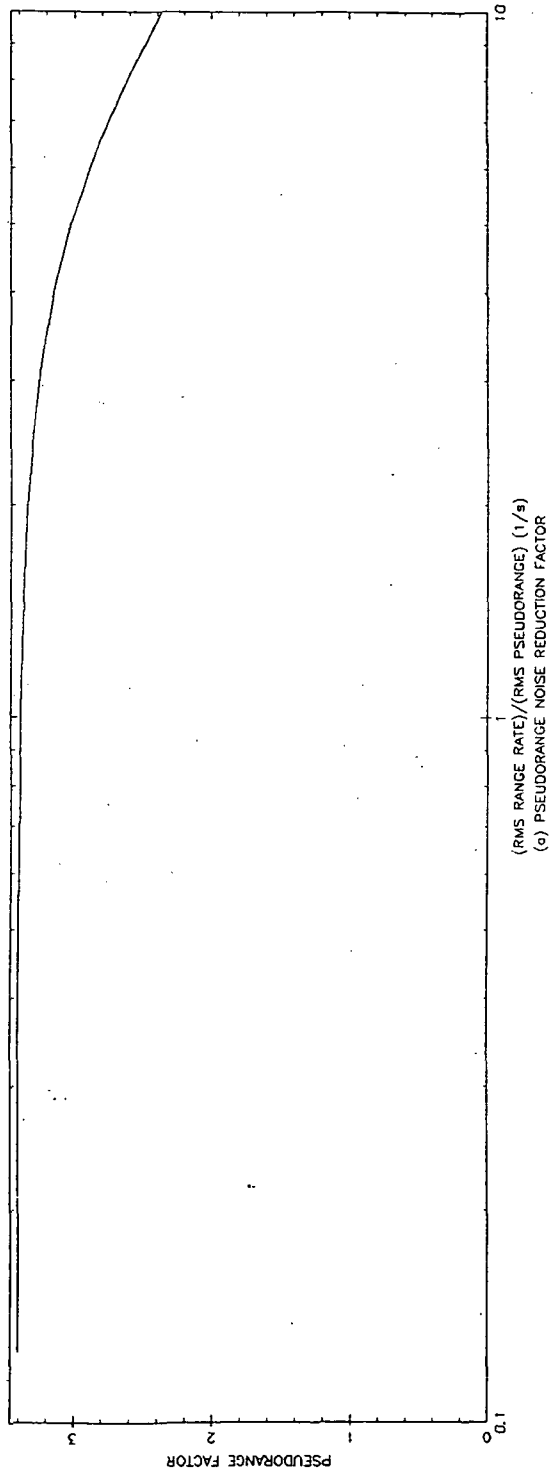
Figure B-15. Third Order Fading Memory Filter - Noise Reduction Factors
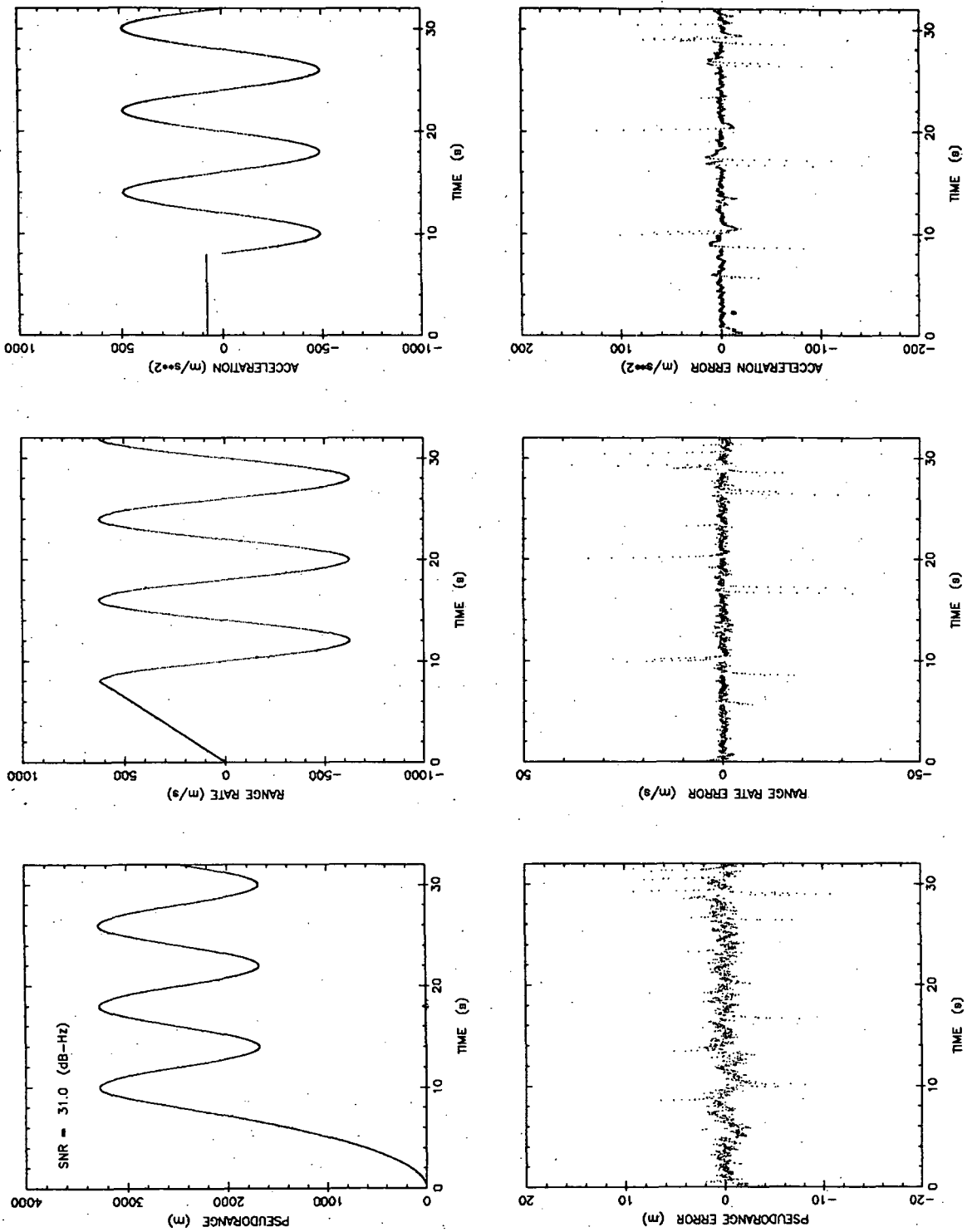
Figure B-16. Simulation Output (Circular Motion, 8 s Period, 50 g Acceleration)
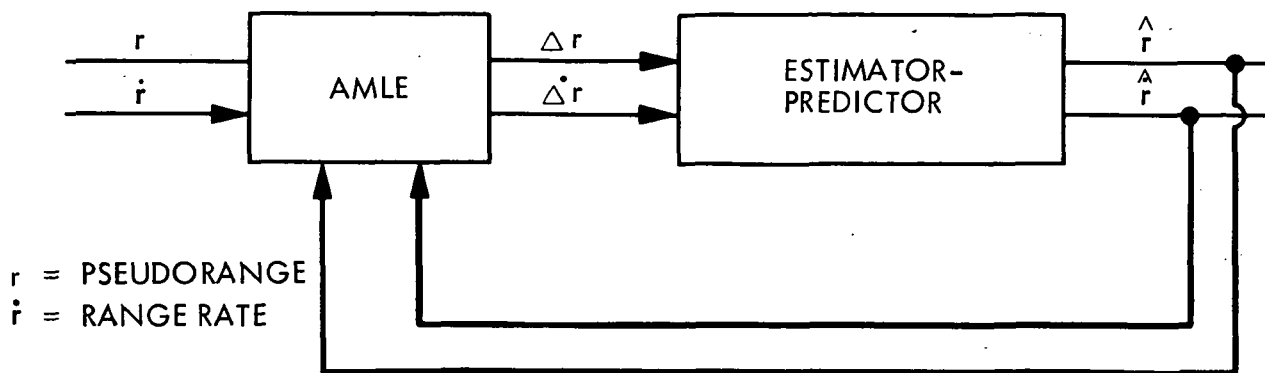
Figure B-17. Demonstration Receiver – Tracking Model

r = PSEUDORANGE
$\dot{r}$ = RANGE RATE
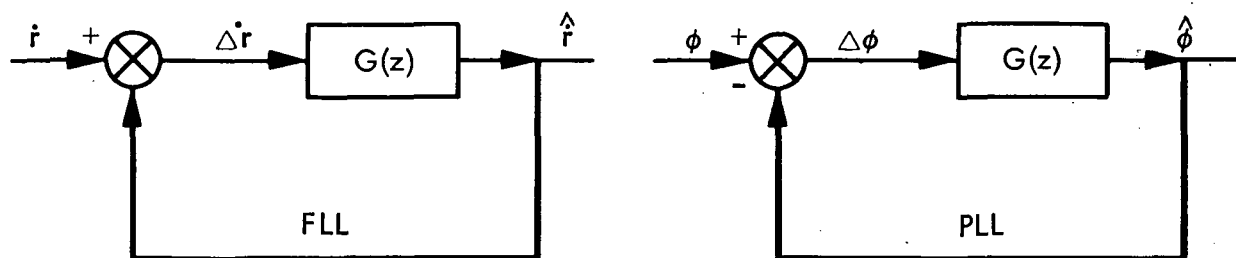


Figure B-18. PLL and FLL Functional Block Diagrams
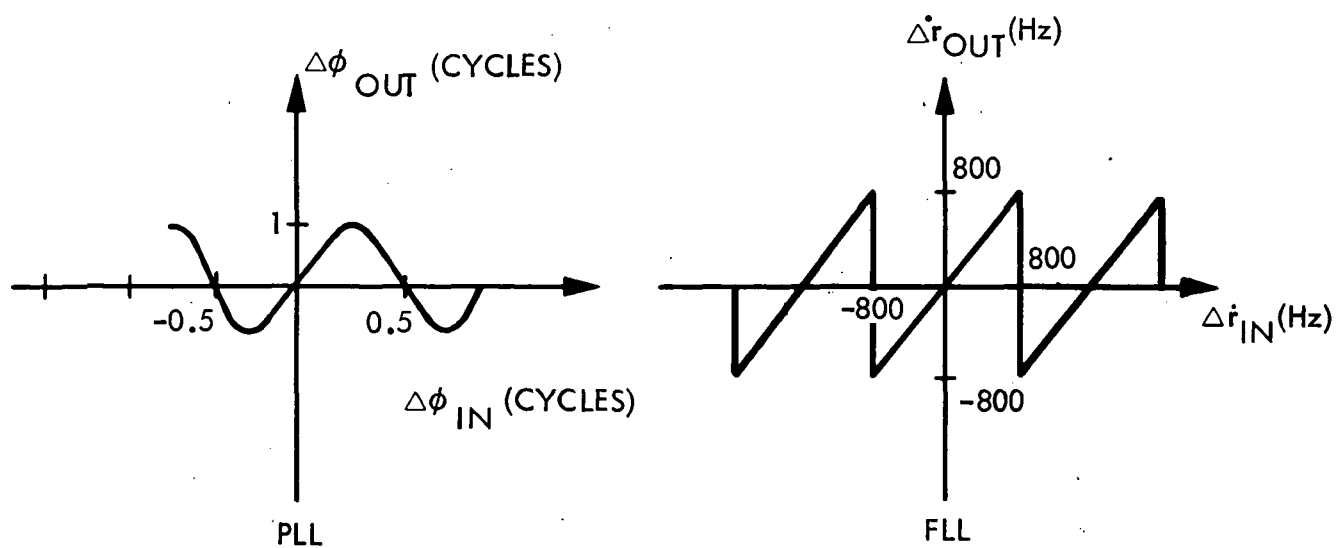


Figure B-19. Discriminator Characteristics
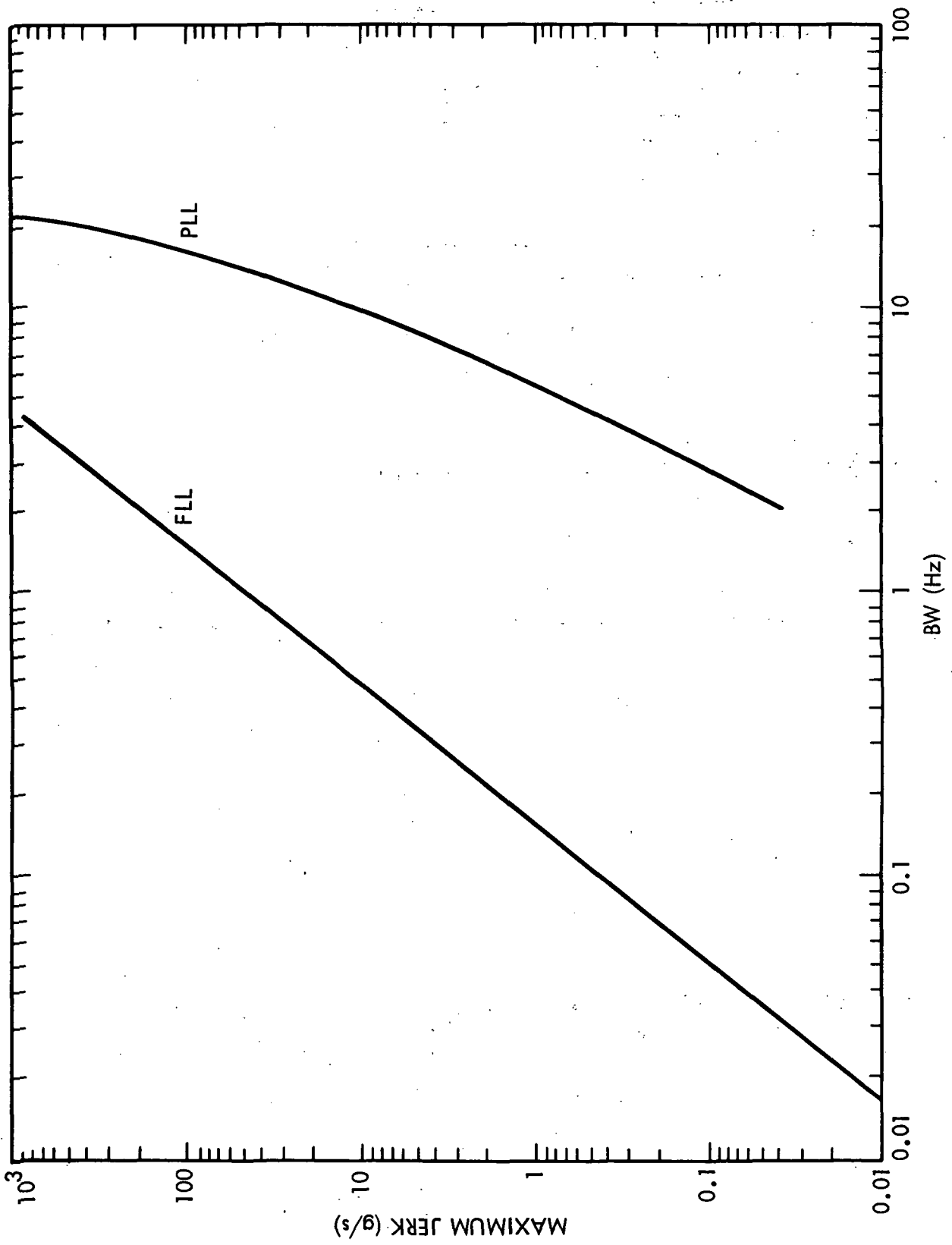
Figure B-20.   Maximum Allowed Input Dynamics for FLLs and PLLs versus Loop Bandwidth

# APPENDIX C

## DETAILED TEST RESULTS

This appendix describes the High Dynamic GPS Receiver Validation Demonstration tests in detail. It starts by defining the test conditions and the statistical significance of the results (C.1 and C.2). Then, for each category of tests, the rationale, test sequence and results are presented. The tests are divided into four categories: AMLE evaluation (C.3), tracking filter evaluation (C.4), tracking under high dynamic conditions (C.5), and performance at low SNR (C.6).

## C.1 TEST CONDITIONS

Each Demonstration test starts with a parameter selection phase, wherein the operator defines the test environment via a set of parameters. Each test is controlled in three areas: simulated trajectories, SNR conditions, and AMLE configuration. This section defines the relevant parameters and relates them to the test conduct.

### C.1.1 Simulated Trajectories

The TIS simulates the Doppler signature associated with a required trajectory by issuing a sequence of computer controlled frequencies to a programmable frequency synthesizer. The synthesizer changes phase coherently. There are three types of generic trajectories: constant velocity, step acceleration, and circular motion. Each of the simulated trajectories consists of five phases, as shown in Figure C-1a:

1. Initial - During the initial phase, typically 10 s to 15 s, the simulated range rate is zero. Code acquisition is achieved and verified and the average pseudorange bias is computed, so it can be removed from subsequent pseudorange error measurements.

2. Ramp up - For 10 s to 30 s the simulated range rate is linearly varied from zero to the maximum range rate of the test.

3. Test period - During the test period phase, the simulated range rate is varied according to the specified trajectory, as shown in Figure C-1b. In a constant velocity trajectory, the simulated range rate is maintained constant. In a step acceleration trajectory, the simulated acceleration is stepped between 0, a, 0, and -a, where a is the magnitude of the step acceleration. In a circular motion trajectory, the simulated range rate has sinusoidal variation.

4. Ramp down - This phase is the inverse of the ramp up phase. The simulated range rate is linearly varied from its maximum value to zero.

5. Final - During the final phase, typically 10 s to 15 s, the simulated range rate is zero.

Most of the circular motion tests were conducted with a cycle time of 8 s, or radian frequency of 0.78 radians/s. For example, a 50 g circular motion trajectory with cycle time of 8 s has peak pseudorange, range rate and acceleration of 810 m, 630 m/s, and 490 m/s$^2$, respectively.

The acceleration intervals in step acceleration tests were 6 s to 12 s long. As an example, in a 50 g step acceleration trajectory with 6 s acceleration the range rate changes from -1470 m/s to +1490 m/s (i.e. a total change of approximately 9 mach numbers) in 6 s.

The operator has control over the following parameters:

1. In all tests - duration of the initial and ramp up phases.

2. In constant velocity tests - test velocity

3. In step acceleration tests - magnitude and duration of acceleration, and magnitude and duration of constant velocity. Any subset of these specifications that completely defines the trajectory is acceptable.

4. In circular motion tests - cycle time, peak pseudorange, range rate, and acceleration. Again, any subset of these specifications that completely defines the trajectory is acceptable.

## C.1.2 SNR Conditions

Most tests were conducted at three SNR levels - high (60 dB-Hz), medium (40 dB-Hz) and low (34 dB-Hz). High SNR tests examine the signal dynamic range and the performance of the instrumentation. Medium SNR tests simulate operation with minimum nominal signal level, a 3.5 dB noise figure front end, and a 0 dBi antenna. Low SNR is the condition that occurs when a -6 dBi antenna is used, which is likely to happen in missile applications. In addition, tests were performed at SNRs lower than 34 dB-Hz to examine the receiver performance at very low SNRs and to determine the minimum SNR for reliable tracking.

The operator controlled the SNR by changing the fixed and variable attenuators in the signal path (see chapter 4). The measured values (signal power, noise power, and fixed attenuator) were entered in the TIS computer. The computer used these and the values of noise bandwidth and pre-determined SNR calibration to compute the SNR.

## C.1.3 AMLE Configuration

The AMLE configuration is determined by two controls: feedback to the AMLE window and selection of interpolation formulas. During normal tracking, there is feedback to center the window on the predicted pseudorange and range rate. For some of the tests this feedback is disabled, so the AMLE function can be evaluated over the complete window.

After identifying the pseudorange and range rate that maximize the AMLE function over a discrete set of points, interpolation formulas are used to estimate the location of the AMLE peak. The operator can select among several different formulas both for the pseudorange and the range rate. Detailed descriptions of the formulas appear in Appendix B.

## C.2 STATISTICAL SIGNIFICANCE

The main objective of the Data Evaluation Subsystem (DES) is to provide statistical evaluation of receiver performance. Specifically, the DES computes the sample mean and sample standard deviation for a finite sample set, and uses these as approximations to the mean and standard deviation of the corresponding random variables. This section discusses the processing steps and the quality of the approximation. It shows that for typical tests, two to ten minutes, the rms pseudorange and range rate noise were within 0.1 m and 0.1 m/s, repectively, of the standard deviation of the corresponding random variable, with probability 95 percent.

The DES computes three error measures for each of the pseudorange, range rate and acceleration variables: AMLE noise, total tracking error, and filtered noise. The AMLE noise is the variable at the output of the AMLE minus the same variable for the simulated trajectory. At low SNR, AMLE noise is dominated by (random) thermal effects, justifying the term "noise". The total tracking error is the variable at the output of the

tracking filter minus the same variable for the simulated trajectory. For a specific test, the total tracking error is affected by the random input, or AMLE noise, and by the deterministic lag introduced by the tracking filter. The third error measure, filtered noise, is generated when the lag introduced by the tracking filter is subtracted from the total tracking error.

Neither the AMLE noise, nor the filtered noise, are Gaussian variables. They contain instrumentation effects, biases and other non-random components. Still, for SNRs above 32 dB-Hz, both are approximated by Gaussian noise, and the AMLE noise samples are approximately independent. At lower SNRs, outliers (see B.3) occur, changing the statistical characteristics of these variables.

The statistical significance results presented in the remainder of this section are accurate only when the Gaussian noise approximation is valid. This is generally true for the AMLE noise and the filtered noise at SNR above 32 dB-Hz. Specifically excluded are the total tracking errors. The generic term "noise" refers both to AMLE noise and filtered noise.

In DES data processing, the non-zero sample mean of pseudorange noise is interpreted as clock bias between transmitter and receiver, and is removed. This is done because the Demonstration system can not separate the clock offset from the simulated pseudorange. The sample mean of the range rate noise was usually under 0.05 m/s, which is close to the modelled zero mean of the random variable.

The sample means and standard deviations are used as estimates of the means and standard variations of the corresponding random variables. The quality of the approximations can be represented by confidence intervals. For example, a 95 percent confidence interval for the mean of the random variable is the interval, centered at the sample mean, that includes the sample mean with probability 95 percent. Size of the confidence intervals depends on three quantities: the number of independent data points, the sample mean and the sample variance.

Data were recorded at the rate of ten points per second, each point representing 0.02 s. The data before the filter are statistically independent from point to point. The data after the filter are approximately independent as long as the filter time constant is longer than the 0.1 s sample spacing, which is the case for the selected third order fading memory filter with a time constant of 0.14 s. Thus, the number of independent data points can be computed by multiplying the test duration in seconds by 10, the number of samples per second. Typical tests lasted two to ten minutes, resulting in 1200 to 6000 points.

Given sample mean, sample standard deviation, and confidence level, the confidence interval for the mean of the random variable is:

$$\{M-b, \ M+b\} \tag{C-1}$$

where:

$$b = zS/(N-1)^{0.5}$$

M = sample mean
S = sample standard deviation
N = number of data points
z = 1.96 for 95% confidence level
    2.58 for 99% confidence level
    3.30 for 99.9% confidence level

As an example, let the pseudorange sample set contain 6000 points, the sample standard deviation be 1 m, and the confidence level be 95 percent. Then the mean of the random variable is within 0.025 m of the sample mean, with probability 95 percent. A similar result applies to range rate data. This example is typical of the Demonstration tests, where at SNRs higher that 32 dB-Hz, the sample standard deviation (or sample rms) were less than 1 m and 1 m/s, for pseudorange and range rate, respectively.

The confidence interval for the standard deviation of the random variable is:

$$\{aS,\ bS\} \tag{C-2}$$

where:

$$a = (1/(1+d))^{0.5}$$
$$b = (1/(1-d))^{0.5}$$
$$d = z(2/N)^{0.5}$$

z = 1.96 for 95% confidence level
    2.58 for 99% confidence level
    3.30 for 99.9% confidence level

For the previous example, The standard deviation of the random variable is between 0.98 and 1.02 of the sample standard deviation, with probability 95 percent.

## C.3 APPROXIMATE MAXIMUM LIKELIHOOD ESTIMATION EVALUATION

Approximate Maximum Likelihood Estimation (AMLE) is performed in three steps. First, discrete correlation data are collected over a bit time, and converted, by FFT, to the frequency domain. The result is a 64 by 11 window of FFT energy values. Then the peak energy over the AMLE window is identified, providing rough estimates of pseudorange and range rate. Finally, interpolation formulas are applied to the discrete AMLE values, generating finer estimates of the pseudorange and range rate. The AMLE evaluation tests measure the shape of the discrete AMLE function, evaluate various interpolation formulas, and assess the effect of NCO setting and input SNR on the AMLE pseudorange error.

The rms pseudorange and range rate errors caused by the originally selected AMLE interpolation formulas are 0.5 m and 0.1 m/s, respectively. Better formulas, introduced after the end of the formal tests, reduced the rms errors to less than 0.1 m and 0.1 m/s, respectively.

C.3.1 Measurement of Discrete AMLE Function

The discrete AMLE function was measured in six tests, all conducted under high SNR conditions:

1. SCH100 - In this test the simulated pseudorange was varied at 0.5 m/s for 500 seconds. The AMLE was restricted to maximize over frequency only, for lag 6, the center lag. The maximum amplitude over the AMLE window was recorded. Neglecting the effects of maximizing over frequency, this results in the cross correlation function between the simulated signal and the local code. Figure C-2a shows the maximum AMLE amplitude (in internal units) as a function of the simulated pseudorange. The resulting shape resembles the triangular autocorrelation function of PN sequences. The deviation of this waveform from triangular is caused primarily by the receiver lowpass filter. The "random" variation is caused primarily by instrumentation effects.

2. SCH101 - This test is similar to SCH100, except that the maximization is not restricted to lag 6. Figure C-2b shows that the maximum amplitude as a function of pseudorange is the envelope of nine overlapped correlation functions, separated by one half P code chip (i.e. one correlator lag). For pseudorange within the nine lag window, the maximum amplitude does not fall below 0.75 of the maximum amplitude when the codes are aligned (-2.5 dB). This means that there is at most 2.5 dB variation in detectability of the correct lag, as a function of pseudorange, modulo the pseudorange spacing. The width of the window is nine lags, rather than eleven, since the first and last lags are excluded from the maximization, and are used only for interpolation.

3. SCH102 - In this test the simulated pseudorange was constant, while the NCO frequency was swept at 0.01 Hz/bit (0.5 Hz/s). The sweep lasted 500 s with NCO frequencies between -125 Hz and +125 Hz. The test simulated fixed pseudorange with changing Doppler. The AMLE was restricted to maximize over the zero frequency bin. Figure C-3a shows the maximum AMLE amplitude (in internal units) as a function of the NCO setting. The resulting shape is of the sin(x)/x variety, with first nulls at 50 Hz, agreeing with the shape of the FFT filter. The dispersion of the results at zero NCO frequency is attributed to instrumentation effects. During the tests, the feedback to the NCO was always quantized to a multiple of 50 Hz, excluding zero, thus eliminating the dispersion.

C-6

4. SCH104 - This test is similar to SCH102, except that the maximization was restricted to frequency bin 1. Figure C-3b shows that the resulting response has a similar shape to that of C-3a, shifted by 25 Hz. Again the dispersion of results at zero NCO frequency is apparent.

5. SCH105 - This test is similar to SCH102, except that the maximization was not restricted. Figure C-3c shows that the the maximum amplitude is the envelope of sin(x)/x type curves with nulls at 50 Hz and spacing of 25 Hz. The minimum amplitude, at the intersection of filters is 0.9 of the peak amplitude (-0.9 dB). Thus detectability varies at most 0.9 dB with frequency, and the average amplitude is 0.3 dB relative to the peak. This figure was used in the processing loss budget.

6. SCH103 - This test is similar to SCH105, except the sweep covers the range of -800 Hz to +800 Hz. Figure C-3d shows the maximum AMLE amplitude as a function of the NCO setting. The resulting shape is the envelope of 64 of the filters shown in C-3a, separated by 25 Hz. The peaks of the waveform are on a sin(x)/x shape with nulls at 1600 Hz. This is caused by the lowpass filtering by integration over the correlation time, 1/1600 s. The amplitude at 800 Hz is 0.6 of the peak at 0 Hz. This agrees with the theoretical degradation of $2/\pi$ =0.63 (-4 dB).

## C.3.2 Effect of Code Adjustment

As shown in Appendix B, the clocking of the local P code generator must be adjusted each correlation interval to maintain the alignment of the local code and the predicted incoming code, to within one lag. The effect of this adjustment was demonstrated by two tests. In the first, the adjustment mechanism was active, while in the second it was deactivated. The tests show that in the absence of code adjustment, there is a significant reduction in signal level at the AMLE output, at high dynamics.

1. 841218T1 - This test measured the effect of range rate on the amplitude of the AMLE, with normal receiver configuration. The TIS simulated a 1 g acceleration from 0 m/s to 5000 m/s. Figure C-4a shows maximum AMLE amplitude vs. simulated range rate, showing no degradation due to range rate.

2. 841218T2 - This test is similar to 841218T1, except that the range rate adjustment was disabled. Figure C-4b shows that as the range rate increases, the signal at the AMLE output decreases, (i.e. the SNR decreases). Comparison between this test and the previous one illustrates the significance of code adjustment.

## C.3.3 Evaluation of Original Interpolation Formulas

The estimation of the peak of the continuous AMLE is performed by interpolating between points of the discrete AMLE. The procedure has three steps: first, the point with the highest AMLE amplitude is identified, then two adjacent points in frequency and two adjacent points in pseudorange are selected, and last, interpolation formulas are applied for pseudorange and range rate. Originally, four interpolation formulas were evaluated. The formulas are:

a. Triangular fit to the AMLE power output

b. Triangular fit to the AMLE amplitude output

c. Parabolic fit to the AMLE power output

d. Parabolic fit to the AMLE amplitude output

The formulas are described in Appendix B. To evaluate the formulas, tests were conducted at high SNR and under low dynamics. In all these tests the feedback that repositions the AMLE window was disabled. To evaluate the range rate interpolation formulas, the range rate error was computed as a function of the simulated range rate, where the simulated range rate is modulo a range rate bin (approximately 4.75 m/s), then the rms range rate error was computed. The rms errors for the four interpolation formulas are shown in Table C-1. Formula (d), parabolic interpolation of amplitude, has the lowest error, 0.1 m/s, and was chosen. The range rate error vs. range data is shown in Figure C-5a.

Table C-1 - Range rate Interpolation Formulas Evaluation

| case | METHOD | INPUT | RMS (m/s) | FOURIER COEFF (m/s) |
|------|--------|-------|-----------|---------------------|
| a | triangular | power | 0.102 | 0.110 |
| b | triangular | amplitude | 0.201 | 0.279 |
| c | parabolic | power | 0.236 | 0.270 |
| d | parabolic | amplitude | 0.106 | 0.100 |

The evaluation of pseudorange interpolation formulas was performed in a similar way. The pseudorange error was computed as a function of the simulated pseudorange, where the simulated pseudorange is modulo a pseudorange bin (approximately 14.7 m). The rms pseudorange errors for the four formulas are presented in Table C-2. Formula (b), triangular interpolation on amplitude, has the lowest error, 0.5 m, and was chosen. Pseudorange error vs. pseudorange is presented in Figure C-5b.

Table C-2 - Pseudorange Interpolation Formulas Evaluation

| case | METHOD | INPUT | RMS (m) | FOURIER COEFF (m) |
|------|-----------|-----------|-------|-------|
| a | triangular | power | 0.865 | 0.128 |
| b | triangular | amplitude | 0.512 | 0.073 |
| c | parabolic | power | 1.529 | 0.448 |
| d | parabolic | amplitude | 0.984 | 0.223 |

C.3.4 Evaluation of Upgraded Interpolation Formulas

After the end of the formal demonstration, new interpolation formulas were introduced, both for pseudorange and range rate. The formulas, described in Appendix B, are based on fits to the empirical shape of the AMLE function. Figure C-6 presents the pseudorange and range rate errors. Unlike the performance of the previous interpolation formulas, the upgraded formulas introduce very little bias in the interpolation process. The rms biases are under 0.1 m and 0.1 m/s in pseudorange and range rate, repectively.

C.3.5 AMLE Pseudorange Bias Versus SNR and NCO

Since the AMLE operation is nonlinear, the performance of the AMLE at medium and low SNR may be different than at high SNR. In a similar way, the NCO setting may affect the AMLE errors. A series of tests measured the AMLE pseudorange errors at low, medium and high SNR, and at various NCO settings. The tests showed that rms errors caused by the AMLE processing, i.e., after averaging of random noise, are independent of SNR and NCO setting.

## C.4 TRACKING FILTER EVALUATION

The pseudorange and range rate estimates generated by the AMLE are processed by a tracking filter. The filter has three objectives: to reduce the measurement noise, to estimate the receiver state (e.g., pseudorange, range rate, and acceleration), and to provide pseudorange and range rate predicts to the AMLE window. The tracking filters considered for the Demonstration Receiver are formulated and analyzed in Appendix B.4. This section describes the experimental results of filter evaluation tests.

Three classes of tracking filters were evaluated: second order fading memory filters, third order fading memory filters, and second order Kalman filters. In each class, 12 to 15 filters with different parameter combinations were tested. The common test bed was a 50 g step acceleration test, with peak range rate of 1470 m/s. The filters were compared in terms of noise response, steady state tracking error, and transient errors.

All test results agreed with theory. This is significant because it indicates that there were no significant unmodelled error sources. As a result of these tests, a third order fading memory filter with time constant of 0.14 s and range rate weight of 0.1 was selected for the rest of the demonstration tests.

The following sections describe the filter evaluation tests in detail.


### C.4.1 Second Order Fading Memory Filter

The second order fading memory filter operates on the raw pseudorange and range rate estimates and produces smooth estimates of the same variables. For a fixed update rate, it is defined by two parameters: filter time constant and range rate weight. Fifteen combinations of time constant and weight were selected, and the tests were repeated at high and low SNR, for a total of 30 tests.

Figure C-7 shows typical pseudorange and range rate errors as functions of time. This particular example is for a filter with a time constant of 0.14 s and range rate weight of 0.01. In general, the second order fading memory filter has zero pseudorange and range rate errors when the simulated range rate is constant, but generates lag errors in both variables when under constant acceleration. The lag errors are proportional to the acceleration. No transient overshoot errors are caused by the step acceleration. The fast variation of pseudorange error is caused by the original pseudorange interpolation formula.

Figure C-8 shows the coordinates of the AMLE maximum amplitude for the same test. The frequency detection occurs in bins -20 to +20. When compared to the total AMLE window width of 64 bins, this represents over 60% of the window width. This indicates that if the dynamics are increased from 50 g to 80 g, detection will occur on the window edge, and regardless of the random noise the receiver will lose lock. The pseudorange detection occurs mostly in bin 6 and rarely in bins 5 and 7. When compared to a total window

width of 11 bins, the pseudorange detection raises less concern about loss of lock than the frequency (or range rate) detection.

Figure C-9 presents the lag errors due to dynamics as functions of filter parameters, for high and low SNR. The errors appear independent of the SNR level. The pseudorange error increases with increase in filter time constant and with increase in range rate weight. In fact, for time constant of 0.14 s, only filters with range rate weight of under 0.02 meet the 10 m maximum error required by the Plan. The range rate error increases with increase in filter time constant, but has a minimum value when the range rate weight is between 0.02 and 0.1. Still, with a filter time constant of 0.14 s, the minimal range rate error is 60 m/s and, as seen in Figure C-8, the AMLE is close to loss of lock. The poor range rate performance when under constant acceleration is the main reason this filter was not selected for the rest of the Demonstration.

Figure C-10 summarizes the rms noise at the filter input and output, under low SNR conditions. The noise before and after the filter was defined in C.2 as the AMLE noise and the filtered noise. The rms noise at the input of the tracking filter is independent of the filter parameters, and is approximately 1.8 m and 0.6 m/s for pseudorange and range rate, respectively. The filter reduces the pseudorange rms noise to 0.5 m to 0.8 m, depending on the filter parameters. The improvement increases as filter time constant and range rate weight are increased. The effect of the filter on range rate is similar to the effect on pseudorange, except that it is more sensitive to change in range rate weight. In fact, at range rate weight of under 0.05, the range rate noise at the filter output is higher than that at the input.

Similar results were obtained at high SNR. The main difference from low SNR cases is that there is a smaller improvement in the pseudorange rms noise. This is because at high SNR the pseudorange noise is dominated by AMLE bias and not by random noise.

In summary, the second order fading memory filter, though providing adequate noise response and pseudorange response when under 50 g dynamics, is rejected because of high range rate error when under high dynamics.

C.4.2 Third Order Fading Memory Filter

The third order fading memory filter operates on the raw pseudorange and range rate estimates and produces smooth estimates of pseudorange, range rate and acceleration. For a fixed update rate, it depends on two parameters: filter time constant and range rate weight. Twelve combinations of these parameters were selected, and the tests were repeated at high and low SNR, for a total of 24 tests.

As shown in B.4, the third order fading memory filter has zero pseudorange and range rate error when the acceleration is constant. It has pseudorange and range rate errors proportional to jerk, when under constant jerk. In the case of step acceleration trajectory, the only lag errors are expected during the transient following the acceleration step. Figure C-11

presents typical pseudorange and range rate errors as functions of time, derived for a filter with a time constant of 0.14 s and range rate weight of 0.01. The transient pseudorange error is less than 0.2 m and cannot be separated from the ambient noise. The transient range rate error appears as a step error that decays within one or two filter time constants.

Figure C-12 presents the coordinates of the AMLE maximum amplitude for the same test. Unlike the second order filter results, the frequency detection deviates from the vicinity of the zero bin only during the short transient. For filters with identical time constant and range rate weight, the peak frequency deviation for third order filter is 14 bins, which is significantly smaller than that of the second order filter, 20 bins. The smaller deviation indicates that the third order filter can track higher dynamics, without loss of lock, than the second order filter. The pseudorange detection for the third order filter is in bins 5 to 7, similar to the second order filter.

Figure C-13 presents the peak transient errors caused by the step acceleration as functions of SNR and filter parameters. The pseudorange transient error cannot be reliably separated from the ambient noise. The peak transient range rate error increases with increasing filter time constant and with decreasing range rate weight.

The effect of the tracking filter on the AMLE pseudorange and range rate noise is shown in Figure C-14, for the low SNR case. Performance of the third order filter is similar to that of the second order filter. Again, when the range rate weight is less than 0.05, the rms range rate noise at the output of the tracking filter is higher than that at the input. Results are similar for high SNRs, except that the pseudorange noise reduction by the filter is smaller than for the low SNR case. This is because the noise is dominated by the AMLE bias and instrumentation effects rather than by random effects.

In summary, the third order fading memory filter exhibits many desired features, both in noise performance and dynamic performance. The filter selected for the rest of the demonstation is a third order filter with filter time constant of 0.14 s and range rate weight of 0.1. At 34 dB-Hz, it reduces the pseudorange and range rate rms errors by 3.5 and 1.2, respectively. In a 50 g step acceleration test, the peak transient errors are 0.2 m and 24 m/s, respectively.

C.4.3 Second Order Kalman Filter

The second order Kalman filter operates on the raw pseudorange and range rate estimates, producing smooth estimates of the same variables. It depends on three variables: standard deviation of pseudorange input, standard deviation of range rate input, and standard deviation of receiver acceleration. Details of filter formulation and a model for process noise are given in B.4. After normalizing the standard deviation of the pseudorange measurement to 1 m, the filter can be defined in terms of two variables: standard deviation of range rate (SIGV) and standard deviation of acceleration (SIGA). Twelve combinations of SIGV and SIGA were selected,

and tests were repeated at high and low SNR, for a total of 24 tests.

Results are similar to those of the second order fading memory filter except that for the Kalman filter it is easier to adjust the filter parameters to obtain lower range rate error. Figure C-15 shows an example of results from a test using a Kalman filter with SIGV=10 and SIGA=6000. The pseudorange and range rate errors are proportional to the acceleration, i.e. no errors at constant velocity. For this particular selection of parameters, there is almost no range rate error. Figure C-16 presents the locations of the AMLE maximum amplitude during the test, revealing peak frequency deviations of $\pm 7$ bins.

Figure C-17 present the errors induced by acceleration as functions of filter parameters and SNR level. As seen, the SNR level has no effect on the errors.

Figure C-18 summarizes the rms noise before and after the tracking filter. The rms range rate noise is not decreased by the filtering, and for some parameter combinations it even increases. The rms pseudorange noise is decreased by the filter, with the amount of decrease depending on the filter parameters. Similar results were obtained at high SNR.

In summary, the second order Kalman filter offers similar performance to that of the second order fading memory filter. When selecting a Kalman filter, the range rate error can be reduced, at a cost of increased rms noise at the output of the tracking filter. The superior range rate performance of the Kalman filter makes it a candidate for tracking at very high dynamics, e.g., accelerations in excess of 100 g; however, the corresponding pseudorange error may not be acceptable.

## C.5 TRACKING UNDER HIGH DYNAMIC CONDITIONS

The tests described in this section evaluate the Demonstration Receiver performance under various dynamics. Three types of generic trajectories are considered: constant velocity, step acceleration and circular motion. Performance is characterized for low, medium, and high SNR. The third order fading memory filter, selected in the previous section, is used for all the tests.

The total tracking errors consist of two components: a dynamic component, caused by the tracking filter lag error, and a static component, caused by random noise and instrumentation effects. The static effects include some indirect dynamic-dependent components. To separate the two components, the filtered noise, or the noise at the output of the tracking filter, is defined as the total tracking error minus the theoretical dynamic lag, where the theoretical dynamic lag is the error when passing the input trajectory through the receiver tracking filter.

As shown in Figure 6-9, the total pseudorange tracking error is very close to the filtered pseudorange noise even for dynamics as high as 50 g, 40 g/s, circular motion. This is true because the theoretical pseudorange

lag error for this case is 0.04 m rms. This approximation cannot be used directly when the dynamic component is not small relative to the static component.

C.5.1 Constant Velocity Tests

The constant velocity tests measured the receiver performance at velocities up to 10,000 m/s. The following tests were conducted:

1.  CVHnn - These were five tests, 160 s each, with constant range rate between 0.1 m/s and 10000 m/s, at high SNR.

2.  CVMnn - These tests were similar to CVHnn, except at medium SNR.

3.  CVLnn - These tests were similar to CVHnn, except at low SNR.

In these tests, the total tracking errors and the filtered noise errors are the same, because the dynamic components of the pseudorange and range rate errors are zero. Tables C-3, C-4, and C-5 summarize the rms noise levels at the tracking filter input and output.

Figure 6-3 shows rms noise at the input and output of the tracking filter. As the simulated range rate increases, there is slight increase in rms noise caused by higher instrumentation errors. At very low velocities, the rms errors increase because of AMLE bias introduced by the original AMLE interpolation formulas. This effect disappears when using the upgraded interpolation formulas.

Table C-3 - Constant Velocity Evaluation, High SNR

| TEST ID | | | RMS NOISE BEFORE FILTER | | RMS NOISE AFTER FILTER | |
|---|---|---|---|---|---|---|
| | | VELCTY (m/s) | RANGE (m) | VELCTY (m/s) | RANGE (m) | VELCTY (m/s) |
| CVH01 | | 300.0 | 0.421 | 0.062 | 0.044 | 0.050 |
| CVH02 | | 1000.0 | 0.454 | 0.071 | 0.063 | 0.057 |
| CVH03 | | 3300.0 | 0.431 | 0.116 | 0.082 | 0.064 |
| CVH11 | | 0.1 | 0.513 | 0.049 | 0.484 | 0.114 |
| CVH12 | | 10000.0 | 0.676 | 0.185 | 0.146 | 0.101 |

Table C-4 - Constant Velocity Evaluation, Medium SNR

| TEST ID | | RMS NOISE BEFORE FILTER | | | RMS NOISE AFTER FILTER | |
|---|---|---|---|---|---|---|
| | VELCTY (m/s) | RANGE (m) | VELCTY (m/s) | RANGE (m) | VELCTY (m/s) | |
| CVM01 | 300.0 | 0.923 | 0.235 | 0.229 | 0.211 | |
| CVM02 | 1000.0 | 0.950 | 0.327 | 0.256 | 0.235 | |
| CVM03 | 3300.0 | 1.000 | 0.422 | 0.285 | 0.260 | |
| CVM11 | 0.1 | 0.916 | 0.260 | 0.610 | 0.210 | |
| CVM12 | 10000.0 | 1.144 | 0.462 | 0.318 | 0.336 | |

Table C-5 - Constant Velocity Evaluation, Low SNR

| TEST ID | | RMS NOISE BEFORE FILTER | | | RMS NOISE AFTER FILTER | |
|---|---|---|---|---|---|---|
| | VELCTY (m/s) | RANGE (m) | VELCTY (m/s) | RANGE (m) | VELCTY (m/s) | |
| CVL01 | 300.0 | 1.739 | 0.496 | 0.480 | 0.416 | |
| CVL02 | 1000.0 | 1.856 | 0.691 | 0.527 | 0.484 | |
| CVL03 | 3300.0 | 1.845 | 0.794 | 0.567 | 0.525 | |
| CVL11 | 0.1 | 1.735 | 0.506 | 0.807 | 0.420 | |
| CVL12 | 10000.0 | 2.128 | 1.206 | 0.642 | 0.652 | |

## C.5.2 Step Acceleration Tests

The step acceleration tests measured performance with step accelerations of up to 100 g. The tests consisted of:

1.  SAHnn – These were seven tests, 240 s each, with accelerations between 3 g and 100 g, at high SNR. The acceleration lasted for 6 s.

2.  SAMnn – These tests were similar to SAHnn, except at medium SNR.

3.  SALnn – These tests were similar to SAHnn, except at low SNR.

Tables C-6, C-7, and C-8 list transient tracking errors and rms noise at the inputs and outputs of the tracking filter.

Figure 6-5 shows the transient tracking errors. The transient pseudorange error could not reliably be separated from the ambient noise. The theoretical peak pseudorange error for 50 g step acceleration trajectory is 0.2 m. The transient range rate error is proportional to the acceleration and is approximately 50 m/s at 100 g, well within the tracking capabilities of the system.

Figure 6-4 shows rms noise at the inputs and outputs of the tracking filter. These errors are independent of the acceleration. There is better noise reduction at low SNR, where random errors dominate, than at high SNR, where instrumentation effects dominate.

## Table C-6 - Step-Acceleration Evaluation, High SNR

| TEST ID | | TRANSIENT DURING ACCELERATION | | RMS NOISE BEFORE FILTER | | RMS NOISE AFTER FILTER | |
|---|---|---|---|---|---|---|---|
| | ACCEL (g) | RANGE (m) | VELCTY (m/s) | RANGE (m) | VELCTY (m/s) | RANGE (m) | VELCTY (m/s) |
| SAH01 | 3.0 | (1) | 1.6 | 0.459 | 0.145 | 0.167 | 0.178 |
| SAH02 | 10.0 | (1) | 4.5 | 0.438 | 0.109 | 0.135 | 0.108 |
| SAH03 | 20.0 | (1) | 10.0 | 0.449 | 0.139 | 0.199 | 0.127 |
| SAH04 | 30.0 | (1) | 14.0 | 0.480 | 0.147 | 0.201 | 0.120 |
| SAH05 | 50.0 | (1) | 25.0 | 0.489 | 0.180 | 0.375 | 0.177 |
| SAH11 | 100.0 | (1) | 48.0 | 0.486 | 0.249 | 0.319 | 0.218 |
| SAH12 | 75.0 | (1) | 35.0 | 0.447 | 0.203 | 0.338 | 0.185 |

(1) Transient pseudorange error is low, and cannot be separated from the random noise reliably.

Table C-7 - Step-Acceleration Evaluation, Medium SNR

| TEST ID | | TRANSIENT DURING ACCELERATION | | RMS NOISE BEFORE FILTER | | RMS NOISE AFTER FILTER | |
|---------|------------|--------------|----------------|--------------|----------------|--------------|----------------|
| | ACCEL (g) | RANGE (m) | VELCTY (m/s) | RANGE (m) | VELCTY (m/s) | RANGE (m) | VELCTY (m/s) |
| SAM01 | 3.0 | (1) | 1.8 | 1.031 | 0.355 | 0.318 | 0.296 |
| SAM02 | 10.0 | (1) | 5.0 | 0.983 | 0.312 | 0.279 | 0.240 |
| SAM03 | 20.0 | (1) | 10.0 | 0.962 | 0.356 | 0.312 | 0.255 |
| SAM04 | 30.0 | (1) | 15.0 | 1.010 | 0.393 | 0.321 | 0.275 |
| SAM05 | 50.0 | (1) | 25.0 | 1.005 | 0.338 | 0.460 | 0.269 |
| SAM11 | 100.0 | (1) | 47.0 | 1.041 | 0.454 | 0.399 | 0.330 |
| SAM12 | 75.0 | (1) | 36.0 | 1.007 | 0.395 | 0.407 | 0.299 |

(1) Transient pseudorange error is low, and cannot be separated from the random noise reliably.

## Table C-8 - Step-Acceleration Evaluation, Low SNR

| TEST ID | ACCEL (g) | TRANSIENT DURING ACCELERATION | | RMS NOISE BEFORE FILTER | | RMS NOISE AFTER FILTER | |
|---|---|---|---|---|---|---|---|
| | | RANGE (m) | VELCTY (m/s) | RANGE (m) | VELCTY (m/s) | RANGE (m) | VELCTY (m/s) |
| SAL01 | 3.0 | (1) | 2.0 | 1.676 | 0.579 | 0.448 | 0.452 |
| SAL02 | 10.0 | (1) | 5.5 | 1.581 | 0.521 | 0.433 | 0.389 |
| SAL03 | 20.0 | (1) | 10.0 | 1.602 | 0.592 | 0.456 | 0.405 |
| SAL04 | 30.0 | (1) | 15.0 | 1.697 | 0.666 | 0.508 | 0.461 |
| SAL05 | 50.0 | (1) | 24.0 | 1.652 | 0.578 | 0.563 | 0.452 |
| SAL11 | 100.0 | (1) | 50.0 | 1.761 | 0.769 | 0.560 | 0.546 |
| SAL12 | 75.0 | (1) | 38.0 | 1.654 | 0.669 | 0.573 | 0.520 |

(1) Transient pseudorange error is low, and cannot be separated from the random noise reliably.

## C.5.3 Circular Motion Tests

Circular motion tests measured the tracking performance for a simulated circular motion trajectory with acceleration up to 150 g and jerk up to 157 g/s. The circular motion tests consist of the following:

1. CMHnn - These were five tests, each containing twenty loops of 8 s each, for a total of 160 s, with accelerations between 10 g and 100 g, at high SNR.

2. CMMnn - These tests were similar to CMHnn, except at medium SNR.

3. CMLnn - These tests were similar to CMHnn, except at low SNR.

Tables C-9, C-10, and C-11 summarize rms tracking errors and rms noise at the inputs and outputs of the tracking filter.

Figure 6-7 shows the rms tracking errors. The rms pseudorange error is less than 0.6 m, it varies with the SNR, and it is almost independent of acceleration. The rms range rate error is proportional to the acceleration and is less than 11 m/s at 100 g. As shown in Figure 6-2, the range rate

error is sinusoidal and thus has a peak of 1.4 times the rms value.

Figure 6-6 shows the rms noise at the inputs and outputs of the tracking filter. The increase in noise level at higher accelerations is caused by higher instrumentation effects. Note that filtered noise is under 0.5 m and 0.8 m/s rms for pseudorange and range rate, respectively.

In addition, tests were performed using a cycle time of 6 s and accelerations of 100 g and 150 g. The corresponding jerks are 104 g/s and 157 g/s, respectively. Figures C-19 and C-20 show the tracking errors and the location of the AMLE maximum amplitude for the 150 g test.

Table C-9 - Circular Motion Evaluation, High SNR

| TEST ID | | RMS LAG ERROR | | RMS NOISE BEFORE FILTER | | RMS NOISE AFTER FILTER | |
|---------|---------|---------|---------|---------|---------|---------|---------|
| | ACCEL (g) | RANGE (m) | VELCTY (m/s) | RANGE (m) | VELCTY (m/s) | RANGE (m) | VELCTY (m/s) |
| CMH01 | 10.0 | 0.2 | 1.1 | 0.476 | 0.109 | 0.234 | 0.143 |
| CMH02 | 20.0 | 0.1 | 2.2 | 0.462 | 0.119 | 0.141 | 0.124 |
| CMH03 | 50.0 | 0.1 | 5.4 | 0.445 | 0.200 | 0.157 | 0.161 |
| CMH11 | 100.0 | 0.2 | 10.7 | 0.475 | 0.298 | 0.144 | 0.225 |
| CMH12 | 75.0 | 0.2 | 8.0 | 0.505 | 0.251 | 0.199 | 0.210 |

### Table C-10 - Circular Motion Evaluation, Medium SNR

| TEST ID | | RMS LAG ERROR | | RMS NOISE BEFORE FILTER | | RMS NOISE AFTER FILTER | |
|---------|-----------|-------------|---------------|-------------|----------------|-------------|----------------|
| | ACCEL (g) | RANGE (m) | VELCTY (m/s) | RANGE (m) | VELCTY (m/s) | RANGE (m) | VELCTY (m/s) |
| CMM01 | 10.0 | 0.3 | 1.1 | 0.969 | 0.319 | 0.306 | 0.273 |
| CMM02 | 20.0 | 0.3 | 2.1 | 0.983 | 0.329 | 0.294 | 0.252 |
| CMM03 | 50.0 | 0.3 | 5.3 | 1.035 | 0.374 | 0.300 | 0.297 |
| CMM11 | 100.0 | 0.3 | 10.7 | 1.080 | 0.470 | 0.320 | 0.330 |
| CMM12 | 75.0 | 0.3 | 8.0 | 1.057 | 0.441 | 0.305 | 0.298 |

### Table C-11 - Circular Motion Evaluation, Low SNR

| TEST ID | | RMS LAG ERROR | | RMS NOISE BEFORE FILTER | | RMS NOISE AFTER FILTER | |
|---------|-----------|-------------|---------------|-------------|----------------|-------------|----------------|
| | ACCEL (g) | RANGE (m) | VELCTY (m/s) | RANGE (m) | VELCTY (m/s) | RANGE (m) | VELCTY (m/s) |
| CML01 | 10.0 | 0.5 | 1.1 | 1.590 | 0.653 | 0.471 | 0.434 |
| CML02 | 20.0 | 0.4 | 2.1 | 1.593 | 0.594 | 0.446 | 0.426 |
| CML03 | 50.0 | 0.4 | 5.3 | 1.693 | 0.635 | 0.486 | 0.454 |
| CML11 | 100.0 | 0.5 | 10.7 | 1.859 | 0.760 | 0.519 | 0.528 |
| CML12 | 75.0 | 0.5 | 8.C | 1.802 | 0.701 | 0.537 | 0.505 |

## C.6 PERFORMANCE AT LOW SNR

The purpose of these tests, also denoted "extended SNR tests", was to determine the minimum SNR at which tracking is possible, and to evaluate the rms pseudorange and range rate errors as a function of SNR. The tests determined that the receiver can reliably track at SNRs down to 28 dB-Hz, almost independent of dynamics.

Three tests were conducted at each SNR:

1.  3 g, 8 s, circular motion.

2.  50 g, 8 s, circular motion.

3.  100 g, 8 s, circular motion

In all the tests, the third order fading memory filter selected for the Demonstration was used. The tests continued with lower SNR, in steps of 1 dB, as long as one minute of tracking without loss of lock was achieved.

Tables C-12 and C-13 summarize the rms pseudorange and range rate noise at the inputs and outputs of the tracking filter.

Figure 6-8 shows the rms pseudorange noise at the output of the tracking filter, for the different dynamics, demonstrating that the noise performance and the loss of lock SNR are independent of dynamics.

## Table C-12 - Extended SNR, Circular Motion, 8 s, 50 g

| TEST ID | SNR (dB-Hz) | RMS NOISE BEFORE FILTER | | RMS NOISE AFTER FILTER | | TOTAL RMS ERROR | |
|---|---|---|---|---|---|---|---|
| | | RANGE (m) | VELCTY (m/s) | RANGE (m) | VELCTY (m/s) | RANGE (m) | VELCTY (m/s) |
| XES101 | 60.1 | 0.39 | 0.15 | 0.15 | 0.13 | 0.13 | 5.39 |
| XES103 | 50.1 | 0.50 | 0.19 | 0.17 | 0.16 | 0.16 | 5.40 |
| XES105 | 40.1 | 1.03 | 0.36 | 0.32 | 0.28 | 0.31 | 5.40 |
| XES107 | 34.1 | 1.70 | 0.62 | 0.56 | 0.50 | 0.56 | 5.43 |
| XES109 | 32.4 | 2.37 | 0.88 | 0.74 | 0.67 | 0.87 | 5.52 |
| XES113 | 38.0 | 1.31 | 0.45 | 0.39 | 0.35 | 0.38 | 5.41 |
| XES115 | 33.3 | 2.36 | 0.78 | 0.67 | 0.73 | 0.67 | 5.47 |
| XES117 | 31.3 | 3.13 | 6.60 | 1.07 | 2.42 | 1.07 | 5.95 |
| XES119 | 30.3 | 4.00 | 10.30 | 1.80 | 5.32 | 1.80 | 7.59 |
| XES121 | 29.9 | 6.23 | 15.09 | 2.48 | 6.99 | 2.48 | 8.90 |
| XES123 | 28.8 | 8.06 | 22.37 | 4.14 | 12.03 | 4.12 | 13.77 |
| XES125 | 27.9 | 12.55 | 36.60 | 6.84 | 24.03 | 6.84 | 25.56 |
| XES127 | 27.9 | 12.70 | 35.07 | 6.73 | 20.82 | 6.72 | 22.56 |

Table C-13 - Extended SNR, Circular Motion, 8 s, 3 g

| TEST ID | SNR (dB-Hz) | RMS NOISE BEFORE FILTER | | RMS NOISE AFTER FILTER | | TOTAL RMS ERROR | |
|---|---|---|---|---|---|---|---|
| | | RANGE (m) | VELCTY (m/s) | RANGE (m) | VELCTY (m/s) | RANGE (m) | VELCTY (m/s) |
| XES102 | 60.1 | 0.17 | 0.16 | 0.07 | 0.13 | 0.07 | 0.27 |
| XES104 | 50.1 | 0.34 | 0.18 | 0.11 | 0.15 | 0.11 | 0.29 |
| XES106 | 40.1 | 1.01 | 0.34 | 0.29 | 0.28 | 0.29 | 0.37 |
| XES108 | 34.1 | 1.93 | 0.62 | 0.59 | 0.51 | 0.59 | 0.56 |
| XES110 | 32.4 | 2.38 | 0.80 | 0.72 | 0.65 | 0.72 | 0.69 |
| XES114 | 38.0 | 1.17 | 0.43 | 0.34 | 0.33 | 0.34 | 0.41 |
| XES116 | 33.3 | 2.23 | 1.92 | 0.68 | 0.91 | 0.68 | 0.93 |
| XES118 | 31.3 | 2.60 | 0.89 | 0.85 | 1.10 | 0.85 | 1.13 |
| XES120 | 30.3 | 3.93 | 8.26 | 1.47 | 2.93 | 1.47 | 2.90 |
| XES122 | 29.9 | 5.17 | 12.58 | 2.26 | 5.96 | 2.26 | 5.96 |
| XES124 | 28.8 | 7.08 | 19.83 | 3.28 | 9.86 | 3.28 | 9.86 |
| XES126 | 27.9 | 11.61 | 30.88 | 5.68 | 16.52 | 5.68 | 16.52 |
| XES128 | 27.9 | 11.35 | 29.40 | 5.58 | 16.60 | 5.58 | 16.60 |
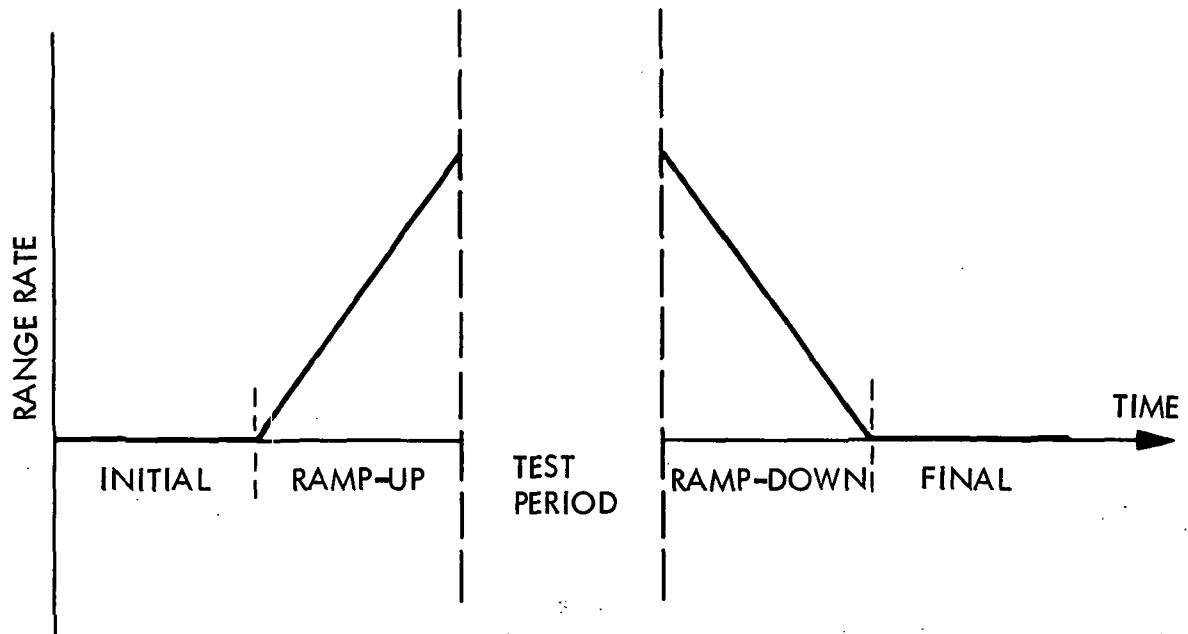
(a). The Five Phases of a Typical Test



CONSTANT VELOCITY    STEP ACCELERATION    CIRCULAR MOTION
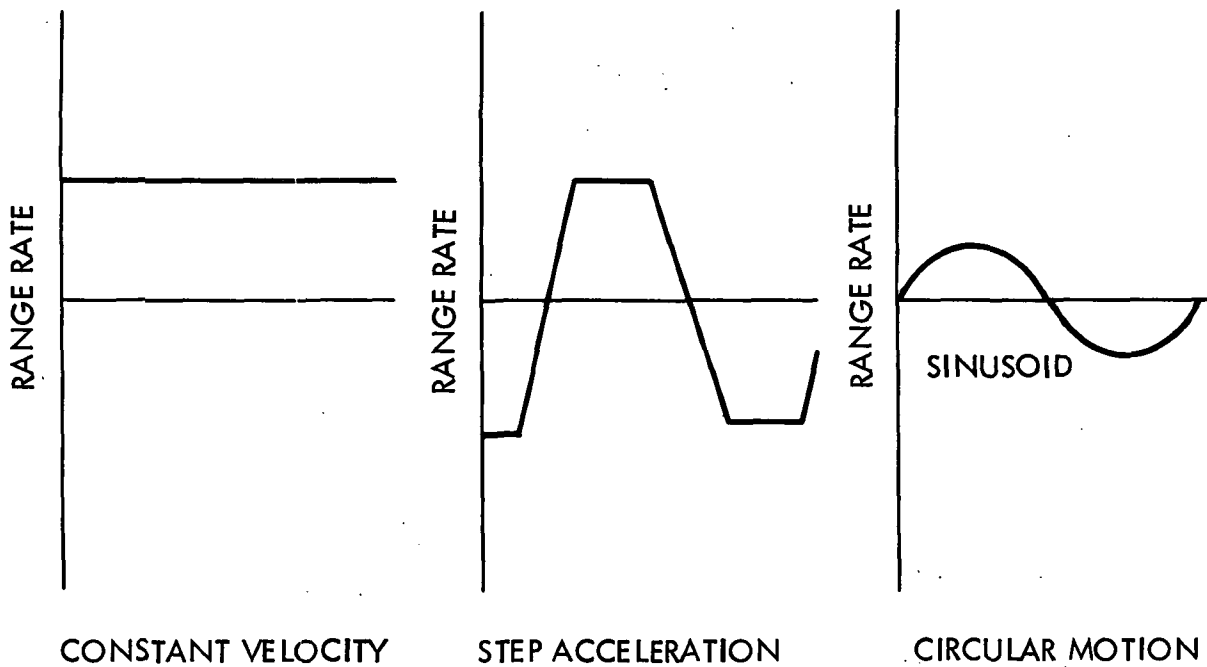
Figure C-1. Simulated Trajectories

(a) MEASURED CROSS CORRELATION FUNCTION



(b) MEASURED AMLE FUNCTION VS. PSEUDORANGE
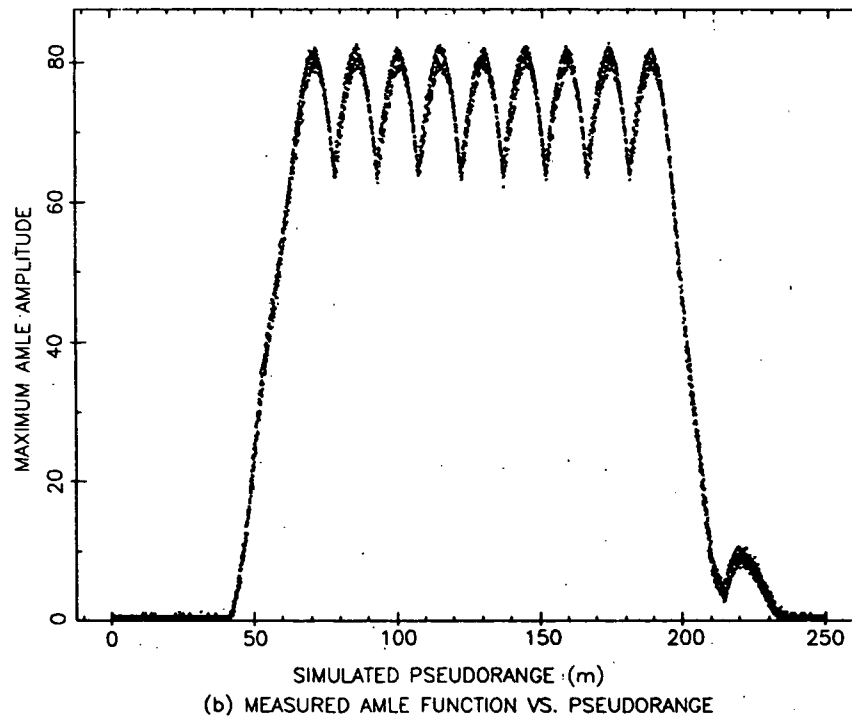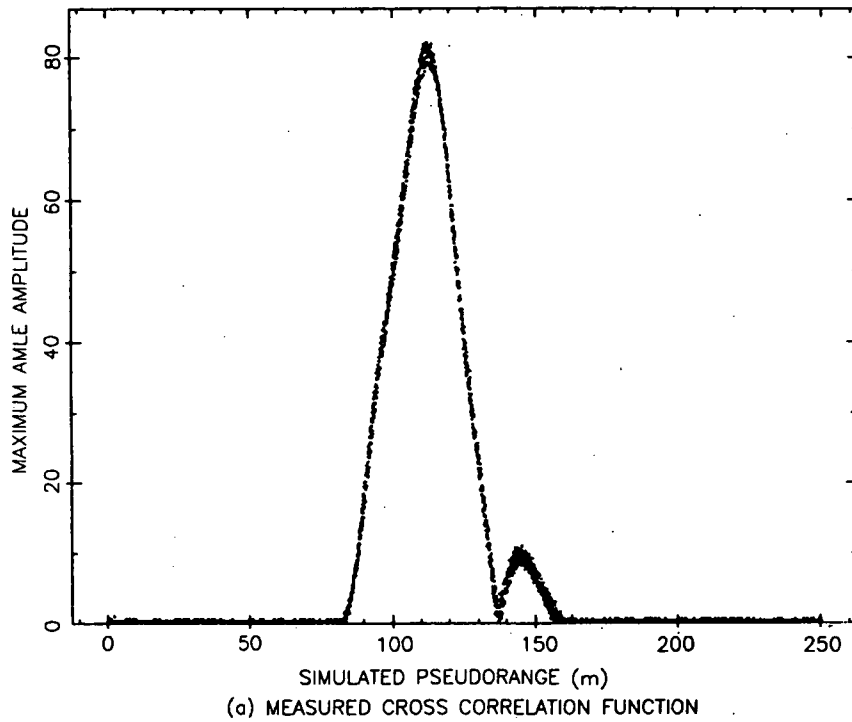
Figure C-2.    AMLE Response Versus Pseudorange
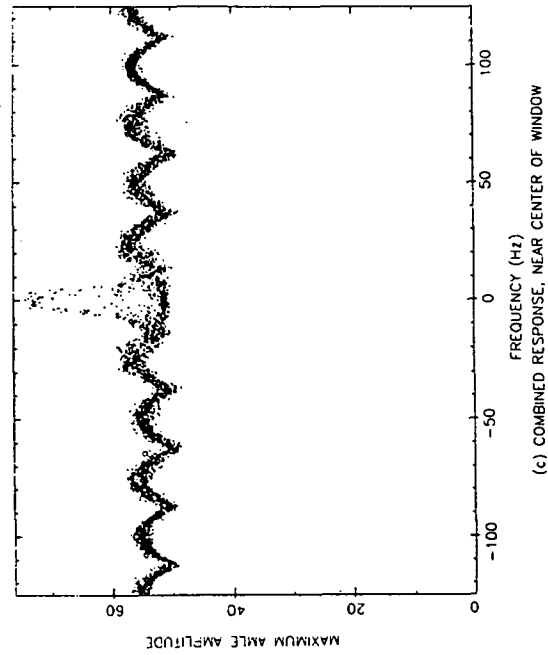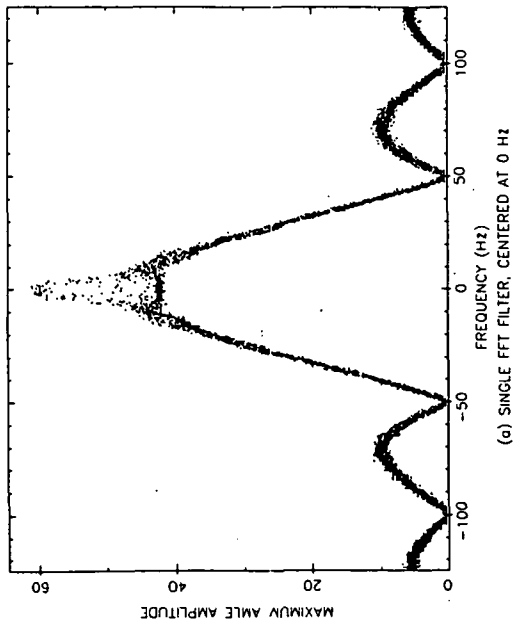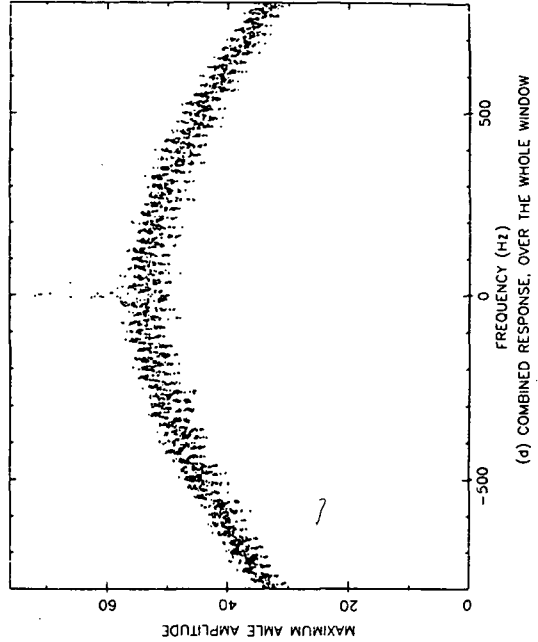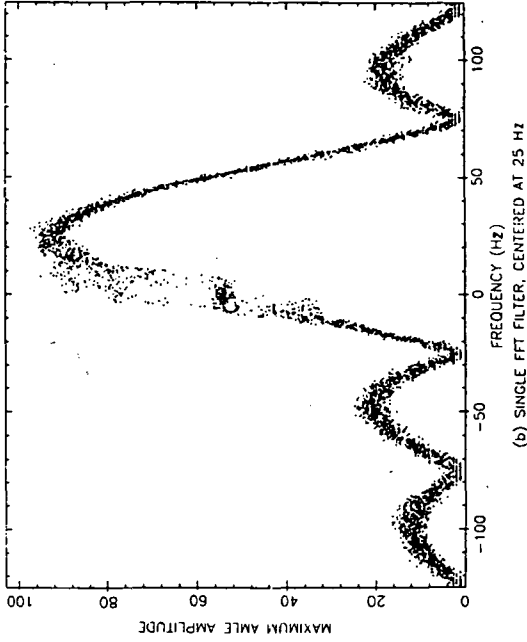
Figure C-3. AMLE Response Versus Velocity
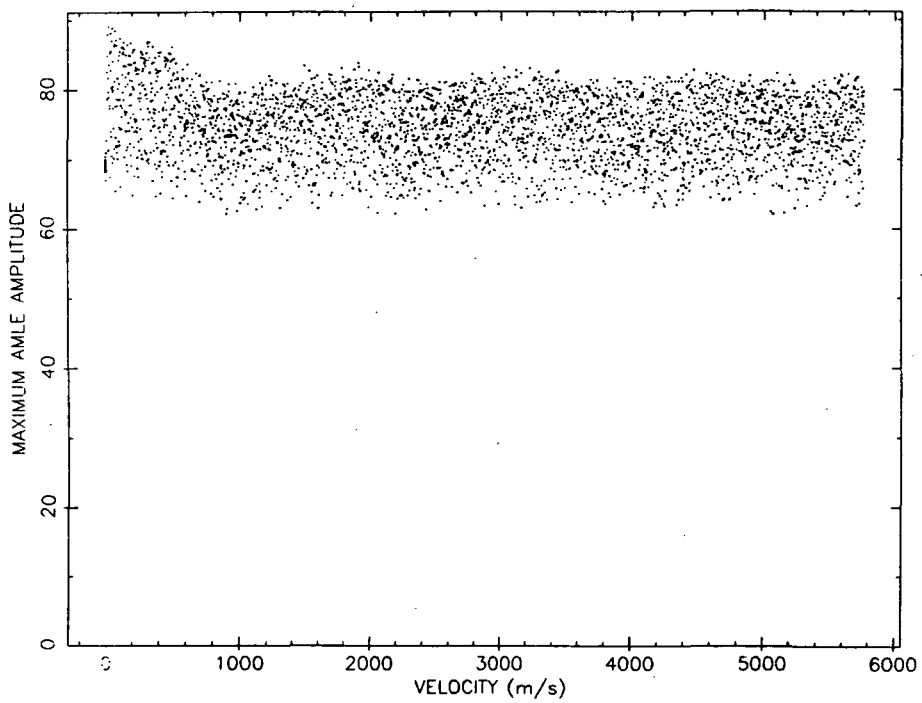
(a) AMLE FUNCTION, CODE ADJUSTOR ENABLED
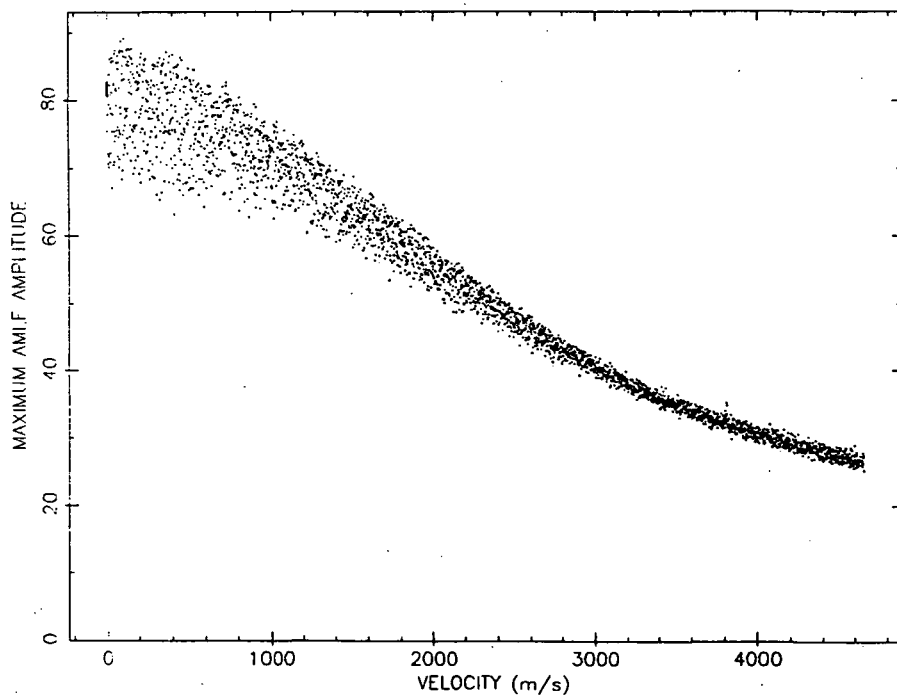


(b) AMLE FUNCTION, CODE ADJUSTOR DISABLED

Figure C-4.    AMLE Amplitude Versus Velocity
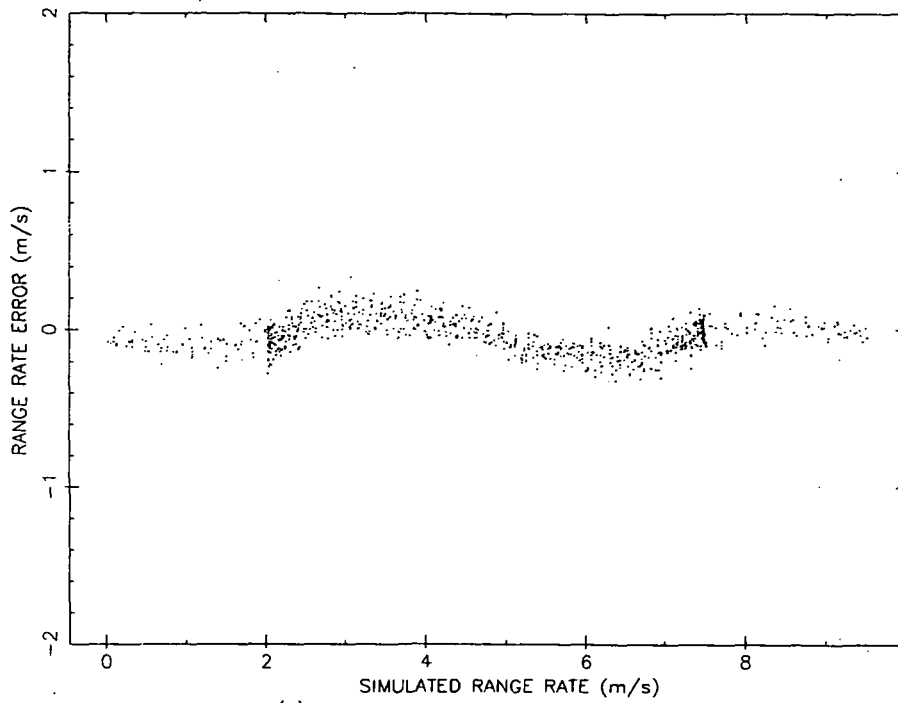
(a) ERRORS DUE TO RANGE RATE INTERPOLATION
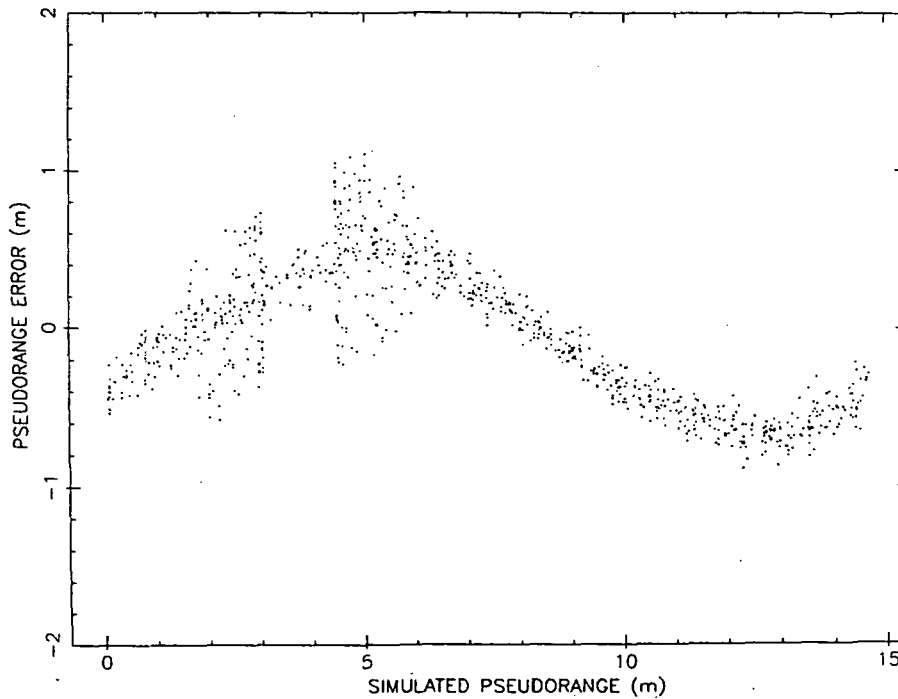
(b) ERRORS DUE TO PSEUDORANGE INTERPOLATION

Figure C-5.    Errors Due to AMLE Interpolation
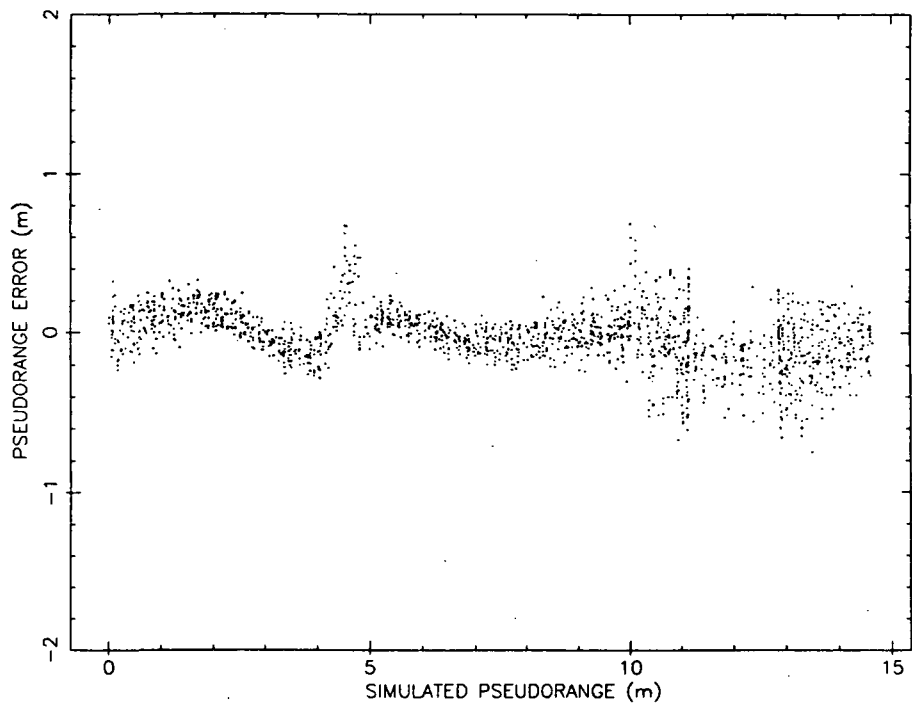
(a) ERRORS DUE TO PSEUDORANGE INTERPOLATION
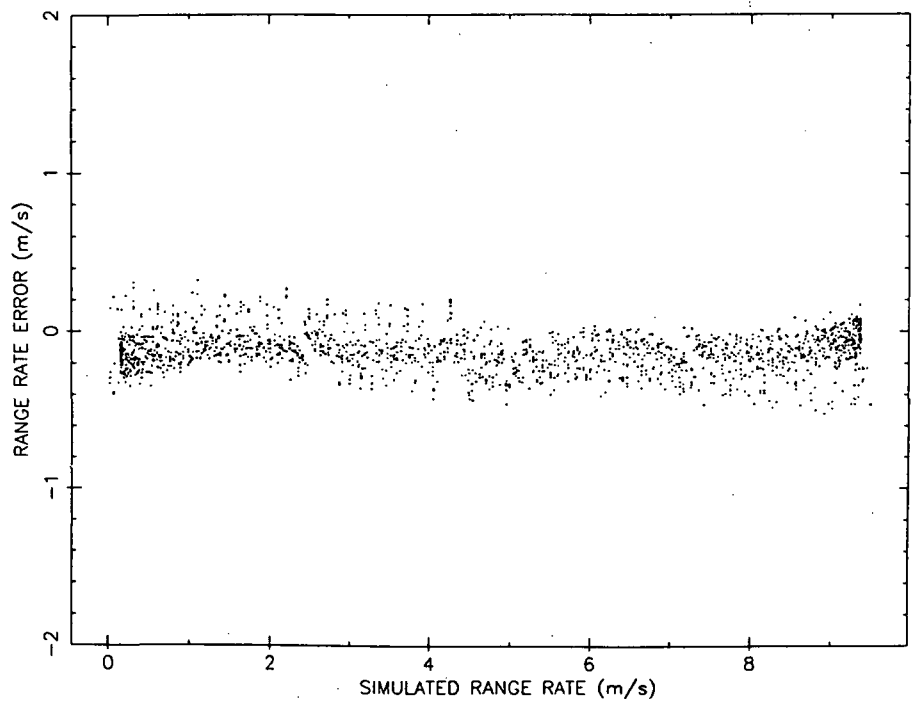
(b) ERRORS DUE TO RANGE RATE INTERPOLATION

Figure C-6.    AMLE Biases with Upgraded Interpolation Formulas

C-30

C - 3
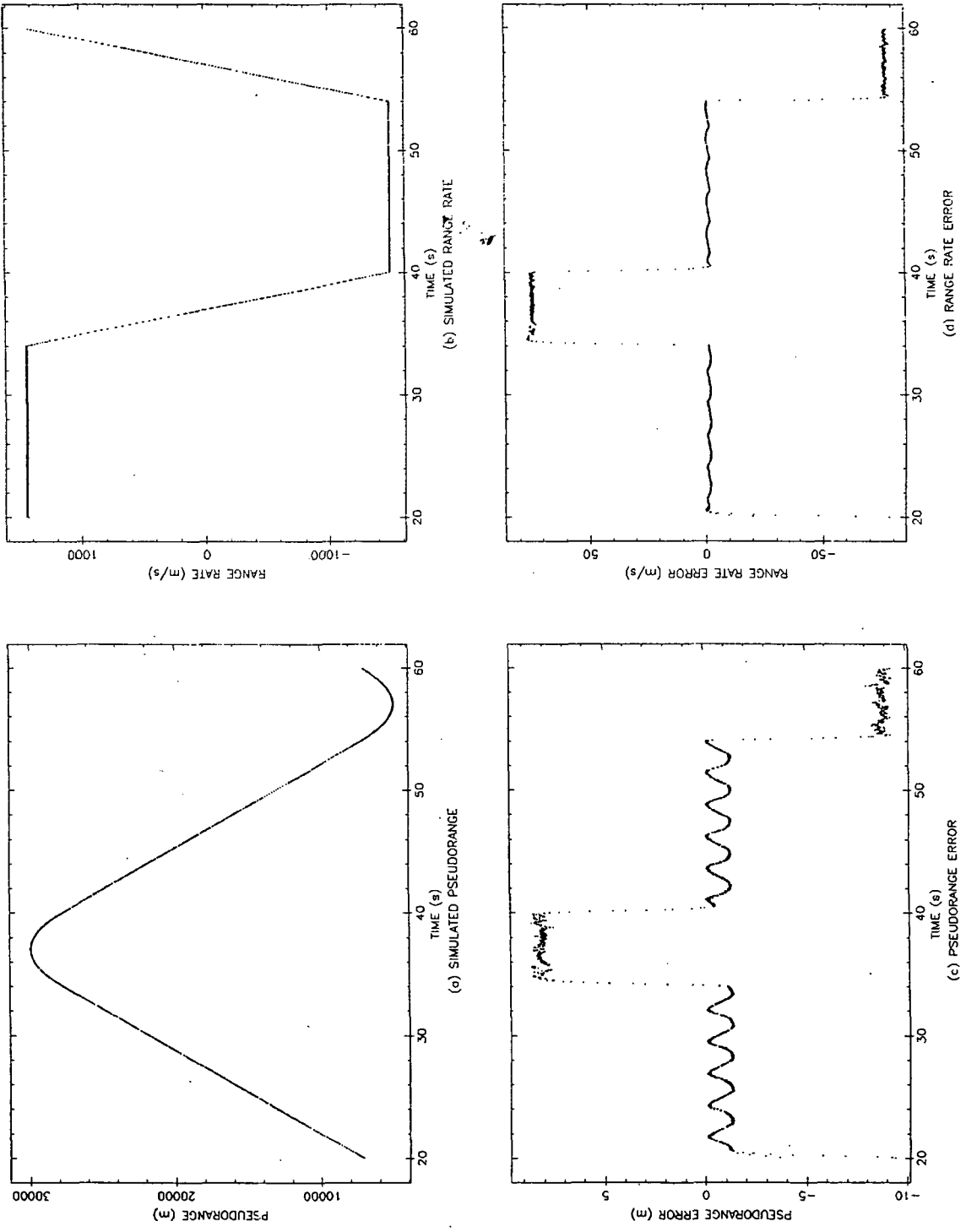
Figure C-7.  Example of Second Order Fading Memory Filter Performance
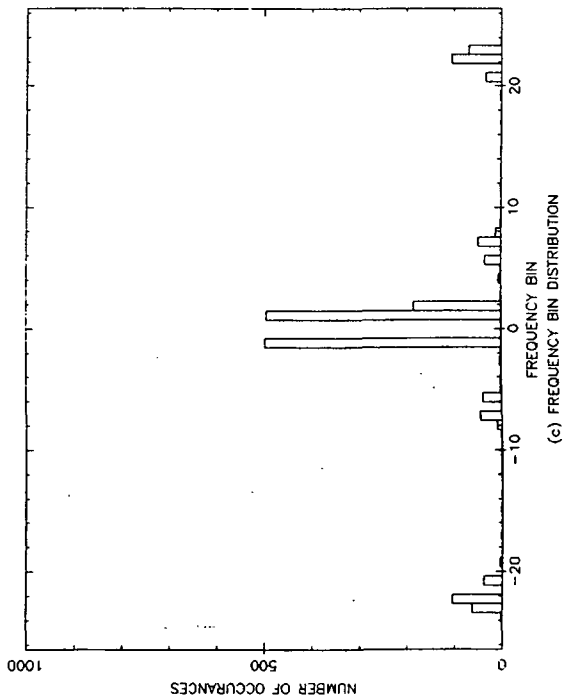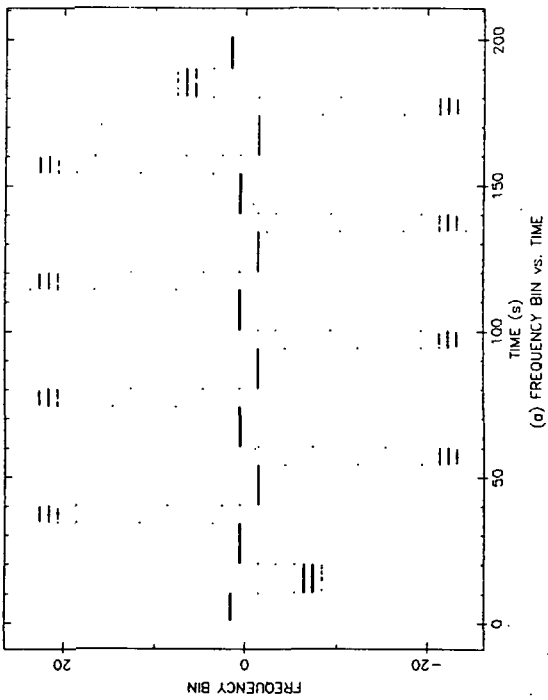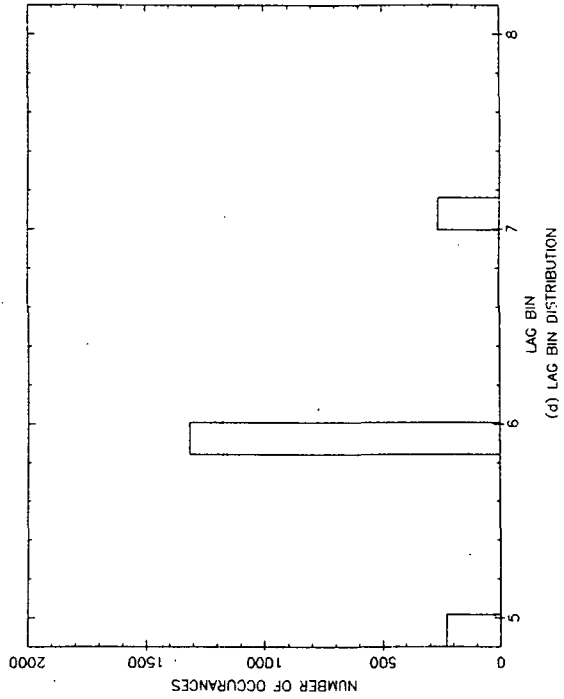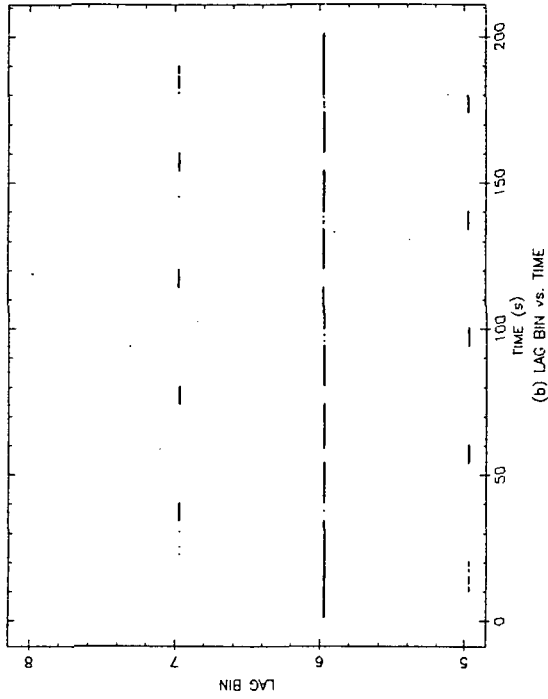
Figure C–8. Variation of AMLE Peak Coordinates – Second Order
Fading Memory Filter
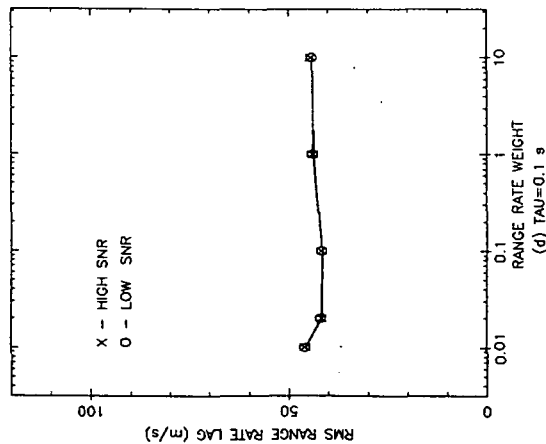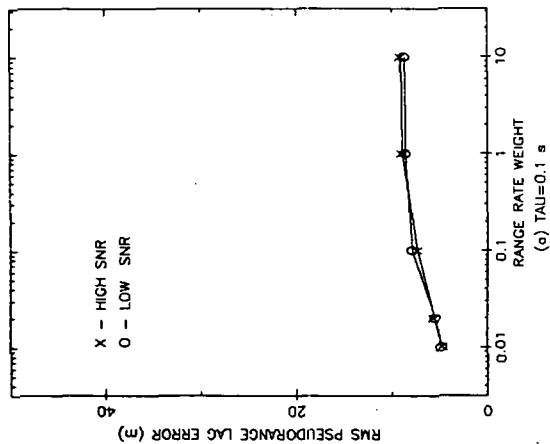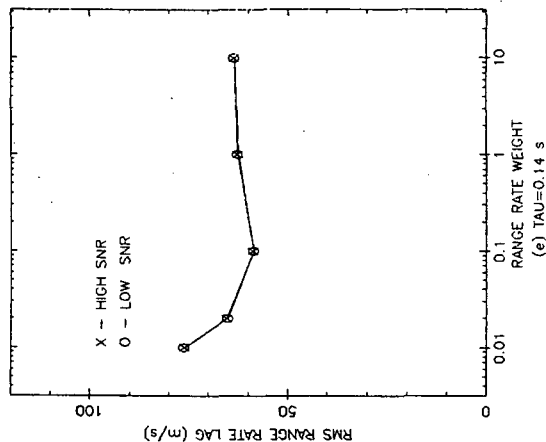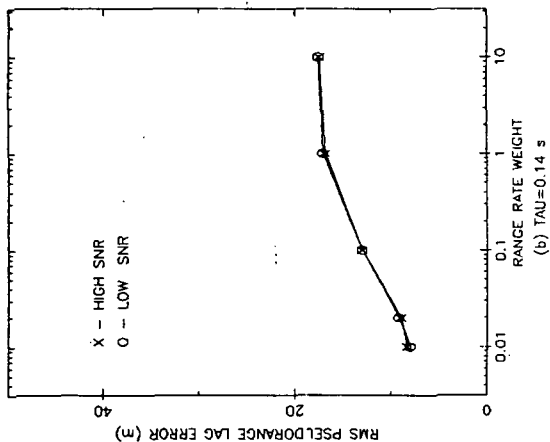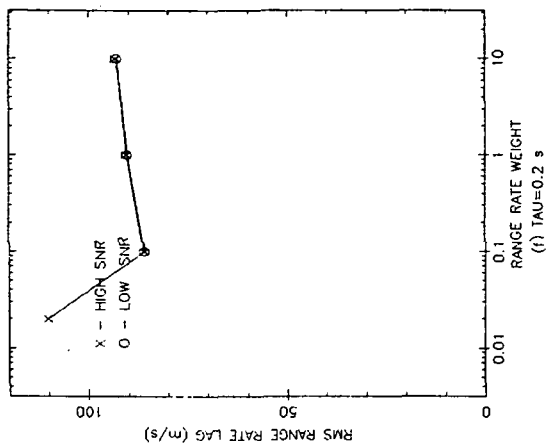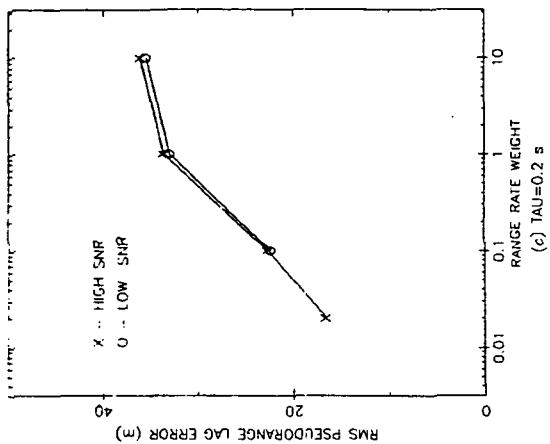
Figure C-9. Dynamic Lag Errors, Second Order Fading Memory Filter
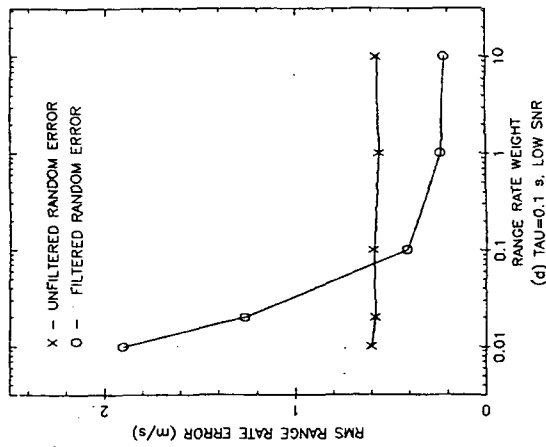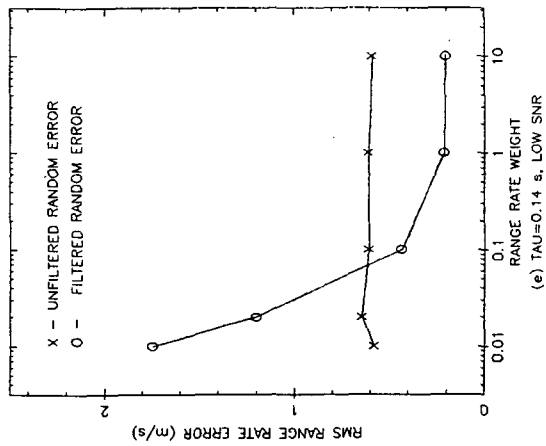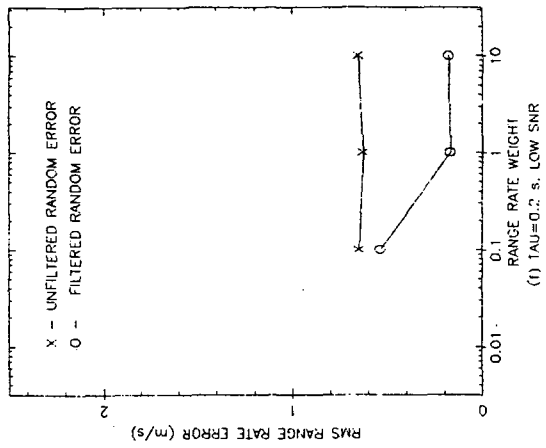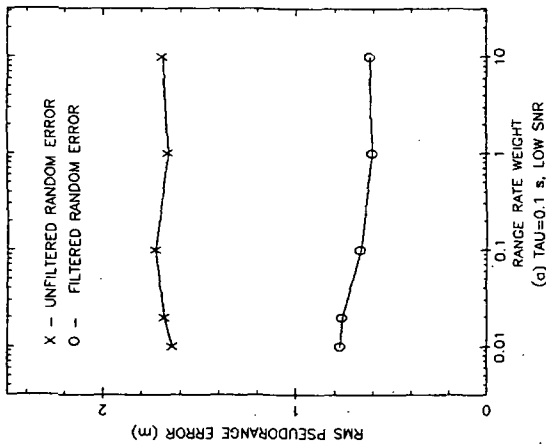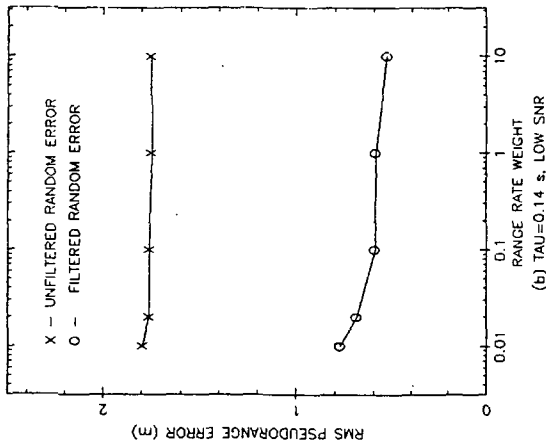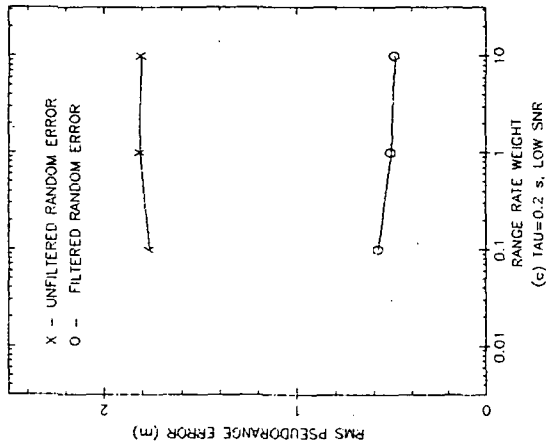
Figure C-10.  Second Order Fading Memory Filter, RMS Noise Before and After Filtering
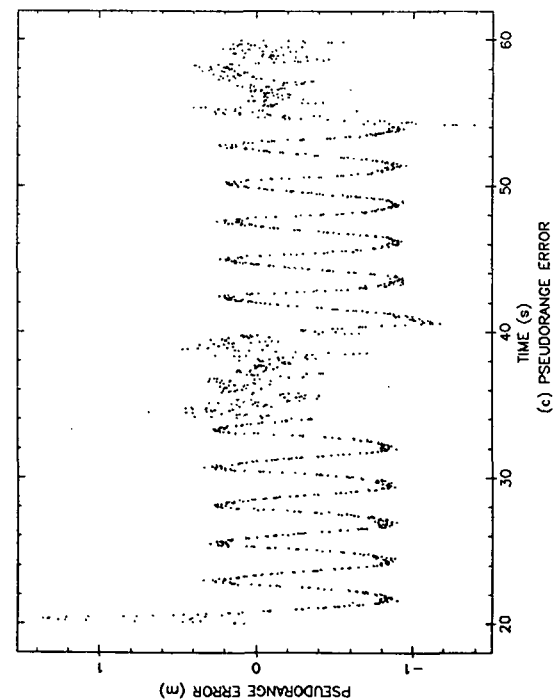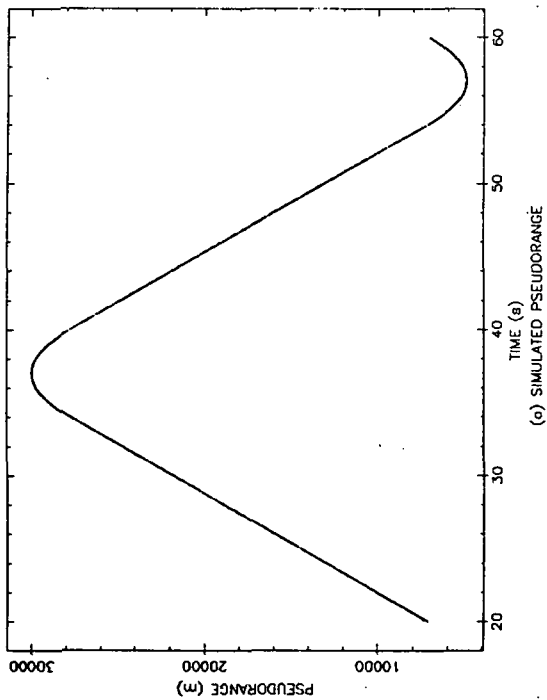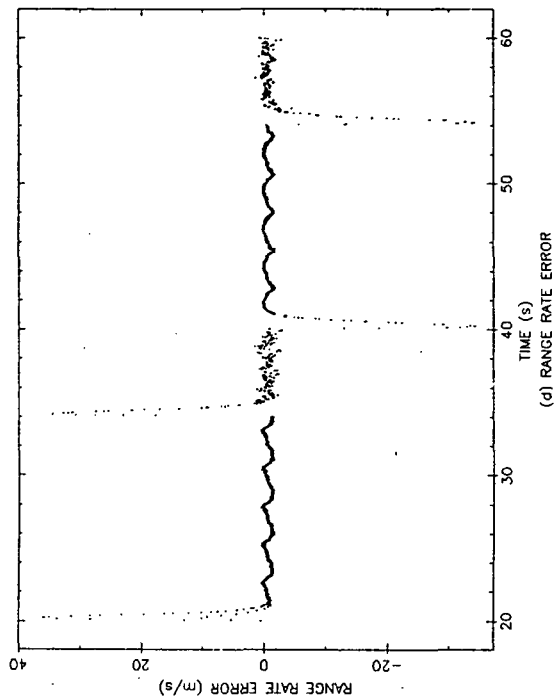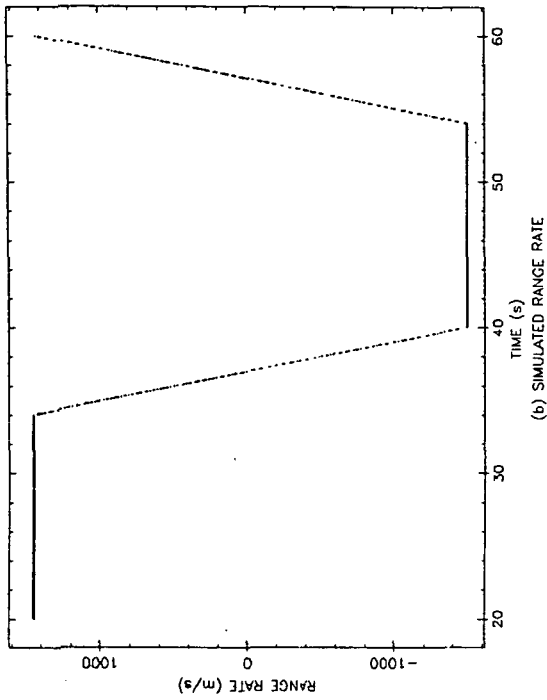
Figure C-11. Example of Third Order Fading Memory Filter Performance
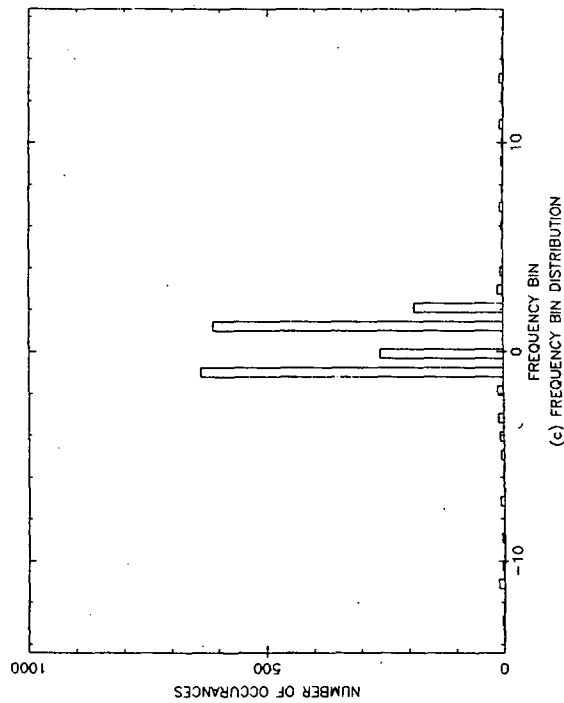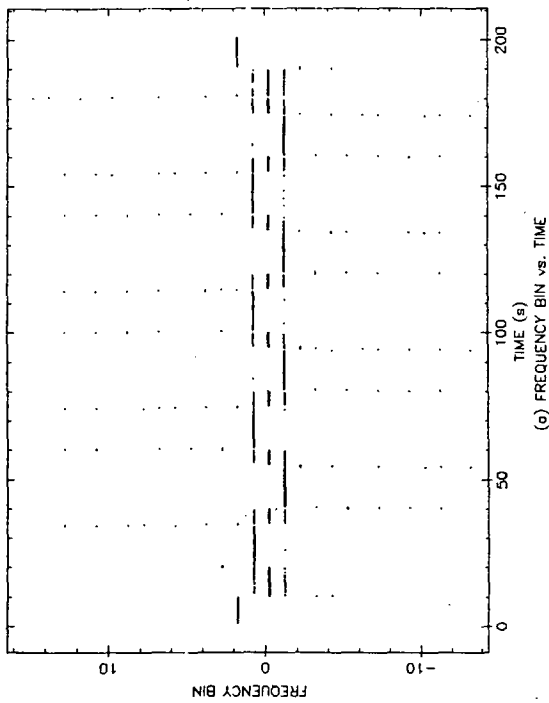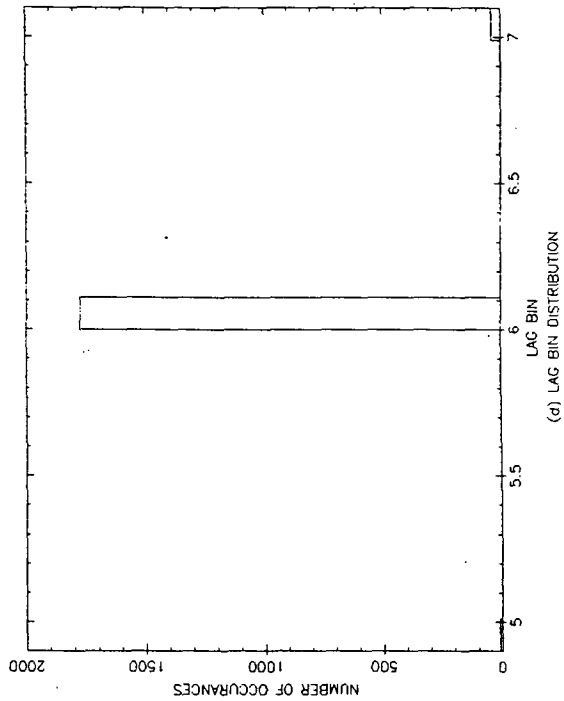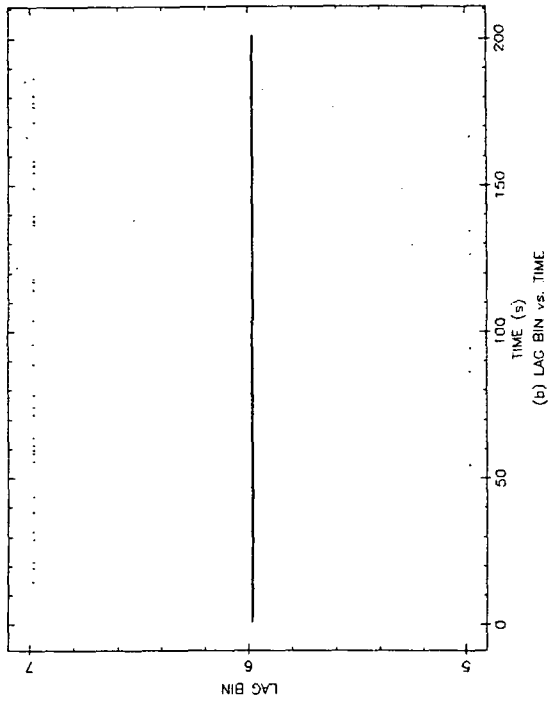
Figure C-12. Variation of AMLE Peak Coordinates - Third Order
Fading Memory Filter

C-36
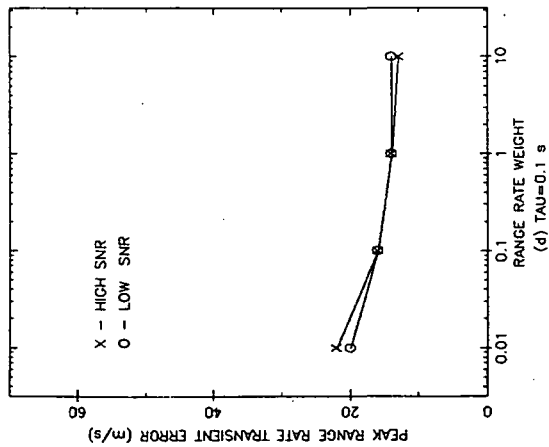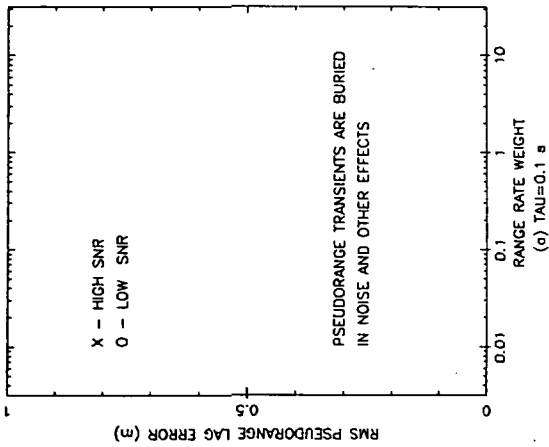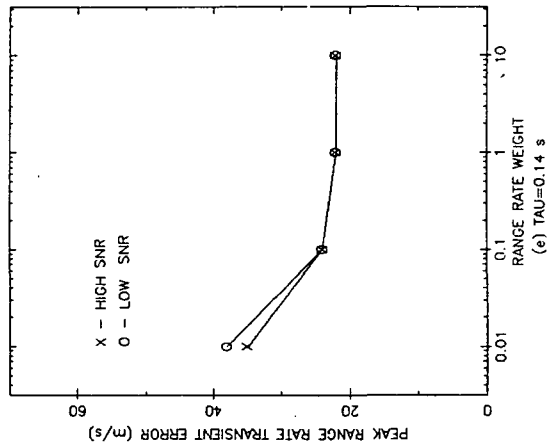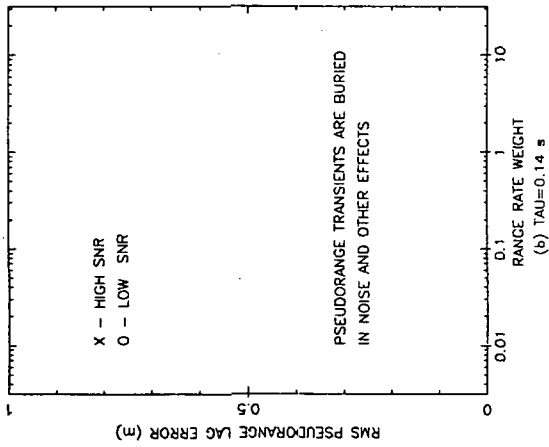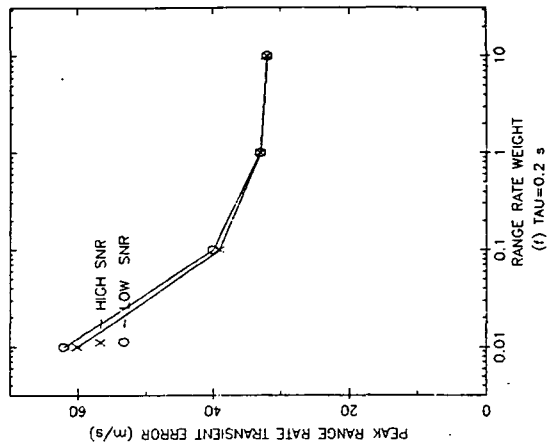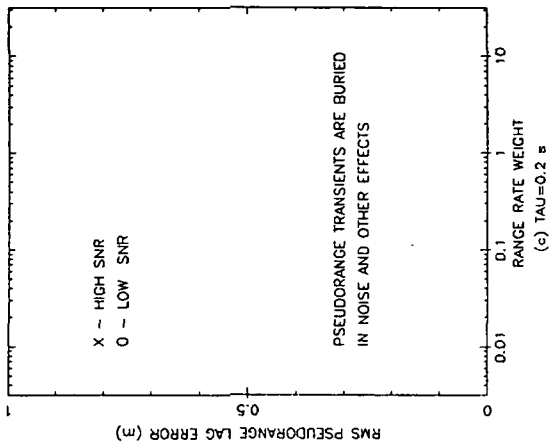
Figure C-13. Dynamic Lag Errors, Third Order Fading Memory Filter
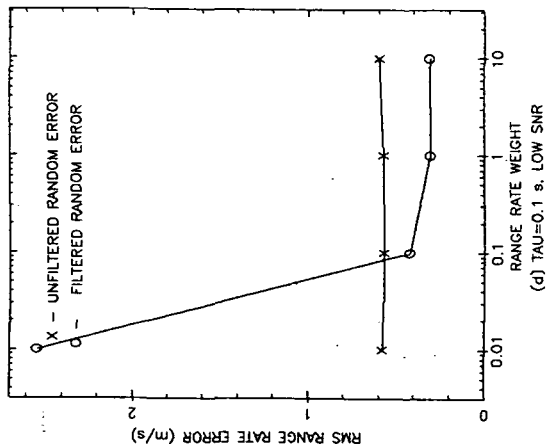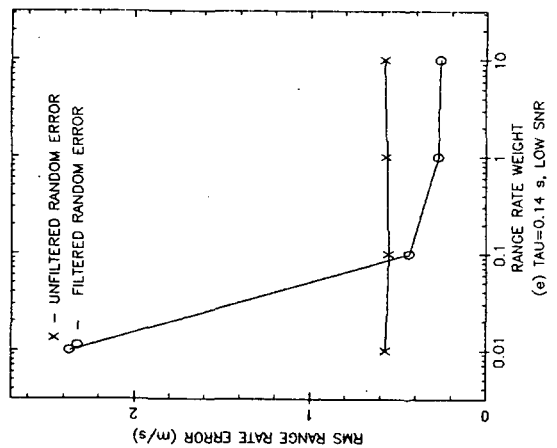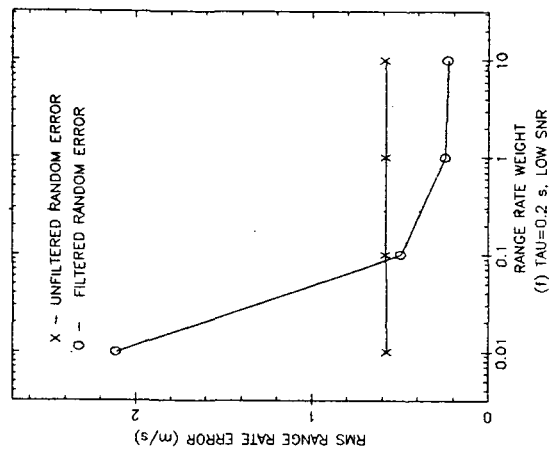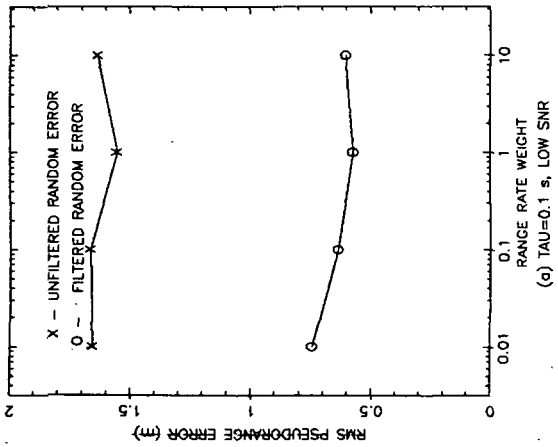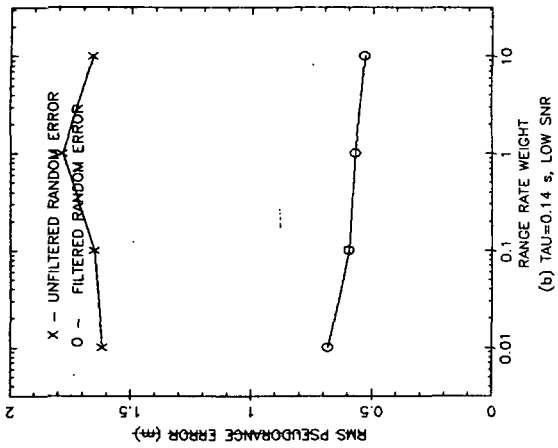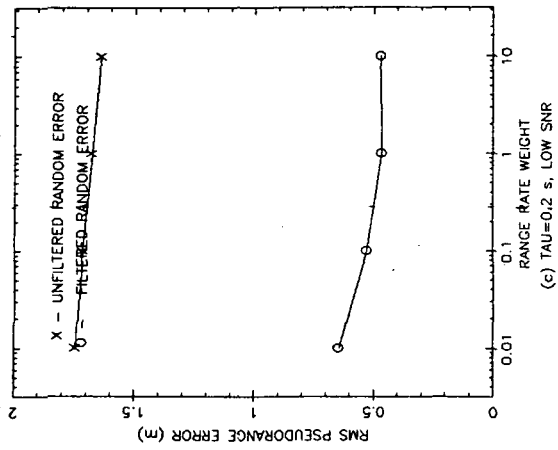
**Figure C-14.** Third Order Fading Memory Filter – RMS Noise Before and After Filtering
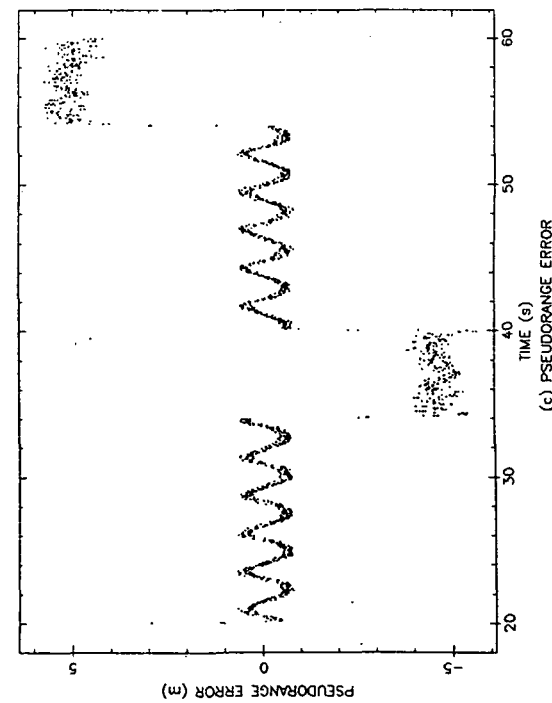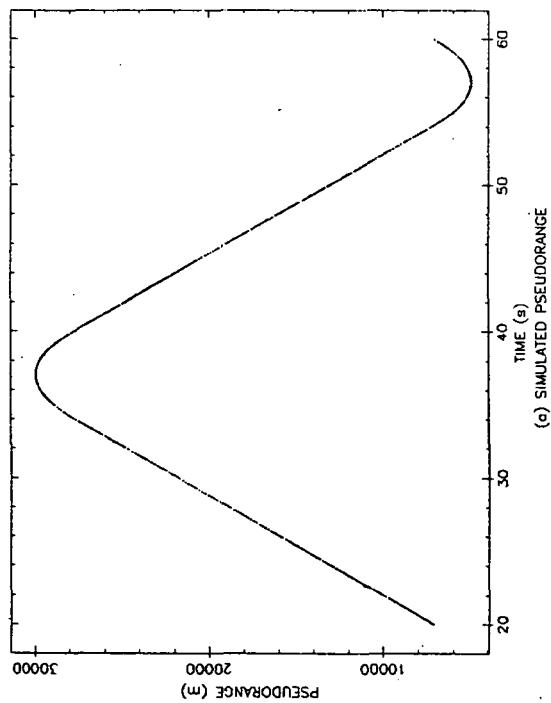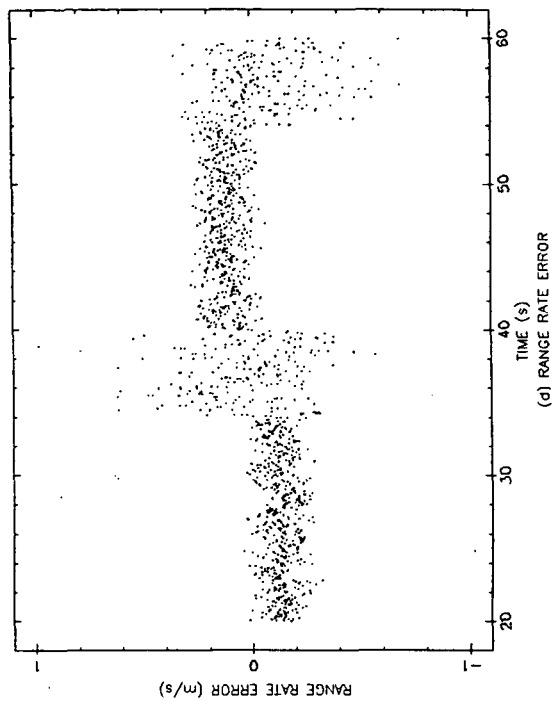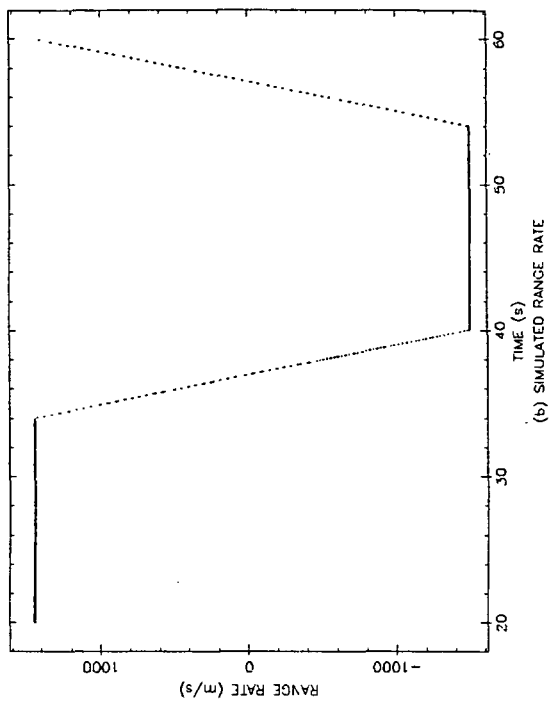
**Figure C-15.  Example of Second Order Kalman Filter Performance**
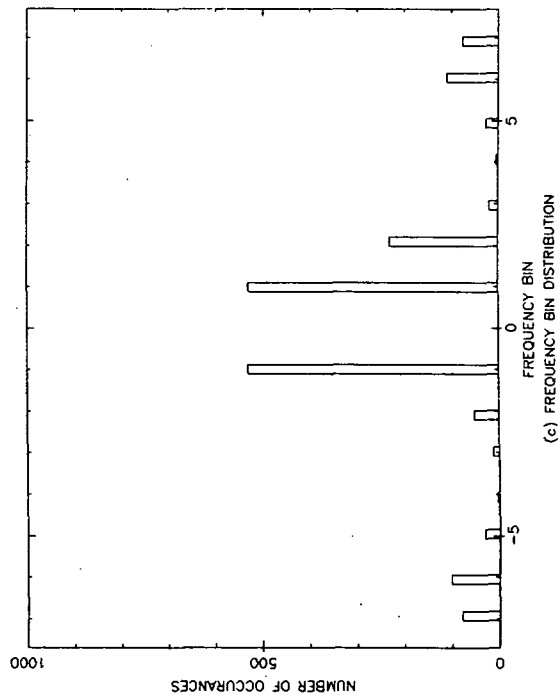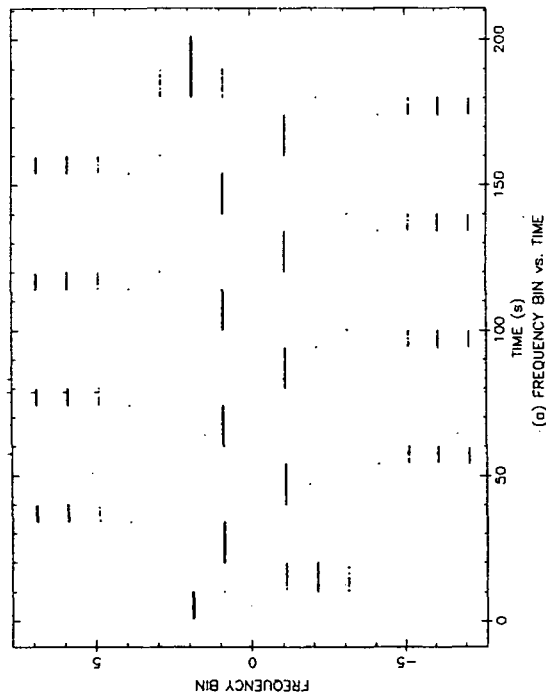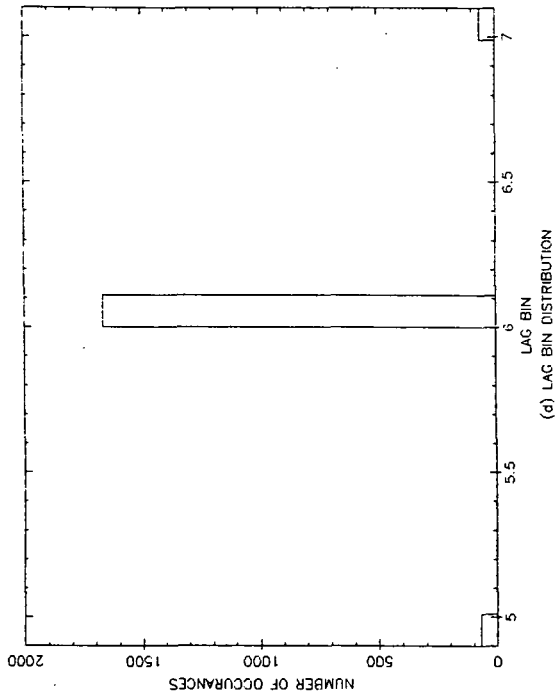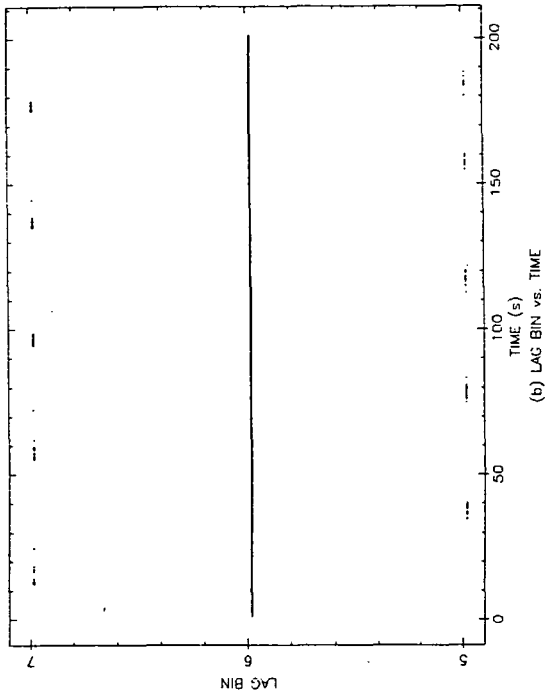
Figure C-16. Variation of AMLE Peak Coordinates – Second Order Kalman Filter
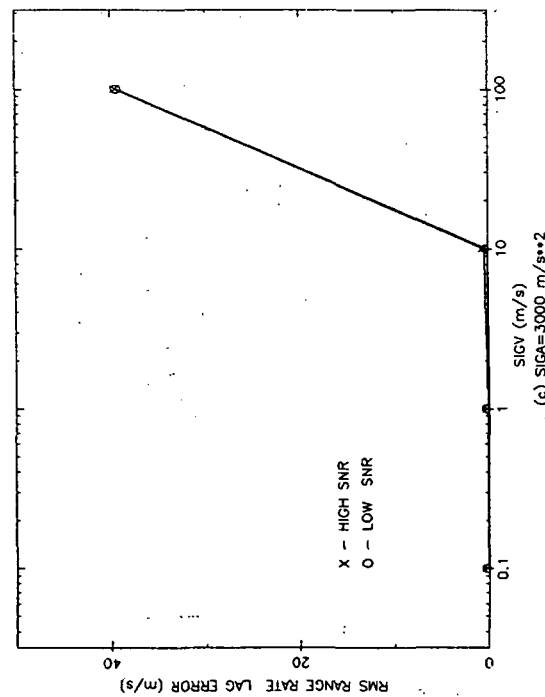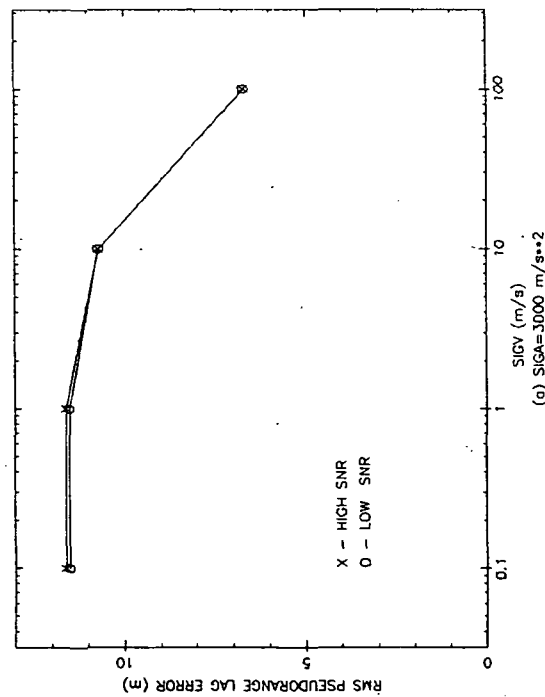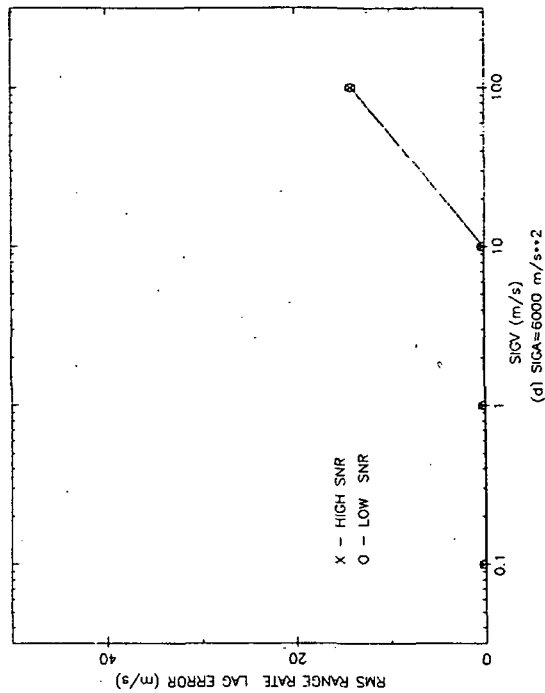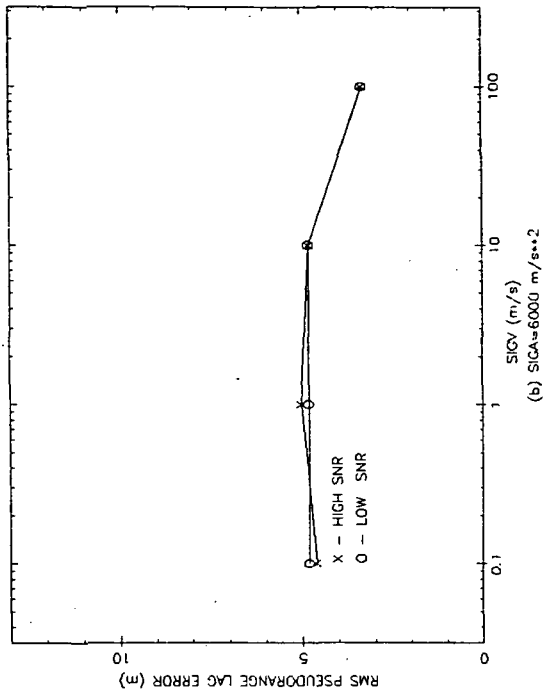
Figure C-17. Dynamic Lag Errors - Second Order Kalman Filter
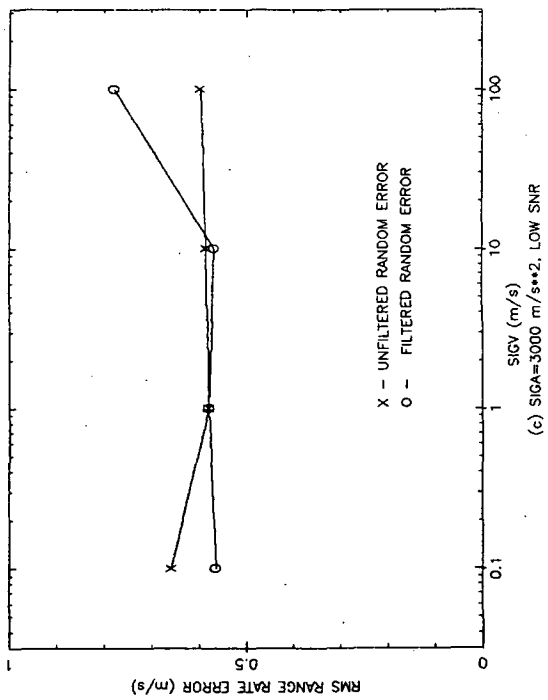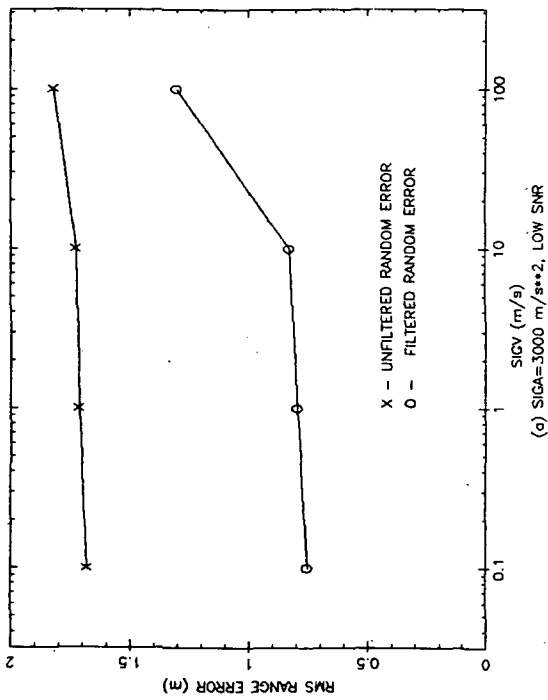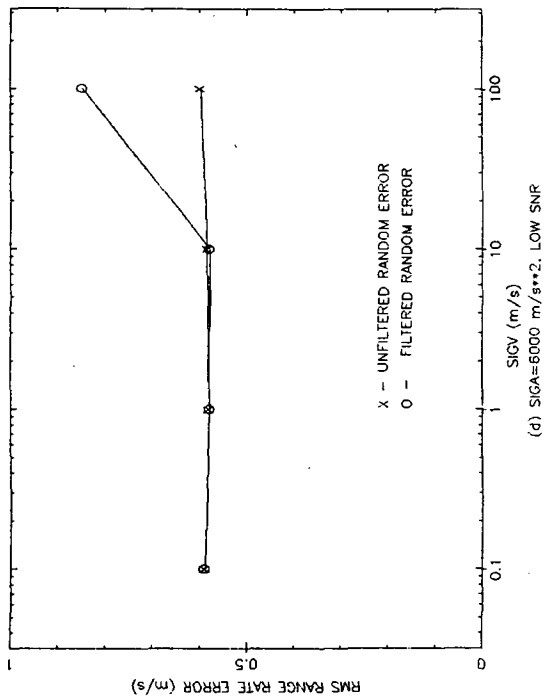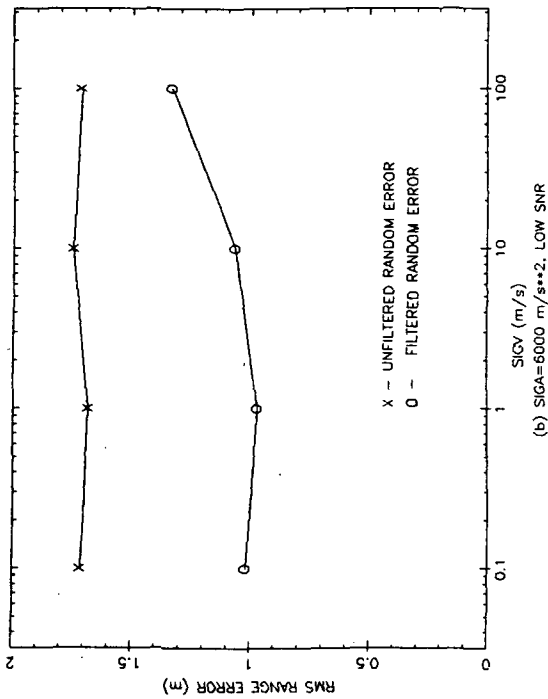
Figure C-18. Second Order Kalman Filter – RMS Noise Before and After Filtering
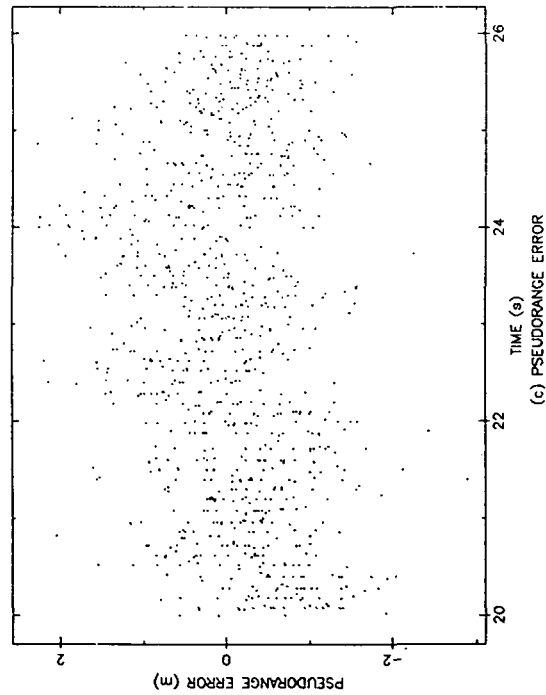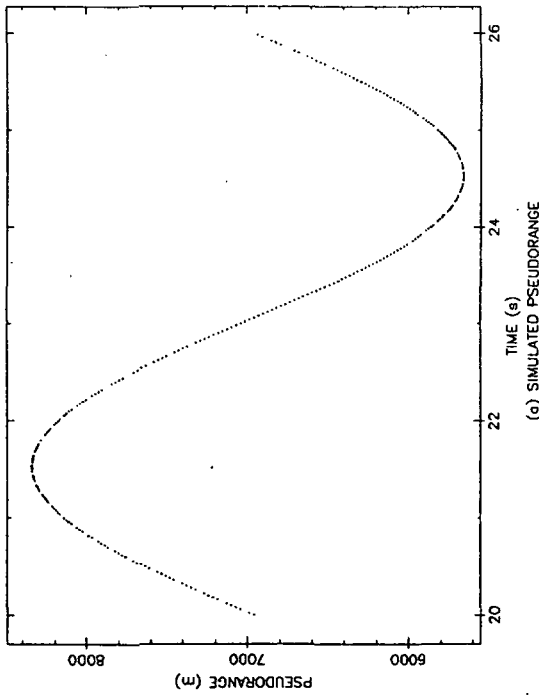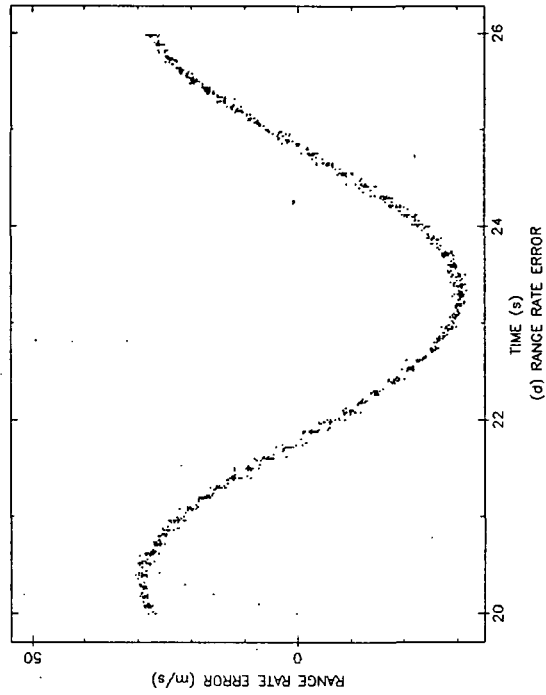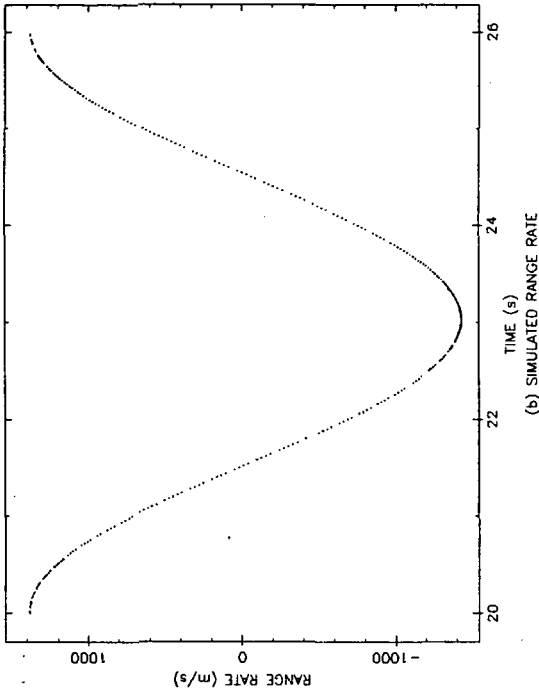
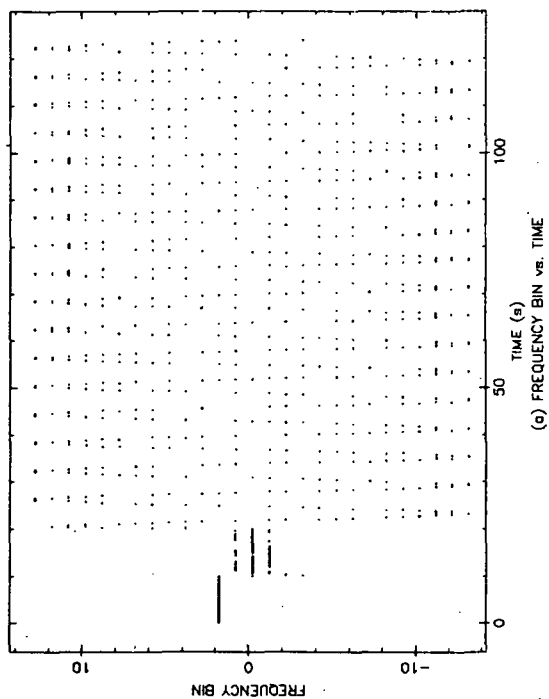Figure C-19. Tracking Errors – Circular Motion 150 g, 157 g/s, 34 dB-Hz
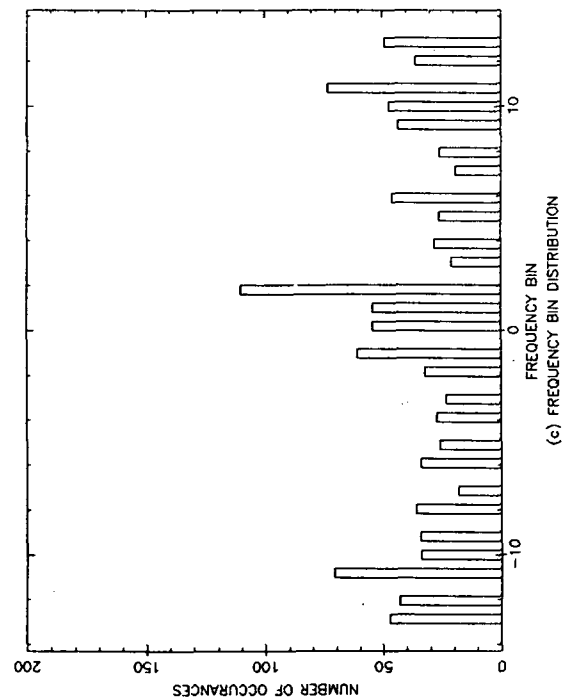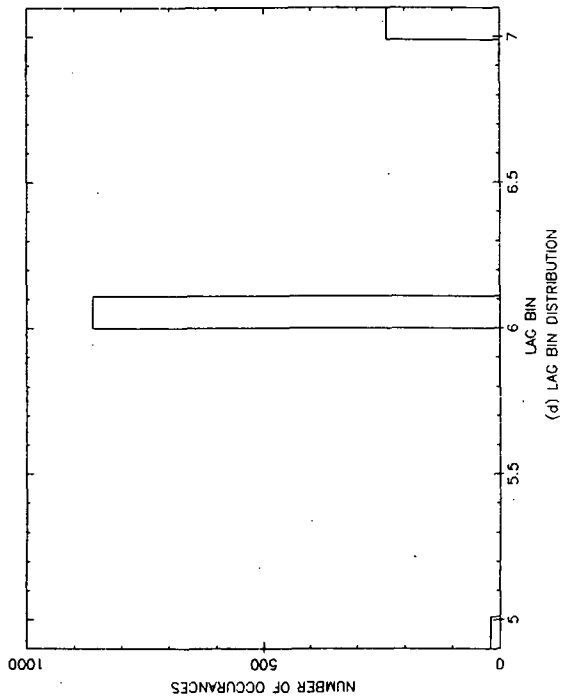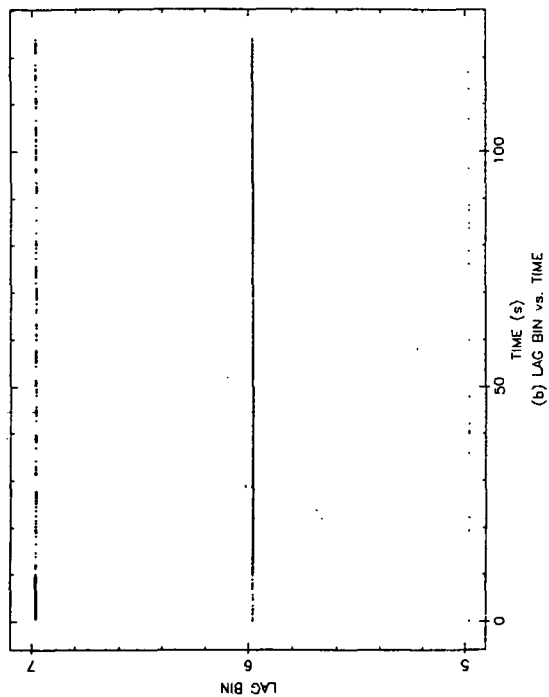
Figure C-20. Variation of AMLE Peak Coordinates - Circular Motion 150 g, 157 g/s